UNIVERSITA' CA' FOSCARI VENEZIA
Dipartimento di Scienze Ambientali, informatica e Statistica

Corso di Dottorato di ricerca in Informatica
ciclo XXXI

Tesi di Ricerca

Computational tools for the safety assessment of engineered nanomaterials

SSD: INF/01

Coordinatore del Dottorato
ch. prof. Riccardo Focardi
Supervisori
prof. Andrea Torsello - ch. prof. Antonio Marcomini

Dottorando
Gianpietro Basei
Matricola 810738

To my love Marina

Abstract

The increasing use of engineered nanomaterials (NMs) in nano-enabled products (NEPs) has raised societal concerns about their possible health and ecological implications. Indeed, despite their clear benefits, NMs may pose environmental, health and safety (EHS) issues. In Europe, the safety of chemicals is subject to the Registration, Evaluation, Authorization and Restriction of Chemicals (REACH) regulation, which requires a thorough Risk Assessment along their life cycles prior to introduction on to the market. To enable this the EU funded SUstainable Nanotechnology (SUN) project, aimed at combining the bottom-up development of EHS tools, knowledge and data with their top-down integration into a Decision Support System (SUNDS, https://www.sunds.gd/) for risk management of NMs. This thesis describes my contribution to developing SUNDS, more specifically aspects of its Human Health Risk Assessment (HHRA) and the Environmental Risk Assessment (ERA) modules, which were eventually tested in two real-world case studies, namely nano-copper oxide-based biocidal paint for wood preservation, and plastic automotive part (bumper) coloured with nano-sized organic pigments.

SUNDS has been designed to perform regulatory risk assessment on a case by case basis. However, the heterogeneity of NMs, with respect to physicochemical properties and observed (eco)toxicological effects, makes such case-by-case risk analyses hardly sustainable in terms of costs, time, and use of test animals, especially in the case of new materials. To address this issue, it has been suggested as essential to develop Integrated Approaches to Testing and Assessment (IATA) in compliance with the 3R (Replacement, Reduction, and Refinement) principles of reducing animal testing. Such strategies can help to make the best use of the available data resources and reduce testing by incorporating *in silico* methods such as (Quantitative) Structure-Activity Relationships ((Q)SARs) and Grouping for Read-Across models.

In this context, the available *in silico* methods to predict the hazard endpoints were critically reviewed as part of this thesis, highlighting their strengths and limitations and proposing a roadmap for future research in this area, including the adoption of more advanced Machine Learning techniques. Moreover, two novel approaches are proposed: the former combines experimental results from simple and fast techniques with multivariate statistical methods to support SbD strategies by highlighting how surface modification can affect the colloidal stability of nanoscale titanium dioxide (TiO2), while the latter uses Subspace Clustering as a tool for Read-Across and the Classification of NMs, by finding clusters in different Subspaces of the source data, learning a model in these Subspaces, and applying a basic Transfer Learning by projecting the target data on the subspace.

Acknowledgements

First, I would like to thank my supervisors prof. Andrea Torsello and prof Antonio Marcomini for their help and really precious suggestions and advices during the 3 years of my PhD.
My gratitude goes to the reviewers of this thesis, prof. Lang Tran and prof. Marco Loog. I'm very proud of them accepting this role and I thank them for the time spent in reading this work.
I owe much to many people in Ca' Foscari and in Greendecision Srl. Many thanks go to Danail, who gave me the opportunity of collaborating in the EU US Roadmap for Nanoinformatics, who always guided me during these three years, and who gave me precious suggestions while writing this thesis. I am really grateful also to Alex, who together with Danail co-supervised my PhD, and who together to Matteo worked with me in the technical development of SUNDS. Many thanks also to Lisa, Lara, Elena S., Elena B and Elisa G. for the opportunity of collaborating with them in different projects, and to Sara and Silvia. Thanks to my PhD colleagues Anna, Elisa F., Virginia, Vrishali, Alessandro "Jack", Artur, Marco and Vuong at INCA, and to the PhD students in Computer Science, especially Martina, Giorgia, Bruno, Francesco, Marco F., Marco S., and Mauro.
Thanks to dr. Andrea Haase for giving me the opportunity to spend three months at the German Federal Institute for Risk Assessment (BfR), and to the really nice people that I found there, especially Anna, Aileen, Anne, and Murat.
Many thanks to all the students that I had the privilege to help during the first two year of my PhD as a tutor of the courses of Calcolo and Istituzioni di Matematica, and to the professors Flavio Sartoretto and Enrico Bertuzzo.
Many thanks for the nice time spent together (and for the beers) to Diletta, Andrea and Mauro.
Thanks to my family for always supporting me, and to my friends.
Lastly but most importantly thanks to Marina, and to her family. Without her and her support all of this would not have been possible.

Contents

Abstract v
Acknowledgements vii
Contents ix
Preface xv
1 Introduction 1
2 A critical review on the *in silico* tools for hazard assessment 7
2.1 Introduction 7
2.2 Methods 9
2.2.1 Critical appraisal of peer-reviewed literature 9
2.2.2 Evaluation criteria 10
2.3 Results 11
2.3.1 Data storage and curation 11
2.3.2 Grouping for Read-Across of NMs 14
2.3.3 (Q)SARs applied to NMs 19
2.4 Discussion 35
2.5 Conclusions 38
3 A methodological approach for NMs categorization by multivariate statistical analysis 39
3.1 Introduction 39
3.2 Materials and methods 40
3.2.1 Case-study nanomaterial and other reagents 40
3.2.2 Synthesis of surface modified TiO_2 nanoparticles 41
3.2.3 Physico-chemical characterization 42
3.2.4 Dispersion stability testing 42
3.2.5 Clustering and Principal Component Analysis 43
3.3 Results and discussion 44
3.3.1 Binding of organic ligands to P25 NMs surface 44
3.3.2 Colloidal stability assessment as a function of electrolyte concentration and pH 50
3.3.3 Colloidal stability assessment as a function of dispersion media 62
3.4 Conclusions 66
4 Subspace Clustering as a tool for the Read-Across and Classification of NMs 67
4.1 Introduction 67

4.2 Materials and Methods 68
4.2.1 Case study datasets 68
4.2.2 Subspace Clustering based Read-Across and Classification 73
4.3 Results 74
4.3.1 Cytotoxicity of poly (amido amine) (PAMAM) dendrimers 74
4.3.2 Cytotoxicity of Metal Oxides 78
4.3.2 NanoTox Class dataset 81
4.4 Conclusions 81
5 SUNDS: SUN Decision Support System 83
5.1 Introduction 83
5.2 SUNDS modules 84
5.2.1 CENARIOS® module 84
5.2.2 Tier 1 - LICARA NanoSCAN 85
5.2.3 Tier 2 modules 85
5.3 Software architecture and server-side structure 98
5.3.1 Software Architecture 98
5.3.2 Server-side structure 100
5.4 Conclusions 103
6 SUNDS Human Health Risk Assessment module and its application to “Ferrari Red” Pigments 105
6.1 Introduction 105
6.2 Materials and methods 106
6.2.1 Case study description 106
6.2.3 SUNDS HHRA module 108
6.2.3 Hazard assessment 108
6.2.4 Exposure Assessment 110
4.2.5 Risk characterisation & Uncertainty analysis 111
6.3 Results 112
6.3.1 Hazard assessment 112
6.3.2 Exposure assessment 115
6.3.3 Risk characterization & Uncertainty analysis 118
6.4 Discussion 119
6.5 Conclusions 121

7 A quantitative Human Health Risk Assessment along the lifecycle of nano-scale copper-based wood preservatives using SUNDS 123
7.1 Introduction 123
7.2 Methods 124
7.2.1 Case study products 124
7.2.2 Risk assessment by means of SUNDS 126
7.3 Results 137
7.3.1 Exposure assessment 137
7.3.2 Hazard Assessment 139
7.3.3 Risk characterization 143
7.3.4 Uncertainty assessment 145
7.4 Discussion 150
7.5 Conclusions 152
8 Ecological risk along the lifecycle of nano-enabled products by means of SUNDS Environmental Risk Assessment module 155
8.1 Introduction 155
8.2 Materials and methods 156
8.2.1 Case study products 156
8.2.2 Exposure assessment 156
8.2.3 Hazard assessment 159
8.2.4 Risk characterization 159
8.3 Results 160
8.3.1 Exposure assessment results 160
8.3.2 Hazard assessment results 166
8.3.3 Risk characterization results 170
8.4 Conclusions 178
9 Conclusions and future work 179
References 181

Preface

The work presented in this thesis is based on some published (and not yet published) research papers written during my Ph.D. studies in Computer Science at Università Ca' Foscari Venezia from September 2015 to August 2018.

Chapter 2 presents a critical review on the available *in silico* tools making use of Machine Learning approaches for hazard assessment of nanomaterials. This work was recently submitted to a journal for publication:

- **G.Basei**, D.Hristozov, L.Lamon, A.Zabeo, N.Jeliazkova, G.Tsiliki, A.Marcomini, and A.Torsello, *Making use of available and emerging data to predict the hazards of engineered nanomaterials by means of in silico tools: a critical review*, (submitted to NanoImpact).

Moreover, I recently presented this work as a poster in an international conference:

- **G.Basei**, D.Hristozov, L.Lamon, A.Zabeo, N.Jeliazkova, G.Tsiliki, A.Marcomini, and A.Torsello, *Making use of existing and emerging data to predict the hazards of engineered nanomaterials: a critical review*, 3rd Nanosafety Forum for Young Scientists, La Valletta, Malta, September 10-11 (2018).

Chapter 3 presents a study on how organic functionalization of TiO_2 nanoparticles affect their colloidal stability, by using unsupervised Machine Learning techniques. Results of this work were recently published in a journal:

- A.Brunelli, E.Badetti, **G.Basei**, F.C.Izzo, D.Hristozov, and A.Marcomini, *Effects of organic modifiers on the colloidal stability of TiO_2 nanoparticles. A methodological approach for NPs categorization by multivariate statistical analysis*, NanoImpact, Volume 9, January 2018, Pages 114-123, ISSN 2452-0748, https://doi.org/10.1016/j.impact.2018.03.001.

Moreover, this work was presented in two different conferences:

- A.Brunelli, E.Badetti, **G.Basei**, and A.Marcomini, *Colloidal stability assessment of TiO_2 nanoparticles in aqueous media by analytical and statistical techniques*, 16thn International Conference on Chemistry and the Environment (ICCE), Oslo, June 18-22 (2017).
- E.Badetti, A.Brunelli, **G.Basei**, and A.Marcomini, *Assessment of nano-TiO_2 colloidal stability in aqueous media by analytical techniques and principal component analysis,* XXVI CONGRESSO NAZIONALE SCI, Paestum (NA), September 11-14 (2017).

Chapter 4 presents the current results of the work that I started during my 3 months at the German Federal Institute for the Risk Assessment (Bundesinstitut für Risikobewertung, BfR) in Berlin. The work presented in this chapter is not yet complete, since we plan to perform more tests on different datasets, however a paper is in preparation starting from it:

- **G.Basei**, A.Bahl, A.Haase, D.Hristozov, A.Zabeo, A.Marcomini, and A.Torsello, *Subspace Clustering as a tool for the Read-Across and Categorization of Nanomaterials*, (in prep.).

Moreover, I recently presented this preliminary results in an international conference:

- **G.Basei**, A.Bahl, A.Haase, D.Hristozov, A.Zabeo, A.Marcomini, and A.Torsello, *Subspace Clustering as a tool for the Read-Across and Classification of Nanomaterials*, 3rd Nanosafety Forum for Young Scientists, La Valletta, Malta, September 10-11.

Chapter 5 provides an overview on SUNDS, the Decision Support System created in the context of the EU FP7 SUN project, which was one of the biggest projects in the FP7 program (13,5 mln € of total budget). A considerable part of my Ph.D. was indeed dedicated to collaborating with the team developing SUNDS. It resulted in the following contributions in international conferences:

- A.Zabeo, D.Hristozov, E.Semenzin, L.Pizzol, V.Subramanian, **G.Basei**, and A.Marcomini, *SUN Decision Support System (SUNDS)*, New tools and approaches for nanomaterial safety assessment, Malaga, February 7-9 (2017).
- A.Zabeo, D.Hristozov, E.Semenzin, L.Pizzol, V.Subramanian, **G.Basei**, and A.Marcomini, *SUNDS, a decision support system for nanotechnology risk assessment & management based on multi attribute value theory*, Risk Governance for Key Enabling Technologies, Society for Risk Analysis Policy Forum, Venezia, March 1-3 (2017).
- A.Zabeo, D.Hristozov, E.Semenzin, L.Pizzol, V.Subramanian, **G.Basei**, and A.Marcomini, *SUNDS, a MCDA based nanotechnology sustainability Decision Support System*, 85th Meeting of the EURO Working Group on MCDA, Padova, April 20-22 (2017).

Chapter 6, 7 and 8 present some practical application of SUNDS in assessing the Risks of nanomaterials for the Environment and for Human Health. Specifically, Chapter 6 and 7 presents two application of the Human Health Risk Assessment module of SUNDS, the former more focused on the methodology, with an application on Organic Pigments used in the automotive sector (Ferrari red pigments) and the latter presenting a comprehensive Risk Assessment of copper based wood preservatives in the whole lifecycle of such nanomaterials. These two chapters are extrapolated from the following journal papers:

- D.Hristozov, L.Pizzol**, G.Basei**, A.Zabeo, J.Habicht, N.Neubauer, W.Wohlleben, A.Sanchez Jimenez, E.Semenzin, V.Subramanian, I.Gosens, F.R.Cassee, W.De Jong, S.F.Hansen, A.Mackevica, A.J.Koivisto, K.A.Jensen, V.Stone, and A.Marcomini, *Probabilistic Human Health Risk Assessment along the Lifecycle of Copper-Based Wood Preservatives*, Nanotoxicology, Volume 12, Issue 7, Pages 747-765, 2018, DOI: 10.1080/17435390.2018.1472314
- L.Pizzol, D.Hristozov, A.Zabeo, **G.Basei**, W.Wohlleben, A.J.Koivisto, K.A.Jensen, W.Fransman, V.Stone, A.Marcomini, SUNDS probabilistic human health risk assessment methodology and its application to organic pigment used in the automotive industry, 2018 (accepted by NanoImpact, DOI: 10.1016/j.impact.2018.12.001).

In addition, these two works were presented in several international conferences, specifically:

- L.Pizzol, D.Hristozov, A.Zabeo, E.Semenzin, V.Subramanian, **G.Basei**, W.Fransman, I.Gosens, F.R. Cassee, J.Koivisto, K.A.Jensen, V.Stone, A.Sanchez, S.F.Hansen, W.Wohlleben, and A.Marcomini*, Human Health Risk Assessment Module implemented in SUNDS, New tools and approaches for nanomaterial safety assessment*, Malaga, February 7-9 (2017).
- D.Hristozov, A.Zabeo, E.Semenzin, L.Pizzol, V.Subramanian, **G.Basei**, and A.Marcomini, *Decision support system for nanotechnology risk assessment and management*, SETAC 27th Annual Meeting, Brussels, May 7-11 (2017).
- L.Pizzol, D.Hristozov, A.Zabeo, E.Semenzin, V.Subramanian, **G.Basei**, W.Fransman, I.Gosens, F.R.Cassee, J.Koivisto, K.A.Jensen, V.Stone, A.Sanchez, S.F.Hansen, W.Wohlleben, and A.Marcomini, *Human Health and Ecological Risk Assessment and*

Management of nano-enabled products through the lifecycle, SETAC 27th Annual Meeting, Brussels, May 7-11 (2017).

Chapter 8 presents different case studies of using SUNDS for evaluating risks for the environment. Currently, a journal paper is being prepared starting from the results presented in the chapter:

- E.Semenzin, **G.Basei**, A.Caballero-Guzman, J.J.Scott-Fordsmand, F.Gottschalk, V.Ricottone, V.Subramanian, A.Zabeo, E.Giubilato, B.Nowack, D.Hristozov, and A.Marcomini, *Ecological risk along the lifecycle of nano-enabled products*, to be submitted to Environmental Pollution (in prep.).

In addition, it was presented in two international conferences:

- E.Semenzin, A.Caballero-Guzman, J.J.Scott-Fordsmand, F.Gottschalk, **G.Basei**, V.Subramanian, A.Zabeo, B.Nowack, D.Hristozov, and A.Marcomini, *Ecological risk along the lifecycle of nano-enabled products,* NanoImpact Conference, Monte Verità, March 12-17 (2017).
- E.Semenzin, V.Subramanian, A.Zabeo, L.Pizzol, **G.Basei**, W.Fransman, T.Wilkins, D.Hristozov, and A.Marcomini, *Human Health and Ecological Risk Assessment and Management of nano-enabled products through the lifecycle*, SETAC 27th Annual Meeting, Brussels, May 7-11 (2017).

In addition to the SUN project, during my Ph.D. I marginally collaborated in the EU H2020 project caLIBRAte, further developing SUNDS, in the EU H2020 project GRACIOUS, and in the EU FP7 NanoToxClass project (during my period at the BfR).

I also collaborated in writing a chapter of the **EU US Roadmap for Nanoinformatics 2030**, which is a joint work between scientists working in the nanosafety context in Europe and in the USA, aimed at addressing future research in the field of nanoinformatics:

- T.Puzyn, G.Verheyen, S.Van Miert, B.Xing, S.Iqbal, Q.Zhao, V.Lobaskin, **G.Basei**, A.G.Papadiamantis, Y.Cohen, *Chapter 6: Nanochemoinformatics and Statistical modelling,* in EU US Roadmap Nanoinformformatics 2030, editors: A.Haase, F. Klaessig (2018), (DOI: 10.5281/zenodo.1486012).

Finally, I marginally collaborated in two additional works presented in an international workshop and in a national conference, which are not reported in this thesis:

- A.Brunelli, E.Badetti, **G.Basei**, A.Zabeo, A.Marcomini, G.Gheno, R.Ganzerla, *On the stability of colloidal calcium hydroxide nanoparticles dispersions for stone conservation*, XVI CONGRESSO NAZIONALE DI CHIMICA DELL'AMBIENTE E DEI BENI CULTURALI, Lecce. June 26-29 (2016).
- N.Jeliazkova, P.Ritchie, S.Rashid, **G.Basei**, A.Zabeo, G.Tsiliki, and D.Hristozov, *Data curation, model development and integration: the GRACIOUS platform*, Scientific workshop on Grouping of Nanomaterials: NanoReg2 and GRACIOUS projects, Paris, France, September 12-13 (2018).

1 Introduction

Nanotechnology is one of the Key Emerging Technologies identified in the European Union (EU) 2020 Strategy. The EU, in his recommendation of 18 October 2001 (2011/696/EU), defines a nanomaterial as a "*A natural, incidental or manufactured material containing particles, in an unbound state or as an aggregate or as an agglomerate and where, for 50% or more of the particles in the number size distribution, one or more external dimensions is in the size range 1 nm - 100 nm. In specific cases and where warranted by concerns for the environment, health, safety or competitiveness the number size distribution threshold of 50% may be replaced by a threshold between 1 and 50%*" [1].

In the last 20 years this class of products have been increasingly used in a wide variety of industrial applications and consumer products [2], often referred as nano-enabled products (NEPs). Applications of nanomaterials (NMs), indeed, include among the others: i) medicine, e.g. by being used as a carrier for delivering drugs to tumours, break up clusters of bacteria, stimulate immune response, or dental applications, ii) Manufacturing and Materials, by providing e.g. odour-resistant clothes, barrier to gases in plastic film, fill gaps between carbon fibres, iii) industrial coating, by e.g. providing resistance to UV rays, fungi or algae, iv) clean up environment, by breaking down oil and pollutants, and vi) applications in energy and electronics, such as batteries and transistors.

Such enormous potential of NMs for innovation has fostered large investments in developing new industrial applications and consumer products. However, the outlooks for a rapid growth in the sector have raised not only high expectations, but also societal concerns about the adequacy of existing regulation to address the risks posed by nanotechnologies. Indeed, despite their clear benefits, NMs may pose environmental, health and safety (EHS) issues. In Europe, the safety of chemicals is subject to the Registration, Evaluation, Authorization and Restriction of Chemicals (REACH) regulation [3], which requires an assessment of their risks along their lifecycles prior to introduction to the market. Risk Assessment consists in the estimation of the probability of health and environmental effects emerging from exposure to chemical substances.

This paradigm has been considered applicable to NMs if properly implemented to address the complexity associated with their physicochemical identity, biological and environmental interactions and fate [4]. However, the large diversity of NMs [5] used in NEPs has made their case-by-case Risk Assessment very demanding both in terms of cost and use of animal experiments. Indeed, NMs are available in many different grades optimised in size, morphology, purity and surface properties for integration into products. Such modifications are denoted as NanoForms (NFs). This is challenging as the physicochemical identity of the nanomaterials can be easily affected upon contact with any biological, environmental or industrial dispersion media. These fast and often unpredictable modifications pose challenges not only to the safety assessment of these materials, but also to the reproducibility of product performance, which are major barriers to nanotechnology innovation. To reduce this high regulatory burden of proof of the nanotechnology industry it has been suggested to employ *in silico* modelling as well as Grouping and Read-Across approaches to enable safety by design (SbD) strategies that target the early stages of product innovation [6].

The implementation of SbD strategies for NMs for either reducing their hazards or reducing their exposure due to release on the lifecycle stages is a young and trending topic [7], that will be advanced by a better understanding of the relationship between safety and material properties [8] and between functionality and properties [9], even though,

depending on NM properties and on the specific application, it might not be possible to maximise both at the same time [7,10].

The NANoREG and ProSafe initiatives[a] worked towards the development of a SbD concept for NMs which could be implemented by industry and accounted as a reference tool by regulators [7]. The SbD implementation concept, as defined in such initiatives, is based on the Cooper Stage-Gate innovation model [11], which is the industrially standard process to manage technology innovation. It has five stages, incorporating a risk/cost-benefit analysis to inform decisions on project termination, the need for stage reiteration to improve the safety, and/or progression to the next stage [11]. The main idea behind this model is that in an innovation process it is better to "fail often, fail fast, and fail cheaply" [11] on the way to successfully launching a new product. In each of the stages in Figure 1, a series of cycles, with each cycle producing a more refined product design, "spiralling" toward a complete product, is performed [11], which comprises testing and asking feedbacks from the final user, until eventually the product is allowed to go to the next stage through each gate.

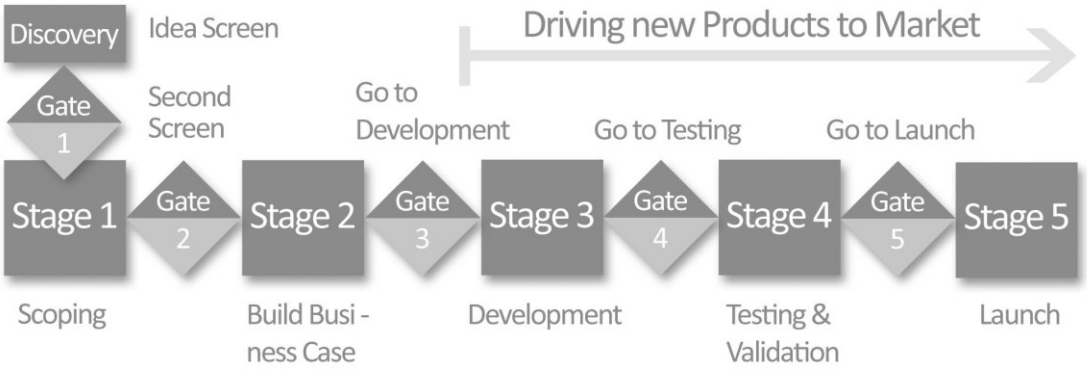

Figure 1: Cooper Stage-Gate innovation model [11].

The rationale behind this thesis builds upon this model and the insights provided by NANoREG and ProSafe initiatives, indeed, the content of this thesis is based on it and its purpose is to contribute to industry's capacity to apply Stage-Gate reasoning in the process of developing safer NEPs that eventually reach the market as well as to regulators' capacity to oversee this process: the first part of this thesis will discuss predictive *in silico* models, also providing two novel approaches, which can be contextualized in screening level modelling in the early stages of NEP development (up to stage 3). On the other hand, the second part of the thesis deals with regulatory risk assessment and management to allow NEPs to go the market (stage 5).

Specifically, Chapter 2 critically reviews the available in silico methods to predict the hazard posed by NMs by applying the OECD (Q)SAR model validation principles, identifying the hotspots that should be better addressed in future reserach. Moreover, in the chapter is provided an overview on the existing databases, highlighting the importance of data curation and data integration, to provide larger datasets more suitable for modelling. Indeed, we found that current approaches do not build on existing data sources, but on in-house datasets or on data retrieved from the literature. Moreover, we find that almost all the investigated *in silico* approaches for the prediction of

[a] http://www.nanoreg.eu/

hazard endpoints model *in vitro* endpoints. In addition, our analysis shows that more efforts are needed to properly validate in silico models for hazard prediction, and that the Applicability Domain (highlighting the chemical space where such models were trained and hence provide more reliable results) is not always properly assessed. Finally, the uncertainty and sensitivity of the current methods are not sufficiently evaluated. To address these challenges, we propose future development for new research in this area, including the adoption of more advanced Machine Learning techniques.

Chapter 3 proposes an approach informing SbD strategies by studying how surface modification, by means of attaching organic ligands, can affect the colloidal stability of nanoscale TiO_2 in different environmental media with changing electrolyte concentrations and pH levels. The functionalization was performed by using four catecholate derivatives (catechol, 3,4-dihydroxybenzaldehyde, 3,4-dihydroxybenzoic acid, dopamine hydrochloride), salicylic acid and polyethylene glycol (PEG) polymer. Surface charge, hydrodynamic diameter and sedimentation velocity were measured to assess the colloidal stability of each of the dispersions. Then, statistical clustering techniques and Principal Component Analysis (PCA) were applied to the obtained experimental data to identify physicochemical descriptors and classes of stability, which were used to classify the investigated surface modifications, thus combining experimental results from simple and fast techniques with multivariate statistical methods.

Chapter 4 provides instead a novel *in silico* tool for the Read-Across and Classification of NMs, based on subspace clustering. The approach consists in the following steps: i) find clusters in different Subspaces, ii) learn an SVM model in these Subspaces, and iii) apply a basic transfer learning in these subspaces, by projecting the target data on the subspace. The approach has been tested against 3 different datasets, showing promising initial results. The methodology presented in this chapter is indeed in "work in progress", as will be thereby described.

As part of my PhD, I collaborated in the EU-FP7 SUN (Sustainable Nanotechnology) project, working with the SUN development team to create a Decision Support System (DSS) addressed to industries, regulators and the insurance sector, to make informed decision in evaluating environmental and health risks in the complete lifecycle of the NMs. This work, as already mentioned, can be contextualized in the final stage of the Copper Stage-Gate innovation model. Chapter 5 gives an overview on the functionalities of SUNDS, mainly focusing on the modules that I actively participated in developing. Chapter 6 and 7 demonstrates the ability of SUNDS to provide and communicate Human Health Risk Assessment (HRA) in the whole lifecycle of NMs, and similarly chapter 8 demonstrates the ability of SUNDS to assess and communicate Environmental Risk Assessment (ERA).

Specifically, chapter 6 demonstrates HHRA methodology, applying SUNDS it in a real case study involving a nanoscale organic red pigment used in the automotive industry. Our analysis clearly showed that the main source of uncertainty was the extrapolation from (sub)acute *in vivo* toxicity data to long-term risk. This extrapolation was necessary due to a lack of (sub)chronic *in vivo* studies for the investigated nanomaterial. Despite the high uncertainty in the results due to the conservative assumptions made in the risks assessment, the estimated risks are acceptable for all investigated exposure scenarios along the product lifecycle.

On the other hand, chapter 7 we performed quantitative (probabilistic) human health risk assessment (HHRA) along the lifecycles of nano-scale copper oxide (CuO) and basic copper carbonate ($Cu_2(OH)_2CO_3$) products in both ionic and micronized wood preservatives used in antifungal wood coatings and impregnations. The results from the risk analysis revealed inhalation risks from CuO in exposure scenarios involving workers handling dry powders

and performing sanding operations as well as potential ingestion risks for children exposed to nano $Cu_2(OH)_2CO_3$ in a scenario involving the hand-to-mouth transfer of impregnated wood. There are, however, substantial uncertainties in these results, so some of the identified risks may stem from the safety margin of extrapolation to fill data gaps and may be resolved by additional testing. The adopted stochastic approach was preferred to deterministic analyses in the sense that it can communicate the contribution of each source of uncertainty and therefore can help in developing strategies to reduce it.

Finally, chapter 8 provide a quantitative methodology for the estimation of ecological risks along the lifecycle of specific nanoapplications to key environmental compartments e.g. surface water, soil (natural and urban or sludge), and sediments, was developed. Ecological risk is calculated by integrating outputs from: a) environmental exposure models deriving Predicted Environmental Concentrations (PECs) in different environmental compartments, and b) deterministic procedures or Species Sensitivity Distributions (SSDs)-based probabilistic procedures that estimate Predicted No Effect Concentrations (PNECs) for various species in the specific environmental compartment. An ecological risk portfolio along the lifecycle is calculated by choosing the maximum risk for each lifecycle stage to characterise it. The resulting ecological risk is either deterministic (i.e. PEC/PNEC) or probabilistic (i.e. percentage of Risk Characterization Ratio (RCR) distribution greater or equal than 1) depending on the nature of exposure and effect input data. The ERA methodology was implemented as specific module in the SUNDS DSS, applying it to the same case studies of chapters 6 and 7, according to the exposure and effect data generated in the frame of SUN and available in the literature. Acceptable risks were obtained for all the investigated compartments along the lifecycle.

2 A critical review on the *in silico* tools for hazard assessment

The work presented in this chapter is based on the following journal article, currently in peer review:
G.Basei, D.Hristozov, L.Lamon, A.Zabeo, N.Jeliazkova, G.Tsiliki, A.Marcomini, and A.Torsello, *Making use of available and emerging data to predict the hazards of engineered nanomaterials by means of in silico tools: a critical review*, (submitted to NanoImpact).

2.1 Introduction

The large number of nanoforms (NFs)[b] and the high complexity associated with their interactions in biological and environmental systems have raised the call for Amendments of the REACH Annexes [12] to require additional information for the safety assessment of NMs. To address these challenges, it has been widely agreed by regulators, industries and scientists that the way forward is to develop robust Integrated Approaches to Testing and Assessment (IATA) that should be compliant with the 3R (Replacement, Reduction and Refinement) principles for reducing animal testing [13]. These IATA would involve both experimental and modelling tools [14] to facilitate intelligent testing and Grouping and Read-Across to inform both regulatory Risk Assessment and safer design of quality products.

The application of *in silico* methods for Grouping and Read-Across is subject to the REACH Annex XI. A group or category, according to REACH, is the arrangement of substances based on similar physicochemical and (eco)toxicological, toxicokinetic and/or environmental fate properties [15]. OECD goes beyond identification of toxicological properties to support Grouping and identifies also mode of toxicological action as a relevant principle of similarity [16]. Other possible ways to group NMs are based on commercial importance and volume of production, composition/chemistry (e.g. carbon-based; metal and metalloid oxides; metals, metal salts and metalloids; semiconductor quantum dots; organics and other classes) [17,18], on properties (such as dimension, shape, morphology, complexity and surface functionalization), or basing on synthetic and biological identity [19]. Grouping can serve several purposes such as informing targeted testing for Risk Assessment, facilitating Safe-by-Design (SbD) practices, and filling data gaps. The latter is typically achieved through Read-Across, an established approach used to predict properties and/or effects for a "target" substance by using information from analogous "source" substance(s) [20]. Furthermore, Grouping for Read-Across is not only accepted under REACH, but is also applicable under different chemicals regulatory frameworks [21]: for instance for risk assessment of NMs in the food and feed chain, the European Food Safety Agency supports grouping for read-across from (other) NFs or non-NFs [22].

The foundations and basic principles for the Grouping and Read-Across of NMs/NFs have been established in a number of conceptual schemes [23–25], which were developed in the EU research projects MARINA, NANoREG, GUIDEnano and ITS-NANO, as part of the European Centre of Ecotoxicology and Toxicology of Chemicals (ECETOC) Nano Task Force [26], and as a result of the ECHA's Partner

[b] Under REACH, a nanoform (NF) is a form of a substance, which fulfils the EC recommended definition of nanomaterial. In addition to size, NFs are characterised by shape and surface chemistry [12].

Expert Group (PEG) [15]. Moreover, a few case studies addressing Grouping of NMs for Read-Across hazard endpoints are available [27]. The H2020 GRACIOUS project[c] is currently building upon these developments to generate a highly innovative science-based framework to enable practical application of Grouping, leading to Read-Across and classification of NMs.

REACH Annex XI recommendation to use when possible *in silico* methods such as (Quantitative) Structure-Activity Relationships ((Q)SARs) for either inferring whether material properties will produce biological effects by means of classification models (SARs) or predicting in numerical terms these relationships by means of regression models (QSARs). The goal is to reduce unnecessary testing by more effectively using the large volume of existing and emerging experimental data, generated in over a decade of nanosafety research [28,29]. Moreover, *in silico* models can help designing NMs with desired properties and known (eco)toxicity [19,30]: a first practical proof-of-concept of applying the SbD concept to NMs was recently published [31].

For classical chemical compounds, thousands of descriptors (directly derived or computed starting from physicochemical properties) are available and can be modelled, however the largest part of these descriptors are not applicable or not useful with respect to NMs [32–34]. Indeed, recently ECHA provided a guidance on how to identify and characterize NMs and NFs [15]: in addition to "substance identity" parameters specified in Section 2 of Annex VI of REACH regulation [3], which include composition of the substance, of impurities or additives, as well as information of surface chemistry and crystalline structure, other parameters that are relevant to characterize NFs are physical parameters such as Size, Shape and Surface area. Other relevant parameters include Solubility, Hydrophobicity, Zeta potential, Dispersibility, Dustiness, as well as Biological (re)activity and Photoreactivity. These properties are indeed the basis to implement the "Stepwise strategy for Grouping and Read-Across" [15]. In addition to physicochemical descriptors, other nanospecific biological descriptors may be adopted, such as protein-corona [35–37] and omics descriptors [38].

It is generally accepted that the difference between (Q)SAR and Grouping for Read-Across approaches lies in the fact that the latter are applied "when a small quantity of data is available", while the former are applied "when more data is available" [39–41]. The difference between (Q)SARs and Read-Across approaches relies indeed in the fact that in the latter the endpoint information is inferred using data on the same endpoint from other (similar) substances, while in (Q)SARs the prediction is based on a model derived from the chemical structure or relevant nanospecific descriptors. The need for larger datasets for (Q)SARs is indeed a consequence to the fact that, in general, it is harder to build a relevant and predictive model when the available samples are limited in number.

The use of (Q)SARs for the safety assessment of NMs in general has been previously reviewed, but not in the specific context of Grouping and Read-Across. Puzyn et al. (2009) were the first to discuss the role of *in silico* models for predicting the hazard of NMs [42], followed by Winkler et al. (2013) who provided an overview on the existing methods [33]. More recently, Tantra et al. (2015) investigated the theoretical and experimental descriptors adopted to train (Q)SAR models [43], while Oksel et al. (2015,2017) highlighted additional descriptors and endpoints for *in silico* modelling [34,44]. Jones et al., (2016) reviewed the application of data mining and Machine Learning (ML) techniques for the prediction of biomedical properties and fate of NMs used in medical applications [45], while Sizochenko

[c] https://www.h2020gracious.eu/ (web address accessed in summer 2018).

and Leszczynsky (2016) focused on inorganic NMs, considering not only ML approaches, but also statistical (e.g. dose-response) models [46]. Chen et al. (2017) in two different works investigated *in silico* methods for the prediction and classification of hazard endpoints for metallic NMs, discussing data sources and mechanistic interpretation of reported (Q)SARs [47], and proposing a roadmap for computational toxicology aimed at designing safer NMs [48]. Finally, Quik et al. (2018) analysed a selection of models used for hazard and exposure assessment of NMs, giving an overview on available mechanistic models related to NMs properties, and their parameterization, identifying the best descriptors to use to characterize intrinsic and extrinsic properties, or measured hazard and exposure [49].
In this chapter, we critically analyse the existing approaches that make use of ML techniques for predicting human health hazard endpoints in terms of their predictive ability, thus providing a starting point for researchers, evaluating the existing methods and proposing possible future developments in the field. In addition, we provide an overview on the existing databases, highlighting the current limitations of such data systems.
To be able to predict the adverse (eco)toxicological effects of NMs by means of *in silico* tools, it is indeed fundamental to have access to high quality (meta)data. Many nanosafety projects have produced a huge amount of relevant physicochemical, toxicokinetics [50], fate, exposure and (eco)toxicity data in over a decade of focused research [51]. However, these data have not been properly curated and are accessible mainly via disparate and heterogeneous sources, offering different types of data in different formats (e.g. technical reports, excel sheets, data inventories, knowledgebases, scientific publications). The data sources are also sparse, thus limiting data analysis and modelling [48]. This has led to the need to develop advanced natural language processing (NLP) techniques and text mining methods to convert these unstructured sources to machine-interpretable format [52,53]. This issue has been partially addressed in the biomedical domain through bioinformatics approaches [54], and there are tools for automatic retrieval of data from the literature, such as ContentMine [55]. In addition, platforms like eNanoMapper [56], which is soundly collaborating with Jaqpot [57], a data analytics web tool, were created as means for collection and curation of data to establish their completeness and quality.
It is essential to make the best use of these data resources to develop robust *in silico* models as part of IATA for Grouping and Read-Across to inform regulatory Risk Assessment and SbD decision making. To facilitate this, the objectives of this work are: (i) to critically review the *in silico* approaches (QSARs and other ML techniques) of relevance for predicting human health hazard endpoints, and discuss their data requirements, methodological strengths and limitations; (ii) to provide an overview on the available databases that may be useful for training and validating these *in silico* modelling tools, and (iii) to identify further steps in addressing the identified data and methodological concerns in order to contribute to the future adoption of *in silico* tools as part of IATA for the regulatory safety assessment of NMs.

2.2 Methods

2.2.1 Critical appraisal of peer-reviewed literature

In this work, we have selected and reported peer-reviewed research papers that described specific *in silico* tools relevant for Grouping and Read-Across hazard endpoints in the context of the regulatory safety assessment of NMs. In the case of (Q)SARs we focused on peer-reviewed approaches that make

use of ML techniques to predict human health hazard endpoints, while for Read-Across approaches, due to the small number of existing studies, we included environmental and human health hazard endpoints as relevant case studies, and considered approaches that make use of statistical methods (such as dose-response analysis), as well as approaches proposing Grouping or ranking of NMs by applying computational tools, as already suggested in the literature [27]. This accounted for 11 articles reporting Read-Across approaches, and in 41 articles on (Q)SARs.

Moreover, we provided an overview on nanosafety databases that are freely available online or accessible by requesting registration. It is worth nothing that in addition of these databases, other relevant sources are available for supporting the development of *in silico* approaches, including datasets deriving from European and internationally funded projects.

2.2.2 Evaluation criteria

The usefulness of *in silico* tools in the context of Grouping and Read-Across lies in their predictive ability. To address the reliability of predictive *in silico* models, the OECD designed five principles for the validation of (Q)SARs [16,58], which consist in a set of rules that such models must comply with. According to these principles, each model should be associated with (i) a well-defined endpoint, (ii) an unambiguous algorithm, (iii) a defined domain of applicability, (iv) appropriate measures of goodness-of-fit, robustness and predictivity, and (iv) a mechanistic interpretation, if possible [16,58]. These principles are fundamental also when dealing with Read-Across and with *in silico* models in general; however they are not always respected, even in the case of conventional chemicals [59]. The OECD principles on the validation of (Q)SARs inspired the eight evaluation criteria adopted in this review to critically evaluate the selected *in silico* models. These criteria, their evaluation rules and a scientific justification for adopting each of them are summarized in Table 1. In the case of Read-Across approaches, since the selected case studies do not necessarily imply model development and do not follow a standard reporting, some of these criteria were adapted as described in the table.

Table 1: Criteria adopted to evaluate in silico tools that predict (eco)toxicity endpoints of NMs and are applicable to Grouping for Read-Across (inspired by the OECD QSAR validation principles [16,58]); explanation on how the evaluation based on such criteria is performed in this chapter.

Criterion	Motivation	Evaluation	Selected references
Modelled endpoint	The model must describe a (set of) well-defined endpoint(s), thus addressing a defined scientific or regulatory purpose. Moreover, response data should ideally be derived and measured through the same (internationally accepted) protocol. For Read-Across approaches the criterion reads "Endpoint to Read-Across".	✓ A well-defined endpoint has been modelled. ✗ The modelled endpoint was not well-defined.	16,58
Dataset size	While it is generally true that representativeness is more important than dataset size, it is well recognized that ML methods work better when trained with a sufficiently large number of samples. Moreover, the dataset must exhibit similar mechanisms of influence between the endpoint that is being modelled and descriptors, and it must be as homogeneous as possible.	Quantitative: dataset size is highlighted, together with the original reference.	60,61

Criterion	Motivation	Evaluation	Selected references
Modelling approach	Relationships between intrinsic/extrinsic NM properties and biological effects can be discovered both using linear and nonlinear models, but in general these relationships are, by nature, highly non-linear. It is possible to describe some families of non-linear relationships using linear models by proper non-linear transformations of descriptors, but often this is not sufficient. The adopted model and the descriptors should be clearly reported. As Read-Across approaches do not necessarily present a model, the criterion reads "Applied method".	✓ Adopted model/method and descriptors have been reported. ✗ Adopted model/method and/or descriptors have not been reported.	16,44,58,62
Model validation	Internal validation provides an optimistically biased estimation of the real predictive ability of the provided model: for this reason, models that have been validated both internally and externally are considered more reliable than models that have been only internally validated.	✓ Both internal and external validation have been properly performed. ≈ Only internal validation has been performed; for Read-Across, comparison with measured data is provided. ✗ No validation or biased validation has been performed.	16,58,61,63–66
Statistics and metrics	The goodness of fit of the model or of the classification can be measured by means of different statistics: each statistic highlights different aspects of the predictive ability of the model. Moreover, statistics that have grounds on statistical theorems should be preferred over heuristic measures.	✓ Proper statistic and metrics have been used. ≈ The statistics/metrics used were not proper or insufficient. ✗ Proper statistics or metrics have not been used.	16,58,61,63–70
Applicability Domain (AD) assessment	It is important to indicate the descriptor space in which the model has been trained: predictions extrapolated outside the AD, indeed, may be less accurate than prediction on data that fall into the AD of the model.	✓ AD have been assessed. ✗ AD have not been assessed.	16,58,61,65,71
Uncertainty and variability assessment	Information regarding robustness, sensitivity and variability help to better understand the uncertainty in model results, and hence facilitate subsequent decision making based on model predictions.	✓ Uncertainty and variability have been assessed. ≈ Only a rough assessment has been provided. ✗ Uncertainty and variability have not been addressed.	14,61,72
Model interpretation	A mechanistic interpretation of the model is needed, at least by giving a justification to the relation between selected descriptors and model output, possibly enforced by evidence reported in the literature. If this it is not reported, the model application would be hardly acceptable in regulatory submissions and for research purposes.	✓ A mechanistic interpretation of the model has been provided. ✗A mechanistic interpretation of the model has not been provided.	16,58,73,74

2.3 Results

2.3.1 Data storage and curation

In silico modelling requires access to data on the investigated endpoint(s) that are sufficient both in terms of quantity and quality. Plenty of nano-EHS data have been generated over the last decade in many national, European and international research projects. Unfortunately, a lot of these data were

never published and are therefore lost to the community, but there have been initiatives to collect as many of the data as possible in the inventories reported in Table 2 [75–78].

Table 2: Nano specific databases.

Name	Address *	Access	Description
eNanoMapper	http://search.data.enanomapper.net /	Freely accessible **	Contains primary research data from various nano-EHS projects and from literature.
EUON	https://euon.echa.europa.eu/enanomapper	Freely accessible	ECHA hosted user interface to eNanoMapper and NANoREG databases.
OCHEM	http://ochem.eu/	Freely accessible	Contains experimental data on nano and non-nano materials. Allows to build and validate computational models from the available data using ML techniques.
NECID	http://www.necid.eu/	Registration required	Contains information on occupational exposure to manufactured NMs.
NanoDatabank	http://nanoinfo.org/nanodatabank/	Registration required	Includes data on NMs toxicity, characterization, fate and transport.
Nanowerk	https://www.nanowerk.com/nanomaterial-database.php	Freely accessible	Contains physicochemical information and details on manufacturers of 4000 nanomaterials from more than 150 suppliers worldwide.
NM-Biological Interactions Knowledgebase	http://nbi.oregonstate.edu/	Freely accessible	Contains annotated data on NMs characterization, synthesis methods, and NMs biological interactions. Computational and data mining tools are included.
NanoMILE	https://ssl.biomax.de/nanomile/	Registration required	Contains characterisation data and high throughput screening toxicity data.
ModNanoTox	http://www.birmingham.ac.uk/generic/modnanotox	Freely accessible	Curated database on ecotoxicity data, focussed mainly on silver NMs. Currently included in the eNanoMapper database.
MARINA	http://marina.iom-world.co.uk	Registration required	Inventory of occupational and consumer exposure scenarios for different NMs, together with their physicochemical characterization. Currently included in the eNanoMapper database.
SUN	http://sun.iom-world.co.uk	Registration required ***	Includes physicochemical, release, exposure, in vitro and in vivo toxicological data.
NIKC	http://nikc.egr.duke.edu/	Freely accessible	The CEINT NanoInformatics Knowledge Commons (NIKC) platform consists of a data repository and associated analytical tools that allows visualizing and interrogating integrated datasets.
DaNa	https://www.nanopartikel.info/en/	Freely accessible	Contains information about products and applications with nanomaterials, including physicochemical properties and EHS information.
Nanomaterial Registry	http://www.nanomaterialregistry.org/	Freely accessible	Contains data related to NMs characterization and biological environmental interactions
Nanoparticle Information Library	http://nanoparticlelibrary.net/	Freely Accessible	Data resource for NMs properties (including chemical composition, size, surface area and morphology) and nanoEHS information.

Name	Address *	Access	Description
NanoSolutions	-	Registration required ***	Includes physicochemical and hazard data.

* Web addresses were accessed in the summer of 2018; ** No registration needed for public available eNanoMapper and NANoREG data. Private access after registration for project specific data; *** Data access is currently granted only to project partners, but the data will be made publicly available by the end of 2018.

Today these repositories contain a huge amount of data, but in most cases, there is need for substantial curation efforts as the data are often incomplete and their quality has not been properly verified. This is a critical issue as proper data curation is essential to ensure robust model predictions. The role of data curation in nanoinformatics was comprehensively studied in the USA as part of the Nanomaterial Data Curation Initiative (NDCI) [79]. This study resulted in a proposal for a data curation workflow [80] that consists of: (i) assessing the quality and completeness of the selected data, (ii) extracting and annotating the data, (iii) contacting authors for any missing data, (iv) formatting the data for inclusion into the databases, (v) reviewing the data, (vi) releasing the curated data to target communities, and (vii) updating the curated data as new information is provided by the authors.

Within the same initiative, the question of how to evaluate and score the degree of completeness and quality of curated NM data was addressed by reviewing existing approaches and proposing guidelines [81]. "Data completeness" was defined as the measure of the extent to which data and metadata addressing a specific need are available, while "data quality" is the measure of the degree to which a single datum or finding is clear and can be considered correct. The NDCI also highlighted the importance of metadata in allowing the assessment of uniqueness and equivalence of data derived from different sources and different studies, thus making data integration for subsequent modelling possible. This is an important point as while a single datum can be considered of insufficient quality for certain purpose, it can become useful if combined with other (e.g. more reliable) data.

Due to the heterogeneity of methods and the paucity of standard operating procedures (SOPs) available to derive related (eco)toxicological data, standard specifications to represent and share data are needed: ISA-TAB-NANO is the most popular specification aimed at reaching this goal [82]. Moreover, when evaluating completeness and quality of nano-EHS data, it is important to address several challenges related to uncertainties associated with the complex physicochemical identity of the NMs and the variability in the outputs of (eco)toxicological assays [81].

Another known issue is related to data fragmentation. Indeed, being nanotechnology an intrinsically interdisciplinary field [83], researchers need to use data from different sources across diverse domains. This results in the fact that often the same concept (e.g. material composition, material core, surface modifiers, but also the relationship among them) is referred using completely different names, or incomplete. At the same time, the methods and techniques adopted to characterize the NM are often not accurately reported, or not comparable [81]. It is thus important to develop common ontologies to be able to integrate such different sources [83], paying attention on providing unique identifiers for describing simple concepts. A recent article by Karcher et al. (2018) [84] addressed such issues, proposing strategies to accelerate the process of integrating the available data sources.

The NDCI guidance on assessing data completeness and quality, the respective challenges and the ISA-TAB-NANO protocol have been taken into account in the process of developing the GRACIOUS data curation system. This system will be based on the eNanoMapper database and ontologies and will

assemble much of the data currently in the repositories reported in Table 2. The curation system will offer users a number of data analytical tools: it will apply quality assessment algorithms and will automatically enable the use the data in combination with statistical methods (e.g. principal component analysis, partial least squares regression, cluster analysis), and *in silico* modelling tools (e.g. (Q)SAR, physiologically-based pharmacokinetic (PBPK) modelling) for predicting the toxicokinetics and hazard of NMs for the purposes of Grouping and Read-Across to inform nanosafety assessments. Moreover, a lot of attention is being paid by the team developing the NIKC database (which allows a mapping to the ISA-TAB-nano file sharing format) for curating the existing data, and in future the system will include a web-enabled curation tool. Data curation based on a set of information about NMs [85] is performed also for the Nanomaterial Registry database. Similar efforts for curating and integrating the existing data in publicy available databases are being conducted in international projects such as NanoFASE [d], NanoCommons [e] and ACENano [f].

2.3.2 Grouping for Read-Across of NMs

Once suitable curated data are selected from one or more of the available sources, it is possible to start modelling to predict (eco)toxicity, kinetics, fate, and/or exposure. A detailed and unambiguous physicochemical and structural characterization of the materials is a fundamental prerequisite to correctly predict human health or environmental endpoints, as required by the REACH Annex XI. Specifically, when Grouping for Read-Across is applied, information on (at least) chemical and physicochemical properties on source and target substance, hazard/toxicokinetic data of the source materials relevant to the endpoint of interest, good data quality and a well described/documented test procedure are needed.

There are not many case studies on Grouping for Read-Across of NMs as defined by the REACH Annex XI [27]. The *in silico* modelling approaches adopted in the few reported cases are critically evaluated in Table 3, by applying the criteria from Table 1. In addition of such criteria, the descriptors used for modelling and other information (such as whether the developed model is available as a web tool, or the approach is contextualized into an existing Grouping framework, cfr. Section 2.1) are highlighted, together with a brief description of the reviewed approach.

[d] http://www.nanofase.eu/ (web address accessed in summer 2018).
[e] https://www.nanocommons.eu/ (web address accessed in summer 2018).
[f] http://www.acenano-project.eu/ (web address accessed in summer 2018).

Table 3: Selection of peer-reviewed studies Grouping for Read-Across of hazard endpoints, evaluated using the criteria described in Table 1

Reference	Description	Modelled endpoint	Dataset size	Modelling approach	Model validation	Statistics and metrics	AD assessment	Uncertainty and variability assessment	Model interpretation
[86]	*In vitro* tests in combination with computational data analysis (heat maps and SOMs of cell responses at different doses and exposure times) and zebrafish embryo screening are combined for hazard assessment, for metal oxides and a quantum dot.	✗ (*In vitro* sublethal and lethal endpoints and *in vivo* response on Zebrafish embryo)	7 + 1 [87]	✓ *(SOM)*	✗	✗	✗	✗	✓
[88]	Predictive regression tree analysis, using as descriptors material conduction band gap and metal dissolution, to predict acute pulmonary inflammation caused by metal oxide NMs.	✗ (*In vitro* oxidative stress; acute pulmonary inflammation)	24	✓ (Regression tree)	✗	✗	✗	✗	✓
[89]	Biological surface adsorption index (BSAI) for NMs surface characterization and biological/environmental prediction of metal oxides, Ag, and organic NMs, using five descriptors (molar refraction, polarity, hydrogen-bond acidity and basicity, and McGowan characteristic volume) obtained from adsorption measurements of a set of organic molecules.	✗ (Biological surface adsorption index)	23	✓ (BSAI modelling [90] and PCA)	≈	≈	✗	✗	✓
[91]	Ranking of metal oxide NMs for hazard assessment (EC50 of human and murine cell lines), by dose response analysis on different cell lines.	✗ (EC50 of different cell lines)	7	✓ (Dose-Response analysis)	✗	✗	✗	✗	✓
[41]	Approach for Quantitative Read-Across applied on two case studies on E. Coli and HaCaT cell line cytotoxicity (reduction of cells viability, EC50) of metal oxide NMs, reading-across toxicity using two quantum-mechanical calculated descriptors (in CS1 enthalpy of formation of a gaseous cation, in CS2 Mulliken's electronegativity of the cluster).	✓ (Cytotoxicity via reduction of *E. Coli* viability and cytotoxicity via cellular uptake of HaCaT cells)	CS1: 17 [32], CS2: 18 [92]	✓ (One-to-one, one-to-many, -many-to-one, and many-to-many class assignment after hierarchical clustering)	≈	≈	✗	✗	✓

Reference	Description	Modelled endpoint	Dataset size	Modelling approach	Model validation	Statistics and metrics	AD assessment	Uncertainty and variability assessment	Model interpretation
[40]	Approach for quantitative Read-Across, that consists in three steps: (1) exploration of multidimensional space of descriptors to obtain first information on structural similarities, (2) Grouping using pattern recognition techniques based on structural features, and (3) application of their approach, using one, two, or three points depending on availability. In the two Case studies, authors adopted as descriptors two quantum-mechanical calculated descriptors (in CS1 enthalpy of formation of a gaseous cation, plus Mulliken's electronegativity of the cluster in CS2).	✓ (Cytotoxicity via reduction of *E. Coli* viability and cytotoxicity via cellular uptake of HaCaT cells)	CS1: 17 [32], CS2: 18 [92]	✓ (One-point slope, two points formula, plane passing for three points)	✓	✓	✗	✗	✓
[93]	Framework for downloading data and ontologies from the eNanoMapper database and developing and validating NMs Read-Across models. The developed tool is available online (https://nano-lazar.in-silico.ch/predict). In the case study authors compared different NM descriptor sets and local regression algorithms for the Net Cell Association endpoint using physicochemical, structural and protein corona descriptors.	✓ (Cell Association in A549 cells)	121 [94] (retrieved from eNanoMapper)	✓ (Different regression techniques)	≈	≈	✓ (Distance based)	✗	✗
[95]	Web platform (toxFlow, accessible at http://147.102.86.129:3838/toxflow) for Read-Across using physicochemical and omics data. The platform is Similar compounds are defined as such by using two similarity criteria, defined by physicochemical and biological characteristics.	✓ (Cell Association in A549 cells)	84 [94]	✓ (Weighted average of the corresponding values of the similar NMs)	≈	✓	✗	✓ (Sensitivity analysis)	✓
[96]	A quantitative Read-Across case study of *in vitro* cytotoxicity (EC50/IC50) data for bacteria, algae, protozoa, human keratinocyte cell, Balb/c 3T3, on metal oxide NMs taken from different sources, using quantum-mechanical and structural descriptors.	✗ (*in vitro* cytotoxicity EC50/IC50 for a large set of cells)	30 [32,92,97–101]	✓ (SOM)	≈	✗	✗	≈ (Considerations on the variability in toxicity outcomes)	✓

Reference	Description	Modelled endpoint	Dataset size	Modelling approach	Model validation	Statistics and metrics	AD assessment	Uncertainty and variability assessment	Model interpretation
102	Grouping of nano-TiO_2 to Read-Across genotoxicity according to the ECHA guidance [15] including application of chemoinformatic approaches, by using measured physicochemical descriptors and nanospecific descriptors (mainly related to size distribution, zeta potential, and dispersibility).	✓ (*In vitro* genotoxicity via Comet assay)	6 + 2 [103–105]	✓ (PCA, hierarchical clustering, random forest)	≈	✓	✓ (WoE based)	✓ (RAAF)	✓
106	Grouping of MWCNTs to Read-Across genotoxicity according to the ECHA guidance [15] through the application of chemoinformatic approaches, by using measured physicochemical descriptors and nanospecific descriptors (mainly related to size distribution, zeta potential, and dispersibility).	✓ (Genotoxicity measured in *in vitro* and *in vivo* data on Comet assay, micronucleus assay)	19	✓ (PCA, hierarchical clustering, random forest)	≈	✓	✓ (WoE based)	✓ (RAAF)	✓

CS: Case Study; PCA: Principal Component Analysis; SOM: Self Organizing Maps; WoE: Weight of Evidence.

Only half of the approaches in Once suitable curated data are selected from one or more of the available sources, it is possible to start modelling to predict (eco)toxicity, kinetics, fate, and/or exposure. A detailed and unambiguous physicochemical and structural characterization of the materials is a fundamental prerequisite to correctly predict human health or environmental endpoints, as required by the REACH Annex XI. Specifically, when Grouping for Read-Across is applied, information on (at least) chemical and physicochemical properties on source and target substance, hazard/toxicokinetic data of the source materials relevant to the endpoint of interest, good data quality and a well described/documented test procedure are needed.

There are not many case studies on Grouping for Read-Across of NMs as defined by the REACH Annex XI [27]. The *in silico* modelling approaches adopted in the few reported cases are critically evaluated in Table 3, by applying the criteria from Table 1. In addition of such criteria, the descriptors used for modelling and other information (such as whether the developed model is available as a web tool, or the approach is contextualized into an existing Grouping framework, cfr. Section 2.1) are highlighted, together with a brief description of the reviewed approach.

Table 3 defined clearly the endpoint to Read-Across: one considered the *in vitro* Comet assay against different NFs of the same material (nano-TiO_2 with different size, surface chemistry and shape) [107], one took into consideration available *in vitro* and *in vivo* genotoxicity tests (comet and micronucleus assays) against different multi-walled carbon nanotubes (different length, rigidity/straightness, impurities) [106], other two identified cytotoxicity endpoints, by reduction of viability in *E. Coli* and cellular uptake of HaCaT cell line [40,41], and in two of the reviewed approaches cell association was used as endpoint [93,95]. All the other case studies reported in the table build their hypothesis on datasets composed by metal oxides of different composition and on their ability to elicit toxic effects on different cell lines, with different endpoints (EC50, IC50) [96] or taking into consideration different endpoints (e.g. *in vitro* oxidative stress and acute pulmonary inflammation) [88].

It is important to notice that the study of Helma et al. (2017) is the only one in which authors reported retrieving their dataset from one of the databases in **Error! Reference source not found.** [93], while the other approaches reported using datasets already available in literature or created in house. It is also worth reporting on the descriptor selection, or on the selection of the physicochemical properties considered in the case studies reported in Once suitable curated data are selected from one or more of the available sources, it is possible to start modelling to predict (eco)toxicity, kinetics, fate, and/or exposure. A detailed and unambiguous physicochemical and structural characterization of the materials is a fundamental prerequisite to correctly predict human health or environmental endpoints, as required by the REACH Annex XI. Specifically, when Grouping for Read-Across is applied, information on (at least) chemical and physicochemical properties on source and target substance, hazard/toxicokinetic data of the source materials relevant to the endpoint of interest, good data quality and a well described/documented test procedure are needed.

There are not many case studies on Grouping for Read-Across of NMs as defined by the REACH Annex XI [27.] The *in silico* modelling approaches adopted in the few reported cases are critically evaluated in Table 3, by applying the criteria from Table 1. In addition of such criteria, the descriptors used for modelling and other information (such as whether the developed model is available as a web tool, or the approach is contextualized into an existing Grouping framework, cfr. Section 2.1) are highlighted, together with a brief description of the reviewed approach.

Table 3, where only 4 out of 11 case studies included in the final model nanospecific properties (protein-corona descriptors [93], omics descriptors [95], and size distribution, zeta potential, and dispersibility [106,107]) in combination with physicochemical descriptors, while the remaining approaches used descriptors related to the chemical structure of the NMs.

Since Read-Across does not necessarily imply the development of a model, it is not surprising that for three of the reviewed approaches no validation was reported. Gajewicz et al. (2017) provided both internal and external validation of their model [40], while in the other cases either cross-validation was performed, or simple comparison between the expected and the predicted outcomes was reported.

The AD gives the dimension of how the Grouping hypothesis is generic for a set of NMs, and thus it should always be addressed in Grouping for Read-Across case studies, however only the tool presented by Helma et al. (2017) made consideration based on similarity in the training set for building an AD for the model [93], while Lamon et al. (2018) reported on this by stating that the hypothesis may extend to other NMs with the same core composition and that fall in the range of e.g. size and shape of the source NMs taken into consideration in their study [107]. Aschberger et al. suggest extrapolation of their grouping should not be extended to MWCNTs that have different size or surface coatings or have a higher content of oxidising impurities [106].

Only a few case studies in Table 3 report uncertainty related to the prediction or Grouping: Lamon et al. (2018) [107] and Aschberger et al. (2019) [106] addressed this aspect by applying the ECHA's Read-across assessment framework (RAAF), thus providing a systematic assessment of all the uncertainties related to the result of their case study, while Sizochenko et al. (2018) discussed the variability in toxicity outcomes between different datasets, thus qualitatively addressing uncertainty [96]. Varsou et al. (2018), instead, tested the sensitivity of their method varying the thresholds used to define similar compounds [95]. The other case studies do not show or discuss uncertainty in their models or computational approaches.

It is worth nothing that while Lamon et al. (2018) [96] and Aschberger et al. (2019) [106] based their analysis on a systematic, recognised framework [20], thus identifying uncertainties specific to the identified read-across scenario (category approach, different compounds with the same effect, no variation in the effect), the other case studies were not contextualized in any of the existing Grouping frameworks. In most cases the similarities in structural and/or physicochemical properties of the NMs and/or their mechanisms of toxicokinetics and/or mode of action were indeed assessed by expert judgement rather than applying one of the frameworks. Moreover, the mechanistic understanding of the approaches adopted in most of the case studies is provided as a justification of the proposed Grouping hypothesis or hazard classification. Varsou et al. (2018), instead, suggested a different approach by forming grouping hypothesis based on the biological identity of the NPs and achieved that by retrieving prior knowledge from biological pathway databases [95], while Helma et al. (2017) focused on the approach and the performance of the adopted *in silico* tool, without providing a mechanistic interpretation nor giving a justification for the Grouping hypothesis [93].

2.3.3 (Q)SARs applied to NMs

(Q)SARs assume that an observed biological activity is correlated with the chemical structure or properties, enabling the identification of a mathematical function or a model. After this relationship is estimated, it is possible to apply it to newly developed or untested substances, thus assessing their

potential effects. The biological activity can be predicted in a qualitative (toxic/non-toxic) or quantitative way depending on the endpoint of interest and on the datasets, respectively by means of classification and regression models. (Q)SARs are extensively applied in chemical toxicity modelling and drug discovery [62,108,109], and in the last decade lots of efforts have been put in practice to apply QSARs to NMs. A selection of peer-reviewed articles presenting models that predict human health hazard endpoints retrieved from the literature as specified in Section 2.2 is presented in Table 4: these tools were critically evaluated against the criteria described in Table 1. In addition of such criteria, the descriptors used for modelling and other information (such as whether the developed model is available as a web tool, or the approach is contextualized into an existing Grouping framework, cfr. Section 2.1) are highlighted, together with a brief description of the reviewed approach.

Table 4: Selection of peer-reviewed studies in which (Q)SAR models predicting hazard endpoints were provided, evaluated using the criteria described in Table 1.

Reference	Description	Modelled endpoint	Dataset size	Modelling approach	Model validation	Statistics and metrics	AD assessment	Uncertainty and variability assessment	Model interpretation
[110]	CS1: classification of metal cored NMs using four structural descriptors (size, R1/R2 relaxivity, zeta-potential). Activity was described by averaging for each NM 64 features (four doses, four different cell lines, and four different *in vitro* assays), thus setting arbitrarily a threshold that allowed to split the dataset in two balanced classes; CS2: QSAR modelling of cancer PaCa2 cellular uptake by Metal cored NMs, with respect to 150 different calculated chemical descriptors (using MOE software).	✗/✓ (CS1: 64 features were averaged, setting an arbitrary threshold to indicate activity; CS2: cellular uptake in PaCa2 cells)	44 [111], 109 [112]	✓ (CS1: *Linear SVM Classifier* CS2: kNN)	✓	✓	✓ (Distance based)	≈ (Y-scrambling)	✓
[113]	Theoretical model that predicts the oxidative stress potential of oxide NMs by comparing the redox potentials of relevant intracellular reactions with the energy structure, using reactivity descriptors.	✓ (Oxidative stress potential)	70	NA (Theoretical model)	≈	≈	✗	✗	✓
[114]	CS1: regression model to predict cellular membrane damage of TiO_2 NMs via lactate dehydrogenase (LDH) release using five nanospecific descriptors (size, size in water and phosphate buffered saline, concentration and zeta-potential). CS2: classification model to detect dense cell membranes and disrupted cell membrane after the exposure to ZnO NMs via LDH release using three nanospecific descriptors (size in water and cell culture medium, zeta potential).	✓ (CS1 and CS2: Cellular membrane damage via LDH release)	24, 18	✓ (CS1: MLR, CS2: *LDA*)	≈	≈	✗	✗	✓
[115]	Classification-based cytotoxicity of metal oxide NMs at different concentrations, using 14 nanospecific and calculated physicochemical descriptors and exploring all possible combinations of these descriptors, ending up with a model with three descriptors (period of the NM metal, atomization energy, and primary size).	✓ (Cytotoxicity via propidium iodide uptake of BEAS-2B cells)	9	✓ (*Logistic regression*)	✓	≈	✓ (Geometric: convex hull after PCA)	✗	✓
[32]	QSAR model describing the Cytotoxicity of a set of Metal Oxide NMs to bacteria *Escherichia Coli* using a single calculated chemical descriptor (enthalpy of formation of a gaseous catio).	✓ (Cytotoxicity via reduction of *E. Coli* viability)	17	✓ (MLR combined with a Genetic Algorithm)	✓	✓	✓ (Leverage approach)	≈ (Y-scrambling)	✓

Reference	Description	Modelled endpoint	Dataset size	Modelling approach	Model validation	Statistics and metrics	AD assessment	Uncertainty and variability assessment	Model interpretation
116	CS1: Evaluation of a linear and of a non-linear model to predict the smooth muscle apoptosis (SMA) induced by Metal Oxide NMs, by using as descriptors three indicator variables (for core material, surface coating, and surface charge). CS2: linear and non-linear models to predict cellular uptake in PaCa2 dell line and in human umbilical vein endothelial cells (HUVEC), induced a set of NMs with the same core but different surface modifications. After finding best-performing models using the complete set of physicochemical and calculated descriptors, authors provided two additional models that made use of interpretable descriptors only, which were mainly related to molecular size and shape, and hydrogen bonding of the fucntionalization.	✓ (CS1: SMA, CS2: cellular uptake in PaCa2 and HUVEC cell lines)	31 [111], 109 [112]	✓ (CS1: MLR and Neural Network with Bayesian regularization; CS2: MLR with EM, and Neural Network with Bayesian regularization)	✓	✓	✗	✗	✓
117	Application of the CORAL software[g] to evaluate the Cytotoxicity to bacteria *E. Coli* of a set of Metal Oxide NMs, using SMILES descriptors [118].	✓ (Cytotoxicity via reduction of *E. Coli* viability)	17 [32]	✓ (Least Square regression)	✓	✓	✗	≈ (Y-scrambling)	✗
119	Consensus model derived from a pool of 2100 classification models (kNN, NBC, Logistic regression, and SVM) to predict the cellular uptake of metal cored NMs by pancreatic cancer cells. Calculated 3D descriptors included in the final model (from an initial pool of 100 descriptors) were mainly related to lipophilicity and hydrogen bonding.	✓ (Cellular uptake in PaCa2 cell line)	105 [112]	✓ (*Consensus classifier)*	✓	✓	✓ (Multiple threshold method)	✗	✗
120	Non-linear model to predict cellular uptake of metal cored NMs in pancreatic cell lines. The model was described by six chemical descriptors computed by Dragon software and chosen by feature selection thanks to a SOM. Authors also provided a less performing linear model was derived by MLR using the same descriptors.	✓ (Cellular uptake in PaCa2 cell line)	109 [112]	✓ (Multi-layered perceptron neural network*)*	✓	✓	✓ (Descriptor ranges + Leverage approach)	✗	✓
121	Demonstration of the dependence of QSAR models on the selection of trial descriptors sets computed by different	✓/✗	80 [122]	✓	≈	≈	✗	✗	✓

[g] http://www.insilico.eu/CORAL (web address accessed in summer 2018).

Reference	Description	Modelled endpoint	Dataset size	Modelling approach	Model validation	Statistics and metrics	AD assessment	Uncertainty and variability assessment	Model interpretation
	softwares from the chemical structure of the NMs using six different endpoints (BSA binding, CA binding, HB Binding, CT binding, NO response, and Cell Viability) and a combination of these endpoints for decorated nanotubes.	(6 different endpoints, and a combination of such endpoints)		(MLR with Genetic Algorithm*)*					
123	SAR model for metal oxide NMs toxicity using metrics based on dose–response analysis and consensus self-organizing map clustering. Authors explored different classification models (NBC, Linear regression, LDA, Logistic regression, quadratic logistic regression, and SVM) with different combinations of nanospecific, physicochemical and metal oxide descriptors, ending up with a model composed by two descriptors (conduction band energy and ionic index).	✗ (Cell viability in BEAS-2B and RAW264.7 cell lines)	24 [124]	✓ (*SVM classifier with gaussian kernel*)	≈	✓	✓ (Probabilistic, based on kernel density estimation)	✓ (Y-scrambling + considerations on the decision boundaries)	✓
125	SAR binary models using different ML techniques, classifying diverse meta cored NMs based on combinations of different nanospecific, molecular and physicochemical descriptors. Activity was described by a "bioactivity profile" which averaged 64 features (four doses, four different cell lines, and four different *in vitro* assays.	✗ (Normalized SNR ratio with respected to unexposed cell responses of the "bioactivity profile")	44 [111]	✓ (*LDA, Naïve Bayes Classifier (NBC), Logistic regression, and Nearest Neighbour*)	≈	✓	✓ (Probabilistic, based on the Naïve Bayes classifier)	✓ (Y-scrambling + considerations on the decision boundaries of the NBC)	✓
126	Toxicology effects of Cobalt Ferrite NMs, at different doses and different exposure times, with respect to seven different cell types (representing different organs of the human body) and precision-cut lung slices. Descriptors were: cell type, concentration, exposure time, and extent of viability decrease.	✓ (ROS level)	2380	✓ (*Decision Tree compared against an NBC*)	≈	✓	✗	✗	✓
127	Application of the CORAL software to predict, using SMILES descriptors, NMs cellular uptake in PaCa2 pancreatic cancer cells. To validate their approach, authors repeated the model training and testing using five different random splits of the dataset.	✓ (Cellular uptake in PaCa2 cell lines)	109 [112]	✓ (Monte Carlo optimization)	✓	✓	✓ (Defined as NMs containing the same SMILES attributes)	✗	✓
128	Model predicting cellular uptake in PaCa2 cell lines of a set of NMs with common metal core and different surface	✓	109 [112]	✓	✓	✓	✓ (Leverage	≈ (Y-scrambling)	✓

Reference	Description	Modelled endpoint	Dataset size	Modelling approach	Model validation	Statistics and metrics	AD assessment	Uncertainty and variability assessment	Model interpretation
	modifications, in relation with a pool of 307 descriptors (structural, molecular, topological, spatial, and electronic) computed using different software (Cerius, Dragon and PaDeL-Descriptor). Genetic Function Approximation (GFA [129]) was applied to find best descriptors from this pool, ending up with a linear model composed by six calculated descriptors, which were related to hydrophobicity, measure of electronic features relative to molecular size, wiener index of the chemical graph, and relative positive charge surface area.	(Cellular uptake in PaCa2 cell lines)		(Stepwise MLR followed by PLS)			approach + DModX)		
130	Investigation of the reliability of two Ensemble Learning methods (Decision Tree Forests (DTF) and Decision Tree Boost (DTB)) applied to five different datasets (NMs with same metal core, NMs with common metal core and different surface modifications, different metal oxide NMs, surface modified multi-walled carbon nanotubes, and fullerene derivatives NMs), using nanospecific and simple structural descriptors.	✓ (CS1: activity profile as in [110], CS2: cellular uptake in PaCa2 cell lines, CS3: cytotoxicity in *E. Coli,* CS4: Cell viability by dehydrogenase activity, CS5: Binding affinity with the HIV-1 PR virus)	44 [111], 109 [112], 17 [32], 29 [122], 48 [131]	✓ (Two different Ensemble Learning methods, for regression and *classification* purposes)	✓	✓	✓ (Distance based)	≈ (Contribution of each descriptor to the final prediction)	✓
132	Model to simultaneously predict ecotoxicity and cytotoxicity of NMs under different experimental conditions and against different biological targets. The model, defined by authors QSAR-perturbation model, is a variation of the classical (Q)SAR principle that make use of perturbation theory to study how changes in the set of descriptors produce changes in the outcome, by random sampling NM pairs and using one as reference and the other as output. Four descriptors were used for each NM pair: three physicochemical descriptors depending on the chemical composition of the NM (molar volume, electronegativity and polarizability), plus the measured size.	✗ (Different measures of toxicity depending on biological target, namely Cytotoxicity, EC_{50}, IC_{50}, TC_{50}, and LC_{50})	229	✓ (*LDA*)	✓	✓	✗	≈ (Area Under the Curve)	✓
133	QSAR-perturbation model aiming at simultaneously predicting the cytotoxicity of different NMs against several mammalian cell lines, considering different times of exposure of the cell	✗	41 [88]	✓ (*LDA*)	✓	✓	✗	✗	✓

Reference	Description	Modelled endpoint	Dataset size	Modelling approach	Model validation	Statistics and metrics	AD assessment	Uncertainty and variability assessment	Model interpretation
	lines, as well as the chemical composition of NMs, size, conditions under which the size was measured, and shape. Four descriptors were used for each NM pair: three physicochemical descriptors depending on the chemical composition of the NM (molar volume, electronegativity and polarizability), plus the measured size.	(Different measures of Cytotoxicity)							
134	Models to predict cytotoxicity of metal oxide NMs: the first model uses a single descriptor (charge of metal cation corresponding to a given oxide), while the second uses an additional descriptor (metal electronegativity), resulting to be more predictive.	✓ (Cytotoxicity via reduction of *E. Coli* viability)	17 [32]	✓ (stepwise MLR for the first model, and PLS for the second)	≈	✓	✓ (Leverage approach)	≈ (Y-scrambling)	✓
97	QSAR relating photo-induced toxicity of metal oxide NMs to *E. Coli*, after exposure to natural sunlight irradiation in comparison to dark, with respect to different combinations of physicochemical and calculated descriptors.	✓ (Cytotoxicity via reduction of *E. Coli* viability)	17	✓ (Least Square regression)	✓	≈	✗	✗	✓
135	QSAR for the prediction of dark and photo-induced cytotoxicity, using SMILES and quasi-SMILES attributes as descriptors [118].	✓ (Cytotoxicity via reduction of *E. Coli* viability)	17 [97]	✓ (Monte Carlo optimization)	≈	✓	✓ (Probabilistic)	≈ (Y-scrambling)	✓
136	Linear and non-linear methods that employ Bayesian neural networks to model three different data sets using four nanospecific descriptors (size, R1 and R2 relaxivities, and zeta potential).	✓ (CS1: Cellular apoptosis, CS2: cellular uptake in 4 different cell lines, CS3: protein adsorption)	50 [111], 109 [112], 80	✓ (Linear and non-linear Bayesian networks)	✓	✓	✗	✗	✓
137	Model to predict cytotoxicity of SiO_2 NMs by means of mathematical functions of size and concentration, through the CORAL software.	✓ (Cytotoxicity via inhibition ratio of human lung fibroblasts)	18 [138]	✓ (Monte Carlo optimization)	✓	✓	✗	✗	✗
74	Application of causation inference method to assist the development and the mechanistic interpretation of SAR models relating human BEAS-2B cell line and murine myeloid cell line	✗	24 [124]	✓ (*Random Forests*)	✓	✓	✓ (Minimum-cost-tree of	✗	✓

Reference	Description	Modelled endpoint	Dataset size	Modelling approach	Model validation	Statistics and metrics	AD assessment	Uncertainty and variability assessment	Model interpretation
	RAW264.7 towards a series of metal oxide NMs. Ionic, fragmental, and "liquid drop model" [139] based descriptors were used.	(Cell viability in BEAS-2B and RAW264.7 cell lines)					variable importance)		
140	QSAR model for the prediction of the cellular uptake of NMs in pancreatic cancer cells using SMILES descriptors. The workflow was made available online through the Enalos InSilicoNano platform [h].	✓ (Cellular uptake in PaCa2 cell lines)	109 [112]	✓ (kNN)	✓	✓	✓ (Distance based)	✗	✗
94	Characterization of the protein serum corona fingerprint of gold NMs, that have been used as descriptors to predict cell association. Performance of the model have been compared against another one that used only size, aggregation state and surface charge, resulting to be 50% more accurate.	✓ (Cell association in A549 cells)	105	✓ (PLS regression)	✓	✓	✓ (Leverage approach)	✗	✓
99	Investigation of the growth inhibitory for a set of metal oxide NMs in the bacterium *E. Coli*. The resulting model used as descriptors the conduction band energy levels and the hydration enthalpy.	✓ (Cytotoxicity via reduction of *E. Coli* viability)	24	✓ (*SVM classifier)*	✗	≈	✗	≈ (Assessment of the decision boundaries)	✓
141	Investigation on the most responsible factors in gold NMs exocytosis in macrophages, using TEM extracted, experimental parameters and combinatorial descriptors.	✓ (Exocytosis in macrophages)	12 [142]	✓ (PLS regression)	≈	✓	✗	✗	✓
143	Comparison of different classification techniques to predict the cytotoxicity of poly (amino amine) (PAMAM) dendrimers using different chemical and structural descriptors. Authors retrieved the data from 12 different nanomedicine journal articles using NanoSifter NLP as a tool for datamining [52], and performed five different analyses to classify NM, using different combinations of descriptors.	✓ (Cytotoxicity in Caco-2 cells)	103	✓ (*NBC, SMO, J48, Bagging, Classification via regression, Filtered classifier, LWL Decision table, DTNB,*	✓	✓	✗	✗	✗i

[h] http://enalos.insilicotox.com/QNAR_PaCa2 (web address accessed in summer 2018)

i A mechanistic interpretation of the model was provided only for the models resulting by the application of the J48 Decision Tree classifier.

Reference	Description	Modelled endpoint	Dataset size	Modelling approach	Model validation	Statistics and metrics	AD assessment	Uncertainty and variability assessment	Model interpretation
				NBTree, Random Forest)					
92	Investigation on difference in modes of action of a set of metal oxide NMs between eukaryotic system (HaCaT cell line) and prokaryotic system (*E. Coli*) starting from a pool of 27 parameters quantitatively describing structure of NMs, and obtaining a model composed by two computed descriptors (enthalpy of formation of metal oxide nanocluster surface and the Mulliken's electronegativity of the cluster).	✗ (Cytotoxicity via reduction of *E. Coli* viability and cytotoxicity via cellular uptake of HaCaT cells)	17 [32], 18	✓ (MLR combined with a Genetic Algorithm)	✓	✓	✓ (Leverage approach)	≈ (Y-scrambling)	✓
144	Regression and classification models for a set of ZnO and TiO_2 NMs tested at different concentrations for their ability to disrupt the lipid membrane in cells by using two empirical descriptors (size and concentration).	✓ (Cellular membrane damage via LDH release)	42	✓ (MLR, SVM, Neural Networks*, and J48 Classification Tree)*	✓	✓	✓ (Leverage approach, convex hull after PCA)	≈ (Y-scrambling)	✓
145	After an unsuccessful attempt to simultaneously find a relationship between a set of descriptors (10 related to NM size and size distribution, 2 derived from TE/SEM images, 2 derived from EPR measurements, 13 relate to surface area, 2 related to reactivity and 5 related to metal content measurements) and 18 different toxicological responses, authors selected a single endpoint and provided a QSAR model using all the available descriptors.	✓ (Cell viability)	10 [146]	✓ (PLS regression)	≈	≈	✗	✗	✗
147	Investigation on the relationships between NM-cell association, and protein corona fingerprints and NM physicochemical properties, through linear and non-linear models. The final (non-linear) model used as descriptors six serum proteins and the zeta potential.	✓ (Cell association in A549 cells)	105 [94]	✓ (SVM regression)	≈	≈	✓ (Leverage approach)	≈ (Y-scrambling)	✓
148	R package (RRegres) for creating and validating multiple regression models, producing unified reports and selecting the best performing one. Authors tested their package against different datasets, including three case studies on nano-particles:	✓/✗ (CS1: Cell association in A549 cells, CS2: Cytotoxicity via	84 [94], 17 [32], 18	✓ (SVM regression, Elastic Net Regression)	✓	✓	✓ (Leverage approach)	≈ (Y-scrambling)	✗

Reference	Description	Modelled endpoint	Dataset size	Modelling approach	Model validation	Statistics and metrics	AD assessment	Uncertainty and variability assessment	Model interpretation
	two of these case studies were related to toxicity, and one to ecotoxicity (short-term aquatic toxicity). In CS1 protein-corona descriptors were included in the models, while in CS2 quantum-mechanical and image derived descriptors were used.	reduction of *E. Coli* viability and cytotoxicity via cellular uptake of HaCaT cells)							
149	Assessment of toxicity of NMs in four different case studies through SAR decision trees, using nanospecific, physicochemical and molecular descriptors. Authors generated for each case study 600 decision trees using a genetic approach, selecting the best 100 trees with respect to the prediction on the training set. Then, for each case study they selected the best decision tree as the one providing the best results in the test set. The selection of the final models (and, consequently, the reported predictive abilities) is thus clearly biased: a better approach would have been for instance to average the results of the 100 trees (resulting in a decision forest).	✗/✓ (CS1: Cell viability in BEAS-2B and RAW264.7 cell lines, CS2: cellular uptake in PaCa2 cancer cell line, CS3: cytotoxicity to via cellular uptake of HaCaT cells, CS4: exocytosis in macrophages)	24 [124], 105 [112], 18 [92], 12 [142]	✓ (*Decision Trees*)	✗	✓	✗	≈ (Y-scrambling)	✓
150	Model composed by two theoretical descriptors (polarization force and enthalpy of formation of a gaseous cation) to predict cytotoxicity to *E.Coli*. Authors tested it to two new NMs and ranked other untested NPs according to predicted toxicity.	✓ (Cytotoxicity via reduction of *E. Coli* viability)	16 [32] + 51	✓ (MLR)	✓	✓	✓ (Leverage approach)	✓ (Y-scrambling + assessment of uncertainty in prediction)	✓
151	Cytotoxicity correlation models between *E.Coli* and HaCaT cell line for cytotoxicity of metal oxide NMs, using as descriptors chemical descriptors, quantum-mechanical descriptors and image descriptors. The resulting model (defined by authors nano-QTTR model) can be thus used extrapolate toxicity related to one species to the other, when data for one species is available.	✗ (Cytotoxicity via reduction of *E. Coli* viability / Cytotoxicity via HaCaT cellular uptake)	17 [32], 18 [92]	✓ (stepwise-MLR + PLS)	≈	✓	✓ (Distance based)	✗	✓
152	Investigation of the quantitative relationships between protein corona and activity by using several linear and non-linear ML approaches. Best performances were achieved by using six serum proteins as descriptors.	✓ (Cell association in A549 cells)	84 [94]	✓ (MLR, SVM, Projection pursuit regression, kNN, Multivariate regression splines,	✓	✓	✓ (Distance based after PCA + Leverage	✗	✓

Reference	Description	Modelled endpoint	Dataset size	Modelling approach	Model validation	Statistics and metrics	AD assessment	Uncertainty and variability assessment	Model interpretation
				Neural Networks, Random Forest)			approach for MLR)		
153	QSAR modelling for predicting the cytotoxicity of various metal oxide NMs, making use of a descriptor that includes physicochemical features into SMILES descriptors, by means of the CORAL software.	✗ (Cytotoxicity via reduction of *E. Coli* viability / Cytotoxicity via HaCaT cellular uptake)	17 [32], 18 [92]	✓ (Monte Carlo optimization)	✓	✓	✗	✓ (Y-scrambling + sensitivity analysis)	✓
154	Multi-Quantitative Structure Toxicity Relationship for simultaneous prediction of multiple toxicity of metal oxide NMs to four different endpoints, having results comparable with ones provided for single QSAR models, using physicochemical calculated descriptors and constitutional and quantum mechanical descriptors retrieved from previous works.	✗ (Cytotoxicity via reduction of *E. Coli* viability / Cytotoxicity via HaCaT cellular uptake)	17 [32] + 17 [97] + 2 [150] + 18 [92]	✓ (Random Forests)	✓	✓	✓ (Leverage approach)	≈ (Y-scrambling)	✓
155	Three SAR models built starting from a pool of 285 descriptors and resulting in models that use respectively one, two and three descriptors (size, surface area and a quantum-mechanical calculated descriptor). The approach was contextualized to support the DF4nanoGrouping scheme, classifying NMs according to one *in vivo* and two *in vitro* studies.	✓ (Protein carbonylation, ROS, NOAEC of a short-term inhalation study)	19 [156]	✓ (*Decision Trees*)	✓	✓	✓ (Assessment in both test and training sets by standardization approach [157])	✗	✓

CS: Case Study; EM: Expectation Maximization; LDA: Linear Discriminant Analysis; MLR: Multiple Linear Regression; NA: Not Applicable; NBC: Naïve Bayes Classifier; kNN: k-Nearest Neighbours; PCA: Principal Component Analysis; PLS: Partial Least Square; ROS: Reactive Oxygen Species; SOM: Self organizing maps; SVM: Support Vector Machines.

(Q)SAR models have often been criticized not being sufficiently accurate when applied in practice [158]. This may be due to a different number of motivations.

As highlighted in Table 4, many studies analysed small datasets, and none of the reviewed approaches reported using any of the databases listed in Table 2. Although the modelling approach and the descriptors used in the final model were always clearly indicated, excluding the model provided by Burello and Worth (2011) where instead a theoretical model was applied [113], in roughly 50% of the reviewed approaches the descriptors used by the final model are related to the chemical composition of the NM and are not related to nanospecific properties, while the most common nanospecific descriptors included in the reviewed models are size (measured in different media), zeta potential, reactivity and surface area, plus in three cases [147,148,152] protein-corona descriptors. The predicted endpoint was in general clearly identified: in roughly 25% of the reviewed approaches (11 out of 41) more cell lines or endpoints were combined to predict a generic biological activity (e.g. viability and cellular uptake). Furthermore, only in one of the case studies of Gajewicz et al. (2018) an *in vivo* endpoint was predicted [155], thus confirming the model landscape presented elsewhere [159]. It is worth noting that in some cases activity was assessed by arbitrarily defining a threshold on endpoint values, in such a way to have half of the dataset classified as "active", and half as "non-active".

The 65% of the reviewed approaches (27 out of 41) performed both internal and external validation, while roughly 25% of the approaches reported performing only internal validation through cross-validation, and one of the reviewed models was not validated at all [99]. The validation of one of the reviewed approaches resulted to be biased, because authors reported selecting the final model by looking at the one maximizing performances in the test set [149]. The statistics used to evaluate the goodness-of-fit or the classification accuracy were clearly reported in the 80% of the reviewed approaches (33 out of 41), while in 8 out of 41 of the approaches the reported statistics were not sufficient to fully evaluate model performances.

The Applicability Domain of the model was assessed in more than half of the reviewed approaches (24 out of 41), and usually in such cases the data samples that felt outside the AD were highlighted. The most used approach to evaluate the AD of the models resulted to be the Leverage Approach, often through a William's Plot (i.e.: leverage values vs standardized residuals), but also geometric and distance-based approaches were adopted, as well as approaches that assess the AD basing on statistical properties of the model. It should be noted that the leverage approach is only scientifically valid when applied to linear regression models.

The robustness of the model was assessed in more of the 40% of the reviewed methods: in 16 out of 41 cases it was assessed by means of the Y-scrambling [61,160], while in one of the approaches [132] the Area Under the Curve method was adopted. The uncertainty assessment of the model prediction is insufficient, which is expected, given that the estimation of confidence intervals is an open research problem for ML beyond linear regression models. In only 3 cases the decision boundaries of the classification model were highlighted [99,123,125], only Mu et al. (2016) provided a raw uncertainty assessment of their linear regression model [150], indicating the confidence intervals of the predictions, while only Singh and Gupta (2014) highlighted the contribution of the selected descriptors to the final prediction [130], and only Pan et al. (2016) provided a sensitivity analysis of their model [153].

A mechanistic interpretation was provided for 34 over 41 of the reviewed approaches, while the remaining case studies focused only on comparing the predictive ability of the models with respect to previous studies on the same dataset.

2.4 Discussion

In this chapter, we provided an overview of the available databases encompassing physicochemical and (eco)toxicological endpoints that may support development and application of predictive *in silico* models for engineered NMs, highlighting some of the known issues of such platforms and referencing relevant papers in which such issues are discussed and solutions for future developments are suggested. Moreover, we critically reviewed the available *in silico* methods for predicting human health hazard endpoints for NMs against eight criteria inspired to the OECD principles on the validation of QSARs. These principles have also been adapted to evaluate the existing Grouping and Read-Across approaches. Datasets currently modelled in material sciences are significantly smaller than those available in domains where ML is more established [161], like for instance computer vision or bioinformatics. Zhang and Ling (2018) [162] reviewed 15 recent case studies on the band gap of binary semiconductors, lattice thermal conductivity, and elastic properties of zeolites, to propose a strategy on how to increase the predictive ability of small datasets. Such case studies, selected as representative works modelling "small datasets", modelled datasets ranging from 100 to about 20000 samples. Nanoinformatics usually deals with even smaller datasets: indeed, the approaches reviewed in this chapter modelled datasets ranging from a minimum of 7 samples [91] to a maximum of 2308 samples [126] (cfr. Table 3 and Table 4), with roughly the 70% of the approaches modelling less than 100 samples, and being the approach of Horev-Azaria et al. (2013) [126] the only one dealing with thousands of samples. This is a potential issue affecting the predictive ability of he reviewed models, since it is well recognized that ML algorithms usually work better when trained with a sufficiently large number of samples [60,61].

It is thus fundamental to address the issues highlighted in Section 2.3.1, curating existing data in available datasources [79,80], improving the completeness and the quality of data in existing databases [81], and integrating as much as possible existing databases and datasets [84], to allow modellers to deal with larger sets of data: hence, we encourage scientists to share their (curated) data in those data repositories. At the same time, it is worth noting that some of the approaches reviewed in this chapter have been implemented as web services that are freely available to the community [93,95,140,148]. Such practices should be encouraged as well, being the availability of data and *in silico* tools fundamental for the definition of IATAs for Grouping and Read-Across.

There are not many case studies in the literature on Grouping for Read-Across of NMs (cfr. Section 2.3.2 and Table 3). Most of the 11 approaches reported in Table 3 are built on small datasets and do not predict well-defined endpoints. In case the endpoint selected to Read-Across is of relevance for REACH (i.e. *in vitro* or *in vivo* genotoxicity) it is either (i) not applied as an alternative method to animal testing (as the prediction is made for an *in vitro* assay) [107], or (ii) the data of the source materials are not provided following an internationally accepted SOP [106]. In addition, because of the small dataset size, many of the case studies neither report on model validation, nor provide a comparison to experimental data. Moreover, in most cases the possibly large uncertainties in the predictions are not properly evaluated. On the other hand, almost all the case studies have a clear presentation of the Grouping hypothesis or relationship and provide mostly satisfactory interpretation of the results.

Similar conclusions may be drawn from the evaluation of (Q)SAR models for the prediction of human health hazard endpoints (cfr. Section 2.3.1 and Table 4) where 41 published studies have been reviewed: most of the approaches modelled small datasets, and none of the approaches reported using any of the databases in Table 2. It is also of note that 12 studies over the total studies reported in Tables 3 and 4 rely on the same datasets [32,92]. The modelled outcome was in general well communicated. The prediction was related to *in vitro* endpoints, except in a single case study [163], and in roughly a third of the reviewed approaches the model outcome consisted in a combination of different endpoints. Even though the modelling approach, as well as the descriptors, were in most of the cases clearly reported, model validation was not always properly assessed, and in some cases the statistics supporting model performance are insufficient. The AD of the model was assessed only in half of the reviewed approaches, and the evaluation of the uncertainty, of the sensitivity, and of the robustness of the model predictions is missing in most of the reviewed approaches. A mechanistic justification of the model, on the other hand, is generally provided.

Roughly 50% of the approaches reviewed in this chapter included in the final model nanospecific descriptors: it is worth noting that some of these approaches reported including in their analysis proteomics [35–37] and omics descriptors [38], with encouraging results (cfr. Section 2.3.2 and Section 2.3.3). Future research should keep in consideration such informative descriptors, which can complement physicochemical descriptors and nanospecific descriptors indicated in Appendix R6.1 of REACH [15].

Structured sources (e.g. databases), where data are well-defined, and semantics are implicit, could be easily mined with automatic methods that are already available for the scientific community. On the other hand, unstructured sources (e.g. technical reports, journal articles) generally provide data in free text format, making it more difficult to automate the process of information extraction and consequently making it harder for modellers to retrieve such data [164]. It is thus surprising that only Helma et al. (2017) reported retrieving their dataset from one of the available databases (eNanoMapper) [93], and only Jones et al. (2015) reported using data mining techniques [143], while the other approaches modelled datasets created ad-hoc or fetched from previous studies or from the literature. On the other hand, Liu et al. (2013) [165], Kovalishyn et. al. (2018) [166], and Chen et al. (2016) [167], fetched their datasets from the OCHEM and the NBI databases for modelling ecotoxicity. This may indicate that for ecotoxicity endpoints data in publicly available databases is in the current state more suitable for modelling than data related to human health hazard endpoints. At present, indeed, research efforts are carried out in the nanosafety community in improving data curation and integration (cfr. Section 2.3.1), to enable subsequent development of *in silico* modelling as part of IATA for Grouping and Read-Across.

In most of the reviewed approaches, despite the small sample size, many descriptors have been included in the final models (cfr. Section 2.3.1 and Table 3, Section 2.3.2 and Table 4). However, ideally most of the ML algorithms work better when a high number of samples is used to train them, and as the number of descriptors used by the model increase, the minimum number of samples required to train it should increase as well. Moreover, the concept of proximity, distance or nearest neighbour exploited by distance-based ML algorithms become less meaningful as the number of dimension become higher: this problem is known as the "curse of dimensionality" [168–170]. Even though there are no general rules specifying the minimum number of samples required to train a model, experiments demonstrated that at least 10 samples per variable are required for logistic regression [171], while a more conservative rule [172] can be adapted from Latent Class Analysis, where the minimal sample size to include is suggested

to be no less than 2^k (where k is the number of variables), preferably $5*2^k$. Zhang and Ling (2018) [162], instead, suggested that 100 should be in their opinion the lowest sample size of the dataset to apply ML in materials research. In our opinion it is more meaningful to have a rule which is dependent to the number of descriptors used by the model and has statistical grounds, rather than having a fixed threshold derived heuristically or set up by scientists' judgement, thus the most conservative rule proposed by Dolnicar (2002) [172] of having a training set with a sample size of at least $5*2^k$ should be taken in consideration in future research. In many of the reviewed cases studies these rules are not fulfilled. In addition, it is fundamental to validate models both internally and externally, and to cross-validate models when the number of samples is not sufficiently high to perform also external validation, to provide an unbiased evaluation of the predictive ability of the models [29–32], and to reduce the risk of overfitting.

Other potential biases that may cause derived models to be inaccurate or even not useful in practice are related to non-i.i.d selection of samples. This results in poor representativeness of the data being modelled as compared to what the resulting model is expected to predict. Representativeness, indeed, is as important as sample size: it can potentially magnify bias effects in case of non-representative or not properly collected samples, instead of correcting it [173]. Heckman (1979) studied the problem of sample selection bias in econometric problems and proposed a method to correct it for regression models, assuming that it is possible to estimate the probability that an observation is selected into the sample [174], being awarded to the Nobel prize for this work (there exists implementation of Heckman-type methods in different programming languages, including R [175]). Later it has been shown that the same problem affects also classification models [176], and methods to correct it were proposed. It will be useful to study how these bias affects *in silico* models for NMs, and to test and if necessary, propose methods to correct it.

Moreover, it is rarely taken into account that ML algorithms require that training and test data are drawn from the same distribution and the same feature space. However, in many real-world applications this assumption does not always hold. Transfer Learning [177,178], also known as Knowledge Transfer, is a trending topic in the ML community. It aims at extracting knowledge from one or more domains and to apply this extracted knowledge to the target domain and has been also shown to be a powerful tool to correct biases related to non-random sample selection. This class of approaches fits almost perfectly with the task required by Read-Across, where knowledge extracted within a group of NMs is to be applied to other NMs for which data are missing and may provide a powerful tool to try and correct the limitations of (Q)SARs (being also able to more reliably extrapolate outside the applicability domain of the models). The definition of the chemical space in which models provide reliable predictions is indeed fundamental, however it is not always properly assessed for (Q)SARs, and its assessment is currently lacking for most of the Read-Across approaches. In addition to Transfer Learning, another trending topic in ML is Deep Learning, where a neural network with a large number of hidden layers composed by nonlinear units is trained [179]. Such class of algorithms are usually applied on dataset composed by thousands/millions of samples, even though there exist algorithms capable to deal with smaller datasets (i.e. datasets composed by few thousands of samples) [180], thus its application for nanoinformatics in the current state of the art is particularly suitable when dealing with electronic images. Another possible future development for nanoinformatics research is to apply Transfer Learning from a pre-trained deep learning model, adapting it for the task of interest [181–183].

Another issue that should be carefully addressed relies on the fact that hazard classes (toxic/non-toxic) are sometimes not balanced, meaning that the number of samples belonging to one class is higher than the number of samples belonging on the other class [184,185], and this is not always properly accounted in the modelling and in the evaluation phase. It is also important to provide proper metrics and statistics when evaluating model performances, possibly discussing it: for instance, for regulatory purposes, a model that overestimates the hazard of a NM would be preferred to another one having better performances, but which tends to underestimate it.

Expert judgement is essential for Grouping, especially because a rigorous scientific justification of the Grouping hypotheses should be provided [15]. It is straightforward to apply computational tools and combine them to expert judgement to strengthen the validity of the prediction or grouping hypothesis. Unsupervised learning techniques (e.g. Principal Component Analysis, Clustering and Self-Organizing Maps) have been already employed for instance to assist the development of (Q)SAR models and Read-Across approaches for NMs [31,41,92,110,116,123,125], for NMs classification [186,187], for quality assessment of nano-based dispersions [188], and to study how surface modifications by means of attaching organic ligands can affect the colloidal stability of NMs [189].

Finally, there are several sources of uncertainty that must be taken into account when applying Read-Across and when dealing with (Q)SARs. Specifically, it may be required to apply assessment factors depending on the nature of uncertainty related to the endpoint taken into consideration [190], and there is a perception of greater uncertainty while reading across starting from non-toxic substances (negative Read-Across), while Read-Across to toxic substances is generally more accepted. Moreover, it is generally more accepted that Read-Across is performed on a substance that "falls" between substances already taken into account (interpolation), while extrapolation is less accepted, and it is considered more important to demonstrate the correctness of the Grouping than considering whether Read-Across results in interpolation or extrapolation.

2.5 Conclusions

In silico models to predict properties of concern and (eco)toxicological endpoints should be seen as highly relevant components of IATA for the safety assessment of NMs. In this chapter, we critically reviewed the available *in silico* computational approaches applied specifically in the context of Grouping and Read-Across. The main conclusions of our analysis are that: (i) considerably more efforts need to be invested into curating the available nano-EHS databases in order to establish the completeness and quality of the data, integrating as much as possible existing databases, thus providing larger datasets to modellers, (ii) Unsupervised ML techniques should be further explored as useful tools to facilitate Grouping for Read-Across of NMs, (iii) attention should be paid in future research on properly communicating model performance, (iv) the *in silico* models should be properly validated (both internally and externally) to avoid overfitting and to provide more reliable results, (v) the AD of the model is fundamental: while for (Q)SARs it is often assessed, it is needed to further explore methods to define it also for the Read-Across approaches, (vi) the uncertainty and sensitivity of the *in silico* models are often not evaluated or reported, while this is essential for interpreting the reliability of results, (vii) future research should explore advanced ML techniques, such as Transfer Learning and Deep Learning, to improve the current state of the art and to face the limitations of currently adopted approaches.

3 A methodological approach for NMs categorization by multivariate statistical analysis

The work presented in this chapter is based on the following journal article:
A.Brunelli, E.Badetti, **G.Basei**, F.C.Izzo, D.Hristozov, and A.Marcomini, *Effects of organic modifiers on the colloidal stability of TiO_2 nanoparticles. A methodological approach for NPs categorization by multivariate statistical analysis*, NanoImpact, Volume 9, January 2018, Pages 114-123, ISSN 2452-0748 (https://doi.org/10.1016/j.impact.2018.03.001).

3.1 Introduction

The high heterogeneity of NMs offered in different NFs has made their safety assessment very demanding in terms of testing. To reduce the regulatory burden of proof of the nanotechnology industry, as described in Chapter 1, it has been suggested to employ *in silico* modelling as well as grouping and read-across approaches to enable safety by design (SbD) strategies that target the early stages of product innovation [6]. This is challenging as the physicochemical identity of the nanomaterials can be easily affected upon contact with any biological, environmental or industrial dispersion media. One of the most frequently observed phenomena is agglomeration of the NMs in the medium as a result of e.g. its chemical composition, pH, ionic strength, dissolved concentration of oxygen and sulphide, light, suspended particle matter, or content of natural organic matter. Thus, changes in the size distribution, shape, surface area and charge of the agglomerated NMs can be frequently observed, maybe varying their industrial functionality, exposure potential, and/or adverse (eco)toxicological effects. These fast and unpredictable modifications pose challenges not only to the safety assessment of these materials, but also to the reproducibility of product performance, which are major barriers to nanotechnology innovation.

Therefore, understanding how the interactions between NMs and the surrounding medium can alter their colloidal dispersion stability is essential not only to predicting their risks, but also to developing SbD strategies [191] that can prevent these risks early in the R&D process [192]. Specifically, elucidating the NM-medium interaction can help to derive descriptors for *in silico* and materials modelling of both properties and effects and to design *in vitro* (eco)toxicological tests as part of IATA that aim at reducing testing costs and the use of animal experiments. It can also help in the better interpretation of the modelling/testing results [193] to derive criteria and guiding principles for grouping and/or read-across and for classification according to regulatory requirements and industrial product quality criteria.

To contribute to the above priorities, the goal of this chapter is to investigate the influence of surface modification on the extrinsic properties of the NMs, defined as the "characteristics that are linked to the material's functionality in its environment" [194], e.g. agglomeration, surface charge, dispersibility etc. Indeed, the approach employed and the outcomes achieved by this work are not intended to replace the huge efforts already carried out on describing methods as well as standardized and validated protocols for synthesis, purification, and characterization of nanomaterials [29,195] but rather to support nanomaterials categorization within relative stability classes by combining easy-to-use analytical and statistical techniques.

Our case study is nanoscale titanium dioxide (TiO_2), which was selected due to its widespread use in many consumer products, very low solubility, and surface which can be easily modified [196,197].

Specifically, we used different modifying substances: catecholate derivatives (i.e. catechol, 3,4-dihydroxybenzaldehyde, 3,4-dihydroxybenzoic acid, dopamine hydrochloride), salicylic acid (SAL), and polyethylene glycol (PEG), exploiting the optimal geometry of these ligands to get covalently linked to the NMs' surfaces. The catecholate-type ligands were chosen because of their versatile chemistry, which allowed easier attachment of different functional groups, leading to new optically active nanomaterials [198] as well as to fundamental building blocks for the synthesis of more complex architectures [199–201]. Salicylic acid was chosen for its similarity to catechols in terms of structure, functional groups, and way of binding to TiO_2 surface. The surface modification with PEG was performed because polymeric coatings are considered one of the main approaches to effectively control physicochemical properties such as size, surface charge and solubility, all of which are parameters known to determine the toxicokinetic and toxicity of nanomaterials [202].

Once the surfaces of the materials were functionalized, the investigation of the stability of colloidal dispersions, which by definition is defined in terms of a change in one or more physical properties over a given time period [203], was assessed in different dispersion media varying electrolyte concentrations and pH levels, by combining Electrophoretic Light Scattering (ELS), Dynamic Light Scattering (DLS) and Centrifugal Separation Analysis (CSA) techniques. The obtained data were analysed through statistical clustering methods and Principal Component Analysis (PCA) [204]. Clustering have been already employed to assist the development of (Q)SAR models for nanomaterials [31,110,116], and as a tool for grouping NMs into different toxicity classes, which were used to predict toxicity of untested materials [41], while PCA was previously applied for nanomaterials classification [146,186] as well as for quality assessment of nano-based dispersions [205]. In this work, clustering was adopted to subdivide the dataset into categories of samples showing similar stability, while PCA was used to display in a bi-dimensional space the obtained classification into high-, moderate- and low-stability dispersions, which helped us to understand which extrinsic properties affected the most this categorization. This approach is one of the first attempts to *in silico* modelling the colloidal stability of TiO_2 NMs, and it could be a useful starting point for developing SbD strategies.

3.2 Materials and methods

3.2.1 Case-study nanomaterial and other reagents

The inorganic Aeroxide® P25 titanium dioxide nanopowder was purchased from Evonik Degussa (Germany). P25 powder (declared average particle size: 21 nm) is a mixture of approx. 80% anatase and 20% rutile, with 99.5% purity. According to a previous work [206], P25 pristine powder showed a size distribution ranging approximately from 10 to 65 nm, with a shape partly irregular and semi-spherical, 50 ± 15 m^2/g as surface area, and a bulk density of 3.8 g/cm^3. Catechol (CAT), 3,4-dihydroxybenzaldehyde (CHO), 3,4-dihydroxybenzoic acid (COOH), dopamine hydrochloride (DOP), salicylic acid (SAL), polyethylene glycol (PEG, Mv 100000) and all the other chemicals were of the highest purity available and were used without further purification (Sigma Aldrich, St. Louis, MI, USA). Ethanol (Romil Ltd, Cambridge, UK), deionized water (resistivity 18.2 MΩ/cm), NaCl (1 and 10 mM) solutions, Artificial Fresh Water (AFW, 2 mM ionic strength) and Artificial Marine Water (AMW, 630 mM ionic strength) were used as dispersant media. The pH of NaCl solutions was adjusted by adding HCl or NaOH. AFW and AMW were prepared according to standardized protocols [207,208].

3.2.2 Synthesis of surface modified TiO_2 nanoparticles

According to recommendations and guidelines for NMs dispersion procedures from a powdered material source for both human health and environmental testing applications [209], an ethanolic suspension of P25 NMs (2 g/L) was sonicated with an ultrasonic probe (UP-200S Hielscher Ultrasonics GmbH, Germany) in an ice bath, delivering a power of 200 W for 15 min using a pulsed 80% mode. The surface modification of P25 NMs was achieved, following the procedure described by Burger et al. (2015) [210] with minor modifications, by the addition of each surface-active ligand up to concentrations highest than the theoretically required to cover all surface sites: catecholate type ligands (20 mM), salicylic acid (20 mM) and PEG (2 mM), all dissolved in EtOH. The formation of modified P25 NMs dispersions was obtained by mixing 25 mL of each ligand solution to 100 mL of P25 NMs suspension, which was sonicated in an ice bath by ultrasonic probe over 1h and then it was consequently let stirring overnight at room temperature. Afterwards, each suspension was centrifuged until the P25 NMs settled completely. The supernatant was removed, and the particles were washed three times by adding 10 mL of EtOH to remove the possible excess of unlinked ligand, followed by ultra-sonication and finally by centrifugation of the new suspension until the complete settling of the NMs. After the last washing step, the NMs were dried leading to powders with different colours, depending on the functionalization performed (Figure 2). Schematics of the functionalized nanomaterials is reported in Figure 3.

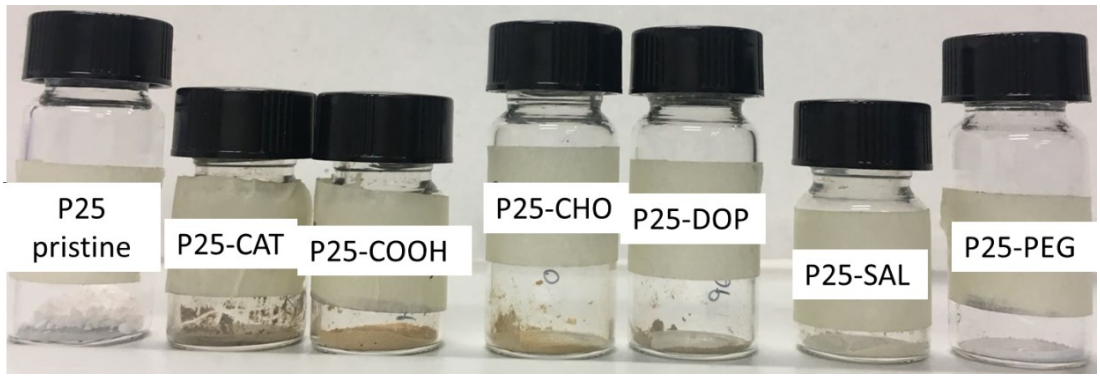

Figure 2: Pristine and functionalized P25 NMs powders.

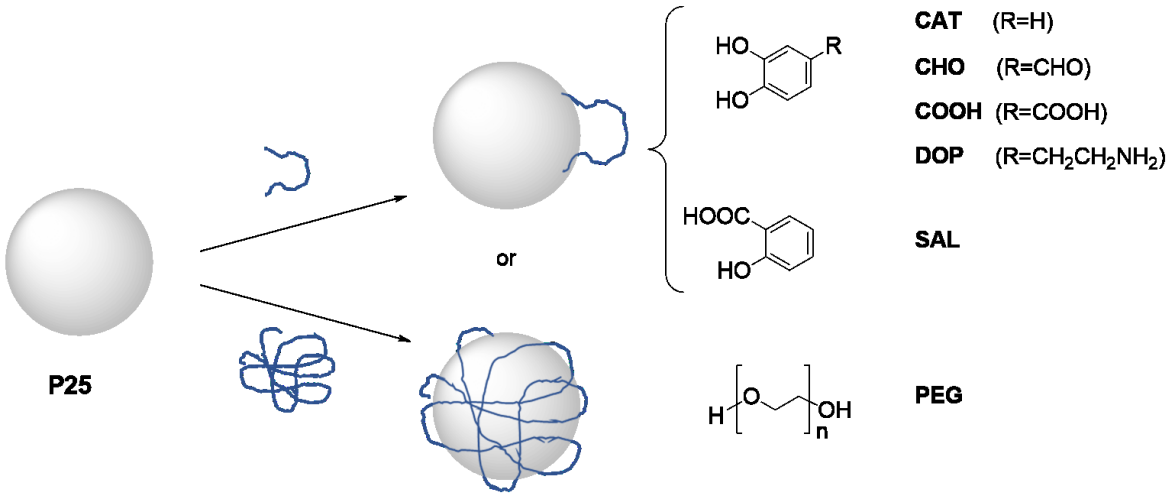

Figure 3: Schematics of P25 NMs surface functionalization with the selected organic ligands: catechol (CAT), 3,4-dihydroxybenzaldehyde (CHO), 3,4-dihydroxybenzoic acid (COOH), dopamine (DOP), salicylic acid (SAL), and polyethylene glycol (PEG).

3.2.3 Physico-chemical characterization

The physico-chemical characterization on the dry powders was performed by means of Fourier-Transformed Infrared spectroscopy (FTIR), Thermo-Gravimetric Analysis (TGA) and Differential Scanning Calorimetry (DSC).

In detail, FTIR analysis was performed with a Thermo Nicolet Nexus 670 FT-IR spectrophotometer equipped with a Smart Orbit Single Reflection Diamond ATR (Attenuated Total Reflection) accessory, from 4000 to 400 cm^{-1} for 64 scans with 4 cm^{-1} resolution. FTIR data were elaborated with Omnic 8.0 and Origin 8.0 softwares.

TGA and DSC were performed simultaneously using a Netzsch 409/C apparatus. The temperature program used was set up experimentally from 30 °C, 10 °C min^{-1} to 600 °C. The TG-DSC analyses were performed in air and the instrument was purged with N_2 at a flow rate of 40 mL/min. The samples masses ranged between 4 and 8 mg; samples were put in a platinum crucible and alumina was used for the internal calibration. Three replicates were performed for each sample. Data were collected with STA Netzsch software and then elaborated with Origin 8.0 software.

3.2.4 Dispersion stability testing

The colloidal characterization was performed by means of Dynamic Light Scattering (DLS), Electrophoretic Light Scattering (ELS) and Centrifugal Separation Analysis (CSA), re-dispersing the NMs at 50 mg/L in the following media: NaCl solutions, deionized water, AFW and AMW. The NMs concentration was selected to obtain the optimal signal-to-noise ratio during the analysis. Before performing the colloidal characterization, every suspension was pre-equilibrated for 15 minutes for reaching stable pH values and then probe sonicated in an ice bath at 200 W for 15 min, pulsed 80% mode. New fresh dispersions for each measurement point and for each replicate were prepared.

In detail, DLS and ELS were performed by means of the multi-angle Nicomp ZLS Z3000 (Particle Sizing System, Port Richey, FL, USA). The hydrodynamic diameter was measured with an optical fiber set at 90° scattering angle (W=25 mW and λ=639 nm) over at least 6 min at room temperature. Surface charge of the electric double layer of each sample was determined in two different electrolyte solutions (1 and 10 mM NaCl) in the pH 2-10 range, applying a 5 V electric field to obtain zeta-potential (Z-pot) values. NaCl was chosen as electrolyte for Z-pot measurements due to its inertia toward TiO_2 [211], which allowed to study the role of the different modifiers in the stabilization without altering the main structure of P25 NMs. Generally, Z-pot values of ±30 mV indicate a stable colloidal dispersion [211,212] and the Point of Zero Charge (PZC), defined as the pH of zero net charge, represents the point of maximum instability. However, in the evaluation of colloidal stability it is important to consider that Z-pot gives information only on the electrostatic repulsive forces, without providing any insights on the attractive Van der Waals forces [213–215].

Centrifugal Separation Analysis (CSA) was employed to assess dispersion stability of NMs in terms of sedimentation velocity. This method was already successfully applied to calculate the sedimentation kinetics of TiO_2 NMs and multi-walled carbon nanotubes [186,216] as well as to gather information on the

sedimentation velocity distribution of CuO NMs in both environmental and biological media [192]. In detail, sedimentation velocity was determined through Centrifugal Separation Analysis (CSA), by using the Multiwavelength Dispersion Analyzer LUMiSizer® 651. The transmission profiles obtained by CSA represent the transmittance values over the length of the cuvette containing the sample. Particles migration due to centrifugal force results in a variation of the local particle concentration and, correspondingly, local and temporal variations of transmission occur [217]. The separation of different components in dispersion was achieved at 3000 Rotation Per Minute (RPM), which corresponds to a Relative Centrifugal Force (RCF) of 1207 at 120 mm far from the rotor of the centrifuge. Sedimentation velocity data were calculated from the transmittance values obtained setting the wavelength of the transmitted light at 470 nm and collecting the transmittance (%) over time at three different positions (115, 120 and 125 mm far from the rotor) over the length of the cuvette. The runtime of each analysis (i.e. 50 min) was chosen according to the lowest time needed to reach the plateau, i.e. the maximum transmittance values, indicating the complete sedimentation of NMs. The linear dependency between RCF and sedimentation velocity allowed to extrapolate sedimentation velocity data at gravity by dividing these values, calculated by the instrument, for the RCF applied. Finally, by analysing the instability curves through the LUMiSizer software, the time needed to observe total sedimentation of NMs was provided.
Hydrodynamic diameter, surface charge and sedimentation velocity were measured in triplicate and results are expressed as average for DLS/ELS and as median for CSA.

3.2.5 Clustering and Principal Component Analysis

The experimental data obtained from the ELS, DLS and CSA techniques in NaCl solutions at different pH levels were statistically analysed to categorize the different dispersions into stability classes (i.e. high-, moderate- and low-stability classes). The identification of patterns without any *a priori* knowledge on data categorization was achieved by cluster analysis. Specifically, after data standardization, performed by subtracting the mean and dividing by standard deviation of each descriptor, three different clustering algorithms, namely Hierarchical Clustering (HC), k-Means (KM) and Fuzzy c-Means (FCM), were applied to automatically derive three subsets of data sharing similarities among descriptors. HC builds a hierarchy of clusters, following either a top down approach (it starts from a single cluster containing all data and it splits it recursively) or a bottom up approach (each of data is initially located in separate clusters, which are recursively merged until all data are included in the same cluster). At the end of the process, HC selects clusters from the resulting hierarchy. On the other hand, KM performs the partition of data into clusters by defining k centroids, which are used as barycenters for the clusters, assigning data to the cluster of the closest centroid. Then, centroids are recomputed as the mean of the clusters so derived, repeating this procedure a fixed number of times or until convergence (i.e.: centroids do not change). FCM is similar to KM but assigns data to each cluster probabilistically, thus allowing clusters to overlap.
The resulting clusters were labelled according to CSA values: cluster containing the sample with the highest CSA values was labelled as "low stability", cluster containing the sample with the lowest CSA value was labelled as "high stability", and "moderate stability" was the third cluster in between. By using DLS or ELS values to label the clusters instead of CSA, the same classification was obtained. In addition to these three algorithms, a voting-based consensus clustering (CONS) was employed [218] to

obtain a single classification method which included the information achieved from HC, KM and FCM clustering techniques. Specifically, a voting system was applied as follows: for each clustering technique, 1 was assigned if the sample resulted in “low stability” class, 2 if sample was included in “moderate stability” class and 3 if it was in “high stability” class. Then, votes were averaged and the consensus clustering classified stability of each entry as "low" if average was lower than 1.5, "high" if it was higher than 2.5, and "moderate" in other cases.

Afterwards, a comparison of the classifications provided by each clustering technique was performed using the Adjusted Rand Index (ARI) [219], a widely used measure of agreement between two cluster results [220,221]. ARI is equal to 0 in case of two random partitions, and 1 in case of perfect agreement. ARI can also be negative, meaning that agreement is worse than expected as random.

In the case of samples dispersed in DW, AFW and AMW, in which ELS measurement were not reliable because of the lack or too high concentration of electrolytes in solution, another approach was used. The clustering algorithms previously described were used considering only DLS and CSA data, and the reliability of the procedure was confirmed by comparing the consensus clustering of these results with those obtained using the three techniques. Standardization of new data was performed by subtracting the same mean and dividing by the same standard deviation of each descriptor previously computed.

Then, the stability classes of the different dispersions were predicted using a Nearest Neighbour classifier for each clustering technique. In the case of HC, each data was assigned to the stability class of the closest element of the previous dataset, while by applying KM and FCM algorithms, data were assigned considering the closest centroids. The outcomes were merged following the consensus clustering definition in each of the three stability classes.

Finally, Principal Component Analysis (PCA) was used display data in 2 dimensions, highlighting data assignment from the results obtained by cluster analysis. Data statistical analysis was carried out using R language. HC was performed using *hclust* function, KM was performed using *kmeans* function, and PCA was performed using *prcomp* function, all included in the *stats* built-in package [222]. FCM was provided by the *cmeans* function from the *e1071* package [223], and Nearest Neighbor for class prediction was carried out by means of the *knn* function from the *class* package [224].

3.3 Results and discussion

3.3.1 Binding of organic ligands to P25 NMs surface

The coating of P25 NMs by chemisorption of the ligands selected was investigated by ATR-FTIR and TGA-DSC analysis.

The ATR-FTIR spectra of catechol free and adsorbed on P25 NMs are displayed in Figure 4, as a zoom-in image of the wavelength region between 1800-1000 cm^{-1}. The main bands of free catechol (Figure 4a) are the following: stretching vibration of the aromatic ring ν(C-C)/ν(C=C) at 1618, 1600, 1512, 1467 cm^{-1} and stretching of phenolic group ν(C-OH) at 1278, 1254 and 1237 cm^{-1}, while the bending vibrations of the phenolic group δ(C-OH) occur at 1360, 1183, 1163 and the bending δ(C-H) at 1093, 1039 cm^{-1}. The adsorption of catechol onto P25 NMs (Figure 4b) led to relevant changes in ATR-FTIR spectrum: a loss of the hyperfine structure of bending δ(C-OH) vibration in the region below 1200 cm^{-1} was observed, the bands at 1360 and 1183 cm^{-1} disappeared and a very weak feature centred at 1327 cm^{-1} appeared. The band of stretching ν(C-OH) vibrations merged to one broad band centred at

1263 cm^{-1}. Such signals are assigned to stretching and bending vibrations of phenolic groups which participated in the complex formation with Ti surface atoms. Moreover, the stretching of the aromatic ring in the region above 1400 cm^{-1} was also affected by the binding to P25 NMs, showing a single band at 1484 cm^{-1}. According to the literature [198], the observed signals suggested that catechol is bound at the P25 NMs surface. Moreover, ATR-FTIR spectrum of pristine P25 NMs (Figure 5) did not show any bands in 1800-1000 cm^{-1} region, but only the typical absorption band below 700 cm^{-1} due to the stretching of anatase and rutile TiO_2 (Ti–O–Ti) [225].

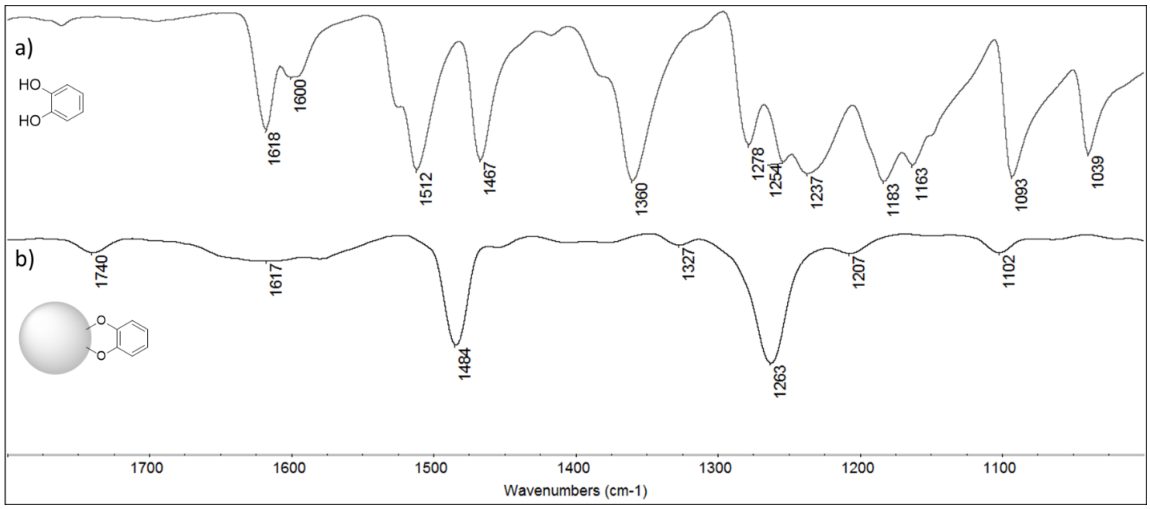

Figure 4: ATR-FTIR spectra of (a) free catechol and (b) P25-CAT NMs in the region between 1800 and 1000 cm^{-1}.

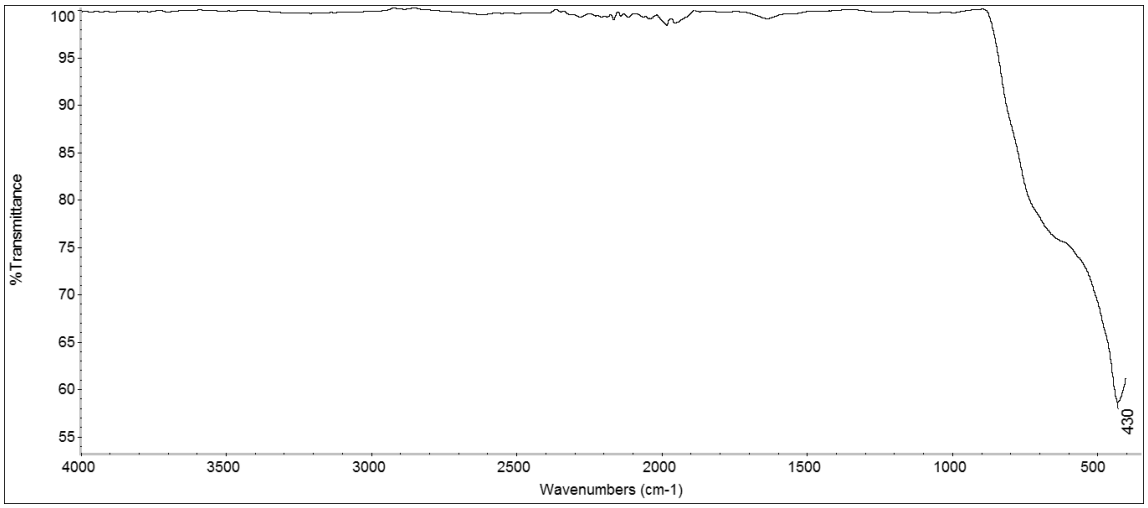

Figure 5: ATR-FTIR spectrum of pristine P25.

The ATR-FTIR spectra of 3,4-dihydroxybenzaldehyde (CHO), 3,4-dihydroxybenzoic acid (COOH) and dopamine hydrochloride (DOP) adsorbed on P25 NMs surface are reported in Figure 6, Figure 7, and Figure 8. As expected, they showed the same way of ligand binding observed for catechol [198]. Moreover, the characteristic signals corresponding to the carboxyl group still appeared in the ATR-FTIR spectra of P25-COOH (stretching absorptions at 1695 and 1606 cm^{-1}) and P25-CHO (stretching band at 1674 cm^{-1}), indicating that these groups are not involved in the formation of the complexes. In the same way, a strong band corresponding to the amine of P25-DOP was observed at 1630 cm^{-1}. As far as salicylic acid, according to Jankovic et al. (2009) [226], both phenolic and carboxylic groups are involved in the

chelation of titanium atoms (Figure 9) since the bands in the region between 1700 and 1560 cm^{-1} merged to one broad band centred at around 1600 cm^{-1}. Finally, ATR-FTIR spectra of P25 NMs functionalized with PEG polymer (Figure 10) showed a strong absorption at around 1100 cm^{-1} corresponding to ether linkage (C-O-C bonds) [227,228], while the signals corresponding to -OH groups appeared very broad, indicating as these groups participated to the bonds formation. The overall results indicated the formation of the desired complexes and proved, for catecholate and salicylate ligands, the most likely formation of bidentate bridging complexes.

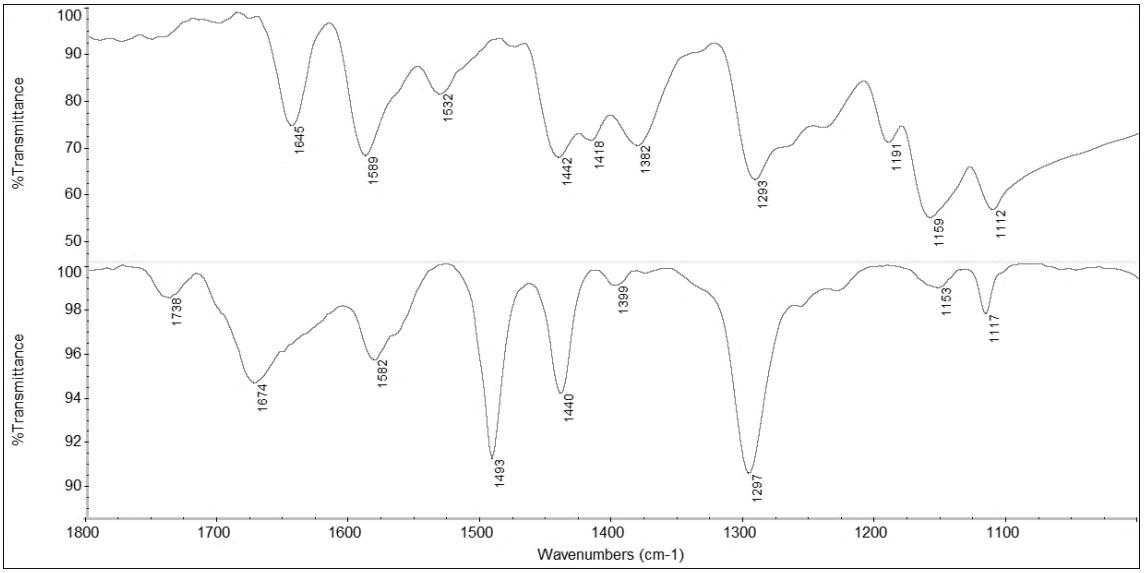

Figure 6: ATR-FTIR spectrum of free 3,4-dihydroxbenzaldehyde (above) and P25-CHO (below).

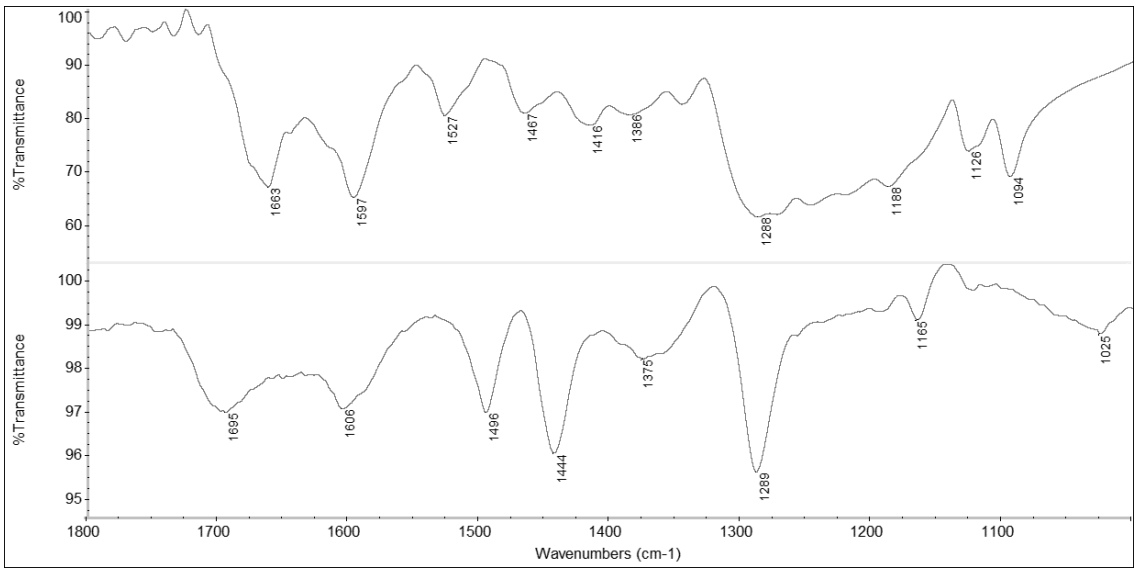

Figure 7: ATR-FTIR spectrum of free 3,4-dihydroxbenzoic acid (above) and P25-COOH (below).

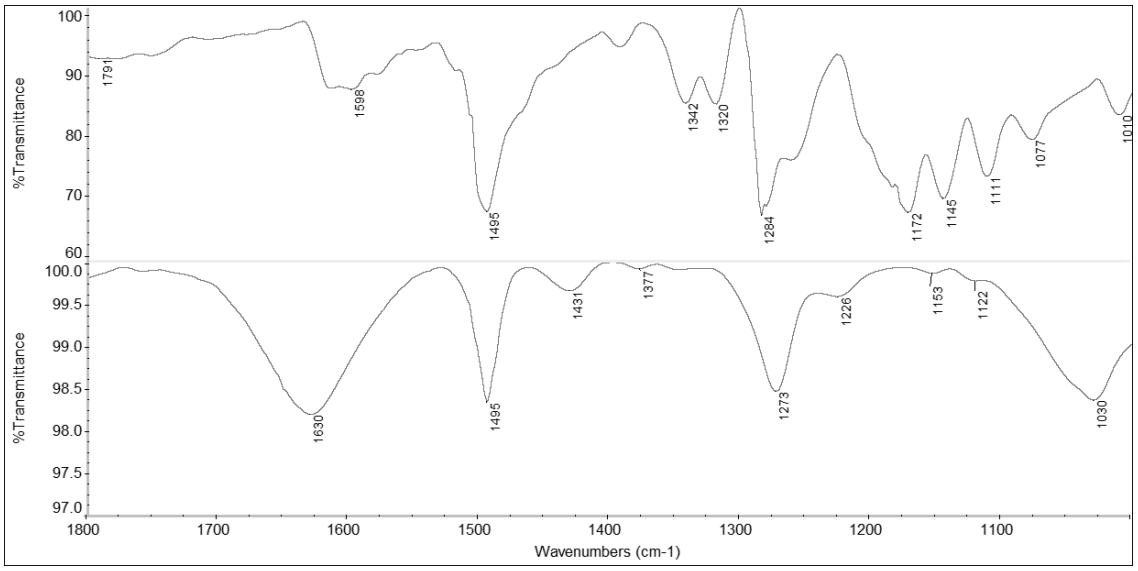

Figure 8: ATR-FTIR spectrum of free dopamine (above) and P25-DOP (below).

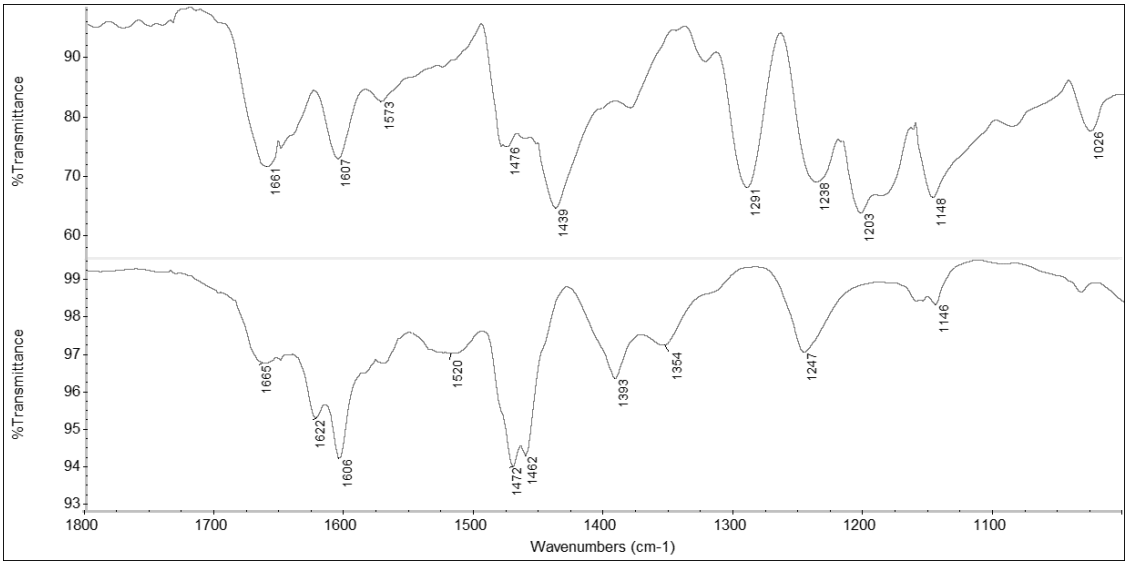

Figure 9: ATR-FTIR spectrum of free salicylic acid (above) and P25-SAL (below).

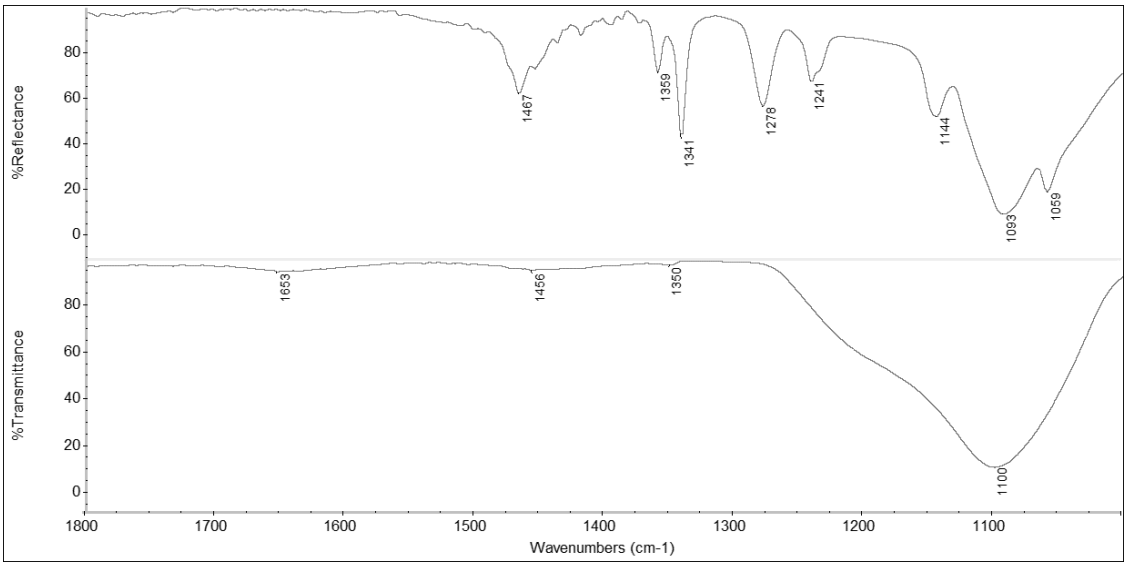

Figure 10: ATR-FTIR spectrum of PEG (above) and P25-PEG (below).

Thermal analysis of pristine P25 and modified P25 NMs, carried out in the 30-600°C temperature range, was performed to estimate the NMs surface coverage rate for each ligand (Figure 11 and Figure 12). TGA of pristine did not show any mass loss in the temperature range investigated, confirming the purity of the starting material already observed by FT-IR analysis. In detail, no organic components or water were adsorbed on pristine NMs surface which resulted to be composed only by anatase and rutile. As far as functionalized P25 NMs, a mass loss of around 3% was observed for NMs functionalized with CAT, COOH and DOP ligands, around 6% for CHO and SAL ligands up to 8% for P25-PEG. DSC analysis finally confirmed the chemisorption of the ligands, showing the exo-thermal processes occurring approximatively between 200 and 400 °C, related to the decomposition of the attached organic fraction.

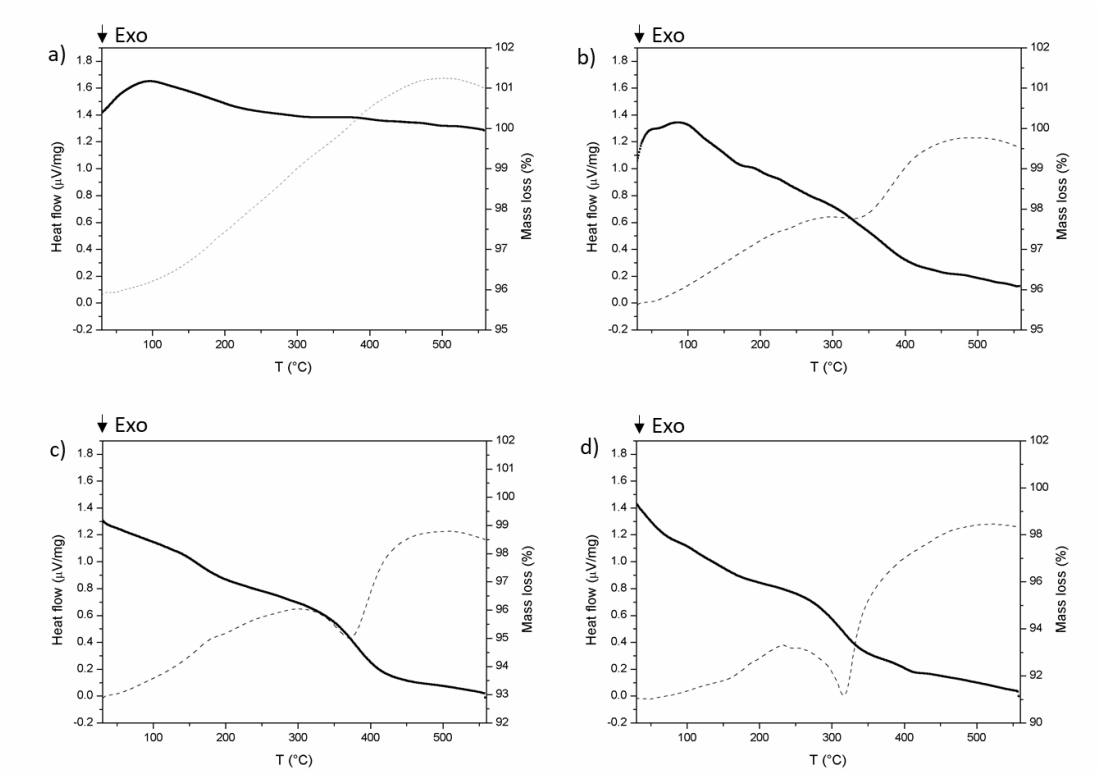

Figure 11: TG-DSC curves of a) P25 NMs, b) P25-CAT, c) P25-SAL, d) P25-PEG in the range of 30-600 °C. TG curve (solid line), DSC curve (dash line).

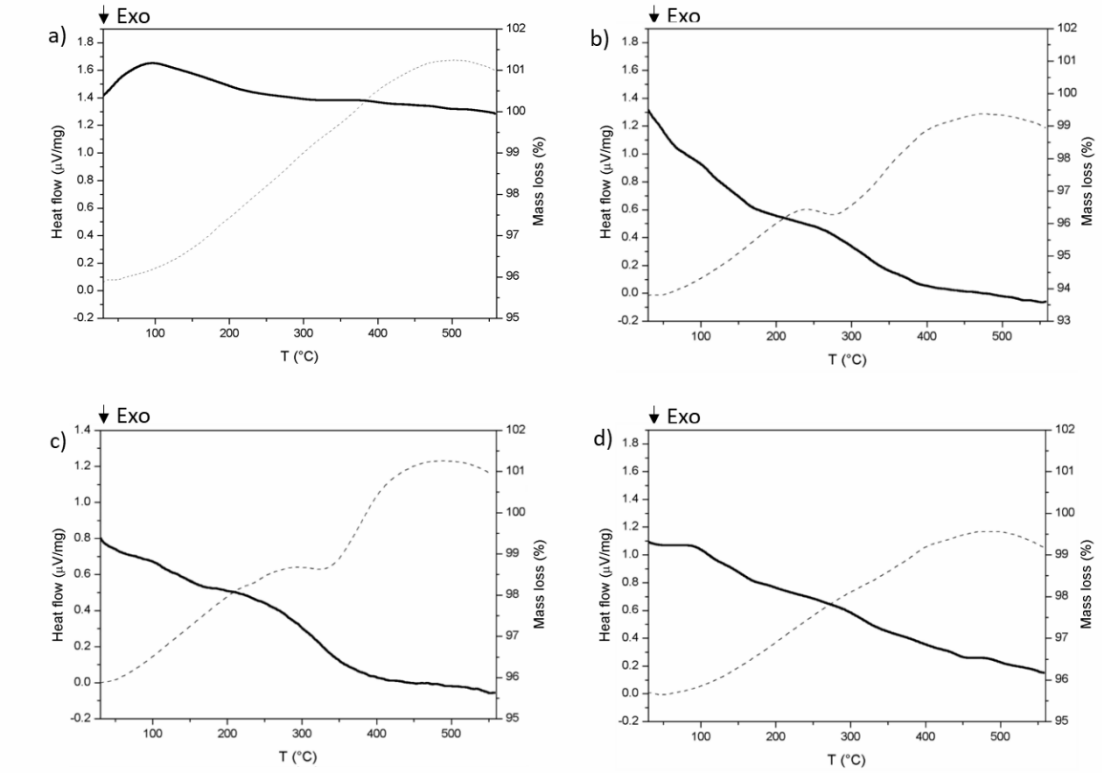

Figure 12: TG-DSC curves of a) P25 NMs, b) P25-CHO, c) P25-COOH, d) P25-DOP in the range of 30-600 °C. TG curve (solid line), DSC curve (dash line).

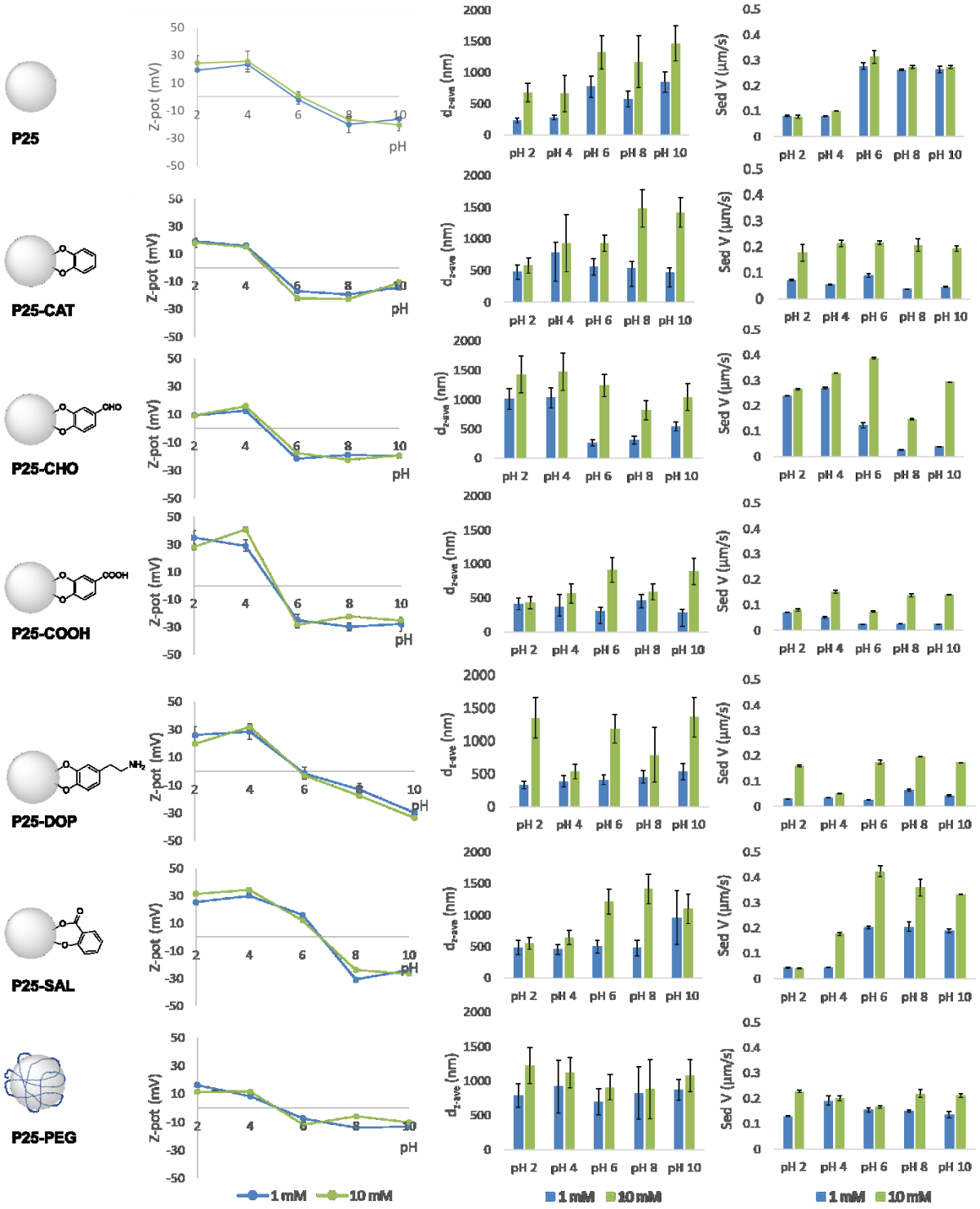

Figure 13: Zeta-potential (Z-pot), hydrodynamic diameter ($d_{z\text{-}ave}$) and sedimentation velocity (Sed V) data of pristine and functionalized P25 NMs dispersed in 1 and 10 mM NaCl solution in the pH range from 2 to 10. An overview of mass loss %, FT-IR bands shifted after NMs functionalization and point of Zero Charge (PZC) for all the samples investigated is reported in Table 5. Estimated time to reach total sedimentation of NMs by CSA are reported in Table 9.

3.3.2 Colloidal stability assessment as a function of electrolyte concentration and pH

The colloidal stability of pristine and functionalized P25 NMs was investigated within the 2-10 pH range at 1 and 10 mM NaCl electrolyte concentrations, by combining ELS, DLS and CSA techniques.

The overall results concerning zeta-potential, hydrodynamic diameter and sedimentation velocity of the different NMs were reported in Table 6, Table 7 and Table 8, and graphically represented in Figure 13. In Table 5, instead, we reported an overview of the percentage of mass lost, FT-IR bands shifted after NMs functionalization, and Point of Zero Charge (PZC) of all the samples investigated.

Table 5: Overview of mass loss %, FT-IR bands shifted after NMs functionalization and point of Zero Charge (PZC) for all the samples investigated.

NMs	TGA (mass loss %)	FT-IR bands involved in chemisorption	PZC (at 1 and 10 mM NaCl)
P25	n.d.	-	6.2
P25-CAT	3	1263 cm^{-1} ν(C-OH)	4.8
P25-CHO	6	1297 cm^{-1} ν(C-OH)	4.8
P25-COOH	3	1289 cm^{-1} ν(C-OH)	5.2
P25-DOP	3	1273 cm^{-1} ν(C-OH)	5.8
P25-SAL	6	1247 cm^{-1} ν(C-OH) 1606, 1622, 1665 cm^{-1} ν(C=O)	6.5
P25-PEG	8	1100 cm^{-1} ν(C-O-C)	5.1

3.3.2.1 Electrophoretic Light Scattering (ELS)

A curve of Z-pot vs pH was obtained for each NMs dispersion (Figure 13 and Table 6). As generally expected, Z-pot of TiO_2-based samples moved from positive values in the acid pH region before the PZC, to negative values in the region after the PZC, regardless of the surface functionalization. Both pristine P25 and all the functionalized NMs led to Z-pot values between ± 30 mV. The curves displayed in Figure 13 showed, for each compound, very similar values of Z-pot vs pH at the two NaCl concentration studied. The independence between IS and surface charge is consistent with data reported in literature [211] and it can be ascribed to the electrolyte nature of the salt investigated, i.e. NaCl is inert for TiO_2 without any specific adsorption of Na^+ and Cl^- by titania NMs.

Moreover, Z-pot vs pH curves were used to determine the PZC for each NMs dispersion. PZC of pristine P25 NMs resulted at pH 6.2 in accordance to the literature data [229,230]. As far as functionalized NMs, PZC of P25-CAT and P25-CHO was 4.8, reaching 5.2 for P25-COOH and 5.8 for P25-DOP. As already reported [231], the adsorption of catechol derivatives onto NMs surface produced an excess of negative surface charge, determining a shift of the PZC to lower pH values. These results suggest that the effect induced by catechol type ligands on PZC exceeded the possible effect of the functional residues. A similar decrease of PCZ was observed for P25-PEG (PCZ of 5.2) while P25-SAL showed a slightly increase of PZC up to 6.5, which is somehow expected due to the different binding mode of salicylic acid.

Table 6: Average and standard deviation (mV) of zeta-potential values at 1 and 10 mM NaCl in the 2-10 pH range.

pH / NMs	P25-Pristine	P25-CAT	P25-CHO	P25-COOH	P25-DOP	P25-SAL	P25-PEG
				1 mM NaCl			
pH 2	19.3 ± 0.8	19.1 ± 0.4	9.3 ± 1.3	35.1 ± 5	26 ± 6.2	25.5 ± 4.6	16.3 ± 2.4
pH 4	23.3 ± 3.2	15.9 ± 0.7	12.6 ± 0.7	29.1 ± 4	28.5 ± 5.8	30.1 ± 0.8	8.6 ± 1.1

pH / NMs	P25-Pristine	P25-CAT	P25-CHO	P25-COOH	P25-DOP	P25-SAL	P25-PEG
				1 mM NaCl			
pH 6	-2.3 ± 3.1	-16.8 ± 1.2	-21.5 ± 1.6	-24.7 ± 4	-1.4 ± 4.1	16.1 ± 1.4	-7.3 ± 0.7
pH 8	-20.2 ± 5.9	-19.3 ± 1.8	-18.9 ± 1.3	-29.6 ± 3	-13.2 ± 4.5	-30.9 ± 0.8	-13.8 ± 1.9
pH 10	-16.2 ± 1.4	-14.2 ± 1.6	-19.6 ± 2.5	-27.6 ± 5	-30 ± 1.2	-24 ± 2.4	-13.2 ± 1.4
				10 mM NaCl			
pH 2	24.4 ± 5.2	18.2 ± 3.3	9.2 ± 5.3	28.2 ± 2.3	19.8 ± 3.8	31.5 ± 4.9	11.6 ± 1.1
pH 4	25.5 ± 7.7	15.3 ± 1.6	15.9 ± 4.4	41 ± 1.6	31.8 ± 3.6	34.5 ± 3.5	11.8 ± 1.6
pH 6	0.8 ± 2.6	-21.9 ± 1.6	-17.5 ± 1.8	-28.2 ± 2.1	-3 ± 1	12.2 ± 3.6	-11.7 ± 1.2
pH 8	-16.5 ± 2.2	-22.6 ± 0.3	-22.5 ± 3.3	-22.1 ± 0.8	-17.7 ± 4.8	-23.8 ± 7.9	-5.9 ± 1.7
pH 10	-20.5 ± 4.3	-10.5 ± 1.6	-19.4 ± 2	-25.1 ± 0.6	-33.5 ± 1.6	-26.6 ± 9.7	-10.2 ± 1.4

3.3.2.2 Dynamic Light Scattering (DLS)

Dynamic Light Scattering (DLS) was employed as one of the most common and easy-to-use light scattering techniques to determine the hydrodynamic diameter of NMs dispersions. According to the classical Derjaguin-Landau-Verwey-Overbeek (DLVO) theory, to an increase of the ionic strength (destabilization event) corresponds agglomeration of NMs, leading to a raise of their hydrodynamic particles size [232]. The relationship between the hydrodynamic diameter and the ionic strength was confirmed for all the dispersions tested along the entire pH range investigated, increasing up to four times the hydrodynamic size from 1 to 10 mM NaCl (Figure 13 and Table 7). This trend was not observed for ELS results. A possible explanation could be that this small increase of ionic strength led to a compression of the electronic double layer which resulted in an increment of particles agglomeration, but it did not significantly affect the zeta potential.

Concerning the effect of pH, P25 pristine dispersions within the acid pH range (from 2 to 4) displayed hydrodynamic particles size < 700 nm. An increase of the hydrodynamic diameter from 800 to 1320 nm was observed at pH 6, which corresponds to the PZC, and at basic pH (8-10), reaching 1470 nm size. Concerning the functionalized NMs, different behaviours were observed depending on the functional group attached on the NMs surface. As depicted in Fig. 4, hydrodynamic diameters of P25-CAT and P25-DOP were more affected by electrolyte concentration than by pH (increasing approximatively from 500 nm at 1 mM NaCl to 1000 nm at 10 mM NaCl). As far as P25-CHO and P25-SAL, the main parameter affecting hydrodynamic particles size was pH, showing an opposite trend between the two samples. The lowest hydrodynamic particles size values (< 550 nm) were measured at pH ≥ 6 for P25-CHO while an increment of size around 1000 nm was observed under acid conditions. This behaviour could be related to the formation of hemiacetals. On the other hand, P25-SAL reached the highest size values around 1400 nm at pH ≥ 6 and lowest hydrodynamic size at around 500 nm in the acid pH range (2-4). The pH variation could somehow affect the binding of salicylic acid to the P25-NMs surface. As far as the hydrodynamic diameter of P25-COOH, it was slightly affected by electrolyte concentration and pH with respect to the other dispersions, showing agglomerates < 500 nm and < 900 nm at 1 and 10mM NaCl respectively. Finally, the coating of P25 with PEG polymer led to NP dispersions not significantly influenced by the two parameters investigated (electrolyte concentration and pH), showing an average of hydrodynamic particles size always around 1000 nm. These findings confirmed that PEG is able to reduce non-specific binding of molecules to NMs, as well as interactions with salts or with local concentration of ions [233].

Table 7: Average and standard deviation (nm) of hydrodynamic diameter values at 1 and 10 mM NaCl in the 2-10 pH range.

pH / NMs	P25-Pristine	P25-CAT	P25-CHO	P25-COOH	P25-DOP	P25-SAL	P25-PEG
				1 mM NaCl			
pH 2	235 ± 35	480 ± 103	1008 ± 178	413 ± 84	333 ± 58	489 ± 114	789 ± 174
pH 4	279 ± 39	787 ± 158	1031 ± 177	373 ± 176	385 ± 86	455 ± 78	917 ± 383
pH 6	771 ± 173	558 ± 123	262 ± 50	305 ± 60	411 ± 76	499 ± 103	697 ± 188
pH 8	577 ± 131	538 ± 97	308 ± 70	468 ± 83	455 ± 93	271 ± 54	823 ± 380
pH 10	846 ± 162	469 ± 74	544 ± 74	282 ± 52	532 ± 122	957 ± 427	874 ± 151
				10 mM NaCl			
pH 2	678 ± 148	577 ± 118	1428 ± 314	430 ± 88	1351 ± 305	553 ± 95	1227 ± 263
pH 4	665 ± 294	933 ± 453	1475 ± 322	563 ± 138	536 ± 110	640 ± 110	1123 ± 220
pH 6	1321 ± 268	932 ± 128	1242 ± 190	913 ± 179	1184 ± 221	1215 ± 199	909 ± 182
pH 8	1174 ± 418	1481 ± 292	814 ± 163	589 ± 113	787 ± 416	1415 ± 233	880 ± 428
pH 10	1470 ± 281	1417 ± 231	1042 ± 225	893 ± 197	1364 ± 301	1095 ± 233	1081 ± 235

3.3.2.3 Centrifugal Separation Analysis (CSA)

CSA technique allows to compare different colloidal dispersions and to establish a relative stability ranking under specific experimental conditions. In general, at increasing sedimentation velocity corresponds a decrease of dispersion stability. As far as pristine P25 NMs, the sedimentation velocity of NMs dispersions was mainly affected by pH values rather than by electrolyte concentration (Figure 13 and Table 8, estimated time to reach total sedimentation of NMs by CSA is reported in Table 9). Low sedimentation velocity values < 0.10 μm/s were collected in the acid pH range from 2 to 4, while values increased up to 0.30 μm/s at pH ≥ 6. On the contrary, as already observed from DLS results, sedimentation velocity values of P25-CAT and P25-DOP were mainly driven by electrolyte concentration, in fact they increased from 0.03 μm/s to 0.22 μm/s. According to DLS data, a strong effect of pH on sedimentation velocity values was clearly observed for P25-CHO and P25-SAL. P25-CHO showed the lowest values at basic pH, especially at 1 mM NaCl (< 0.04 μm/s), while P25-SAL displayed analogous sedimentation velocity values in the acid pH range (2-4). Similar to the trend observed from DLS results, P25-PEG sedimentation velocities were quite constant along the whole pH range investigated (0.15-0.23 μm/s) and P25-COOH presented very low values (all < 0.15 μm/s) at each pH examined, also at the highest electrolyte concentration. As a result, the overall CSA and DLS data were in good agreement to assess colloidal stability for almost all the samples analysed. Nevertheless, although to an increase of the sedimentation velocity corresponded an increase of the hydrodynamic particles size and vice versa, few exceptions were observed. This finding was expected since the two techniques are based on different forces driving particle-migration: diffusion for DLS and centrifugal forces for CSA. Moreover, DLS is more sensitive to the scattering signal of larger particles size and often masks the signal of the smaller counter parts [205].

Although it is difficult to gather clear-cut considerations from the experimental data obtained, it can be highlighted that catechol ligands with polar functional groups (COOH and DOP with an unexpectedly similar trend for what pH is concerned) lead to more stable colloidal dispersions.

Table 8: Median and standard deviation (μm/s) of sedimentation velocity values at 1 and 10 mM NaCl in the 2-10 pH range.

pH / NMs	P25-Pristine	P25-CAT	P25-CHO	P25-COOH	P25-DOP	P25-SAL	P25-PEG
				1 mM NaCl			
pH 2	0.08 ± 0.01	0.07 ± 0.01	0.24 ± 0.01	0.07 ± 0.01	0.03 ± 0.01	0.04 ± 0.01	0.13 ± 0.01
pH 4	0.08 ± 0.01	0.05 ± 0.01	0.27 ± 0.01	0.05 ± 0.01	0.04 ± 0.01	0.04 ± 0.01	0.19 ± 0.02
pH 6	0.28 ± 0.01	0.09 ± 0.01	0.12 ± 0.01	0.02 ± 0.01	0.03 ± 0.01	0.2 ± 0.01	0.15 ± 0.01
pH 8	0.26 ± 0.01	0.04 ± 0.01	0.03 ± 0.01	0.03 ± 0.01	0.07 ± 0.01	0.21 ± 0.02	0.15 ± 0.01
pH 10	0.26 ± 0.01	0.04 ± 0.01	0.04 ± 0.01	0.02 ± 0.01	0.04 ± 0.01	0.19 ± 0.01	0.14 ± 0.01
				10 mM NaCl			
pH 2	0.08 ± 0.01	0.18 ± 0.03	0.27 ± 0.01	0.08 ± 0.01	0.16 ± 0.01	0.04 ± 0.01	0.23 ± 0.01
pH 4	0.10 ± 0.01	0.21 ± 0.01	0.33 ± 0.01	0.15 ± 0.01	0.05 ± 0.01	0.18 ± 0.01	0.20 ± 0.01
pH 6	0.31 ± 0.02	0.22 ± 0.01	0.39 ± 0.01	0.07 ± 0.01	0.17 ± 0.01	0.42 ± 0.02	0.17 ± 0.01
pH 8	0.27 ± 0.01	0.21 ± 0.02	0.15 ± 0.01	0.14 ± 0.01	0.20 ± 0.01	0.36 ± 0.03	0.22 ± 0.01
pH 10	0.27 ± 0.01	0.19 ± 0.01	0.29 ± 0.01	0.14 ± 0.01	0.17 ± 0.01	0.33 ± 0.01	0.21 ± 0.01

Table 9: Estimated time (expressed in hours) to reach total sedimentation of NMs calculated from CSA data.

pH/NMs	P25-Pristine	P25-CAT	P25-CHO	P25-COOH	P25-DOP	P25-SAL	P25-PEG
				1 mM NaCl			
pH 2	105	105	66	105	138	104	86
pH 4	105	103	63	103	140	104	66
pH 6	63	100	97	168	138	64	88
pH 8	64	104	138	160	105	63	88
pH 10	64	104	138	168	138	65	87
				10 mM NaCl			
pH 2	105	67	63	105	87	104	61
pH 4	100	65	23	88	103	67	64
pH 6	61	63	17	105	67	11	67
pH 8	65	65	88	87	64	19	62
pH 10	65	67	56	87	67	23	62

3.3.2.4 Stability categorization by statistical analysis

The experimental data from ELS, DLS and CSA techniques (Table 6, Table 7 and Table 8) were statistically analysed by clustering and PCA to categorize the different dispersions into relative stability classes as a function of the investigated extrinsic physicochemical parameters. After data standardization (for each dimension, the mean was subtracted, and data were divided by the standard deviation), NMs were clustered into three main categories, which were labelled as high, moderate, and low stability classes. Data standardization was necessary since the values of each descriptors were not in the same ranges: without standardizing the three descriptors, the dimeter measured by DLS would have indeed prevailed to the others while clustering. Moreover, data standardization should be applied when performing PCA (using the correlation matrix), since in this way more emphasis will be gave to variables with higher variance, thus better finding the right principal components. The three clusters algorithms applied (i.e. Hierarchical clustering (HC), K-means (KM) and Fuzzy c-Means (FCM)),

agreed in arranging data as follows: samples with high CSA and DLS values and low ELS absolute values were grouped together, as well as samples with high ELS absolute values and low CSA and DLS values.

The obtained results are reported in Table 10, together with data from the voting-based Consensus clustering (CONS) performed to merge all the information achieved by the three clustering techniques. In Figure 14, instead, the classification results are displayed through a PCA biplot.

Table 10: Clustering analysis of ELS, DLS and CSA data, dividing them into high (H), moderate (M) and low (L) relative stability classes. Results from k-means, hierarchical clustering, fuzzy c-means were combined to obtain the voting-based consensus clustering.

Class	pH	k-means	Hierarchical clustering	Fuzzy C-means	Consensus
P25-pristine-1 mM-pH 2	acid	H	H	H	H
P25-pristine-1 mM-pH 4	acid	H	H	H	H
P25-pristine-1 mM-pH 6	original pH	M	M	L	M
P25-pristine-1 mM-pH 8	basic	M	M	M	M
P25-pristine-1 mM-pH 10	basic	M	M	M	M
P25-pristine-10 mM-pH 2	acid	H	H	H	H
P25-pristine-10 mM-pH 4	acid	H	H	H	H
P25-pristine-10 mM-pH 6	original pH	L	M	L	L
P25-pristine-10 mM-pH 8	basic	L	M	L	L
P25-pristine-10 mM-pH 10	basic	L	L	L	L
P25-CAT-1 mM-pH 2	acid	H	H	H	H
P25-CAT-1 mM-pH 4	acid	H	H	M	H
P25-CAT-1 mM-pH 6	original pH	H	H	M	H
P25-CAT-1 mM-pH 8	basic	H	H	H	H
P25-CAT-1 mM-pH 10	basic	H	H	H	H
P25-CAT-10 mM-pH 2	acid	M	M	M	M
P25-CAT-10 mM-pH 4	acid	M	M	M	M
P25-CAT-10 mM-pH 6	original pH	M	H	M	M
P25-CAT-10 mM-pH 8	basic	L	L	L	L
P25-CAT-10 mM-pH 10	basic	L	M	L	L
P25-DOP-1 mM-pH 2	acid	H	H	H	H
P25-DOP-1 mM-pH 4	acid	H	H	H	H
P25-DOP-1 mM-pH 6	original pH	M	H	M	M
P25-DOP-1 mM-pH 8	basic	H	H	M	H
P25-DOP-1 mM-pH 10	basic	H	H	H	H
P25-DOP-10 mM-pH 2	acid	L	L	L	L
P25-DOP-10 mM-pH 4	acid	H	H	H	H
P25-DOP-10 mM-pH 6	original pH	M	M	L	M
P25-DOP-10 mM-pH 8	basic	M	M	M	M
P25-DOP-10 mM-pH 10	basic	L	L	L	L
P25-COOH-1 mM-pH 2	acid	H	H	H	H

Class	pH	k-means	Hierarchical clustering	Fuzzy C-means	Consensus
P25-COOH-1 mM-pH 4	acid	H	H	H	H
P25-COOH-1 mM-pH 6	original pH	H	H	H	H
P25-COOH-1 mM-pH 8	basic	H	H	H	H
P25-COOH-1 mM-pH 10	basic	H	H	H	H
P25-COOH-10 mM-pH 2	acid	H	H	H	H
P25-COOH-10 mM-pH 4	acid	H	H	H	H
P25-COOH-10 mM-pH 6	original pH	H	H	H	H
P25-COOH-10 mM-pH 8	basic	H	H	H	H
P25-COOH-10 mM-pH 10	basic	H	H	M	H
P25-CHO-1 mM-pH 2	acid	M	M	L	M
P25-CHO-1 mM-pH 4	acid	M	M	L	M
P25-CHO-1 mM-pH 6	original pH	H	H	H	H
P25-CHO-1 mM-pH 8	basic	H	H	H	H
P25-CHO-1 mM-pH 10	basic	H	H	H	H
P25-CHO-10 mM-pH 2	acid	L	M	L	L
P25-CHO-10 mM-pH 4	acid	L	L	L	L
P25-CHO-10 mM-pH 6	original pH	L	L	L	L
P25-CHO-10 mM-pH 8	basic	H	H	M	H
P25-CHO-10 mM-pH 10	basic	L	M	L	L
P25-SAL-1 mM-pH 2	acid	H	H	H	H
P25-SAL-1 mM-pH 4	acid	H	H	H	H
P25-SAL-1 mM-pH 6	original pH	M	M	M	M
P25-SAL-1 mM-pH 8	basic	H	H	H	H
P25-SAL-1 mM-pH 10	basic	M	H	M	M
P25-SAL-10 mM-pH 2	acid	H	H	H	H
P25-SAL-10 mM-pH 4	acid	H	H	H	H
P25-SAL-10 mM-pH 6	original pH	L	L	L	L
P25-SAL-10 mM-pH 8	basic	L	L	L	L
P25-SAL-10 mM-pH 10	basic	L	L	L	L
P25-PEG-1 mM-pH 2	acid	M	M	M	M
P25-PEG-1 mM-pH 4	acid	M	M	M	M
P25-PEG-1 mM-pH 6	original pH	M	M	M	M
P25-PEG-1 mM-pH 8	basic	M	M	M	M
P25-PEG-1 mM-pH 10	basic	M	M	M	M
P25-PEG-10 mM-pH 2	acid	L	M	L	L
P25-PEG-10 mM-pH 4	acid	M	M	L	M
P25-PEG-10 mM-pH 6	original pH	M	M	M	M
P25-PEG-10 mM-pH 8	basic	M	M	M	M
P25-PEG-10 mM-pH 10	basic	M	M	L	M

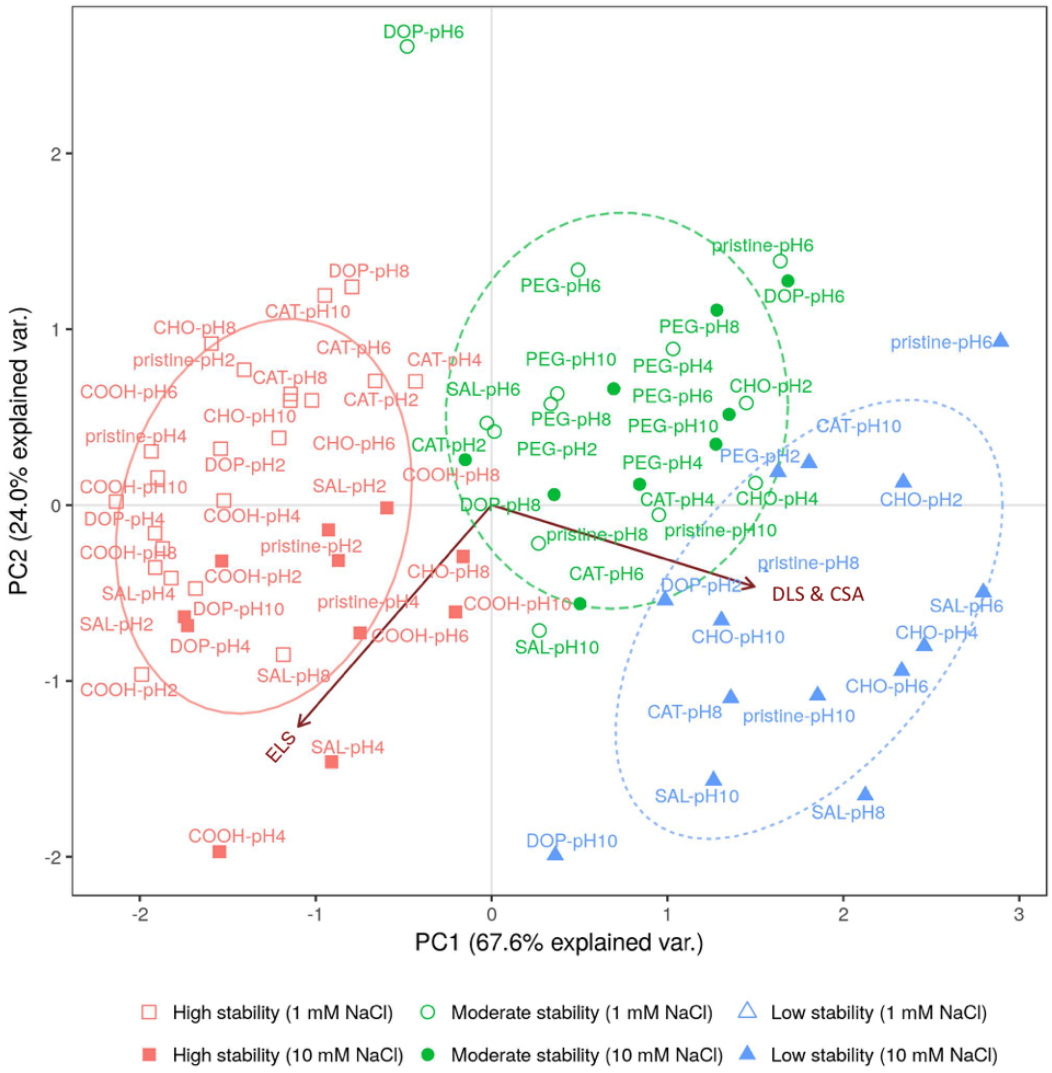

Figure 14: PCA biplot of the P25 NMs dispersed in 1 and 10 mM NaCl in the pH range 2-10. The ellipses represent a 68% confidence interval for experimental data, highlighting the regions corresponding to high, moderate, and low stability. For clarity, only the functional group of P25 functionalized NMs was reported in PCA labels.

The Adjusted Rand Index (ARI) was used to assess the similarity in the classifications provided by the four different clustering algorithms (Table 10) and the results are reported in Table 11, showing in general a good agreement among the statistical techniques.

Table 11: Adjusted Rand Index (ARI) results from the comparison of partitioning obtained by Consensus clustering (CONS) with respect to Hierarchical clustering (HC), K-means (KM) and Fuzzy c-Means (FCM).

	HC	**KM**	**FCM**	**CONS**
HC	1	0.72	0.47	0.72
KM	0.72	1	0.63	1
FCM	0.47	0.63	1	0.63
CONS	0.72	1	0.63	1

The categorization obtained by Consensus clustering displayed by PCA in Figure 14 was split for clarity into three different PCA biplots with respect to pH: (I) acid pH range between 2 and 4 (Figure 15); (II) around the Point of Zero Charge, i.e. pH 6 (Figure 16); (III) basic pH range between 8 and 10 (Figure 17). The ellipses depicted in each stability region represented the 68% confidence interval of data, under the reasonable assumption of normal distribution. Moreover, the loading arrows are displayed for all the original variables in the biplots presented in the PCA plots. Squared length of loading arrows approximates the variance of original variables, scalar products between any two arrows approximate the covariance between the corresponding original variables, and cosines of the angles between two arrows approximate the correlation between corresponding original variables [234].

In general, almost the same direction for the arrows corresponding to DLS and CSA data was observed, showing a high correlation between these two techniques. Both hydrodynamic particles size and sedimentation velocity values increased along with the direction of the arrows, indicating a decrease of the dispersion stability. On the contrary, zeta-potential data considered as absolute values, showed an increase of the stability. A change of ELS arrow orientation along the pH scale was observed moving from the acid to the basic pH. In fact, the ELS arrow became practically orthogonal to DLS and CSA arrows, indicating an increased contribution of zeta-potential to PC2 at basic pH. In detail, as far as strong acid pH (2-4), the first principal component PC1 accounted for 80.8% of the whole variance while PC2 accounted for 13.9% of the total variability (Figure 15). This translates in a quite good agreement among the three analytical techniques under strong acid conditions. On the other hand, PC1 of pH 6 biplot (Figure 16) accounted for 63.9% of the total variance and the second accounted for 27.7%. Finally, PC1 from the basic pH (8-10) biplot (Figure 17) accounted for slightly more than half, i.e. 57.7%, and the second for roughly one third, i.e. 32.3%, indicating the same contribution from each technique to the total variability. The increment in the contribution of PC2 from acid to basic pH was mainly ascribed to ELS.

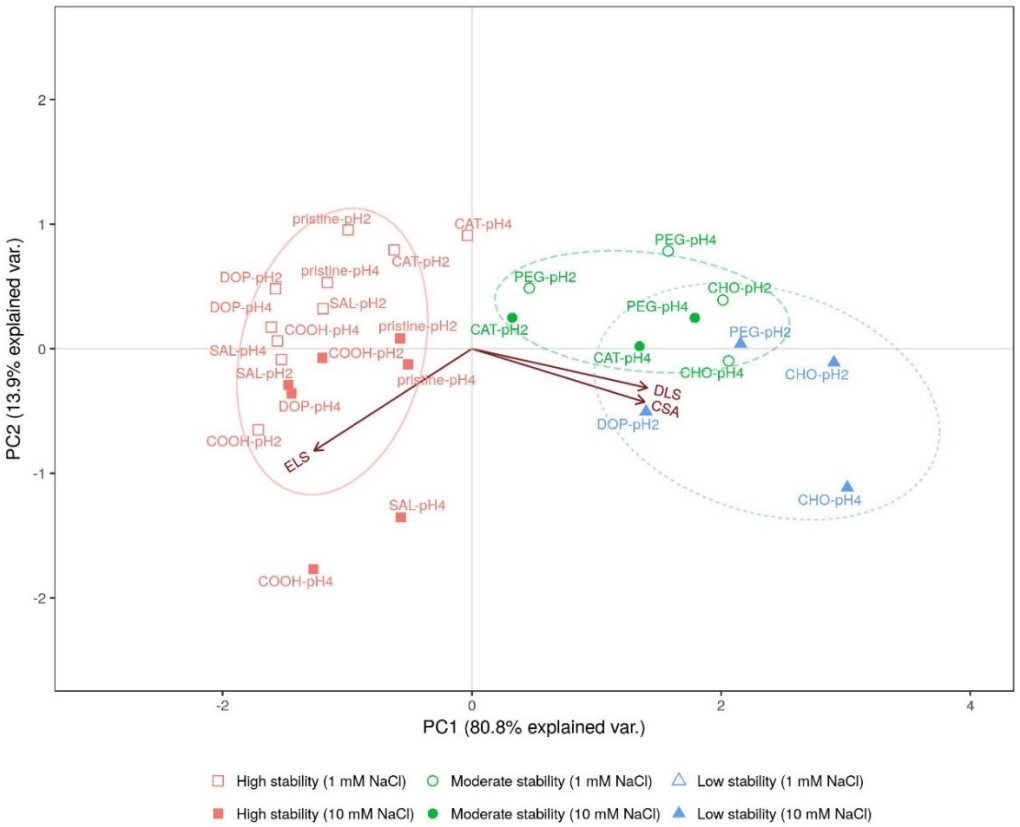

Figure 15: PCA biplots of the P25 NMs dispersed in 1 and 10 mM NaCl at strong acidic pH (2 and 4).

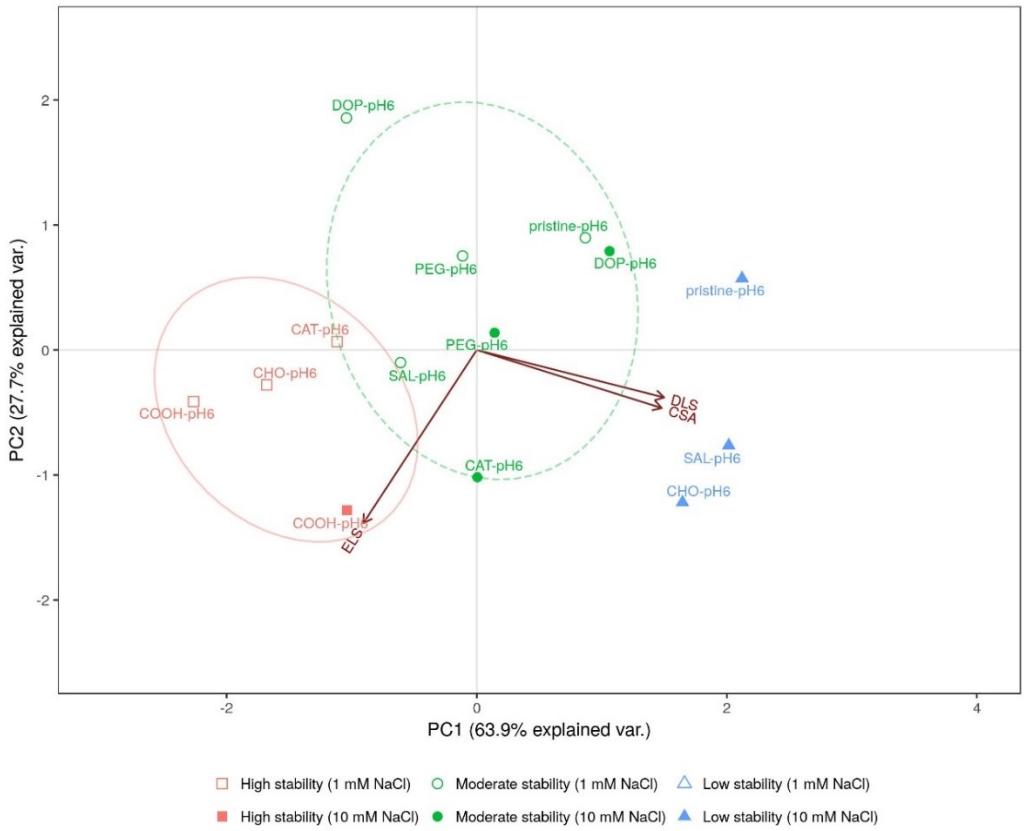

Figure 16: PCA biplots of the P25 NMs dispersed in 1 and 10 mM NaCl around the Point of Zero Charge (pH 6).

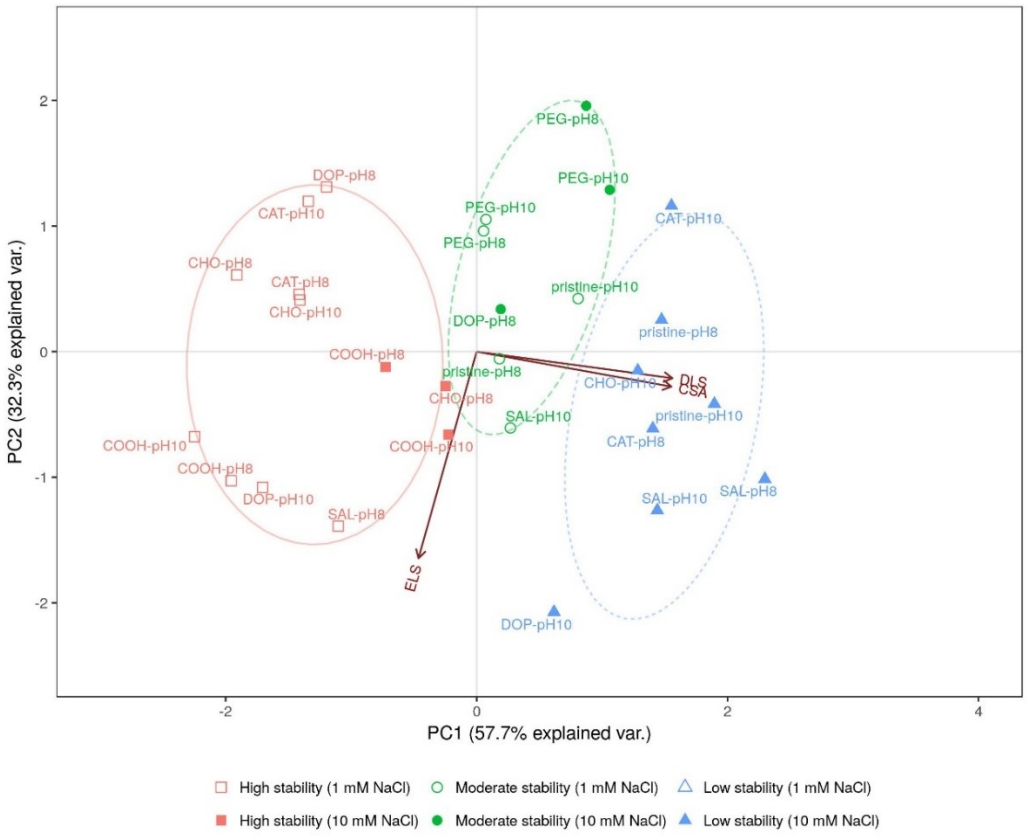

Figure 17: PCA biplots of the P25 NMs dispersed in 1 and 10 mM NaCl at basic pH (8 and 10).

An increase of surface functionalized NMs colloidal stability with respect to pristine was observed in PCA plots from pH 6 to 10 (Figure 16 and Figure 17). As expected [235], pristine dispersions already resulted highly stable under acid conditions (Figure 15), along with all the P25-COOH and P25-SAL dispersions tested. A possible explanation of the high stability of these two functionalized NMs can be ascribed to the carboxylic group. In fact, as far as P25-COOH, -COOH group was not involved in the modification of P25 surface, as highlighted by FTIR spectrum (Figure 12). Moreover, in the case of P25-SAL, the protonation of the carboxylic group attached on titanium might occur under strong acid conditions, leading to a monodentate conformation and to the free COOH group. On the other hand, P25-CAT and P25-PEG were mainly located in the moderate stability class while the less stable dispersions were represented by P25-CHO. P25-DOP was an exception, resulting highly stable at pH 4, but varying its stability class at pH 2 depending on the electrolyte concentration. Taking into account the results at pH 6 (Figure 16), P25-COOH, P25-CHO and P25-CAT were categorized within the high-stability class. However, while P25-COOH was highly stable regardless the NaCl concentration, P25-CHO and P25-CAT moved respectively to the low- and moderate-stability classes at 10 mM NaCl solutions. The sensitivity to the salt concentrations was also observed for P25-SAL, which moved from moderate- to low-stability class at increasing NaCl concentration. As far as P25-DOP and P25-PEG, they were always located within the moderate-stability class. Finally, at pH ≥ 8 (Figure 17), the functionalized P25-NMs dispersed in 1 mM NaCl were almost all classified as highly stable, except for the P25-PEG dispersions, again categorized as moderate stable. Based on the relative stability classification proposed, Table 12 highlights at which percentage and within which range the different dispersions fitted, for each technique used.

Table 12: Values (%) of the distribution of results within high, moderate and low stability classes gained from consensus clustering.

			ELS ranges (mV)			
Stability class	**<5**	**5-10**	**10-15**	**15-20**	**20-25**	**≥25**
High	0%	0%	6%	21%	15%	58%
Moderate	14%	18%	27%	27%	14%	0%
Low	7%	7%	20%	33%	20%	13%
			DLS ranges (nm)			
Stability class	**<400**	**400-600**	**600-800**	**800-1000**	**1000-1200**	**≥1200**
High	30%	49%	12%	9%	0%	0%
Moderate	0%	18%	18%	41%	23%	0%
Low	0%	0%	0%	0%	20%	80%
			CSA ranges (µm/s)			
Stability class	**<0.03**	**0.03-0.1**	**0.1-0.17**	**0.17-0.24**	**0.24-0.31**	**≥0.31**
High	12%	67%	15%	6%	0%	0%
Moderate	4%	0%	23%	55%	18%	0%
Low	0%	0%	6%	27%	27%	40%

In summary, at strong acid pH (2-4) the colloidal stability of the P25-NMs dispersions appeared to be functional group-dependent, while from pH 6 to 10 the colloidal stability seemed to be electrolyte concentration-dependent. A comparison among the different functional groups revealed that P25-COOH and P25-PEG dispersions were always located in the high- and moderate-stability class respectively, regardless of the pH and NaCl concentrations. As commented before, the polarity of COOH and the steric hindrance of PEG are probably the main factors which limited destabilization of NMs dispersions.

3.3.3 Colloidal stability assessment as a function of dispersion media

The results obtained so far have highlighted the role of the different organic ligands in the colloidal stabilization of functionalized NMs dispersed in simple electrolyte solutions. The study was further extended to deionized water and ecotoxicological media i.e. AFW and AMW, to investigate how media characteristics (such as ionic strength and ionic composition) can affect the colloidal stability of the NMs dispersions, with respect to pristine P25. The results from DLS and CSA techniques are summarized in Table 13, showing a decrease of hydrodynamic diameter and sedimentation velocity in AFW and AMW for almost all the functionalized P25 NMs with respect to pristine. ELS data were not reported because of the difficulty to obtain reproducible zeta-potential values in DW and ecotoxicological media with our instrumental setup (measurements prevented by the lack or too high concentration of electrolytes in solution).

Table 13: Hydrodynamic diameter (average and standard deviation in nm) and sedimentation velocity (median and standard deviation in µm/s) values in deionized water (DW), 1 and 10 mM NaCl, Artificial Fresh Water (AFW) and Artificial Marine Water (AMW).

Media / NMs	P25-Pristine	P25-CAT	P25-CHO	P25-COOH	P25-DOP	P25-SAL	P25-PEG
				Hydrodynamic diameter (nm)			
DW	386 ± 85	178 ± 34	309 ± 54	237 ± 45	375 ± 94	420 ± 96	435 ± 93
1 mM NaCl	771 ± 173	558 ± 123	262 ± 50	305 ± 60	411 ± 76	499 ± 103	697 ± 188
10 mM NaCl	1321 ± 268	932 ± 128	1242 ± 190	913 ± 179	1184 ± 221	1215 ± 199	909 ± 182
AFW	2100 ± 598	705 ± 155	838 ± 158	1251 ± 213	937 ± 163	985 ± 193	1095 ± 180
AMW	2396 ± 470	1180 ± 239	1175 ± 240	1260 ± 214	941 ± 163	933 ± 162	1168 ± 202
				Sedimentation velocity (µm/s)			
DW	0.12 ± 0.01	0.02 ± 0.001	0.02 ± 0.001	0.02 ± 0.001	0.03 ± 0.001	0.02 ± 0.001	0.03 ± 0.001
1 mM NaCl	0.28 ± 0.01	0.09 ± 0.01	0.12 ± 0.01	0.02 ± 0.001	0.03 ± 0.001	0.2 ± 0.01	0.15 ± 0.01
10 mM NaCl	0.31 ± 0.02	0.22 ± 0.01	0.39 ± 0.001	0.07 ± 0.001	0.17 ± 0.01	0.42 ± 0.02	0.17 ± 0.01
AFW	0.45 ± 0.02	0.34 ± 0.02	0.36 ± 0.01	0.34 ± 0.01	0.38 ± 0.02	0.44 ± 0.01	0.28 ± 0.01
AMW	0.41 ± 0.01	0.32 ± 0.02	0.34 ± 0.01	0.37 ± 0.01	0.33 ± 0.02	0.33 ± 0.01	0.29 ± 0.01

For this reason, before applying the same statistical approach to the new dataset, DLS and CSA data were standardized and further analysed by consensus clustering. The results from the statistical analysis considering 3 vs 2 techniques were compared and summarized in Table 14.

Table 14: Consensus clustering data of 2 (DLS and CSA, named Consensus (2)) vs 3 techniques (ELS, DLS and CSA, named Consensus (3)), dividing them into high (H), moderate (M) and low (L) relative stability classes. In italic the different categorization between Consensus (3) and Consensus (2).

Class	**pH**	**Consensus (3)**	**Consensus (2)**
P25-pristine-1 mM-pH2	acid	H	H
P25-pristine-1 mM-pH4	acid	H	H
P25-pristine-1 mM-pH6	original pH	M	M
P25-pristine-1 mM-pH8	basic	M	M
P25-pristine-1 mM-pH10	basic	M	M
P25-pristine-10 mM-pH2	acid	H	H
P25-pristine-10 mM-pH4	acid	H	H
P25-pristine-10 mM-pH6	original pH	L	L
P25-pristine-10 mM-pH8	basic	L	L
P25-pristine-10 mM-pH10	basic	L	L
P25-CAT-1 mM-pH2	acid	H	H
P25-CAT-1 mM-pH4	acid	H	H
P25-CAT-1 mM-pH6	original pH	H	H
P25-CAT-1 mM-pH8	basic	H	H
P25-CAT-1 mM-pH10	basic	H	H
P25-CAT-10 mM-pH2	acid	M	M
P25-CAT-10 mM-pH4	acid	M	M
P25-CAT-10 mM-pH6	original pH	M	M
P25-CAT-10 mM-pH8	basic	L	L
P25-CAT-10 mM-pH10	basic	L	L
P25-DOP-1 mM-pH2	acid	H	H
P25-DOP-1 mM-pH4	acid	H	H
P25-DOP-1 mM-pH6	*original pH*	*M*	*H*
P25-DOP-1 mM-pH8	basic	H	H
P25-DOP-1 mM-pH10	basic	H	H
P25-DOP-10 mM-pH2	acid	L	L
P25-DOP-10 mM-pH4	acid	H	H

Class	pH	Consensus (3)	Consensus (2)
P25-DOP-10 mM-pH6	original pH	M	M
P25-DOP-10 mM-pH8	basic	M	M
P25-DOP-10 mM-pH10	basic	L	L
P25-COOH-1 mM-pH2	acid	H	H
P25-COOH-1 mM-pH4	acid	H	H
P25-COOH-1 mM-pH6	original pH	H	H
P25-COOH-1 mM-pH8	basic	H	H
P25-COOH-1 mM-pH10	basic	H	H
P25-COOH-10 mM-pH2	acid	H	H
P25-COOH-10 mM-pH4	*acid*	*H*	*M*
P25-COOH-10 mM-pH6	*original pH*	*H*	*M*
P25-COOH-10 mM-pH8	*basic*	*H*	*M*
P25-COOH-10 mM-pH10	*basic*	*H*	*M*
P25-CHO-1 mM-pH2	acid	M	M
P25-CHO-1 mM-pH4	*acid*	*M*	*L*
P25-CHO-1 mM-pH6	original pH	H	H
P25-CHO-1 mM-pH8	basic	H	H
P25-CHO-1 mM-pH10	basic	H	H
P25-CHO-10 mM-pH2	acid	L	L
P25-CHO-10 mM-pH4	acid	L	L
P25-CHO-10 mM-pH6	original pH	L	L
P25-CHO-10 mM-pH8	*basic*	*H*	*M*
P25-CHO-10 mM-pH10	basic	L	L
P25-SAL-1 mM-pH2	acid	H	H
P25-SAL-1 mM-pH4	acid	H	H
P25-SAL-1 mM-pH6	original pH	M	M
P25-SAL-1 mM-pH8	basic	H	H
P25-SAL-1 mM-pH10	basic	M	M
P25-SAL-10 mM-pH2	acid	H	H
P25-SAL-10 mM-pH4	*acid*	*H*	*M*
P25-SAL-10 mM-pH6	original pH	L	L
P25-SAL-10 mM-pH8	basic	L	L

Class	pH	Consensus (3)	Consensus (2)
P25-SAL-10 mM-pH10	basic	L	L
P25-PEG-1 mM-pH2	acid	M	M
P25-PEG-1 mM-pH4	acid	M	M
P25-PEG-1 mM-pH6	original pH	M	M
P25-PEG-1 mM-pH8	basic	M	M
P25-PEG-1 mM-pH10	basic	M	M
P25-PEG-10 mM-pH2	acid	L	L
P25-PEG-10 mM-pH4	acid	M	M
P25-PEG-10 mM-pH6	original pH	M	M
P25-PEG-10 mM-pH8	basic	M	M
P25-PEG-10 mM-pH10	basic	M	M

The comparison highlighted that >88% of samples (62 out of 70, which corresponds to an ARI of 0.67) were included in the same stability class, suggesting the possibility of using the same statistical approach, considering only two descriptors (DLS and CSA results). As a result, the stability classes of data obtained by dispersing P25 NMs in DW, AFW and AMW, were standardized using the mean and the standard deviation computed in the previous step, and predicted starting from NaCl data, using a Nearest Neighbour classifier. Categorization of samples dispersed in DW at original pH as well as in 1 mM NaCl, 10 mM NaCl, AFW and AMW at pH 8 was graphically represented by PCA (Figure 18).
As expected, NMs dispersed in DW were all located in the highest stability class (very low agglomeration and sedimentation of NMs due to the absence of salts) while the ecotoxicological media composition (high salt concentration and presence of divalent cations) increased the destabilization of the dispersions, regardless the functional group on the NMs surface, locating all the data into the low stability class. However, as shown by the position of pristine in AFW and AMW from the PCA biplot (i.e. outside from the ellipses), an increase of the colloidal stability of P25 NMs has been obtained because of the surface functionalization performed.

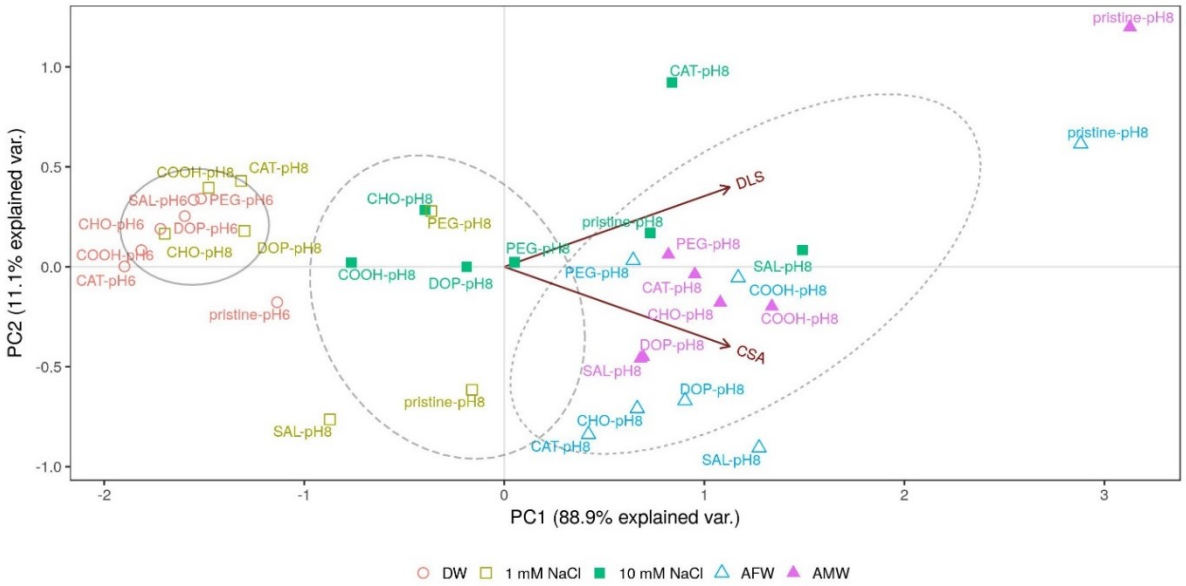

Figure 18: Hydrodynamic diameter (dz-ave) and sedimentation velocity (Sed V) of pristine and functionalized NMs dispersed in Deionized Water (DW) at pH 6 and in 1 and 10 mM NaCl solutions, Artificial Fresh Water (AFW) and Artificial Marine Water (AMW), all at pH 8.

3.4 Conclusions

The work presented in this chapter is one of the first studies employing multivariate statistical analysis methods to categorize experimental data of NMs dispersions into relative stability classes. The study highlighted that even small modifications of the NMs' surfaces can affect their colloidal stability towards the investigated parameters (i.e. dispersion media composition, pH, and electrolyte concentration). The performed statistical analyses helped to derive conclusions on the relationships of these extrinsic characteristics with the intrinsic properties of the modified nanomaterials (e.g. surface modification), which can support *in silico* and materials modelling to develop SbD strategies for TiO_2. In addition, the stability classification itself can directly inform the selection of dispersions/formulations for such strategies as well as for developing standard nano(eco)toxicological experiments for regulatory risk assessment.

4 Subspace Clustering as a tool for the Read-Across and Classification of NMs

The work presented in this chapter will be submitted as a journal article, currently in preparation:
G.Basei, A.Bahl, A.Haase, D.Hristozov, A.Zabeo, A.Marcomini, and A.Torsello, *Subspace Clustering as a tool for the Read-Across and Classification of Nanomaterials*, (in prep.).

4.1 Introduction

Considerable efforts have been made to provide *in silico* models exploiting ML techniques aimed at predicting hazards of nanomaterials, as highlighted in Chapter 2. However, as discussed in Chapter 2, such models were often trained on small datasets, usually described by hundreds of variables. Unfortunately, this setting is in general not good for classic ML algorithms: the concept of proximity, distance or nearest neighbour exploited by distance-based ML algorithms, including Clustering algorithms that automatically group data according to similarity in descriptors, become less meaningful as the number of dimensions become higher. Indeed, given a fixed number of samples, as the number of dimensions of such samples tends to the infinite, the difference between the distance from a fixed sample and its closest and farther neighbours in the dataset, divided by the distance from the closest samples, tends to zero [236].

To address this issue, typically either feature selection or feature transformation techniques are adopted. Feature transformation techniques, such as Principal Component Analysis (PCA), aim at transforming the original (possible correlated) descriptors into a set of linearly uncorrelated ones (called Principal Components (PCs)), by creating a set of linear combinations of the original descriptors. This transformation results in the fact that the first component describes the highest variance in the original set of descriptors, and the others subsequently describe the remining variance under the constraint of being orthogonal to the preceding. These techniques are able to discover latent patterns in datasets, and for this reason are very popular also for modelling properties and hazards of NMs: PCA, indeed, was previously applied for nanomaterials classification [146,186], as a preliminary step for subsequent modelling [89,237], as well as for quality assessment of nano-based dispersions [205], moreover it was suggested as a tool for grouping NMs [19]. However, such techniques preserve the relative distances between samples, since they are combining features and not removing them. Moreover, being the resulting PCs combinations of the original descriptors, they may result to be very difficult to interpret.

Feature selection methods, on the other hand, select only the most relevant of the dimensions from a dataset. There exists many types of feature selection techniques [238] based for instance on looking at variable importance (e.g. through a ROC curve), or based on using a subset of the database and train a number of models, recursively removing features with low weight. While quite successful on many datasets, feature selection algorithms fail when clusters are found in different combinations of descriptors. It is this type of data that motivated the evolution to subspace clustering algorithms. Subspace Clustering is indeed an extension of Clustering, where clusters are searched in different (possibly overlapping) combination of descriptors, called Subspaces [239].

Subspace clustering is still unexplored as a tool to assess similarities in a dataset of NMs for Read-Across and classification purposes. The novel method presented in this chapter finds overlapping clusters in data Subspaces, then it trains an SVM model in this subspace, and predicts an endpoint or categorizes an untested NM extracting information from NMs that appear in the same cluster(s). The methodology has been tested on datasets retrieved from the literature, as well as on data from EU projects, comparing performances to those reported in literature and with those provide by against an SVM model applied on the whole dataset, and against an SVM model trained after PCA.

4.2 Materials and Methods

4.2.1 Case study datasets

4.2.1.1 Cytotoxicity of poly (amido amine) (PAMAM) dendrimers

Jones et al. (2015) retrieved from 12 different nanomedicine journal articles a dataset on the cytotoxicity of poly (amino amine) (PAMAM) dendrimers in human colon carcinoma Caco-2 cells (measured as cell viability) [143], using NanoSifter NLP as a tool for datamining [52]. The resulting dataset is composed by 103 samples, described by 51 physicochemical features (52 including the cytotoxicity concentration). Description, mean, minimum and maximum values of each descriptor is reported in Table 15.

Such NMs, benefiting from their characteristic scaffold structures, have been demonstrated being suitable carriers for a number of diverse bioactive agents, improving the solubility and bioavailability of poorly soluble ones [240–242], moreover, they are also promising for use in the treatment of cancer [243]. However, there are concerns for their use in biomedicine due to their potential toxicological effects, which depend on the structure that is used: indeed, research has demonstrated their surface charge-, generation-, and concentration-dependent toxicity [244–246].

In their work, Jones et al. (2015) [143] performed 5 different analyses to classify NMs as toxic or nontoxic, using different combinations of descriptors: the first analysis utilized all the molecular descriptors available, the second involved an automatic feature selection, the third used only the molecular descriptors selected by experts as suitable candidates to relate to cytotoxicity (molecular weight, atom count, pI, and molecular polarizability), the fourth analysis included the same molecular descriptors used in the second analysis in addition to the experimental concentration (i.e., the amount in mM of PAMAM dendrimer added cells culture during the cytotoxicity analysis), while the final analysis independently assessed the performance by randomly splitting the dataset into a training set, including 83 of the values, and a test set, including 20 of the values in the dataset.

Authors tested 10 different ML approaches in each setting, comparing Accuracy, Sensitivity and Specificity of each approach. To test our approach, we took the same internal and external sets, and compared the results of our approach with ones reported by Jones et al. (2015) [143] in their last analysis.

Table 15: Descriptors computed by Jones et al. (2015) [143], together with computed minimum, maximum and average values.

Descriptor	Description	Min	Max	Mean
Molecular Weight	Average molecular mass calculated from the standard atomic weights.	516.6811	23438.19	8453.289

Descriptor	Description	Min	Max	Mean
Exact Mass	Monoisotopic mass calculated from the weights of the most abundant natural isotopes of the elements.	516.386	23424.61	8448.384
Atom Count	Number of all atoms in the molecule.	84	3396	1294.252
pI	Isoelectric point: net charge of an ionizable molecule is zero at a certain pH.	4.85	12.93	10.95437
logP	The octanol/water partition coefficient. Generally used as a measure of molecular hydrophobicity.	-157.52	-6.45	-78.1327
logD	The octanol-water distribution coefficient at any pH value.	-179.67	-18.95	-101.428
Molecular Polarizability	The electric field generated by partial charges of a molecule spread through intermolecular cavities and the solvent. The induced partial charge tends to diminish the external electric field. This phenomenon is called polarizability.	55.28	2272.27	861.5057
Aliphatic Atom Count	Number of atoms in the molecule having no aromatic bond (excluding hydrogens).	36	1636	591.3398
Aliphatic Bond Count	Number of non-aromatic bonds in the molecule (excluding bonds of hydrogen atoms).	35	1635	590.3398
Aromatic Atom Count	Number of atoms in the molecule having aromatic bonds.	0	0	0
Aromatic Bond Count	Number of aromatic bonds in the molecule.	0	0	0
Asymetric Atom Count	The number of asymmetric atoms (having four different ligands).	0	0	0
Bond Count	Number of bonds in the molecule including bonds of hydrogen atoms.	83	3395	1293.252
Chain Atom Count	Number of chain atoms (non-ring atoms excluding hydrogens).	36	1636	591.3398
Chain Bond Count	Number of chain bonds (non-ring bonds excluding bonds of hydrogen atoms).	35	1635	590.3398
Chiral Center Count	The number of tetrahedral stereogenic centres. This function identifies two chiral centres in 1,4-dimethylcyclohexane, which does not contain asymmetric atoms.	0	0	0
Ring Atom Count	Number of ring atoms.	0	0	0
Ring Bond Count	Number of ring bonds.	0	0	0
Rotatable Bond Count	Number of rotatable bonds in the molecule.	0	1131	397.7767
Stereo Double Bond Count	Number of double bonds with defined stereochemistry.	0	0	0
Aliphatic Ring Count	Number of those rings in the molecule that have non-aromatic bonds (SSSR based).	0	0	0
Aromatic Ring Count	Number of aromatic rings in the molecule.	0	0	0
Carbo Ring Count	Number of rings containing only carbon atoms.	0	0	0
Carboaliphatic Ring Count	Number of aliphatic rings containing only carbon atoms.	0	0	0
Carboaromatic Ring Count	Number of aromatic rings containing only carbon atoms (SSSAR based).	0	0	0
Fused Aliphatic Ring Count	Number of aliphatic rings having common bonds with other rings.	0	0	0
Fused Aromatic Ring Count	Number of aromatic rings having common bonds with other rings.	0	0	0

Descriptor	Description	Min	Max	Mean
Fused Ring Count	Number of fused rings in the molecule (having common bonds).	0	0	0
Hetero Ring Count	Number of rings containing hetero atom(s).	0	0	0
Heteroaliphatic Ring Count	Number of aliphatic heterocycles in the molecule.	0	0	0
Heteroaromatic Ring Count	Number of aromatic heterocycles in the molecule.	0	0	0
Largest Ring Size	Size of the largest ring in the molecule.	0	0	0
Largest Ring System Size	Number of rings in the largest ring system.	0	0	0
Ring Count	Number of rings in the molecule. This calculation is based on SSSR (Smallest Set of Smallest Rings).	0	0	0
Ring System Count	Number of disjunct ring systems.	0	0	0
Smallest Ring Size	Size of the smallest ring in the molecule.	0	0	0
Smallest Ring System Size	Number of rings in the smallest ring system.	0	0	0
Platt Index	Sum of the edge degrees of a molecular graph.	80	4024	1418.33
Randic Index	Harmonic sum of the geometric means of the node degrees for each edge.	17.35	777.71	283.7268
Harary Index	Half-sum of the off-diagonal elements of the reciprocal molecular distance matrix of the molecule.	12.45	32238.35	7453.854
Hyper Wiener Index	A variant of the Wiener index.	26135	6.44E+08	2.36E+08
Szeged Index	The Szeged index extends the Wiener index for cyclic graphs by counting the number of atoms on both sides of each bond (those atoms only which are nearer to the given side of the bond than to the other) and sum these counts.	4858	75825090	11112568
Wiener Index	The average topological atom distance (half of the sum of all atom distances) in the molecule.	4858	75825090	11112568
Wiener Polarity	The number of 3 bond length distances in the molecule.	41	2009	730.8641
Cyclomatic Number	The smallest number of bonds which must be removed so that no circuit remains. Also known as circuit rank.	0	0	0
Fragment Count	Number of fragments in the sketch.	1	1	1
H-Bond Donor Count	Hydrogen Bond Donor calculates atomic hydrogen bond donor inclination.	8	252	104.5825
H-Bond Donor Sites	Hydrogen Bond Donor calculates atomic hydrogen bond donor inclination.	12	252	128.8155
H-Bond Acceptor Count	Hydrogen Bond Acceptor calculates atomic hydrogen bond acceptor inclination.	10	506	161.767
H-Bond Acceptor Sites	Hydrogen Bond Acceptor calculates atomic hydrogen bond acceptor inclination.	14	886	259.3592
Refractivity	Molar refractivity is strongly related to the volume of the molecules and to London dispersive forces that has important effect in drug-receptor interaction.	139.82	5823.25	2199.709

4.2.1.2 Cytotoxicity of Metal Oxides

Sizochenko et al. (2015) [74] retrieved from the literature cytotoxicity data of MTS assay on human bronchial epithelial cell line (BEAS2) for 24 Metal Oxide NMs and murine myeloid cell line RAW 264.7 [247]. The original study provided dose response quantitative values for toxicities, while in their study Sizochenko et al. (2015) [74] arranged a classification into toxic and non-toxic classes, by considering the slope of the doe-response curves: NMs with a negative slope were classified as non-toxic, while NMs with a positive curve were classified as toxic.

Each NM was described by: i) Simplex Representations of Molecular Structure (SiRMS) based descriptors [248], ii) Metal-ligand binding descriptors [249], iii) "Liquid drop" model (LDM) descriptors [139], and iv) molecular descriptors, for a total of 203 descriptors. Minimum, maximum and average values of these descriptors (excluding SiRMS descriptors) are reported in Table 16.

Authors split the dataset into a training set composed by 16 NMs and a test set composed by 6 NMs, modelling it using Random Forest. Finally, they assessed the AD of the models basing on minimum-cost-tree of variable importance values, which is usually provided by Random Forests modelling packages, and provided a mechanistic interpretation of the models by means of causal structures [250,251]. In this work, we only considered data on BEAS2 cell line, and we kept the same split into internal and external sets.

Table 16: Descriptors computed by Sizochenko et al. (2015) [252], together with computed minimum, maximum and average values.

Descriptor	Description	Min	Max	Mean
	General properties			
Size	Size of NMs.	10.00	193.00	40.85
Size in BEGM	Size in BEGM medium.	109.20	339.50	245.43
Size in DMEM	Size in DMEM medium.	46.40	351.60	222.97
E_c (eV)	Conduction band energy.	-5.53	-1.51	-3.82
PZZP	Point of zero zeta-potential.	0.30	11.40	6.80
	LDM-based descriptors			
Wiegner-Seitz radius	The minimum radius of the interactions between elementary particles in the cluster.	1.34	2.38	1.90
Number of atoms	Number of atoms in the nanocluster.	13.18	128956.90	8521.77
Volume of cluster	Volume of the nanocluster.	4186.67	30098190.00	1993292.71
Surface area	Surface area of the nanocluster.	1256.00	467847.40	44291.48
Number of surface molecules	Number of surface molecules of the nanocluster.	0.08	1.69	0.71
Surface-area-to-volume ratio	Ratio of surface molecules to molecules in volume.	-25.90	356.90	14.71
AP in BEGM	Aggregation parameter: represents the ratio of the aggregate's size to the size of individual particles (BEGM medium).	1.64	23.85	10.84
AP in DMEM	Aggregation parameter: represents the ratio of the aggregate's size to the size of individual particles (DMEM medium).	1.65	24.52	9.61
	Integral (constitutional) descriptors			

Descriptor	Description	Min	Max	Mean
Molecular weight	Average molecular mass calculated from the standard atomic weights.	60.00	394.00	184.45
Aligned electronegativity	Electronegativity of bonding atoms.	1.10	2.36	1.67
Density	Density of the NM.	2.65	9.68	5.99
Metal-ligand Binding based descriptors				
Ionic radius	Radius of an atom's ion in ionic crystals structure.	40.00	103.20	69.02
Covalent index	Reflects the relative influence of covalent interactions in the binding process.	105.03	334.18	192.67
Cation polarizing power	Reflects the relative importance of covalent interaction with bio-ligands.	0.05	0.60	0.17
Charge of cation	Positive charge of the ion.	2.00	6.00	3.18

4.2.1.3 NanoTox Class dataset

EU FP7 NanoToxClass project[j] aims at facilitating hazard evaluation for the human health by developing grouping approaches for a selection of industrially relevant nanomaterials, integrating publicly available data from with extensive new data with established toxicological endpoints, performing transcriptomics, metabolomics and proteomics studies in vitro as well as in vivo.

The goal of the project is thus to make use of most comprehensive datasets, allowing to find mechanisms of action of nanomaterials and at the same time to follow a bottom-up approach, developing grouping strategies based on mode of action. Furthermore, the project aims at contributing to the establishment of in vitro/in vivo correlations. In the project, selected nanomaterials are examined in different nanoforms on representative stages of their lifecycle.

During my three months at the BfR in berlin, I contributed in modelling such dataset, which at the current state is not yet complete (some of the measurements/test are still missing). The results presented later, indeed, are to be intended as preliminary: the intent here is to demonstrate that our approach provide useful insights even when using small datasets. Indeed, the dataset is composed by only 11 NMs (two organic pigments, TiO_2, seven different NFs of SiO_2, and Graphene Oxide). Even though our approach can deal also with missing entries, for comparison purposes we used as descriptors ones which were available for all NMs. At the current time, 6 descriptors are available: Minimum, maximum and average values of these descriptors are reported in Table 17. Note that all the properties in the table are nano-specific, while on the other hand, for the other datasets modelled in this chapter also (computed) chemical descriptors are used.

For some of the particles, a categorization *in vivo* into toxic and non-toxic classes after short term inhalation was provided by Landsiedel et al. (2014) [253]. In addition, for a subset of NMs results from an *in vitro* test for short term inhalation for macrophages was available from a previous study of Wiemann et al. (2016) [254], and additional *in vitro* tests were performed during the NanoTox Class project, specifically i) metabolomics in epithelial cells/macrophages, ii) proteomics in epithelial cells and macrophages, and iii) SH2 signaling in epithelial cells / macrophages. All the available data was then merged in a single characterization into toxic/non-toxic classes: were results *in vivo* were not available,

[j] http://www.nanotoxclass.eu/project.html

we considered the additional tests and assigned the toxicity categorization by looking at the *in vitro* data available. Note that the resulting categorization is made merging different endpoints, and thus the methodology in this case should not be referred to Read-Across (since Read-Across is defined when predicting a well-defined endpoint), but rather into a categorization (classification) method.
Due to the limited set of samples, we performed Leave-One-Out Cross Validation (LOO CV), and we tested our method against a Random Forest classifier, against a Nearest Neighbour classifier trained on after PCA on the first three PCs, and a simple Read-Across-like method, which averaged the predictions with respect to the Euclidean distance of the closest 3 samples for each particle.

Table 17: Descriptors, together with minimum, maximum and mean values, of the NanoTox Class dataset.

Descriptor	Description	Min	Max	Mean
Density	Density of the NM.	1.62	3.89	2.545455
PPS	Primary Particle Size.	8.913805	75.91112	26.88242
Surface Area	Specific surface area.	33.674	254.005	152.7395
ZP	Zeta Potential at 7.4 pH, in FK12 medium.	-48.0656	-0.36588	-29.7811
Z average	Hydrodynamic diameter computed by DLS.	38.8	4284.767	939.3374
CPH	CPH reactivity.	0	0.102017	0.024269

4.2.2 Subspace Clustering based Read-Across and Classification

Before starting the analysis, to reduce pair-wise correlation among descriptors we performed a basic feature reduction by discarding strongly correlated descriptors (i.e.: correlation cut-off of 0.9) and constant descriptors. Subsequently data was standardized, namely for each descriptor in the training and test set we subtracted the mean of the training set and divided for the Standard Deviation of the training set. After these preliminary steps our approach finds (possibly overlapping) subspaces in the test set by means of the CLIQUE algorithm [255], then for each subspace it trains a Support Vector Machine (SVM) model in each subspace. We choose SVM since they can provide an accurate and robust classification on a sound theoretical basis, even when input data are non-monotone and non-linearly separable [256], which is the case for NMs. It is however noticeable that any other ML classification technique, in principle, can be used in place of SVMs in our method, but of course the application of different techniques at this step is likely to produce different results with respect to the ones presented here.
To provide prediction for the test set, we apply a basic transfer learning on the subspace, by projecting the new data into the PCA coordinate basis of the main PC of the subspace. Then, for each prediction, we check if it is in the Applicability Domain (AD) of the model in the subspace. At current time, the AD assessment is done by checking if the test particle falls between the ranges of the train set descriptors in the subspace, but we plan to perform more experiments to set a different threshold or to use a different method. Finally, the method averages all prediction for the samples in the test set. If one or more of the test set samples have no prediction (this is the case when they always fall outside of the AD of each subspace), we classify the sample as active, following a conservative approach (i.e.: we highlight risk, in presence of no information), highlighting that the sample is outside the AD of the model.

Results (expressed in terms of balanced accuracy, sensitivity and specificity) are then compared with ones provided in the literature. For a risk assessment perspective, sensitivity is a very important measure, since it highlights the ability of the model to recognize toxic NMs.
For comparison purposes, we trained as SVM model using the full set of descriptors (except constant ones and ones discarded being strongly correlated to others), and we trained an SVM model applied on the most important PCs (namely, excluding components which standard deviations are less than or equal than the 50% of the standard deviation of the first component). Finally, the decision regions are plotted in the space of the two principal components of data.
Computation is performed out using R language. CLIQUE algorithm is performed thanks to the *CLIQUE* function of the *subspace* package [257], while SVM is provided by the *svm* function from the *e1071* package [223].

4.3 Results

4.3.1 Cytotoxicity of poly (amido amine) (PAMAM) dendrimers

After removing strongly correlated descriptors and constant descriptors, we end up with a total of 25 descriptors from the initial pool of 51 descriptors. Then we performed the experiments described in section 4.2.1.2: original results and results of our experiments, expressed in terms of balanced accuracy, sensitivity and specificity, are presented in Table 18.

Table 18: Results expressed in terms of Balanced Accuracy, Sensitivity and Specificity for the dataset originally provided by Jones et al. (2015) [143]. Best performances are highlighted in bold font.

	Balanced accuracy	**Sensitivity**	**Specificity**
Original work [74]	**65%**	**65%**	80%
SVM on all descriptors	**65%**	36%	**100%**
SVM after PCA	**65%**	36%	**100%**
Subspace Clustering method	**65%**	36%	**100%**

All the approaches have the same performances in terms of Balanced Accuracy. However, the results provided by Jones et al. (2015) [143] demonstrated a better capacity of correctly classifying toxic substances as such. This is explained by the fact that while we automatically discarded strongly correlated descriptors, in the original work authors chosen the descriptors by expert judgment. The decision regions of the models that we trained are presented in Figure 19 (SVM computed on all descriptors), Figure 20 (SVM after PCA), and Figure 21 (Subspace Clustering method). All the NMs were classified inside the AD of the model.

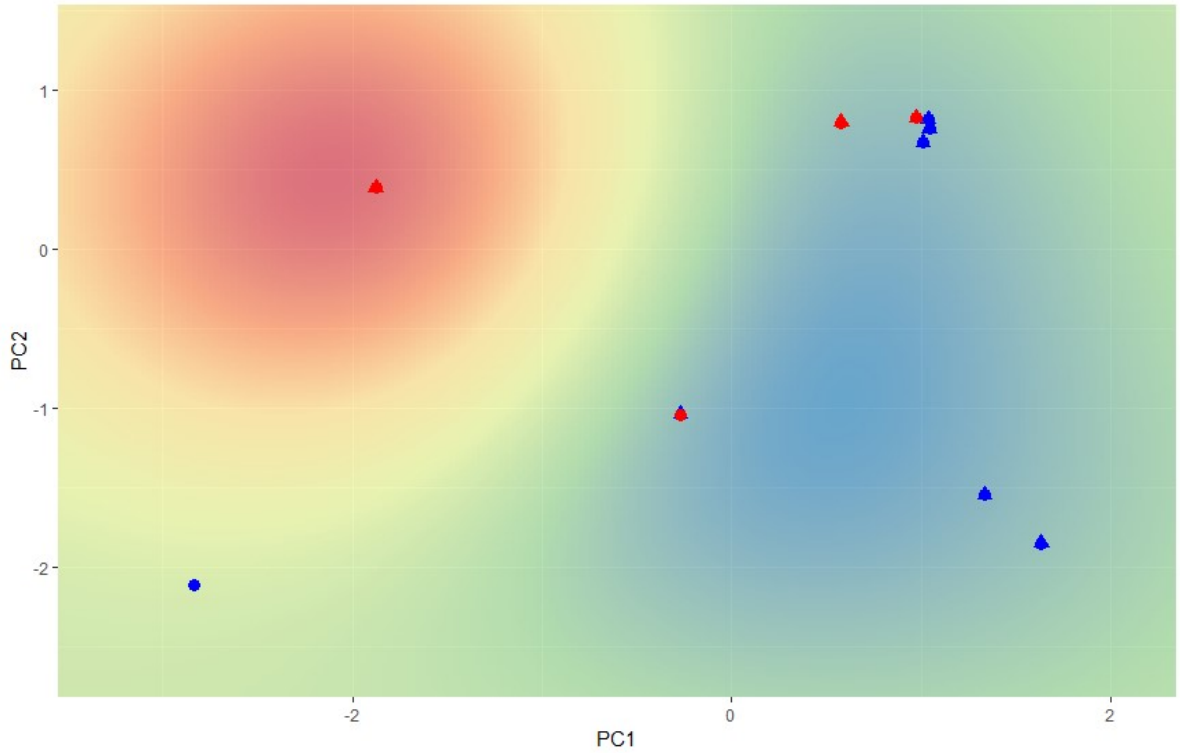

Figure 19: Decision regions of the SVM model applied on all descriptors after removing redundant ones, in the space of the first two principal components. NMs classified as toxic are highlighted in red, non-toxic in blue. Circles are NMs in the training set, triangles represent NMs in the test set.

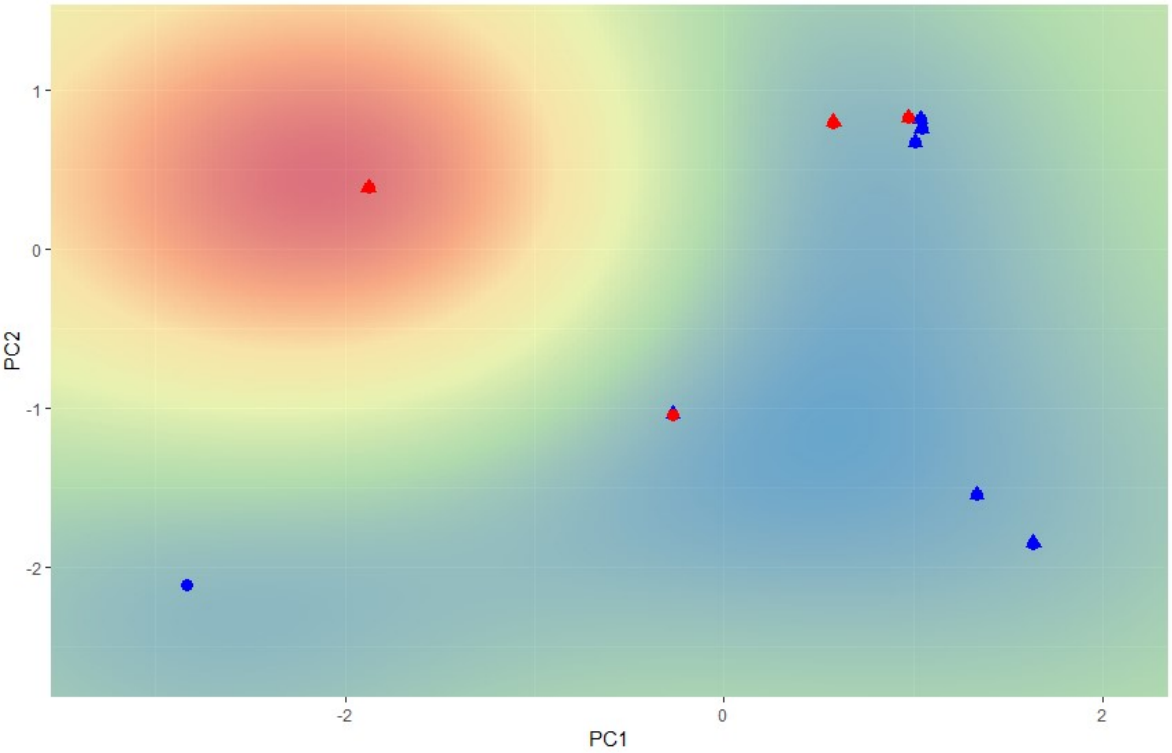

Figure 20: Decision regions of the SVM model applied after PCA, in the space of the first two principal components. NMs classified as toxic are highlighted in red, non-toxic in blue. Circles are NMs in the training set, triangles represent NMs in the test set.

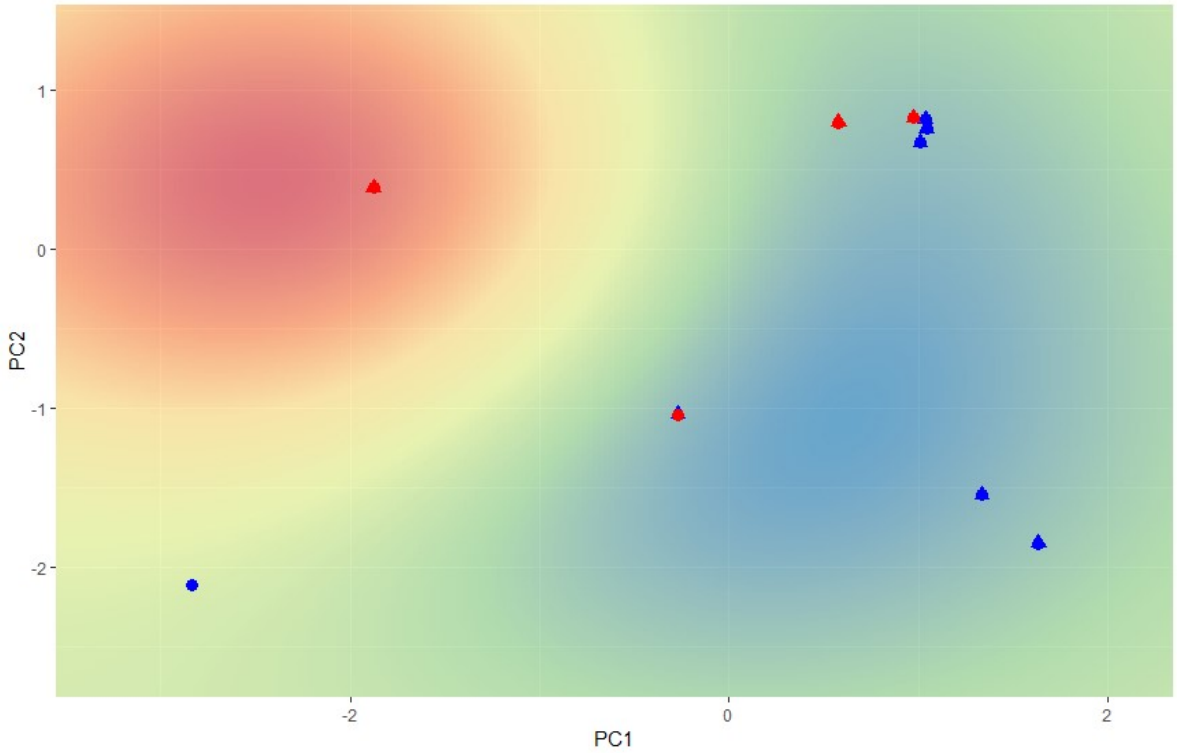

Figure 21: Decision regions of the novel Subspace Clustering method, in the space of the first two principal components. NMs classified as toxic are highlighted in red, non-toxic in blue. Circles are NMs in the training set, triangles represent NMs in the test set.

From such decision region it is possible to understand why the performances of the models (and of original models) are not so excellent: in their test, authors performed their experiments on the same set of NMs, varying the cytotoxicity concentration. Hence data is overlapping.

Thus, as Jones et al. (2015) [143] did, we repeated the modelling including to the pool of descriptors the cytotoxicity concentration. After removing strongly correlated descriptors and constant descriptors, we end up with a total of 4 descriptors from the initial pool of 26 descriptors. Original results and results of our experiments, expressed in terms of balanced accuracy, sensitivity and specificity, are presented in Table 19, while the decision regions of the models that we trained are presented in Figure 22 (SVM computed on all descriptors), Figure 23 (SVM after PCA), and Figure 24 (Subspace Clustering method). All the NMs were classified inside the AD of the model.

Table 19: Results expressed in terms of Balanced Accuracy, Sensitivity and Specificity for the dataset originally provided by Jones et al. (2015) [143], including cytotoxicity concentration as descriptor. Best performances are highlighted in bold font.

	Balanced accuracy	**Sensitivity**	**Specificity**
Original work [143]	65%-**95%**	80-**95%**	65-95%
SVM on all descriptors	**95%**	90%	**100%**
SVM after PCA	**95%**	90%	**100%**
Subspace Clustering method	**95%**	90%	**100%**

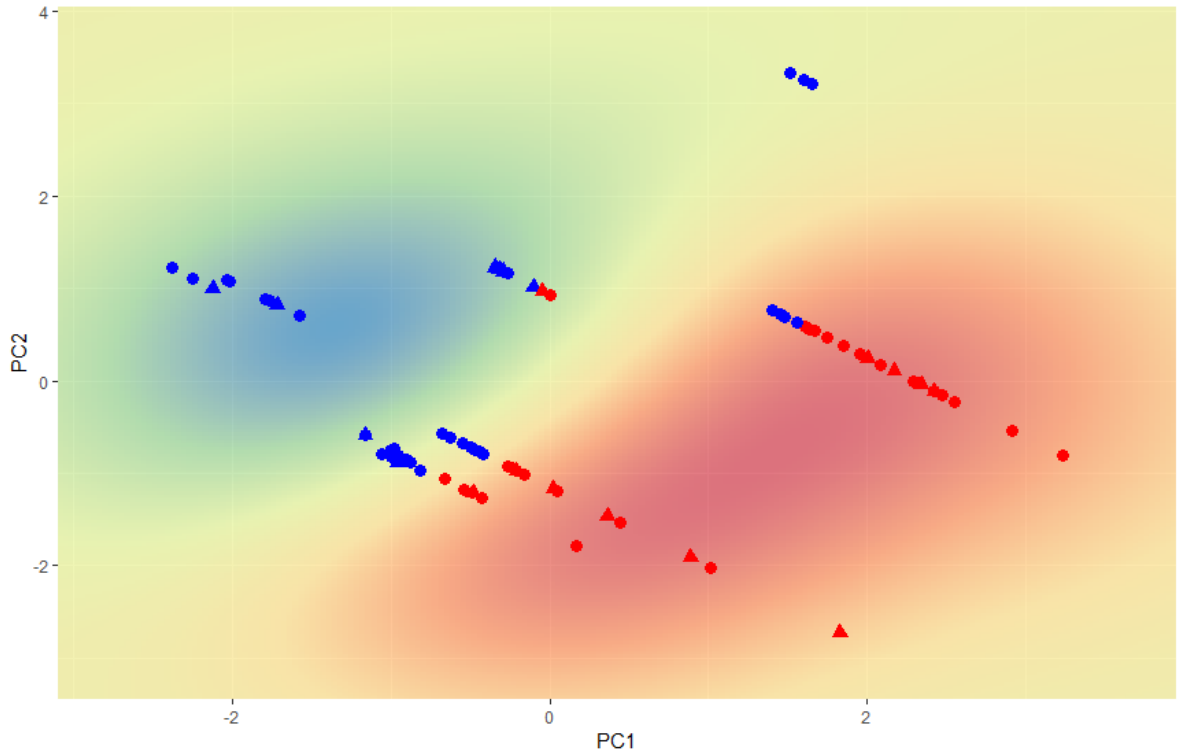

Figure 22: Decision regions of the SVM model applied on all descriptors including cytotoxicity concentration after removing redundant ones, in the space of the first two principal components. NMs classified as toxic are highlighted in red, non-toxic in blue. Circles are NMs in the training set, triangles represent NMs in the test set.

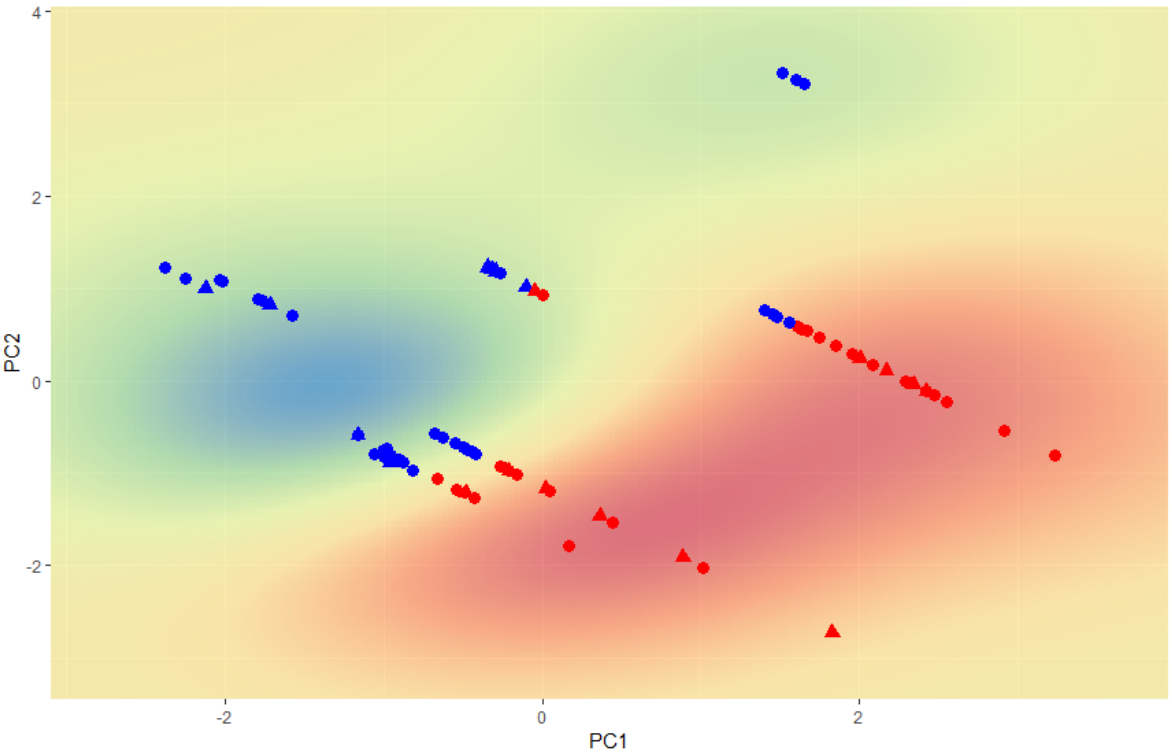

Figure 23: Decision regions of the SVM model applied after PCA including cytotoxicity concentration, in the space of the first two principal components. NMs classified as toxic are highlighted in red, non-toxic in blue. Circles are NMs in the training set, triangles represent NMs in the test set.

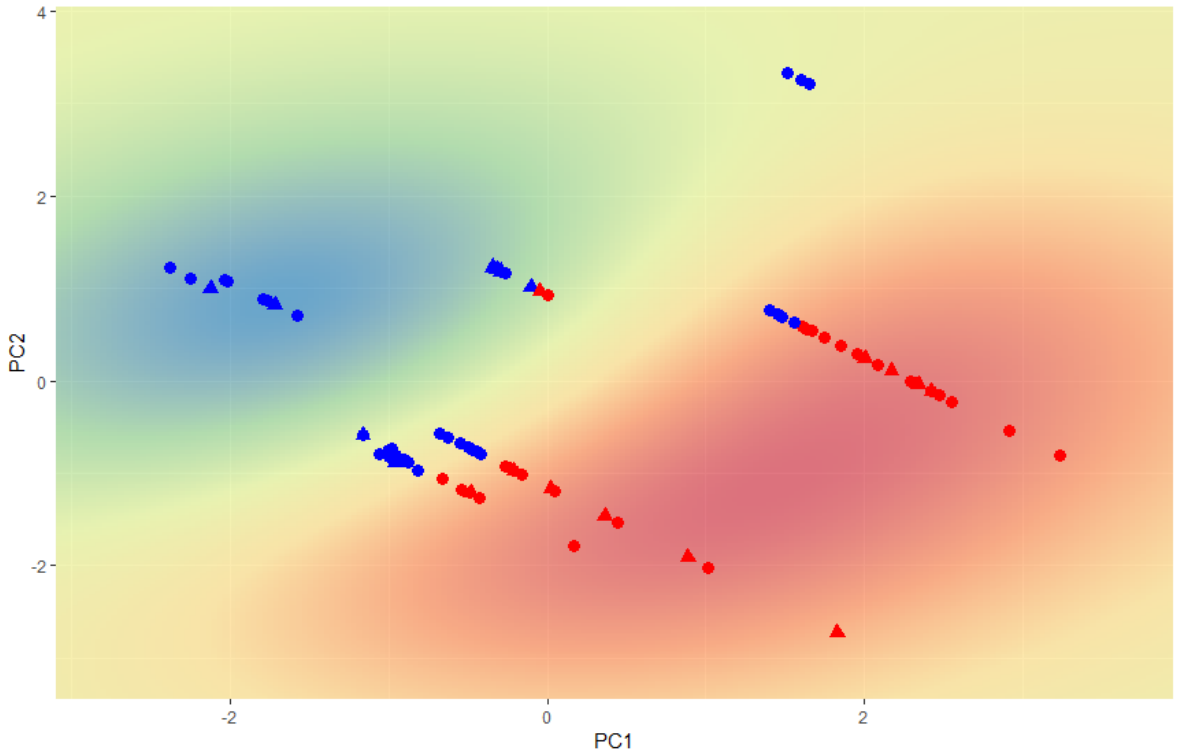

Figure 24: Decision regions of the novel Subspace Clustering method (including cytotoxicity concentration), in the space of the first two principal components. NMs classified as toxic are highlighted in red, non-toxic in blue. Circles are NMs in the training set, triangles represent NMs in the test set.

As expected, with this new setting the performances became almost perfect. All our developed approaches shown the same performance with respect to the best performing approach provided by Jones et al. (2015) [143]. Again, one of the approaches originally provided was able to classify as such an additional NM with respect to our approaches (and at the same time, it classified as active a toxic NM). Again, we stress out that in the original study authors chosen the descriptors to be included to the model by expert judgment.

4.3.2 Cytotoxicity of Metal Oxides

After removing strongly correlated descriptors and constant descriptors, we end up with a total of 26 descriptors from the initial pool of 203 descriptors. Then we performed the experiments described in section 4.2.1.2: original results and results of our experiments, expressed in terms of balanced accuracy, sensitivity and specificity, are presented in Table 20, while the decision regions of the models that we trained are presented in Figure 25 (SVM computed on all descriptors), Figure 26 (SVM after PCA), and (Subspace Clustering method). All the NMs were classified inside the AD of the model.

In this case, our novel approach has exactly the same performance of the original one and of the SVM classifier trained after PCA. On the other hand, the SVM model trained on all descriptors has bad performances (50% balanced accuracy and 33% Sensitivity), demonstrating that when the number of descriptors become high, it is more difficult for ML techniques to provide good results. In this case, indeed, even after discarding correlated descriptors, we used 26 descriptors for modelling.

All the test NMs felt inside the Ad of the models.

Table 20: Results expressed in terms of Balanced Accuracy, Sensitivity and Specificity for the dataset originally provided by Sizochenko et al. (2015) [74]. Best performances are highlighted in bold font.

	Balanced accuracy	**Sensitivity**	**Specificity**
Original work [74]	**83%**	**100%**	**67%**
SVM on all descriptors	50%	33%	**67%**
SVM after PCA	**83%**	**100%**	**67%**
Subspace Clustering method	**83%**	**100%**	**67%**

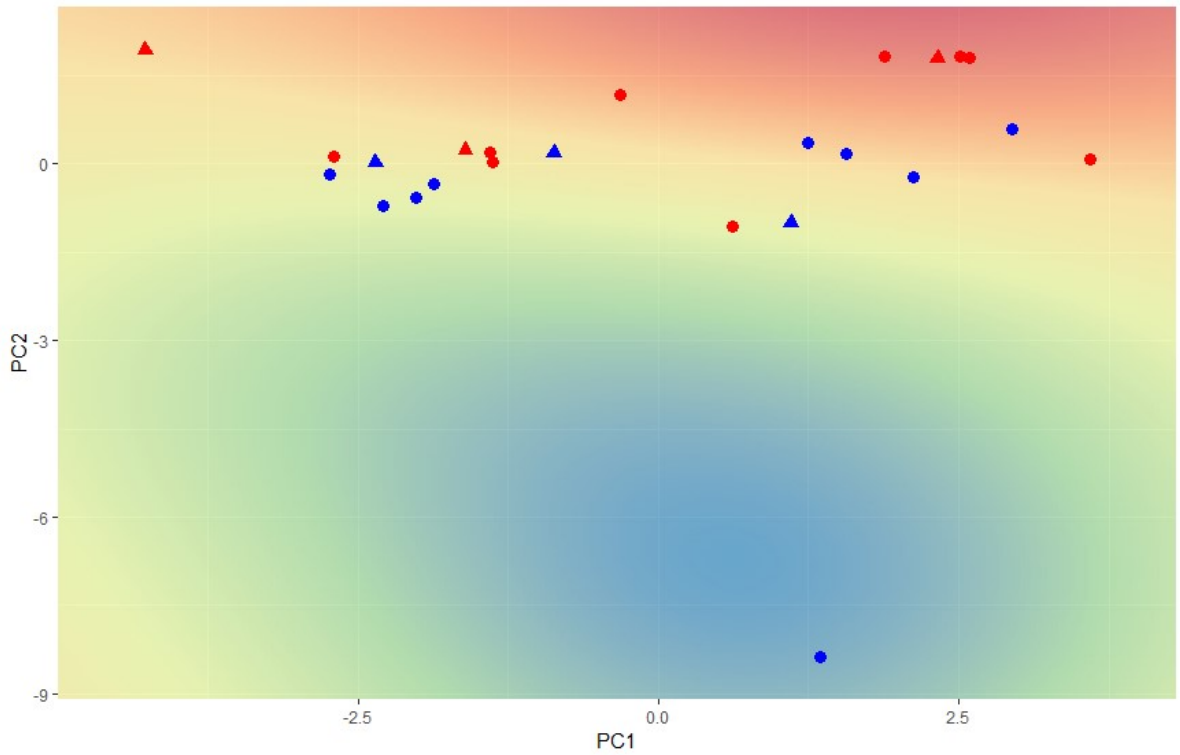

Figure 25: Decision regions of the SVM model applied on all descriptors (26) after removing redundant ones, in the space of the first two principal components. NMs classified as toxic are highlighted in red, non-toxic in blue. Circles are NMs in the training set, triangles represent NMs in the test set.

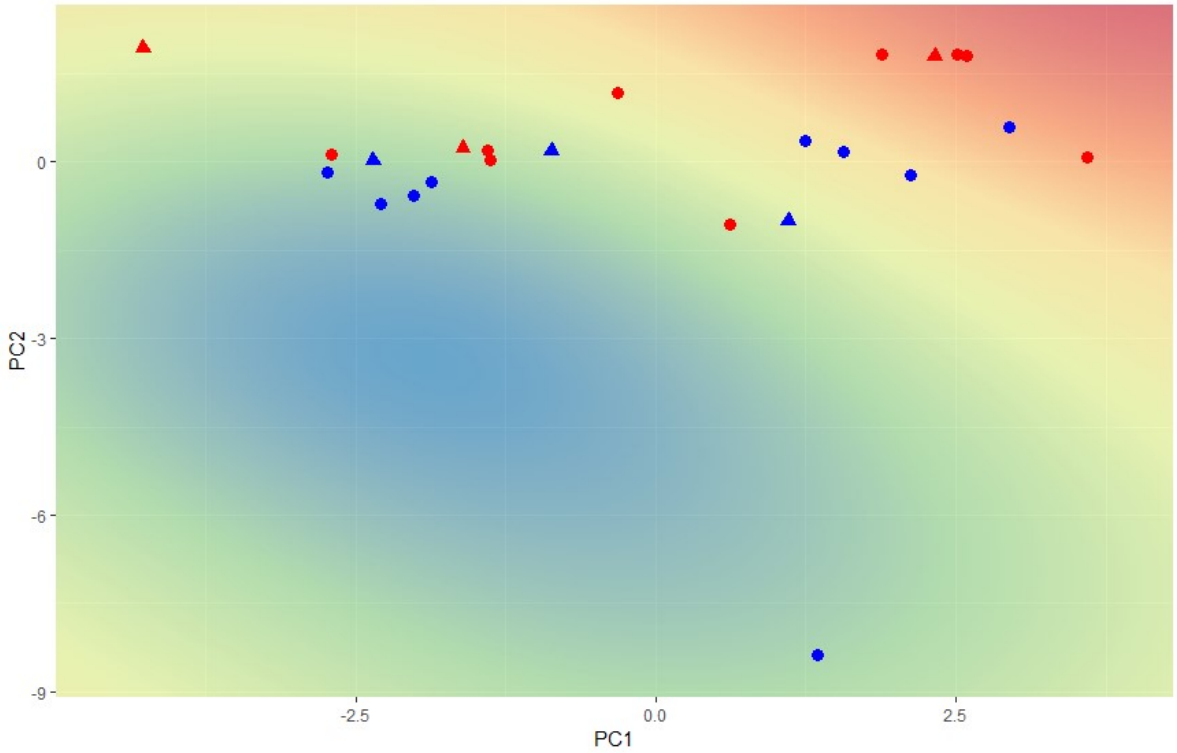

Figure 26: Decision regions of the SVM model applied after PCA, in the space of the first two principal components. NMs classified as toxic are highlighted in red, non-toxic in blue. Circles are NMs in the training set, triangles represent NMs in the test set.

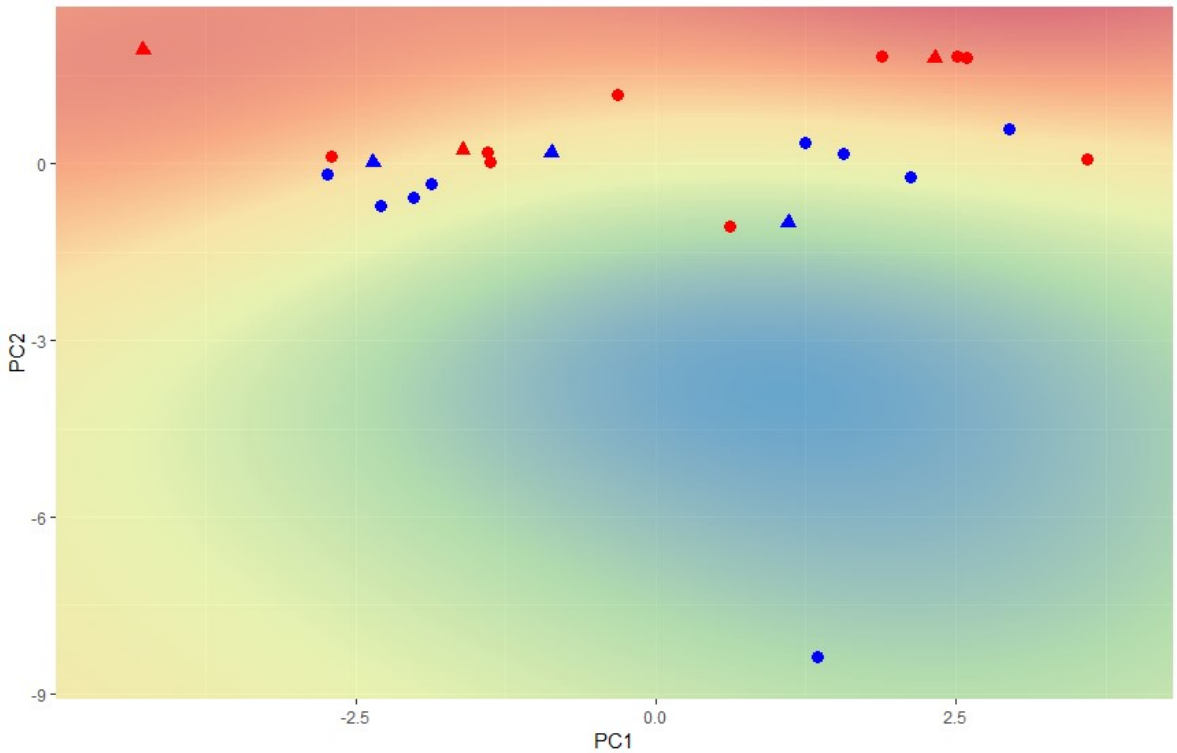

Figure 27: Decision regions of the novel Subspace Clustering method, in the space of the first two principal components. NMs classified as toxic are highlighted in red, non-toxic in blue. Circles are NMs in the training set, triangles represent NMs in the test set.

4.3.2 NanoTox Class dataset

Results of experiments, expressed in terms of balanced accuracy, sensitivity and specificity, are presented in Table 21. All the test NMs felt inside the AD of the models. In this case, our novel approach performed better of all the other tested approaches in terms of balanced accuracy, in addition, together with the Read-Across like method based on Euclidean Distance, it was able to provide the better ability to correctly identify toxic substances as such (60% sensitivity). SVM on all descriptors shown a 100% specificity, but this is because it always classified as non-toxic each NM.

Table 21: Results expressed in terms of (leave One Out) Cross Validated Balanced Accuracy, Sensitivity and Specificity for the NanoTox Class dataset. Best performances are highlighted in bold font.

	LOO CV Balanced accuracy	**LOO CV Sensitivity**	**LOO CV Specificity**
Random Forest	55%	40%	67%
PCA + NN	45%	20%	67%
Read-Across like method	63%	**60%**	67%
SVM on all descriptors	55%	0%	**100%**
SVM after PCA	55%	40%	67%
Subspace Clustering method	**72%**	**60%**	83%

Due to the limited number of samples and the fact that here we performed cross validation, decision regions are not displayed for this case study. It is worth nothing that the dataset is not yet complete, hence these are intended to be preliminary results.

4.4 Conclusions

According to the first results of our methodology presented in this chapter, Subspace Clustering seems to be promising tool for both Read-Across and Categorization purposes, being able to provide better or comparable results with respect to already published ones when applied to existing datasets or on new data. Indeed, we believe that further work can be done following this path, thus providing new insights to scientists and risk assessors.

Future works include testing the method on further datasets, and to predict quantitatively the endpoint value (i.e.: by a regression model, averaging the predictions in each subspace), perform Uncertainty and Sensitivity analysis, and provide a mechanistic interpretation for the model. A good starting point for providing a mechanistic interpretation could be to start looking at each cluster found in the subspace and on the corresponding descriptors, and to try to give a mechanistic interpretation on why each particle is clustered together using that subset of descriptors.

5 SUNDS: SUN Decision Support System

5.1 Introduction

The main idea behind the EU FP7 SUN (Sustainable Nanotechnologies) Project was that the current knowledge on environmental and health risks of nanomaterials – while limited – can nevertheless guide nanomanufacturing to avoid liabilities if an integrated approach addressing the complete product lifecycle (Synthesis, Formulation, Use, and End of Life) is applied. It was launched on 1 October 2013 and continued for 42 months, bringing together 35 partners from 12 EU countries, with a total budget of about 13.5 million EUR.

Within the SUN project, I collaborated with the SUN team of developers an online software Decision Support System (DSS): SUNDS (http://sunds.gd). It estimates the occupational, consumer and environmental risks from manufactured nanomaterials (NMs) in real industrial products along their lifecycles, integrating the bottom-up generation of nano-EHS (Environmental and Health Safety) data and methods with the top-down design of a DSS. SUNDS comprises LICARA NanoSCAN [258], a screening-level tool developed within the FP7 LICARA project specifically for Small and Medium Enterprises (SMEs), who often lack the resources and expertise to apply complex DSS. Indeed, LICARA NanoSCAN is a user-friendly screening-level tool with relatively low data requirements that provides a semi-quantitative evaluation of the environmental, social and economic benefits and the ecological, occupational and consumer health risks of NMs in products from lifecycle perspective. In addition, LICARA NanoSCAN is a tool that can assist SMEs in checking supplier risks, competing products, market opportunities or making an internal risk and benefit analysis. In addition to LICARA, SUNDS includes a more advanced quantitative tool for risk and sustainability assessment, which will be described in this chapter. In situations where the risks are not controlled SUNDS propose suitable Risk Management Measures, including information about their costs compared to the benefits of the nanotechnologies.

Risk control (RC) can be demonstrated by reducing risk to below threshold levels or by investigating feasible alternatives to the substance. If risks are not adequately controlled and no feasible alternatives to a substance are found, Socioeconomic Analysis (SEA) is used to demonstrate that benefits of using a certain MN significantly outweigh the costs. SEA analyses all environmental, economic and social impacts, at both micro and macro levels. Integrating RC and SEA within the SUNDS allows its users to be guided on the technical and economic performance of Risk Management along the lifecycle for nano-enabled products.

Figure 28 shows the general schematic for the conceptual framework behind SUNDS. In addition to the two tiers displayed in the figure, which will be described in details in the following sections, a stand-alone module based on CENARIOS (Certifiable Nanospecific Risk-Management and Monitoring System) ® [259,260] is included in the DSS. It covers a representative selection of the specific requirements stipulated in the certification standard. It thereby enables interested enterprises to assess their level of fulfilment (in terms of requirements of the certification standard) in an independent and inexpensive manner.

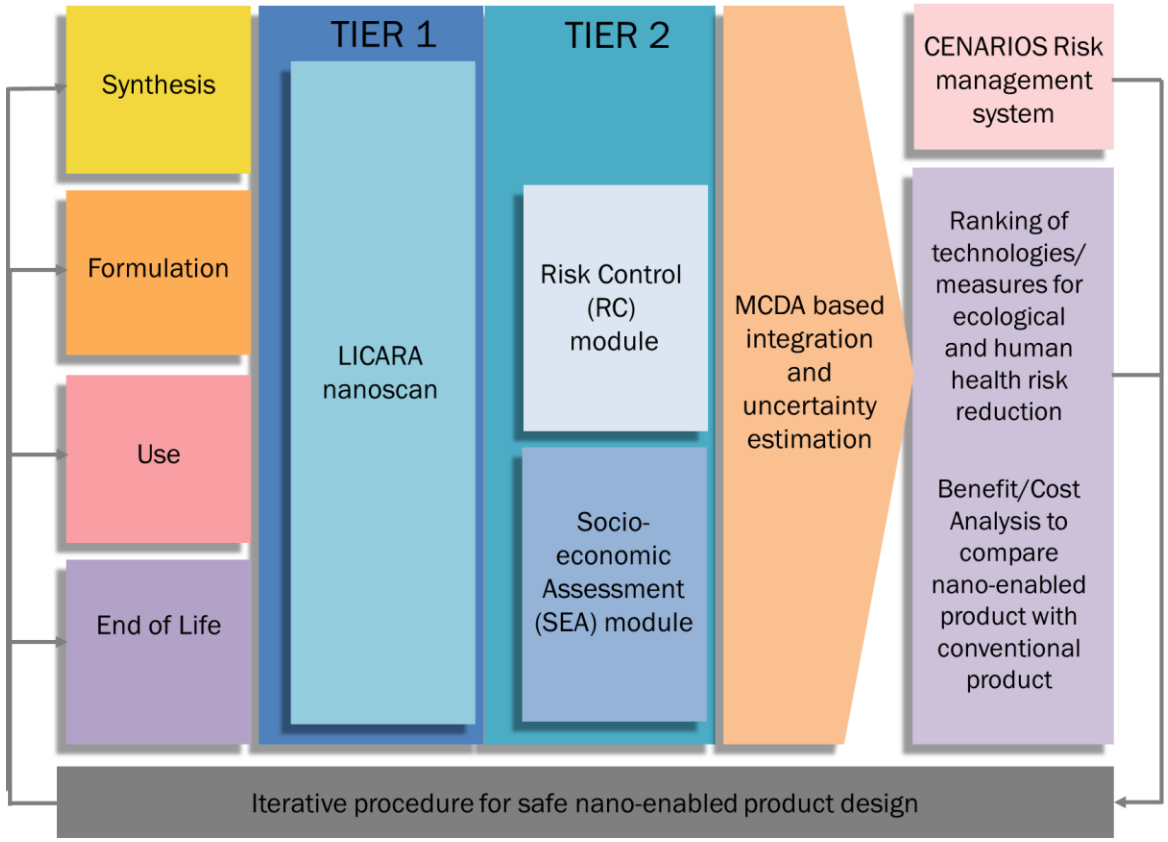

Figure 28: SUNDS Conceptual Decision Framework.

Tier 1 of the DSS comprise of the LICARA NanoSCAN tool, while SUNDS Tier 2 implements the RC and SEA modules.

My contribution in the overall development of SUNDS mainly focused on the Risk Control modules (ERA, HHRA and RC), and on the development of R-SUNDS, a web server which provides a REST API to a set of R models which are included in SUNDS. For this reason, CENARIOS ®, Tier 1, and SEA modules will be shortly introduced in the next section (as well as the RC modules) but will not be further discussed in this thesis. On the other hand, in chapters 6, 7 and 8 different case studies that applied the RC module of SUNDS will be presented in detail.

5.2 SUNDS modules

5.2.1 CENARIOS® module

CENARIOS® module encompasses five sections with specific requirements (general, staff-related, organizational, risk assessment and monitoring requirements and requirements related to risk treatment and communication).

Within SUNDS, a questionnaire linked to the CENARIOS® system is implemented as a stand-alone module. It covers a representative selection of the specific requirements stipulated in the certification standard, thus providing an evaluation of the status of companies' organizational risk management for nanomaterials. Moreover, advices on how to improve organizational Risk Managements Systems (RMS) are provided to users, highlighting existing gaps that need to be addressed to comply with CENARIOS® certification standard [259,260].

5.2.2 Tier 1 - LICARA NanoSCAN

LICARA NanoSCAN is part of the LICARA Guidelines for the sustainable competitiveness of nanoproducts (2014) [261]. It is aimed at guiding SMEs through their decision-making processes about new nanoproducts, by: (i) scanning both the benefits and risks over the nanoproduct's lifecycle in comparison to a conventional product with a similar functionality, (ii) estimating economic, environmental and social opportunities, (iii) identifying the nano-specific risks facing consumers, workers and the public and the environment, (iv) supporting interpretation of the results, reflected in a consistent argument about the weaknesses and strengths of the nanoproduct, (v) giving guidance on next steps, (vi) using little quantitative data, (vii) combining state-of-the-art know-how in Lifecycle Assessment and Risk Assessment, (viii) integrating existing tools that are backed by renowned agencies or private institutions, and (ix) using a modular approach.

The questionnaire is divided in 7 sections: Nano product and Legislation, Environmental Benefits, Economic Benefits, Societal Benefits, Public Health & Environmental Risks, Occupational Health Risks (Figure 15), and Consumer Health Risks. The user Interface is very similar to the one of the CENARIOS® module, while results (displayed to the user by means of graphs) are exportable in PDF.

5.2.3 Tier 2 modules

When a new project is created, and Tier 2 is subsequently selected, the user is asked to specify which Environmental and Human Health exposures scenarios (and associated risks) he wants to assess. It is possible in any time to change this selection, and in such cases all the scenarios associated with the project will be updated accordingly. Such project scenarios comprise the exposure scenarios selected by the users, and the associated hazards, and can be created, cloned or deleted in any moment. It is important to stress out again that the selection of the exposure scenarios is done at project level: each project scenarios inside a project will thus have the same exposure scenarios.

For each project scenario, the user can select one of the four modules of Tier 2: Risk Assessment (that allows to assess risk through probabilistic and deterministic methodologies, both for Human Health and the Environment, along the lifecycle of the substance), Risk Control (that highlights hotspots, i.e. risks derived in Risk Assessment sub-modules that are not acceptable, proposing to apply different technologies to reduce them), Additional Sustainability Aspects (that include LCIA, Economic Assessment and Social Impact Assessment), and Socio-Economic Assessment (a module that considers all the previous sub-modules results, to derive a sustainability portfolio and allow identification of hotspots).

5.2.3.1 Risk Assessment and Control modules

The RC module comprises of two risk sub-modules, namely The Ecological Risk Assessment (ERA) module, and the Human Health Risk Assessment (HHRA) module, plus an additional module that simulates the application of Technological Alternatives and Risk Management Measures (TARMMs) to reduce the risks assessed in the previous two modules. These modules are introduced in the following subsections.

A simplified scenario of application of this module is the following. A manufacturer may be interested in evaluating the risk associated to a nano enabled product (NEP) for a specific application. The RC module first creates a quantitative risk profile using the RA sub-modules embedded in the SUNDS Tier 2. Specifically, outputs from exposure (occupational, consumer and ecological) and hazard ((eco)toxicological profiles) are integrated

using MCDA to obtain an assessment of occupational health (oHRA), consumer health (cHRA), public health (pHHRA) and ecological (ERA) risks. Assume that this profile indicates that some human health risks (e.g. related to specific workers' activities) are not adequately controlled, the TARMM inventory provides a ranking of TARMM based on efficiency of occupational risk reduction and related costs. This ranking is used to build alternative occupational exposure scenarios, leading to alternatives to the initial scenario. If the risk profiles for the alternative scenarios show occupational health risk is reduced to an acceptable level, the user can then select the alternative using which risk is controlled at lowest cost. An overview on the submodules is provided in the following subsections.

The user interface for inserting Environmental and Human Health data is the same: for HHRA exposure routes and types previously selected are listed, in Exposure and Hazard, and user can insert available data, i.e. Derived No-Effect Levels (DNELs) for toxicity endpoints (also called threshold endpoints) and Derived Minimal Effect Levels (DMELs) for carcinogenic and genotoxic endpoints (also called threshold endpoints), and Exposures, either deterministic or probabilistic (by means of confidence values, i.e. 5th and 95th percentile).

Similarly, for ERA, the user can insert available data both for Effect, inserting Predicted No Effect Concentrations (PNECs) and Predicted Environmental Concentrations (PECs), either deterministic or probabilistic.

When both Exposure and Hazard (Effect) are available, SUNDS automatically assess the risk related to the exposure scenario or the environmental compartment. Risks are assessed in terms of Risk Characterization Ratios (RCRs), namely Exposure/Effect (Hazard). This results in a distribution (when either Exposure or Effect/Hazard, or both, are probabilistic) or in a deterministic value. If part of the RCR distribution (or the resulting value in case of deterministic RCR) is greater than 1 (it means that exposure is greater than the DNEL or the PNEC), it means that there is some risk. This risk, however, can be classified in the case of HHRA as acceptable if less than 5% of the probabilistic RCR (1% in case of ERA) is not greater than 1. Similarly, in case of HHRA if the portion of RCR that is greater than 1 is between 5% and 10% (between 1% and 5% in case of ERA), risk needs further consideration. Results are displayed to the user in terms of charts, and intermediate results (e.g. dose response model derived by PROAST) are displayed in the Results subsections of both HHRA and ERA modules.

If, instead, deterministic or probabilistic data are not available, and one needs to run one of the models included in SUNDS, by clicking on the corresponding button in the list of hazards/exposure scenarios, the user is redirected to the corresponding input module, or to an external model. In case of a model included in, the User Interface to provide input to the model is always similar: a set of questions are posed and/or data is requested. Once all data needed is inserted the user can launch the corresponding model. In some cases, to derive results it is necessary to perform more than one step. When possible, intermediate results are displayed to the user within this interface.

On the other hand, in the Risk Control module it is possible to apply different technologies to reduce exposures in each exposure scenario: specifically, the exposure scenarios that resulted in risk (hotspots) are highlighted, and the available technologies applicable in such scenarios are on top of the list, thus making simple to the user to immediately simulate their application to reduce risk.

5.2.3.1.1 Environmental Risk Assessment (ERA) module

The ERA module derives ecological risk quantitatively by integrating outputs from: a) an environmental exposure model that estimates PECs in different environmental compartments (e.g. water, soil), and b) deterministic procedures or Species Sensitivity Distributions (SSDs) that estimate PNECs for various species in the ecosystem in these compartments.

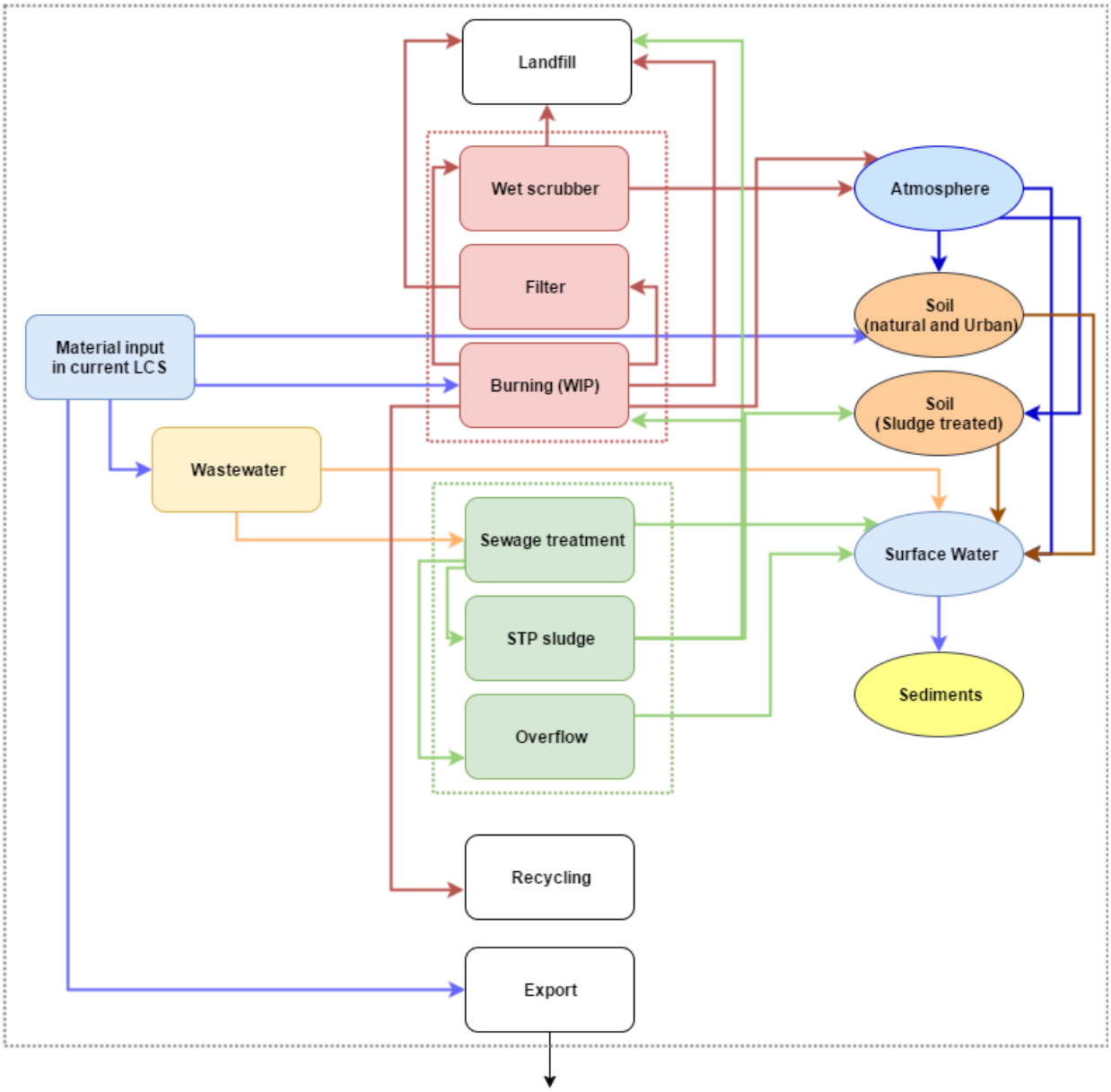

Figure 29: Material Flow. Compartments and possible transfer directions among compartments are fixed, the user is allowed to insert a transfer coefficient for each arrow. Selecting 0 as coefficient means that there is no material transfer between the two compartments.

In case the user wants to derive PECs related to a specific Lifecycle Stage, she/he first needs to specify the quantity (expressed in tons) of material per year in the system (in the current Lifecycle Stage). By default, the system of reference is Europe, but one can change it (in this case he needs to change the volumes of natural compartments, inserting volumes relative to the system under investigation). Subsequently, he can start inserting data related to each natural and technical compartment (possible compartments, and transfer among the compartments, are summarized in Figure 29), specifying transfer coefficient from the compartment to other compartment, and material fate in the compartment, in case a portion of material degrades or is eliminated in the compartment (e.g.

portion of material being burnt and eliminated from the system in a Waste Incineration Plant). The portion of material that is not eliminated and does not transfer to other compartments is assumed to deposit in the compartment.

While a normal distribution is assumed for input material in the system, the user can specify distributions for fate and transfer coefficients. Specifically, he can choose between:

- Uniform distribution: this distribution can be used in case of deterministic (i.e.: constant) coefficients, but also in case of more than one coefficient, in the latter case transfer coefficients are uniformly sampled between min and max coefficients specified by the user, and other values are ignored;
- Triangular distribution: in this case, min and max coefficients are taken as extremes of the distribution, while median value is considered as the peak;
- Normal distribution: mean and standard deviations are derived from input coefficients, and transfer coefficients are sampled from a uniform distribution with such mean and standard deviation;
- Sample from user input (bootstrapping): in this case, transfer coefficients are sampled with replacement from coefficients provided in input.

Once all the data is inserted, and the computation completes, SUNDS is responsible to update PECs of all compartments and to compute (if possible) new risks.

Derivation of Predicted No Effect Concentrations (PNECs)

To derive a PNEC, user is asked to insert information on available (eco)toxicological data. Accordingly, SUNDS applies the suitable Assessment Factor (AF) as proposed by the EU REACH regulation [262] and derives the deterministic PNEC. Specifically, the AFs applied to derive a PNEC for aquatic compartments are reported in Table 22, AFs applied to derive a PNEC for the freshwater sediment compartment are reported in Table 23, AFs applied to derive a PNEC for the marine sediment compartment are reported in Table 24, while in Table 25 are reported the AFs for soil environmental compartments. The AF is applied to the lowest data available.

Table 22: Assessment factors for deriving a PNEC for aquatic environmental compartments [262]. The assessment factor is applied to the lowest data available.

Available data	**Assessment factor**
At least one short-term L(E)C50 from each of three trophic levels (fish, invertebrates (preferred Daphnia) and algae)	1000
One long-term EC10 or NOEC (either fish or Daphnia)	100
Two long-term results (e.g. EC10 or NOECs) from species representing two trophic levels (fish and/or Daphnia and/or algae)	50
Long-term results (e.g. EC10 or NOECs) from at least three species (normally fish, Daphnia and algae) representing three trophic levels	10
At least 10 long-term NOAEC (preferably 15) from at least 8 species are available	1 (pSSD model)
Field data or model ecosystems is available	Case-by-case

Table 23: Assessment factors for deriving a PNEC for the freshwater sediment environmental compartment [262]. The assessment factor is applied to the lowest data available.

Available data	Assessment factor
One long-term test (NOEC or EC10)	100
Two long-term tests (NOEC or EC10) with species representing different living and feeding conditions	50
Field data or model ecosystems is available	10

Table 24: Assessment factors for deriving a PNEC for the marine sediment compartment [262]. The assessment factor is applied to the lowest data available.

Available data	Assessment factor
One acute freshwater or marine test	10000
Two acute tests including a minimum of one marine test with an organism of a sensitive taxa	1000
One long-term freshwater sediment test	1000
Two long-term freshwater sediment tests with species representing different living and feeding conditions	500
One long-term freshwater and one saltwater sediment test representing different living and feeding conditions	100
Three long-term sediment tests with species representing different living and feeding conditions	50
Three long-term tests with species representing different living and feeding conditions including a minimum of two tests with marine species	10

Table 25: Assessment factors for deriving a PNEC for soil compartments [262]. The assessment factor is applied to the lowest data available.

Available data	Assessment factor
L(E)C50 short-term toxicity test(s) (e.g. plants, earthworms, or microorganisms)	1000
NOEC for one long-term toxicity test (e.g. plants)	100
NOEC for additional long-term toxicity tests of two trophic levels	50
NOEC for additional long-term toxicity tests for three species of three trophic levels	10
At least 10 long-term NOAEC (preferably 15) from at least 8 species are available	1 (pSSD model)
Field data or model ecosystems is available	Case-by-case

Once the correct Assessment Factor is selected, and the corresponding PNEC is derived, if exposure data is available risk is computed.

If at least 10 long-term NOECs are available from different species (covering at least 8 taxonomic groups), it is possible to derive a probabilistic PNEC starting from Probability Species Sensitivity Distribution (pSSD). The user has to insert NOECs values as endpoint values (in future, it will be possible to insert other type of values, and the proper transformation will be applied to derive a NOEC from short terms studies [263]). More than one value for a species can be inserted using the same species name. It is also possible to specify confidence values for NOECs,

in this case data will be considered as endpoint value ± confidence value. Moreover, it is possible to specify the number of numerical simulations to perform. Each simulation provides an SSD curve, and once all simulations are performed SUNDS takes the 5th percentile from each SSD, which corresponds to the hazardous concentration for the five percent of the species (HC5), and then uses the distribution of these percentiles as probabilistic PNEC for the environmental matrix in the Lifecycle Stage. If possible, it also computes probabilistic risk using this PNEC.

5.2.3.1.2 Human Health Risk Assessment (HHRA) module

The HHRA module estimates the risks for humans (general population, Occupational and Consumer population) exposed to nanomaterials via the environment by integrating outputs from deterministic and probabilistic procedures for dose-response assessment and intra/inter-species and from exposure assessment. The resulting estimation of human health risk will be always quantitative, but either deterministic (in case of deterministic DNEL/DMEL) or probabilistic (i.e. 5% of the population has at least a 10% response with 95% confidence) depending on the nature, quantity and quality of the input exposure and effects data.

As for ERA module, it is possible to directly provide Exposure and Hazards by means of deterministic values or probabilistic confidence intervals (exposure is assumed normally distributed, hazard log-normally distributed), or to use one of the models included in SUNDS or linked to SUNDS.

For a specific hazard, usually more than a single biomarker is available for a (set of) endpoints(s), thus in SUNDS it is possible to insert all the available data, and the system automatically selects the most conservative biomarker for computing the risk. The user, in any case, is allowed to make a different choice, for instance when he/she has more confidence on a specific result.

Derivation of Exposure

In addition to allowing the possibility to manually enter a deterministic exposure, or confidence intervals for a probabilistic exposure (assumed to be normally distributed), SUNDS provides an interface for NanoSafer to estimate a deterministic exposure for Human Health Risk Assessment. Specifically, questions related to material properties and on the process, which causes the exposure to workers are asked to the user. Once all values are provided, it is possible to send data to NanoSafer API, which in response provides daily and acute exposure results for near and far field, and a toxicity score. The highest daily exposure value is used as deterministic Exposure for HHRA, and if possible (i.e.: DNEL or DMEL are available) risk is computed. Moreover, SUNDS allows users to use other external models, such as Consexpo Nano, but in this case it is requested to retrieve the results and copy it into SUNDS.

Derivation of A Derived No Effect Level (DNEL) for threshold endpoints

In case of threshold endpoints, it is possible to derive a DNEL. Such endpoints are listed, together with a definition, in Table 26.

Table 26: Threshold endpoints, with definition provided by REACH [264] and/or CLP regulation [265].

Endpoint	Definition
Skin corrosion	The production of irreversible damage to skin; namely, visible necrosis through the epidermis and into the dermis, following the application of a test substance for up to four hours. Corrosive reactions are typified by ulcers, bleeding, bloody scabs, and, by the end of observation at 14 days, by discolouration due to blanching of the skin, complete areas of alopecia, and scars.

Endpoint	Definition
Skin irritation	The production of reversible damage of the skin following the application of a test substance for up to 4 hours.
Dermal concern after repeated exposure	Used for a substance which may cause skin dryness, flaking or cracking upon repeated exposure but which cannot be considered as skin irritant.
Serious eye damage	The production of tissue damage in the eye, or serious physical decay of vision, following application of a test substance to the anterior surface of the eye, which is not fully reversible within 21 days of application.
Eye irritation	The production of changes in the eye following application of a test substance to the anterior surface of the eye, which are fully reversible within 21 days of application.
Respiratory tract corrosion*	Destruction of the respiratory tract tissue after a single, limited period of exposure analogous to skin corrosion; this includes destruction of the mucosa.
Respiratory tract irritation*	Transient target organ effect, i.e. an effect which adversely alter(s) human function for a short duration after exposure and from which humans may recover in a reasonable period without leaving significant alteration of structure or function. More specifically, respiratory tract irritation is often used to describe either or both of two different toxicological effects, sensory irritation and local cytotoxic effects. However, classification in STOT SE Category 3 for respiratory tract irritation is generally limited to local cytotoxic effects: respiratory irritant effects are characterized by localized redness, edema, pruritis and/or pain and they impair function with symptoms such as cough, pain, choking, and breathing difficulties.
Skin sensitization	A skin sensitizer is an agent that will lead to an allergic response in susceptible individuals following skin contact. As a consequence of a secondary - usually organ-specific - subsequent re-exposure, adverse health effects on the skin (allergic contact dermatitis).
Respiratory sensitization	an agent that will lead to hypersensitivity of the airways following inhalation exposure to that agent. Respiratory sensitization (or hypersensitivity) is a term that is used to describe asthma and other related respiratory conditions (rhinitis, extrinsic allergic alveolitis), irrespective of the mechanism (immunological or non-immunological) by which they are caused.
Acute toxicity	Adverse effects occurring following oral or dermal administration of a single dose of a substance or multiple doses given within 24 hours, or an inhalation exposure of 4 hours.
Repeated dose toxicity	Comprises the general toxicological effects occurring as a result of repeated daily dosing with, or exposure to, a substance for a part of the expected lifespan (sub-acute or sub-chronic exposure) or for the major part of the lifespan, in case of chronic exposure. Repeated dose toxicity studies provide information on possible adverse general toxicological effects likely to arise from repeated exposure to a substance. Furthermore, these studies may provide information on e.g. reproductive toxicity and carcinogenicity, even though they are not specifically designed to investigate these endpoints.
Reproductive toxicity	Covers both the effects on fertility and development. Fertility is seen as a broad concept covering all the effects on the reproductive cycle except for developmental toxicity.

* There is no EU or OECD TG for respiratory tract corrosion and respiratory tract irritation under REACH.

Again, it is possible to specify deterministic or probabilistic (through confidence intervals of a lognormal distributions) values for each biomarker describing one of the threshold endpoints in Table 25, or it is possible to derive such values by means of the modes included in SUNDS, specifically APROBA [266] and PROAST by RIVM [k].

To compute a Derived No-Effect Level (DNEL) an endpoint value for test species is needed, either deterministic (NOAEL) or probabilistic (Benchmark Dose), where in the latter case the lower confidence limit of the distribution (5th percentile, known as BMDL) is used as Point of departure for test species. Within SUNDS it is possible to

[k] https://www.rivm.nl/en/Documents_and_publications/Scientific/Models/PROAST/

derive a Benchmark Dose (BMD) starting from dose-response values on test species. The PROAST software by RIVM has been included in SUNDS to derive a BMD (with confidence levels, BMDL and BMDU).
The user can define a label for both dependent (response) and independent (dose) variables. Moreover, it is possible to insert data from an Excel spreadsheet, or to download input data as an Excel spreadsheet.
SUNDS provides a simplified version of the original PROAST package. Specifically, SUNDS needs user to insert only two parameters: data type for the Point of Departure (at current time, only continuous variables are allowed) and Benchmark Response (namely, the predetermined change in the response rate of an adverse effect relative to the background response rate of this adverse effect). Once data is inserted (at least two dose-response values are needed), the user can run PROAST. When computation completes, intermediate results are displayed directly in the User Interface. Moreover, BMDL and BMDU derived by PROAST are automatically inserted as input parameter in APROBA user interface.
Once a Point of Departure for test species is derived (or if the user already has a precomputed PoD, either BMDL or NOAEL), indeed, a DNEL for Human Health needs to be evaluated. As previously described, this is done using APROBA, which was integrated in SUNDS by creating a package that performs the same analysis as the original spreadsheet. The user needs to provide input parameters (i.e. parameters related to original test species, such as species weight and PoD, and parameters related to the target species, such as body weight or the percentage of sensitive population that one wants to consider), and to provide Assessment Factors. In addition to default Assessment Factors, one can insert as much extra assessment factors (either probabilistic, inserting confidence values, or deterministic, specifying the same value for both confidence values). Once computation is performed (it is usually almost immediate), the computed DNEL distribution is displayed to the user directly in the module, and if there is at least one exposure associated with the route of exposure being analysed in the current Lifecycle Stage and if the endpoint results to be the most conservative one, risks are computed.

Derivation of A Derived Minimal Effect Level (DMEL) for non-threshold endpoints

In case of non-threshold endpoints, it is possible to derive a DMEL, by either using the Large Assessment Factor approach (also called EFSA approach), or the linearized approach. Such endpoints are listed, together with a definition, in Table 26.

Table 27: Non-threshold endpoints, with definition provided by REACH [264].

Endpoint	Definition
Mutagenicity	Refers to the induction of permanent transmissible changes in the amount or structure of the genetic material of cells or organisms. These changes may involve a single gene or gene segment, a block of genes or chromosomes.
Carcinogenicity	Chemicals are defined as carcinogenic if they induce tumours, increase tumour incidence and/or malignancy or shorten the time to tumour occurrence. Benign tumours that are considered to have the potential to progress to malignant tumours are generally considered along with malignant tumours
Genotoxicity	Refers to processes which alter the structure, information content or segregation of DNA and are not necessarily associated with mutagenicity. Thus, tests for genotoxicity include tests which provide an indication of induced damage to DNA (but not direct evidence of mutation) via effects such as DNA strand breaks, unscheduled DNA synthesis (UDS), sister chromatid exchange (SCE), DNA adduct formation or mitotic recombination, as well as tests for mutagenicity.

The procedure to derive a DMEL, as indicated in Section R.8.1.3 of the REACH [267] is to: (i) select a relevant dose-descriptor(s) for the endpoint concerned; (ii) modify, when necessary, of relevant dose descriptor(s) to correct starting point; and (iii) Application, when necessary, of AFs/High-to-low dose risk EFs to correct starting point to obtain endpoint-specific DMEL(s) for the relevant exposure pattern.

LARGE ASSESSMENT FACTOR APPROACH (EFSA APPROACH)

Similar to the Overall Assessment Factor approach applied for threshold effects in deriving DNELs, the EFSA approach results in DMEL values representing exposure levels where the likelihood that effects (cancer) are avoided is appropriately high and of low concern from public health point of view.

The steps are the following

1) Select the relevant dose-descriptor(s), i.e. $BMDL_{10}$[l] (by default) or T25[m]. In case $BMDL_{10}$ is deviating more than one order of magnitude from the corresponding BMD_{10}, the T25 should be used.
2) Modify, when, the relevant dose descriptor(s) to the correct starting point.
   This applies to the following situations:
   a) If for a human exposure route there is a dose descriptor for the same route in experimental animals, but for that route there is a difference in bioavailability between animals and humans at the relevant level of exposure;
   b) If for a human exposure route there is not a dose descriptor for the same route in experimental animals;
   c) Differences in human and experimental exposure conditions;
   d) Differences in respiratory volumes between animals (at rest) and humans (light activity)**;**
   e) Differences between occupational and lifetime conditions of exposure
      Lifetime: Corresponds to 1.5 to 2 years studies
      Workers: For Oral studies apply a correction factor of 2.8, for inhalation studies apply a correction factor of 1.65
3) Apply assessment factors in Table 28 to the correct starting point to obtain DMEL(s) for the relevant exposure pattern (route and exposed human population).

Table 28: Assessment Factors for the EFSA approach.

AF	Description	Exceptions	Default AF
Interspecies differences	The default factor of 100 for non-genotoxic substances would also be relevant for genotoxic and/or carcinogenic substances	These factors can be reduced or increased when appropriate chemical specific data are available as described e.g. by IPCS	10
Intraspecies differences			General population: 10 Workers: 5
Nature of carcinogenic process (inter-individual variability in cell cycle control and DNA repair)	MoA for substances that are both genotoxic and carcinogenic includes irreversible steps, such as the fixation of DNA lesions into permanent an inheritable mutation. The consequences of these irreversible steps are amplified by clonal expansion of a single mutated cell, accumulation of genetic changes and progression of the mutated cell into cancer.	Any relevant substance-specific or analogue-specific information on this assessment factor should be used to adjust or replace the default factor.	10
The reference point on the animal dose-response -cure is not a NOAEL	Reference point cannot be regarded as a surrogate for a threshold in the case of a	Any relevant substance-specific or analogue-specific information on	BMDL10: 10 T25: 25

[l] Lower confidence interval of the BMD at a BMR of 10%.
[m] Cronic dose rate that will give 25% of the animals' tumors at a specific tissue within the life time of that species.

	substance that both genotoxic and carcinogenic.	this assessment factor should be used to adjust or replace the default factor.	

LINEARISED APPROACH

The linearized approach is an alternative way to derive a DMEL, resulting in a value that represents exposure levels where the likelihood that effects (as asses by lifetime cancer risk) are avoided is high and considered to be of low concern.

This approach assumes a linear does-response relationship[n] between tumour formation and exposure, and which is incorporated in the high to low dose extrapolation assessment factor. It is used when there is an absence of sufficient information on Modes of Action or when MoA information indicates that the dose-response curve at low dose is or it is expected to be linear.

Steps:

1) Select the relevant dose-descriptor(s), i.e. T25 by default or BMD_{10} (note that in this case the BMD is selected, and not its lower confidence interval);
2) Modify, when, the relevant dose descriptor(s) to the correct starting point.
   This applies to the following situations:
   f) If for a human exposure route there is a dose descriptor for the same route in experimental animals, but for that route there is a difference in bioavailability between animals and humans at the relevant level of exposure;
   g) If for a human exposure route there is not a dose descriptor for the same route in experimental animals;
   h) Differences in human and experimental exposure conditions
   i) Differences in respiratory volumes between animals (at rest) and humans (light activity)
   j) Differences between occupational and lifetime conditions of exposure
      Lifetime: Corresponds to 1.5 to 2 years studies
      Workers: apply a correction factor of 2.8 for oral studies, and a correction factor of 1.5 for inhalation studies
3) Derive from correct starting point a DMEL for each relevant exposure pattern by linear high to low dose extrapolation, and by application of assessment factors in Table 29 when necessary.

Table 29: Assessment Factors for the linearized approach.

AF	Description	Exceptions	DEFAULT
Interspecies differences	AF for differences in metabolic rate is to be applied. No AF for remaining uncertainty for non-threshold effects.	Not needed for non-threshold effects that are induced locally at the ports of entry and inhalation studies	Allometric Scaling
Intraspecies differences	NO AF for intraspecies differences for non-threshold effects.		1
Exposure duration	No assessment factor for non-threshold effects. It is indeed already taken into consideration when correcting the starting point.		1
Quality of whole database	If justified. Special consideration should be given when alternative data (QSAR, read-across, categorization, …) is used.	>1 for non-testing data, case-by-case for others → expert judgments	1

[n] It is possible to replace it by a supralinear or sublinear dose response relationship if there is sufficient information in support of this.

4) Apply high to low dose risk extrapolation factor, as in Table 30.

Table 30: High to low extrapolation factors for the Linearized approach.

	Workers	General population
T25	25000	250000
BMD_{10}	10000	100000

It worth noting that the two approaches may result in a very different value for the DMEL, depending on how high the uncertainty of the BMD is (in case of using it as a dose descriptor). In SUNDS, it is possible to choose between the two approaches, and if the $BMD(L)_{10}$ is selected as dose-descriptors, it is possible to derive it by means of PROAST.

Once the DMEL is derived by means of one of the two approaches, if there is at least one exposure associated with the route of exposure being analysed in the current Lifecycle Stage and if the endpoint results to be the most conservative one, risks are computed.

5.2.3.1.3 Risk Control (RC) module

In the RC module outputs of the ERA and HHRA sub-modules are integrated with a risk reduction inventory along the lifecycle using Multi-Criteria Decision Analysis (MCDA). SUN developed an inventory TARMMs along with their efficiency and cost in collaboration with project partners.

Specifically, the RC Alerts submodule, highlights where these risks are in each scenario of the project. It is possible to order and to filter risks, to show only risks assessed in a specific scenario, while the RC Comparison submodule, then, provides an overview of assessed risks in each scenario of the project, displaying also costs (if technologies were applied to reduce risk), or only risks, thus allowing the user to consider also technologies costs when selecting the best scenario or strategy to reduce risks.

Finally, the RC Technologies module allows to apply technologies to reduce risks. A set of TARMMs is proposed, and for each TARMM exposure scenarios in which it can be applied are displayed clicking on the entry in the list, together with the current assessed risk (acceptable risk, unacceptable risk, risk needs further consideration).

If at least one new technology is applied (or at least one is removed), an “APPLY” button appears on top of the page. When clicked, new risks are computed taking into consideration the exposure reduction factor provided by applied TARMMs (risks will be also updated in technologies list).

The best way to use this module consists in first cloning the scenario (thus creating a new one, where one or more technologies will be applied), and then applying technologies on the new one. This can be done from scenarios list and directly in RC Technologies module, by clicking the bottom at top of the page. In the latter case, it is possible to select first TARMMs to apply, without applying it, and then cloning. Application is indeed performed, in this case, after cloning. This allows to compare the original scenario with new scenario(s) with reduced exposures, thus comparing also costs if different combinations of technologies are selected in different scenarios, using the RC Comparison module.

5.2.3.2 Social and Economical Assessment modules

The Socioeconomic Assessment (SEA) module In Tier 2 comprises 3 submodules, namely the Lifecycle Impact Assessment (LCIA) module, the Economic Assessment (EA) module, and the Social Impact Assessment (SIA) module. These modules are introduced in the following subsections.

The SEA module aims at pinpointing hotspots (i.e. high risks and impacts or low benefits) that allow the user to see in which ways the sustainability profile of a NEP can be improved. Each scenario covers the whole lifecycle of a NEP i.e. synthesis of functional components, product manufacturing, consumer use and product end of life (disposal, recycling and reuse). The SEA methodology aims to account for salient sustainability aspects such as transformation of pristine nanomaterial to diverse nano-forms (which constitute different exposure agents), environmental (including human) targets, material and energy fluxes contributing to environmental impacts, economic inputs and social context.

Aligned with the Triple Bottom Line (TBL) formulation of sustainability [268], the SEA module includes the three sustainability pillars through the integration of the following components:

- Human Health Risk Assessment (HHRA), Ecological Risk Assessment (ERA) and Lifecycle Impact Assessment (LCIA) methodologies are included in the environmental pillar;
- Economic Assessment (EA) methodology is included in the economic pillar;
- Social Impact Assessment (SIA) methodology is included in the social pillar.

The different methodologies included in SEA provide heterogeneous results, making the integration of their outputs toward a final sustainability assessment score not straightforward. The option of integrating these outputs to a single scale (e.g. in monetary units or non-dimensional index) was discussed with the group of stakeholders involved in SUNDS design[o]. Stakeholders agreed that an integrated sustainability score could only pinpoint a better scenario in comparative analysis but could not prescribe how product sustainability could be further improved. Therefore, it was decided to differentiate results from each module to create a sustainability portfolio as depicted in Figure 30. Such portfolio comprises single outputs for global and lifecycle stage scores for all methodologies which are assigned communicative labels to provide further guidance to the user. The combination of classifications for each scenario can considered on its own; for example, a NEP with low risks and environmental impacts, low costs and high benefits could be innovative and commercially profitable. In the case of more than one scenario, sustainability portfolio provides the framework for a systematic and detailed comparison of results of each methodology.

[o] http://www.sun-fp7.eu/wp-content/uploads/2015/02/SUN-user-workshopsummaryfinal.pdf

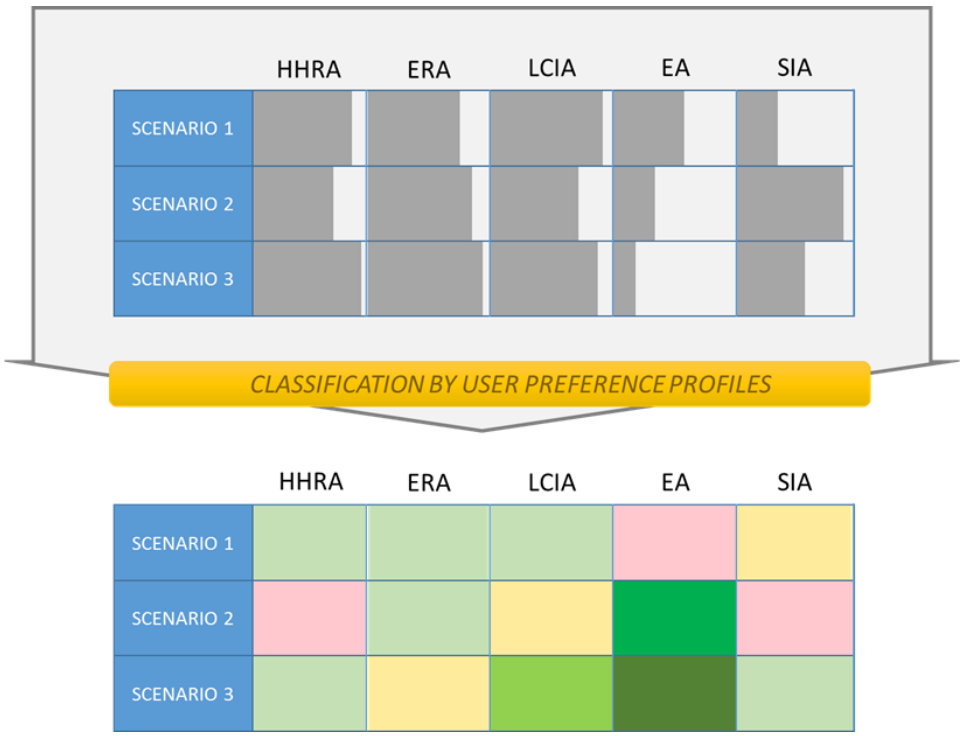

Figure 30: Example of application of the SEA module.

5.2.3.2.1 Lifecycle Impact Assessment (LCIA) module

The LCIA module, which accepts LCA midpoints calculated as per explicitly specified LCIA methodology (e.g. ReCIPe [269], CML [270], etc.). The conduction and interpretation of LCA requires specific expertise; therefore, in order to protect the user-friendliness of SUNDS it was decided not to program an LCA software and database within its platform, but to allow the users to upload the raw results of LCA external softwares (namely Simapro[p] and Umberto[q]) which are then elaborated by SUNDS, showing user friendly graphs and highlighting impacts, costs and benefits.

5.2.3.2.2 Economic Assessment (EA) module

The EA module assesses microeconomic impacts due to a NEP. These are impacts at the individual company level and implement a cost evaluation methodology for nanomanufacturing. BASF[r] has offered know how from its economic module of SEEBALANCE [271], which is based on lifecycle costs from a consumer perspective.

5.2.3.2.3 Social Impact Assessment (SIA) module

The SIA module assesses social impacts due to a NEP. Although this module was not originally planned to be included in SUNDS, given the increasing interest and relevance of this topic to sustainability assessment, it was decided to develop and include it. Much of the research on the social impacts of nanotechnology is qualitative and based on broad scenarios, and it is challenging to construct a comprehensive list of social impacts. This module focuses upon the impacts due to workplaces, products and regional context.

[p] https://simapro.com/
[q] https://www.ifu.com/en/umberto/lca-software/
[r] https://www.basf.com/

5.3 Software architecture and server-side structure

5.3.1 Software Architecture

5.3.1.1 Graphical User Interface (GUI)

A continuous dialogue with stakeholders took place to create the GUI of SUNDS, through dedicated interviews and questionnaires, moreover three stakeholder's meetings were organized throughout the project. This ensured the development of user interfaces which meet stakeholders' requirements as well as the use of agreed default values and thresholds all along the application.

GUI have been developed by following Google Material Design guidelines[s] to ensure maximum user friendliness and propose familiar software interactions. Material Design is a three-dimensional environment containing light, material, and cast shadows. Within the material environment, virtual lights illuminate the scene. Key lights create directional shadows, while ambient light creates soft shadows from all angles. Materials has certain immutable characteristics and inherent behaviours while objects, in material design, possess similar qualities to objects in the physical world such as being stacked or affixed to one another. Objects also cast shadows and reflect light.

5.3.1.2 Meteor

The web application has been created using Meteor.js[t], a framework based on Node.js[u] which offers the tools and the flexibility to build a complete reactive application. Being based on Node.js it uses JavaScript both in the client side and in the server side. It also pre-installs the non-SQL MongoDB[v] as database (cf. section 5.3.1.3). As displayed in Figure 31 the communication between the Node.js server and the client takes place by means of libraries which allows DDP (Distributed Data Protocol) and EJSON (an extension of JSON to support more types). In summary, the following libraries are at the core of Meteor:

- Node.js: JavaScript server.
- Connect: a library for receiving input output HTTP of an app.
- Database Driver (Mongo): a simple drive to interface with MongoDB database.
- Blaze: library for creating user interfaces by writing reactive HTML templates.
- LiveQuery: a library built to query and manage data of database in a reactive way.
- Fibers/Future: a wrapper library for Node.js to make the server synchronous.

[s] https://material.io/
[t] https://www.meteor.com/
[u] https://nodejs.org/
[v] https://www.mongodb.com/

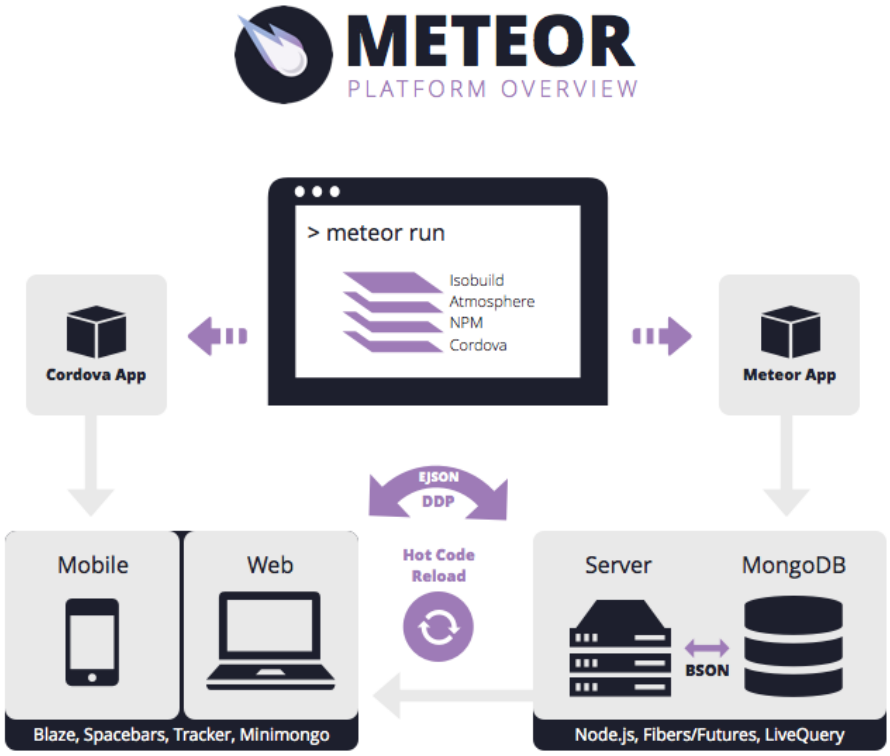

Figure 31: Meteor infrastructure (source: Meteor website)

Meteor's high level of connection between client and server allowed by DDP fosters reactive programming where every change in the underlying data is automatically propagated to all listeners live so that changes appear immediately to all connected users. This is feasible due to the presence of Minimongo, an in-memory non-persistent client-side implementation of a MongoDB in pure Javascript, which serves as a local cache that stores just the subset of the database that this client is working with. Once an insertion/deletion/update query is performed by the client, the command is executed locally immediately, and, simultaneously, it's sent to the server for being executed there.

It is possible to add additional packages/libraries to the application by means of Atmosphere packages (the official package repository for meteor), as well as NPM packages. Moreover, Meteor allows to build an app for three different platforms (web, Android, IOS) starting from the same base of code.

5.3.1.3 MongoDB

MongoDB is a NoSQL database that stores documents into BSON format (a binary form of JSON). For each data collection in SUNDS database an appropriate JSON file is used as template, which is the "skeleton" of the various elements. The NoSQL logic applied in Mongo is substantially the opposite of what used by traditional relational databases such as MySQL, which are based on tables and relationships. In a non-relational database, documents are grouped into collections that can also be heterogeneous. This means that each element in a collection may have different structures.

Mongo database embedded in Meteor can be accessed directly from the server console, thus allowing to directly manage the database.
Like classical SQL databases, mongo allows different types of queries, specifically:

- find, to select documents in a collection given a set of arguments;
- insert, to insert a new document;
- update, to modify an existing document;
- delete, to delete a document

5.3.2 Server-side structure

SUNDS is currently running on a server which uses Ubuntu as Operating System, note however that it can be run in all main Operating Systems, including Windows and MAC OX.
The application, server side, is composed by three entities: the web server (provided by the Meteor app), the database (MongoDB) and the API that allows to run the R models included in SUNDS and retrieve computed results. To keep separate these entities, SUNDS uses Docker[w], a platform available for both Linux and Windows based apps that allows to put applications or parts of applications in separate independent and isolated environments, called "containers". A Docker container, indeed, is an isolated and secure application platform that contains everything needed to run it, independently from the Operating Systems hosting them.
Docker allows to compose two or more containers (i.e.: define and run a multi-container application), moreover it allows to expose a port allowing the container to listen to that port for external requests. Specifically, there are two main applications: SUNDS, composed by the web server and the database, and R-SUNDS, which instead is responsible of running R models included in SUNDS. The web server and the DB constantly communicates with each other, while SUNDS communicates with R-SUNDS when clients (i.e.: users that connect to the application) requests a result that is provided by R models included in the Decision Support System. R-SUNDS, on the other hand communicates with SUNDS notifying the progress of requested computations. A description of R models included in SUNDS as well as a detailed explanation on how SUNDS and R-SUNDS communicate are presented in following subsections.
Currently, the MongoDB container and the SUNDS container are placed in the same machine, while R-SUNDS container is placed in a different one. Docker also allows to replicate containers (for instance in a cluster), to improve the scalability off the whole system. A schematic view of the server-side infrastructure is presented in Figure 32.

[w] https://www.docker.com/

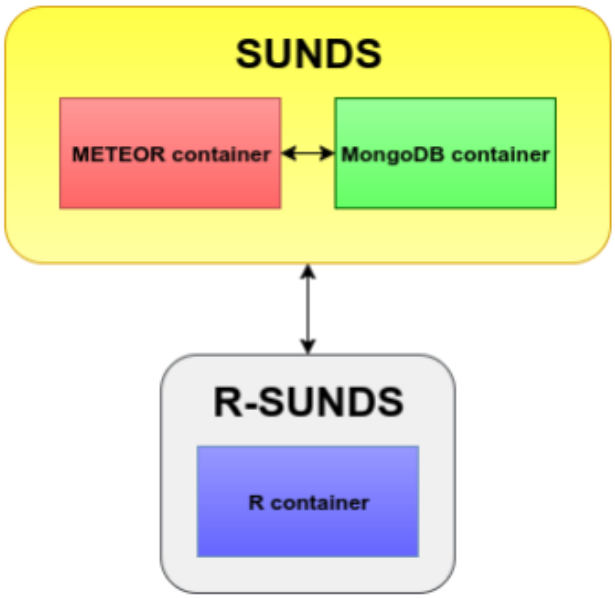

Figure 32: Server-side structure. There are two main applications (SUNDS and R-SUNDS), which are composed by Docker containers.

5.3.2.1 Communication between SUNDS and R-SUNDS

As aforementioned, communication between SUNDS and R-SUNDS is bidirectional. Specifically, R-SUNDS provide a REST API to run R models, producing a JSON object that contains results and data to be stored in the database and then shown to users producing charts. Each call to the APIs is performed by a POST request, with data (e.g.: raw dose-response data for test species) and parameters (e.g.: number of simulations to perform).
R-SUNDS, on the other hand, notifies SUNDS on the execution progress, providing for time consuming models an Estimated Time of Arrival (ETA), i.e.: an estimation of the completion time of current execution.

5.3.2.2 Models included in R-SUNDS

To date, three external packages are included in R-SUNDS, namely PROAST by RIVM, PSSD and PMFA (by courtesy of dr. Fadri Gottschalk, and still not publicly available). Moreover, an R package that performs the same computations and provides the same results as the APROBA spreadsheet [266] has been internally developed and included in R-SUNDS. In addition to these packages, further R functions has been developed to characterize risk for both Environment and Human Health, to generate data starting from confidence values provided in input by users, and to numerically assess the contribution of each parameter to the uncertainty of the results.

5.3.2.2.1 PROAST

PROAST is an R package developed by RIVM for statistically analyse dose-response data. In SUNDS, it is applied on raw dose-response data to test species to derive a Benchmark Dose (BMD). Confidence intervals of BMD, namely BMDL (5^{th} percentile) and BMDU (95^{th} percentile), are then used as input data to derive a Derived No-Effect Level (DNEL) for Human Health, with the former considered as Point of Departure (PoD) for test species. Original PROAST package allows very fine analysis on input data, while in SUNDS its been decided to provide a very basic and simple analysis, thus making it simple to use also for non-experts. Specifically, in SUNDS one can perform dose-response analysis to derive a BMD(L/U) by simply inserting dose-response data (for a single group of test species) for a specific endpoint and specifying Benchmark Response (BMR) for test species.

5.3.2.2.2 APROBA

APROBA (Approximate PROBabilistic Analysis) is an Excel Spreadsheet developed within the IPCS project on the Harmonization of Approaches to the Assessment of Risk from Exposure to Chemicals under the sponsorship of the World Health Organization [266], to estimate a Target Human Dose, i.e. the dose at which the most sensitive part of the population shows an effect of the specified percentage on the considered endpoint, considering uncertainty for many typical hazard characterizations. As already mentioned, APROBA was integrated into R-SUNDS by developing an R package based on the original spreadsheet. APROBA is used to derive a DNEL starting from BMD(L/U) previously derived using PROAST or starting from No Adverse Effect Levels (NOAELs), applying Assessment Factors to consider uncertainty. The original spreadsheet also proposes a non-probabilistic analysis not included in SUNDS, moreover in the original APROBA the user can specify up to 3 additional Assessment Factors, while in SUNDS insertion of as many values as the user desires is allowed.

5.3.2.2.3 PSSD

PSSD is an R package to derive a probabilistic Species Sensitivity Distribution (pSSD) for ecotoxicological assessment. Starting from No Observed Effect Concentration (NOEC) data for different species covering several taxonomic groups (at least eight as requested by EU REACH), a cumulative distribution function (and, consequently, a probability density function) that describes the proportion of species that does not show adverse effects while exposed to the nanomaterial is derived by the package. This process is repeated a specified number of times, thus obtaining a set of curves. Subsequently, R-SUNDS retrieves the 5^{th} percentile of all these curves, thus obtaining a probabilistic PNEC.

5.3.2.2.4 PMFA

PMFA is an R package to simulate material flows (PMFA stands for Probabilistic Material Flow Analysis), to estimate the release of nanoparticles into natural and technical compartments (i.e.: PECs). The original package allows to specify for each compartment (up to 50 natural and technical compartments) (i) material input in the system that directly involves the compartment, (ii) material fate (i.e.: elimination/degradation of material inside the compartment, deposition of the material, delay of the material inside the compartment and unknown fate) and (iii) transfer of material between different compartments. To simplify its use environmental and technical compartments has been fixed, as well as the possible directions of flows between compartments. Moreover, only material degradation/elimination can be input inside each compartment, while deposition is automatically computed (i.e. the material that remains in the compartment and is not eliminated). A schematic overview of the resulting simplified system is presented in Figure 29. Note that this analysis is performed for each lifecycle stage.

5.3.2.3 External models

In principle, the standard way to include a model in SUNDS is to add it to R-SUNDS, providing an API to SUNDS, and/or to create an interface for the model in the DSS. However, for some models is not possible, nor allowed by the model's authors to follow this path. In such cases it is possible either to make use of already existing APIs, thus providing an interface in SUNDS and directly connecting with the original model, or to redirect the user in the external model homepage, asking him/her to insert the results in SUNDS once the computations are performed.

The former scenario applies in the case of Nanosafer[x], which allows to estimate Exposure associated with production and use in occupational. Data is then sent to NanoSafer which responds with a toxicity score assigned to the nanomaterial, resulting exposures (both daily and acute, related to Far-field and Near-field), and intermediate data. SUNDS then selects the highest daily value and uses it as deterministic Exposure to evaluate Human Health risk. Currently, the same setting is being developed for the ECEL database of technologies [272]. The latter set of scenarios, instead, in addition to the already mentioned Simapro and Umberto software, applies for an exposure models, specifically ConsExpo Nano[y] for the quantification of the exposure of spray products in consumer scenarios. Finally, we are currently working together with the RIVM institute to allow to use the web version of PROAST, which allows the full use of the package (while in SUNDS a simplified version is provided). In future, it will be possible to use it and then import the results in SUNDS by simply coping and pasting in SUNDS a special key, which will be provided by the PROAST web app to the user once the analysis is completed.

5.4 Conclusions

One of the goals of the EU funded SUN project was to implement its assessment methodology into the SUNDS decision support system. SUNDS has been developed as a web application by using the Meteor JavaScript development framework. The software has been presented to the Stakeholders in multiple workshops during the project where it received general appreciation; moreover, comments from stakeholders have been collected and properly implemented in the subsequent releases of the software. The software has been successfully applied to two project case studies, Pigments for plastic bumpers and Wood preservation systems, which have been included in the software as demonstrative projects. Part of these case studies will be presented in detail in Chapters 6, 7, and 8. The software code of the SUNDS decision support system and of R-SUNDS is available on bitbucket.org upon request.

[x] http://www.nanosafer.org/.
[y] https://www.consexponano.nl/

6 SUNDS Human Health Risk Assessment module and its application to “Ferrari Red” Pigments

The work presented in this chapter is based on the following journal article, currently in press:
L.Pizzol, D.Hristozov, A.Zabeo, **G.Basei**, W.Wohlleben, A.J.Koivisto, K.A.Jensen, W.Fransman, V.Stone, A.Marcomini, SUNDS probabilistic human health risk assessment methodology and its application to organic pigment used in the automotive industry, 2018 (accepted by NanoImpact, DOI: 10.1016/j.impact.2018.12.001).

6.1 Introduction

The increasing use of NMs in NEPs has raised societal concerns about the adequacy of their risk regulation.
The Risk Assessment for the Human Health is done by performing a Chemical Safety Assessment (CSA) to demonstrate that the produced or imported chemicals do not pose any unacceptable risks for the environment, and for workers, consumers and/or the general population. REACH applies the chemical Risk Assessment paradigm to identify the risks and to propose proportionate risk management measures [3]..
CSA in Europe or Human Health Risk Assessment in the USA are standard systematic procedures to evaluate the likelihood of adverse health effects due to exposure to chemical substances, which have been recognized by major regulatory agencies and international organizations such as the European Chemical Agency (ECHA), the US Environmental Protection Agency (US EPA), the Organization for Economic Cooperation and Development (OECD), and the World Health Organization (WHO).
Current risk assessment paradigms are composed of hazard identification and assessment, exposure assessment, risk characterization and uncertainty analysis [273], and are considered applicable to NMs if aided by proper tools to account for their unique properties and interactions [4]. The standard deterministic HHRA relies on single point estimates of hazard, exposure and risk, which often fail to explicitly report the considerable uncertainties that propagate through the risk assessment process, albeit this can effectively support risk managers from industry and regulation in taking more informed decisions [72,274]. This issue is more pronounced for NMs than for conventional chemicals due the higher complexity of their characterization profiles which influence their safety assessment. Therefore, on the basis of previous works on HHRA applied to nanoscale titanium dioxide and silver [275,276], an extended version of the HHRA approach, which includes probabilistic assessment and uncertainty analysis, was proposed as a suitable mean to better communicate these uncertainties [14]. In comparison to the more conventional deterministic approach, the strength of the proposed probabilistic HHRA methodology is its ability to assess the sources of uncertainty in the estimated risks and to clearly communicate them in order to assist industries and regulators in taking more objective decisions. The methodology was implemented as a specific module in SUNDS.
The aims of this chapter are to present the first probabilistic HHRA of organic nanopigments for automotive plastics and to demonstrate it in a real case study: i.e. nanoscale organic pigment used in the automotive industry. This is highly relevant as the market of high-performance pigments has expanded to reach an estimated size of about $6.32 billion by 2022 [277]. Pigments are defined as coloured, black, white or fluorescent particulate organic or inorganic solids, which are insoluble in, and essentially physically and chemically unaffected by, the vehicle or substrate in which they are incorporated [278]. These pigments are ubiquitously used in plastics because, in contrast to dyes, they have low solubility, can be dispersed better within a matrix and can both absorb or scatter light.

Organic pigments (e.g. azo, phthalocyanines blues and greens, diketopyrrolopyrroles) generally exhibit an increase in colour strength as the particle size is reduced, while with many inorganic pigments (e.g. titanium dioxide, iron oxide, chromates, carbon black) there is an optimum particle size at which the colour strength reaches its maximum [279]. Therefore, organic pigments can have several advantages as colorants in coatings and polymers, including: a) high brightness and good colour strength, b) improved fastness properties (especially migration resistance and mechanical reinforcement), and c) inhibition of polymer degradation [279]. Our case study specifically targets pigment-coloured automotive plastics. Nano-pigments can be defined as organic or inorganic substances, insoluble, chemically and physically inert into the substrate or binders, with a particle size less than 100 nm [280,281]. Such plastics are widely used in interior, exterior, and under bonnet components to reduce automobile weight, improve aesthetics, vibration and noise control, and cabin insulation [282].

6.2 Materials and methods

6.2.1 Case study description

The investigated substance is a nanoscale (median 43 nm, range 14 to 151 nm) diketopyrrolopyrrole (DPP) pigment used to impart red colour to external automotive coatings or plastic parts. Physicochemical characterization of pristine NMs is fundamental for interpreting the risk assessment results. Therefore, we performed detailed physicochemical characterization, the results of which are reported in Table 31.

Table 31: Physicochemical characterization of pristine Organic Pigment.

Parameter	Technique	Results
Primary size distribution Min- Max (average)	TEM	14, 151 (43)
Mode (1st quartile … 3rd quartile) [nm]		26.3 (29.8 - 49.8)
Shape	TEM	Irregular polyhedrons and some small semi spherical particles
Dispersibility in water: D_{50} [nm];	DLS	137.3 ± 4.6
average agglomeration number (AAN)		41
Dispersibility in modified MEM provided by the Heriot -Watt University: D_{50} [nm];	DLS	84.4±5.5;
average agglomeration number (AAN)		9
Z potential in UP water [mV]	ELS	-20.8 ± 1.3
Isoelectric point [pH]	ELS	2.1
Specific Surface Area [$m^2 g^{-1}$]	degradation BET	94 (from producer)

Parameter	Technique	Results
Pore sizes [nm]	BET	80, 200 to 2E05 (from producer)
Surface chemistry [atomic fraction]	XPS	C 77.1
		O 10.9
		N 5.9
		Cl 6.1
		(from producer)
Structure	FT-IR and/or RAMAN	Match with organic pigment Red 254 database
Chemical impurities [mg kg^{-1}]	ICP-MS	No efficient sample digestion. Mass loss in TGA: -2.9% from 35° to 315°

DPP is highly insoluble and extremely resistant to temperature and pressure, which has made it a preferred option for paints of luxury cars [283]. Chemically, DPP is a nitrogenous heterocyclic compound comprising of two five-ring pyrrole and two carbonyl groups (chemical formula: $C_{18}H_{10}Cl_2N_2O_2$). It was first known to have been synthesized in 1974 by the chemist Donald G. Farnum [284]. Ciba-Geigy Ltd. (then Ciba Specialty Chemicals, then acquired and integrated in BASF) patented the first known method of producing the pigment in 1983 [285]. Earlier, red paint used by auto manufacturers tended to fade and develop a dusty look known as "chalking", but the DPP organic pigment was extraordinarily bright, stable and resistant to ultraviolet light and extremes of heat and cold [283]. Nicknamed "Ferrari Red," the pigment was used on all solid-red Ferraris from 2000 to 2002, and on Alfa Romeos, BMWs, Corvettes, Volkswagen GTI models and the Lexus Soarer (SC 430) from 2000 to 2006 [283]. Chemical modifications to DPP can also yield pigments of other colours: e.g. alkylation leads to greater solubility and orange to green colour palette.

Both opaque (non-nano[z], TEM median size around 150 nm) and transparent (nano, TEM median size around 35 nm) grades of this organic pigment are marketed by BASF in the EU, USA, Canada and Mexico. The grade studied in SUN is described as a very transparent and saturated DPP, whose colour index is Pigment Red 254 | 56110. The specific material is relevant to represent nanoscale ("transparent") organic pigments as it also features among the high-tonnage materials.

In the SUN project the Red 254 organic pigment was used to colour plastics with a content of low percent in the polypropylene polymer matrix, specifically with 0.2% for fully saturated colour. Injection moulding was used for the manufacturing of the automotive part. The polymer used was Polypropylene KSR 4525 (Borealis), which is a reactor elastomer modified polypropylene intended for injection moulding automotive applications. Polypropylene KSR 4525 has excellent balanced mechanical properties, it gives a good surface quality and has been developed especially to be used in automotive exterior parts.

[z] According to Recommendation 2011/696/EU.

6.2.3 SUNDS HHRA module

SUNDS implements a probabilistic HHRA module designed to quantitatively estimate and communicate the uncertainties in each step of the risk analysis. The system can simultaneously assess different lifecycle stages of the assessed NMs, human exposed targets, working activities (where applicable) and routes of exposure. A single combination of these relevant components has been called lowest unit of assessment (LUA). The structure of the HHRA module is illustrated in Figure 33.

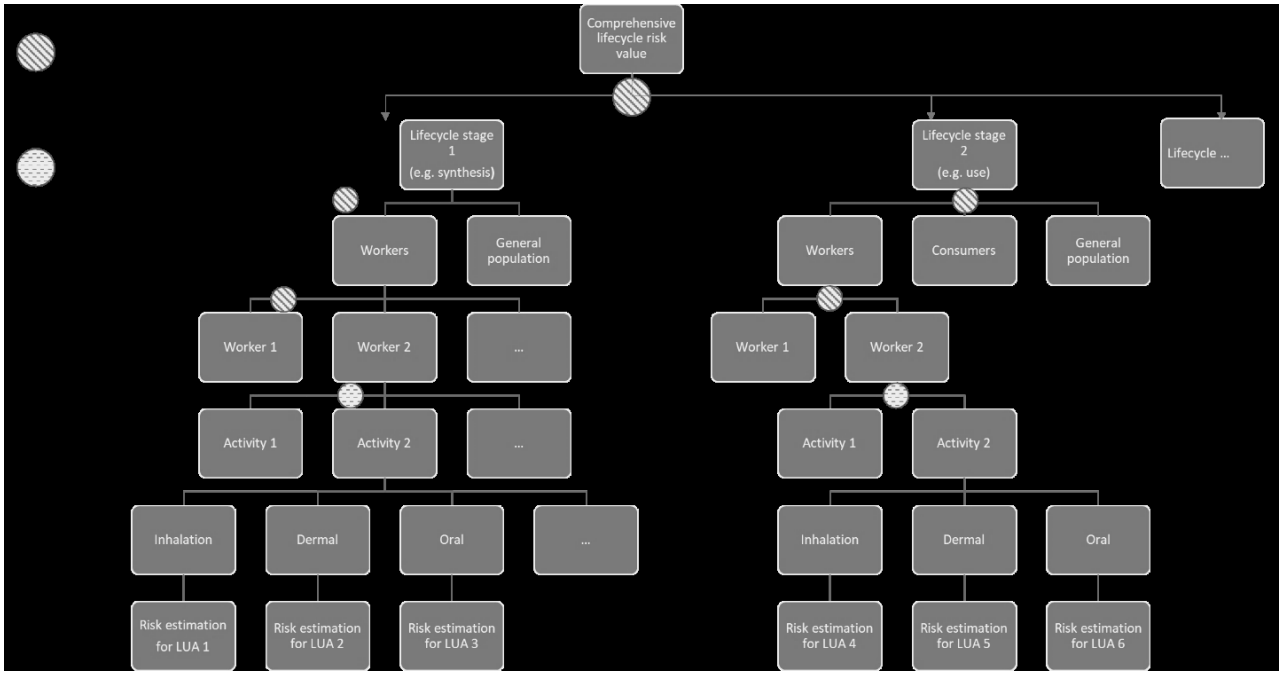

Figure 33: Example of the hierarchical structure of the HHRA module (not exhaustive of all the possible combinations assessed in the HHRA module), including different lifecycle stages, human exposed targets and sub-targets (i.e. worker 1, etc.), working activities, and routes of exposure, all contributing to estimate the risk value for a lowest unit of assessment (LUA). Non-additive and additive aggregation, methods are used to the integration of risk values to provide risk estimations associated to a higher level of assessment.

For each LUA, the combination of the hazard assessment (i.e. estimation of acceptable human dose expressed in terms of concentration levels below which a substance does not adversely affect human health) and exposure assessment (estimation of concentration levels) produces a discrete value or a probability distribution of risk. Once risk is estimated for each LUA, an aggregation step is required to produce a single risk value for each lifecycle stage as well as for the entire lifecycle, considering all relevant targets, activities and routes of exposure. This module is fully functional and can perform hazard, exposure, risk and uncertainty analysis as described in sections 5.2.3-5.2.5.

6.2.3 Hazard assessment

This step consists of hazard identification and dose-response assessment. The hazard identification involves the gathering and evaluation of the available information on the health effects or diseases that a substance can cause

under a particular exposure scenario. The principal question it tries to answer is whether the existing evidence suggests a potential risk for the human health. To identify the relevant hazard information for the organic pigment Red 254 a literature review was performed that focused on the inhalation and ingestion exposure routes as they were considered by the SUN consortium more relevant than the dermal route. To do this, the authors of this research queried the Web of Science database with combinations of the following keywords: nano, organic pigments, organic pigment Red 254, diketopyrrolopyrroles, hazard, toxicity, workers, Occupational Exposure Limit (OEL). The literature search from 2006 to 2017 resulted in a small number of documents (only four peer-reviewed papers) which were carefully analysed.

The dose-response assessment characterises the relationship between the dose of the substance administered during animal studies and the observed *in vivo* effects by means of statistical modelling. The final goal is to estimate an acceptable exposure level such as the Derived No-effect Level (DNEL), which can then be compared to external exposure to calculate risk for specific scenarios. The starting point for estimating human acceptable exposure level is the Point of Departure (PoD), or in other words the highest safe dose based on which adverse effects are not likely to occur in the test animals. It is generally recognised that Benchmark Dose (BMD) method is considered statistically more powerful than the alternative No-Observable Adverse Effect Level (NOAEL) approach [286]. When toxicological information is available, a BMD can be estimated by using PROAST[aa] [287], which is a software package developed by the Netherland's National Institute for Public Health and the Environment (RIVM) and implemented through SUNDS for the statistical analysis of dose-response data. PROAST is suitable for handling *in-vivo* dose-response data to provide probabilistic distributions of BMD.

However, in the specific case of our organic pigment case study, since no toxicological effects was identified up to the highest dose tested, we used the highest dose tested (i.e. NOAEL) as the PoD. SUNDS, however allows the use of both methods for deterministic and stochastic dose-response analyses.

Moreover, in our organic pigment case study, when necessary, NOAEL values have been corrected to consider differences in human and experimental exposure conditions and in respiratory volumes between experimental animals (at rest) and humans (light activity). The "corrected" NOAEL values were then extrapolated to human dose (i.e. DNELs) probabilistic distributions by applying well accepted inter- and intra-species extrapolation factors [288]:

$$HD = \frac{NOAEL\ or\ BMD}{EF_{\text{inter}} * EF_{\text{intra}} * UF_i}$$

In this equation EF_{inter} and EF_{intra} are inter- and intra-species extrapolation factors, while UF_i is reserved for other sources of uncertainty (i) from the dose-response assessment (e.g. representativeness of toxicology data, or uncertainty in the PoD). Log-normal distributions for these factors are defined using similar approaches presented by Slob et al. [289].

In SUNDS, the methodology developed by the WHO/IPCS Workgroup on the evaluation and expression of uncertainty in hazard characterization [290,291] has been used. Accordingly, HDs for both inhalation and oral routes can be estimated on the basis of Equation 1 by means of an embedded version of APROBA (approximate probabilistic analysis (tool)) [290], which is originally a Microsoft Excel-based tool developed by the WHO/IPCS Workgroup. APROBA performs approximate probabilistic (as well as deterministic) analysis of human dose

[aa] PROAST is a software package that has been developed by the Dutch National Institute for Public Health and the Environment for the statistical analysis of dose-response data for chemical substances and here applied to nanomaterials.

extrapolation starting from animal dose-response results. It requires quantitative specification or estimation of: a) PoD, b) population incidence goal (i.e. number of individuals at risk, e.g. 5%), c) target human dose coverage (i.e. the required statistical one-sided confidence level, e.g. 95%), and d) uncertainty related to different parameters, including the inter- and intra-species EF. In APROBA, in the case BMD values are not available, NOAEL values are regarded as a rough estimate of the lower confidence limit of the benchmark dose (BMDLx), where x is the default benchmark response (BMR) [292]. Accordingly, the generic uncertainty in the NOAEL are defined as the precision of the NOAEL in estimating the BMDL. Detailed assessment of uncertainty in using a NOAEL as a surrogate for a BMD is reported in IPCS (2017) [290].The result of the probabilistic hazard assessment is the human dose HD_M^I at which a fraction I of the human population shows an effect of magnitude M after chronic exposure, with a specific confidence interval (e.g. 90%). This fraction I represents the sensitive target population, namely the portion of population which is more vulnerable to effects of exposure to the substance, due to e.g. age or poor health status.

6.2.4 Exposure Assessment

Exposure assessment involves the formulation of Exposure Scenarios (ES) and the estimation of the related intakes of the substance by workers, consumers and/or the general population. An exposure scenario is a set of (contextual) information describing the conditions of use of the nanomaterial which can influence its emissions from processes or release from products and its subsequent exposure potential. In assessing exposure, measured data and/or model estimates can be used as inputs to the SUNDS HHRA module either as deterministic values or as probabilistic distributions.

6.2.4.1 Formulation of ES

To gather the information needed to formulate realistic workplace and consumer ES for our case study (plastic car parts coloured with organic pigment red 254) we performed a comprehensive literature review. Specifically, published literature from 2000 to 2017 was searched for release and exposure assessment studies that involved pigments by querying the Web of Science database with combinations of the following keywords: nano, organic pigments, inorganic pigments automotive plastics, exposure assessment, release, emission, exposure, workplace, consumer, use. The search resulted in a few documents (four peer-reviewed papers), which demonstrated that no specific studies related to organic pigments and their potential releases from plastics are available. Therefore, ES were formulated for each lifecycle stage of our case-study product (i.e. synthesis, formulation, use, end-of-life EoL) mainly based on contextual information obtained from the SUN project and our industrial partner BASF, which is the primary manufacturer of organic pigment red 254.

6.2.4.2 Estimation of exposure

Site-specific measurements of known quality are often preferred over model estimates and are needed to validate and improve models. However, for most consumer scenarios, such measurements are hardly available, which requires the use of models to estimate exposure levels. Therefore, an array of nano-specific exposure models has been implemented through SUNDS (e.g. Nano Safer SQ, ConsExpo Nano Spray model, dARTnano, nanoIEAT, ConsExpo 4.1) based on a comprehensive exposure assessment framework for NMs. These models have been very useful for risk assessments performed by means of the system [275,276], but they were not used for the risk assessment

of the organic pigment reported in this chapter. Instead, measured data from the literature, release experiments performed in the context of SUN as well as a single box and a near-field (NF)/far-field (FF) occupational exposure model that is not strictly part of SUNDS were used as described below. The release experiments were performed to estimate the exposure concentration in air i) of organic pigments during the manufacturing of the master-batch [293], ii) during the injection moulding phase [294], iii) sawing, sanding or drilling of car bumper, and iv) shredding activities in the end of life stage. Artificial weathering studies have shown that release from polyethylene containing 0.2 wt.% DPP was 0.003 mg/MJ, which is very low release considering that the release range is typically from *ca.* 0.001 to 100 mg/MJ [295,296]. Thermal decomposition of polyethylene containing 2 wt.% DPP at 500 °C released 4.19 % of airborne particles from initial mass and residual ash content was 1 % from initial mass where DPP particles were not detected [297]. Because release levels were low these lifecycle stages were not included in the lifecycle exposure assessment.

4.2.5 Risk characterisation & Uncertainty analysis

6.2.5.1 Risk characterisation ratio (RCR)

The $RCR_{i,M}^{I}$ is calculated as reported in Equation 2.

$$RCR_{i,M}^{I} = \frac{EXP_i}{HD_M^I}, \text{ eq. 2}$$

EXP_i represents the exposure value (or the probabilistic distribution of exposure) related to exposure scenario i, while HD_M^I is the result of the hazard assessment (i.e. the level of exposure above which humans should not be exposed; in REACH this is called Derived No-Effect Level (DNEL)). HD_M^I values that can be both deterministic or probabilistic. A risky scenario was defined as RCR values ≥ 1 (i.e. exposure levels higher than human acceptable exposure for the specific incidence goal related to sensitive population).

6.2.5.2 Risk acceptability classification

Once the risk is estimated, it is classified in terms of acceptability according to an approach based on confidence intervals. Specifically, in case the risk is presented deterministically, two classes are identified: acceptable (ratio below one) and non-acceptable (ratio above one). As probabilistic risk distributions typically follow a right-skewed log-normal distribution, it is too rare to have a completely acceptable risk. Literature suggests that, in the case of probabilistic risk assessment, the risk is acceptable if the 90th percentile of the exposed population is safe, but conservative values can also be selected (i.e. the 95th percentile or the 99th percentile) [298–300]. To select the most suitable risk acceptability classes we studied the literature and in addition asked relevant experts by means of a questionnaire specifically designed for this purpose. Ten experts were chosen from our personal networks and contacted by email in December 2015 with a request to participate in SUNDS methodology development. Eight responses were received, including two regulators (one from US and one from Canada) and six researchers (from EU). Data collection through the questionnaires was closed in February 2016. SurveyMonkey platform was used to implement the online questionnaire. Their responses pointed us to the following three classes: 1) acceptable (when the threshold of one is higher than the 95th percentile of the risk characterization ratio distribution), 2) needs further consideration (threshold of one between the 90th and 95th percentile) and 3) non-acceptable (threshold of one below the 90th percentile). The selection of the percentiles for this pre-defined risk acceptability classification profile can be changed depending on specific assessment needs. In our specific case, the selection of a specific

population incidence goal (e.g. 5%) in the dose-response assessment implies that the resulting probabilistic distribution of the RCR protects 95% of the population, thus the RCR probability distribution represents the variability and uncertainty around the 95% of the assessed population. Accordingly, the 90% and 95% percentiles used for the risk classification refer to the probability distribution of the RCR estimated according to the selected population incidence goal (i.e. sensitive population).

6.2.5.3 Risk aggregation across targets and lifecycle stages

The risk aggregation consists in the integration of risk values to provide a risk estimation associated to a higher level of assessment. Some examples considered in this chapter include i) integration of risks estimated for two or more activities performed by the same target (e.g. worker, consumer) with the same material to provide a more comprehensive estimation of risk for that target; or ii) integration of the risks estimated for two or more ES and/or targets in the same lifecycle stage in order to assess the risk for that specific lifecycle stage. Such aggregation may be additive (in the case of risks related to the same target) or non-additive (in the case of risks related to different targets for the same lifecycle stage), as reported in Figure 33.

The instances of additive aggregation include the situation of a worker exposed via more than one exposure routes (i.e. inhalation and dermal contact), or the situation of a worker involved in more than one activity within a single lifecycle stage (e.g. weighing and mixing of nanomaterial in the synthesis or formulation stages). According to the outcomes of the submitted questionnaires, the risk value for a lifecycle stage involving more than one exposure route is calculated by summing the risk for all exposure routes. In the case of a single worker involved in more than one activity, the risk for the worker is calculated by summing the contribution of each activity weighted by the exposure duration which should not exceed the whole working shift.

To produce a single HHRA output for each lifecycle stage and for the entire lifecycle, aggregation of non-additive risks (i.e. risk estimated for different targets) also needs to be addressed. According to the results of the questionnaire, non-additive integration is addressed for each lifecycle stage by presenting the maximum risk value.

6.2.5.4 Uncertainty analysis

Uncertainty contribution to RCR by each involved factor is estimated by means of the Monte Carlo approach with 10 000 trials. At each trial, the RCR is numerically estimated by randomly sampling elements from the BMD distribution, exposure estimates, and from each EF's distribution. The contribution to uncertainty of each factor is quantified by assessing the level of correlation between the factor and the resulting RCR by means of squared Spearman's rank correlation coefficient [301]. The contribution of each EF is selected as the arithmetic mean of each resulting curve and appropriate figures are developed for communication purposes.

6.3 Results

6.3.1 Hazard assessment

Relevant information on the toxicity of the organic pigment Red 254 for the inhalation and ingestion exposure routes was collected from the REACH registration dossier for this substance in the nanoform (CAS no. 84632-65-5), freely available on the ECHA web site. For the Inhalation exposure route, a short-term repeated dose toxicity study was performed in 2012 applying the method developed by Ma-Hock et al. (2009) [302] to organic pigment Red 254 at different size dimensions including that assessed in the present work (i.e. nano-form) [303]. This included

assessing i) effects in the lungs; ii) persistence, progression or regression of effects; iii) effects in organs other than the lung; and iv) lung burden and potential translocation to other tissues. This study assessed a nominal concentration of 30 mg/m³, and defined a NOAEC equal to ≥ 30 mg/m^3 [194,303] as reported in Table 32.
To assess the effect due to ingestion, a subacute (28 days) oral gavage study was performed in 1986 according to the OECD Guideline 407 with a reliability index equal to 1 (reliable without restriction) which assessed the organic pigment Red 254 at different size dimensions including that assessed in the present work (i.e. nano-form) [bb]. Observations for mortality, body weight, food consumption, ophthalmoscopy, haematology, clinical chemistry, urinalysis, gross pathology, histopathology and histotechnology have been performed. The assessed doses were 0, 100, 300, 1000 mg/kg body weight on the basis of actual concertation ingested (intake by gavage) and the study identified a NOAEL > 1 000 mg/kg bw/day. Effects observed are reported in Table 32.

Table 32: Input and output data for APROBA related to organic pigment Red 254. LCL: lower confidence limit, UCL: upper confidence limit.

	Notes	**Organic Pigment (Inhalation)**	**Organic Pigment (Oral)**
Inputs to APROBA			
Data type		Continuous	Continuous
PoD type		NOAEL	NOAEL
Unite of measure		mg/m^3	mg/kg bw/day
Value		30*	1000*
Reference to support the PoD selection		Taken from ECHA chemical safety assessment where the initial data is > 30). Basis for effect level: other: Reversible minimal hypertrophy/hyperplasia in the bronchioles, at the level of the terminal bronchioles and alveolar ducts. Clearance of pigment deposits by macrophages.	Taken from ECHA chemical safety assessment. Starting with day 21 until termination of treatment all rats of the high dose group (1000 mg/kg bw) showed red discoloured extremities. In addition, red and discoloured faeces were observed in the same animals between day 18 and termination of the test. No other symptoms related to test article treatment were observed.
Factor 1	Used to correct PoD to consider differences in human and experimental exposure conditions (6/8 hours per day). **	0.75	-
Exposure conditions in the study		6 h/day	-
Factor 2	Used to correct PoD for differences in respiratory volumes between experimental animals (at rest) and humans (light activity)[5].	0.67	-
Corrected PoD value		15.07	1000

[bb] https://echa.europa.eu/it/registration-dossier/-/registered-dossier/10135

	Notes	Organic Pigment (Inhalation)	Organic Pigment (Oral)
Data route		Inhalation	Oral
Study type		Subacute	Subacute
Test species		Rat	Rat
Species weight		0.251 kg	0.1645 kg
Human weight		70 kg	70 kg
Population Incidence Goal (I)		5%	5%
Probabilistic Coverage Goal		95%	95%
Outputs from APROBA			
NOAEL to BMD (LCL)	Uncertainty to move from NOAEL to BMD	0.07	0.07
NOAEL to BMD (UCL)		1.57	1.57
Intraspecies variability (LCL)	This aspect addresses the interspecies adjustment to consider differences in body size (e.g. allometric scaling).	1***	4.83
Intraspecies variability (UCL)		1***	7.83
Interspecies TK/DK (LCL)	This aspect addresses remaining interspecies TK and TD (toxicokinetic and toxicodynamic differences) differences after accounting for body size differences.	0.333	0.333
Interspecies TK/DK (LCL)		3	3
Duration Extrapolation (LCL)	This aspect addresses uncertainty in using a less-than-chronic study (as specified in "Study type" previously) to estimate a chronic PoD.	0.625	0.625
Duration Extrapolation (UCL)		40	40
Intraspecies variability (LCL)	This aspect addresses the uncertainty in the amount of human variability in sensitivity. It depends directly on the "population incidence goal" entered previously	1.77	1.77
Intraspecies variability (UCL)		14.02	14.02

* Highest concentration tested which did not cause any adverse effects; ** According to the REACH Guidance on information requirements and chemical safety assessment Chapter R.8: Characterisation of dose [concentration]-response for human health v2.1; *** According to REACH.

The derived NOAEC and LOAEL were used as inputs to APROBA, which applied the interspecies and Intraspecies variability and extrapolation factors reported in Table 32 and derived lognormal distributions of

$HD_{long\text{-}term}$ for local and systemic effects due to both inhalation and ingestion of organic pigment Red 254, which are reported in Table 33.

Table 33: Long-term HD log-normal probability distributions statistics for organic pigment Red 254 (inhalation and oral exposure routes).

	OP Inhalation mg/m3	OP Oral mg/kg/day
5%	9.00E-02	9.67E-01
95%	3.65E+01	3.97E+02
50% (median)	1.81E+00	1.96E+01
Mean	9.58E+00	1.04E+02
Geometric Mean (GM)	1.81E+00	1.96E+01
SD factor	6.20E+00	6.23E+00

The estimated HD for inhalation ranges between 9.00E-02 mg/m^3 (P 5%) and 3.65E+01 mg/m^3 (P 95%). Its mean is equal to 9.58E+00 while its median and Geometric Mean (GM) is equal to 1.81 mg/m3. Comparing these values with Occupational Exposure Limit (OEL) values is impossible since such are currently not available for nanomaterials [25,194]. However, BAuA (2013) [304] suggested "assessment criteria" of i) < 0.5 mg/m^3 (considering an average agglomerate density of 2.0 g/cm^3 at the workplace) for biopersistent, non-fibrous nanomaterials without specific toxicity, and ii) <0.1 mg/m^3 for nanomaterials with specific (chemical composition-related) toxicity [26,194,304] (Arts at al., 2015 and Arts at al., 2016). These "assessment criteria" are included in the most conservative part of the probability distribution curve, where 0.1 mg/m^3 is close to P 5%, while 0.5 mg/m^3 falls between the P 5% and P 50%, the latter being more than 3 time higher. This confirms the low inhalation toxicity of the material. In the case of ingestion, neither OELs, not benchmark "assessment criteria" are available for comparison, but it is evident that from Table 33 that the HD statistics again describe a low toxicity material.

6.3.2 Exposure assessment

Realistic occupational and consumer ES were formulated according to the knowledge gained from the literature and the information provided by our industrial partner BASF, which is the primary producer of organic pigment Red 254. These ES (Table 34) showed that occupational exposure to organic pigment can occur during production (synthesis), master-batch manufacturing (formulation), injection melding of car bumpers (formulation), sanding and shredding the plastic (use, EoL). Consumer exposure is mainly relevant for operations such as sawing, sanding or drilling that might lead to release of airborne particles.

The experimental and modelling exposure estimations performed for each of these ES in the SUN project demonstrated that the release of organic pigment Red 254 is negligible in each lifecycle stage and the highest exposure potential is associated with EoL drilling, sanding and shredding operations due to significant release in the air. In the use stage of plastics, the embedded pigments comprise a low release potential due to the strong incorporation in the polymer matrix.

Table 34: Description of the exposure scenarios assessed for nanoscale organic pigment Red 254 used in automotive plastics.

Exposure scenario (ES)	LCS	Target	Exposure route	Exposure concentration	Additional information	References
ES1: Production of organic pigment	SYN	Worker	Inhalation	0.05 mg/m^3	Data collected in workplace for analogous materials	BASF internal data
		Worker	Dermal/Oral	negligible	Surface contamination: dermal and perioral exposure are negligible	EU FP7 SUN D5.4 and D6.6.
ES2: Manufacture of Master-batch containing 10 wt.% organic pigment	FOR	Worker	Inhalation	3*10^{-3} mg/m^3	Boonruksa et al. (2016) measured particle number concentrations varying from $N = 1.9 \times 10^3$ to 7.1×10^3 cm^{-3} during production of PP containing CNTs master-batch. Particles were mainly below 300 nm in diameter. Assuming that particles are spherical PP particles with count median diameter of 100 nm and density of polypropylene (ca. 1 g/cm^3), particle number concentration of 7100 1/cm^3 correspond to a mass concentration of 30 µg/m^3 where 10 % is organic pigment.	[293]
		Worker	Dermal/Oral	negligible	Surface contamination: dermal and perioral exposure are negligible	EU FP7 SUN project D5.4 and D6.6
ES3: Manufacturing of PP (Polypropylen KSR 4525) car bumper containing 0.2 wt.% organic pigment (injection moulding)	USE	Worker	Inhalation	2*10^{-6} mg/m^3	During injection moulding of car bumpers the near field (NF) particle number concentration at the injection mould was 14800 1/cm^3 (particle geometric mean diameter was 60.9 nm) which was at similar level than the far field (FF) level representing the background level. However, if we assume that the NF concentrations are all spherical PP particles, the mass concentration would be 10 µg/m^3 where 0.2% is organic pigment	EU FP7 SUN project D5.4 and D6.6
		Worker	Dermal	migration of pigment from plastics is strongly suppressed	Surface contamination: dermal and perioral exposure are negligible	[305]

Exposure scenario (ES)	LCS	Target	Exposure route	Exposure concentration	Additional information	References
ES4: Consumers handling and working with PP-org Pigment performing operations such as sawing, sanding or drilling that might lead to release of airborne particles.	USE	Consumer	Inhalation	$6*10^{-7}$ mg/m^3	Cutting studies have been performed in a 20 m^3 ventilated chamber (λ=0.5 1/h) using a jig saw. According to the gravimetric analysis of collected airborne respirable particles from 30 to 100 cm from the jig saw the respirable mass concentration was 0.3 µg/m^3 where 0.2% is organic pigment.	EU FP7 SUN project D5.4 and D6.6
		Consumer	Dermal	negligible	Surface contamination: dermal exposure is negligible	
ES5: Shredding	EoL	Worker	Inhalation	$6*10^{-13}$ mg/m^3	At the end-of-use the PP is shredded before incineration, landfill or down-use. Shredding studies have been performed in a 20 m^3 ventilated chamber (λ=0.5 1/h) using a down scaled industrial shredder. According to the gravimetric samples measured from shredder extract and feed inlet, where the concentrations were assumed to be highest and assuming fully mixed concentrations in the room, the respirable mass release was up to 0.3 µg/(kg of PP). Assuming 100*100*20-meter shredding plant ventilated at rate of 5 1/h and shredding 1000 kg/h PP bumpers the mass concentration would be 0.3 ng/m3 in steady state where 0.2% is organic pigment.	
		Worker	Dermal	negligible		

LCS: Lifecycle stage; SYN: Synthesis; FOR: Formulation, EoL: End of Life

6.3.3 Risk characterization & Uncertainty analysis

Figure 34 and Table 35 display the estimated RCR probability distribution for each ES along the lifecycle of our case-study product and the associated sources of uncertainty.

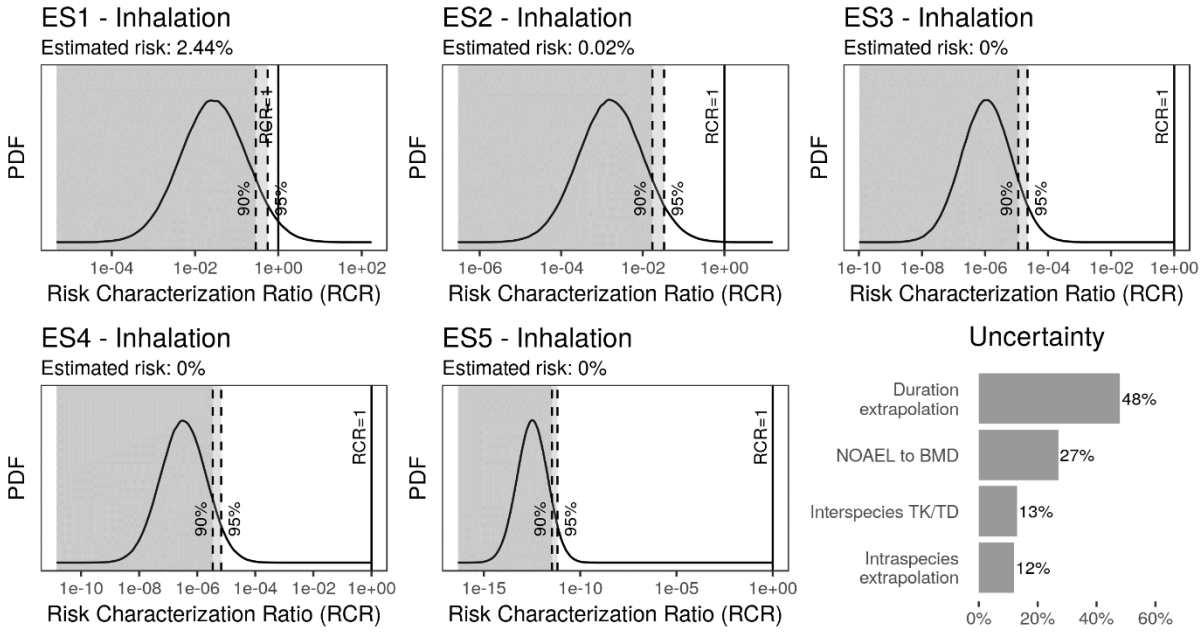

Figure 34: Risks along the lifecycles of the OP based products for all concerning exposure scenarios (ES). Contributions of the different sources of uncertainty to the total uncertainty are highlighted. Sources of uncertainty are related to the derivation of the DNEL for inhalation, which has been used for all the assessed ES.

Table 35: Statistics of distributions of risks along the lifecycles of OP based products for all the assessed exposure scenarios (ES). These statistics are the result from over 10 000 Monte Carlo simulations.

	ES1 Inhalation	**ES1 Dermal**	**ES2 Inhalation**	**ES2 Dermal**	**ES3 Inhalation**
5%	1.37E-03	No Risk (negligible exposure)	8.23E-05	No Risk (negligible exposure)	5.48E-08
95%	5.54E-01		3.33E-02		2.23E-05
50%	2.76E-02		1.65E-03		1.10E-06
Mean	1.46E-01		8.74E-03		5.86E-06
GM	2.76E-02		1.65E-03		1.10E-06
SD factor	6.20E+00		6.20E+00		6.21E+00
Risk (Prob. RCR > 1)	2.44%		0.02%		0.00%
	ES3 Dermal	**ES4 Inhalation**	**ES4 Dermal**	**ES5 Inhalation**	**ES5 Dermal**
5%	No Risk (negligible exposure)	1.65E-08	No Risk (negligible exposure)	1.65E-14	No Risk (negligible exposure)
95%		6.67E-06		6.61E-12	
50%		3.32E-07		3.30E-13	
Mean		1.75E-06		1.74E-12	
GM		3.32E-07		3.30E-13	
SD factor		6.20E+00		6.19E+00	
Risk (Prob. RCR > 1)		0.00%		0.00%	

These results clearly show that for each ES the risk is acceptable as the RCR is equal to 1 for more than 95% of the sensitive population. The cumulative health risks (based on non-additive integration; cf. 6.2.5, Figure 33) posed by the organic pigment Red 254 along its entire lifecycle is reported in Figure 35. The uncertainty associated to the risk estimations can be assessed considering the probabilistic distributions used for the derivation of the long-term HD for inhalation, which has been used in each assessed risk scenario, while variations in exposure have not been considered since the used deterministic values represent conservative estimations. Accordingly, the uncertainties associated to the risk estimations are similar for each assessed scenario. Forty eight percent of the variation in these results can be ascribed to the exposure duration EF used for extrapolation from the subacute short-term inhalation study to a chronic PoD, 27% were caused by the uncertainty of using a NOAEL instead of the BMD as the PoD for the risk assessment, 13% and 12% were related to inter- and intraspecies EF uncertainties, respectively.

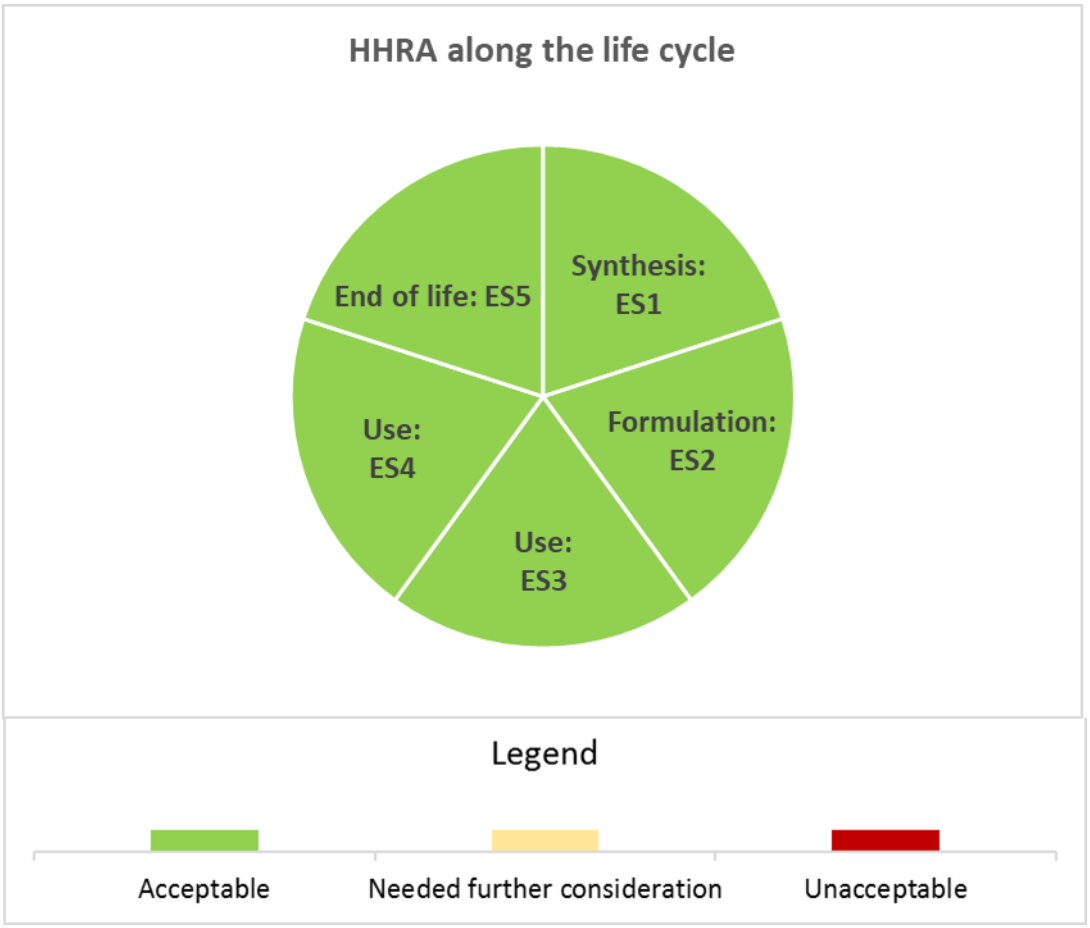

Figure 35: SUNDS interface which provides a comprehensive overview of the human health risks posed by organic pigment Red 254 along the entire lifecycle of the nanomaterial. Green indicates acceptable risks (i.e. exposure levels below DNELs).

6.4 Discussion

This study represents the first probabilistic HHRA of organic nanopigments for automotive plastics. The strength of the proposed probabilistic HHRA methodology (in comparison to the more conventional deterministic approach) is its ability to clearly communicate the sources of uncertainty in the estimated

risks (cf. Figure 34) to support better risk communication for more objective decision making by industries and regulators.

Specifically, it was possible to assess the uncertainty in the dose-response data by means of parametric bootstrapping. This showed that the largest uncertainty can be ascribed to the exposure duration EF used for extrapolation from the subacute short-term inhalation study to a chronic PoD. This uncertainty originated from the fact that (sub)chronic studies for nanoscale organic pigments are currently unavailable, which forced us to resort to short-term data. This had a strong effect on the obtained results and therefore we recommend repeating the assessment once relevant longer-term (at least sub-chronic) *in vivo* studies become available.

The second largest source of uncertainty in the assessment is related to NOAEL that we used as the PoD for risk assessment. There is probably a lot of unknown uncertainty in the NOAEL that our analysis could not capture. The NOAEL represents the highest dose at which no (adverse) effects were observed in the test animals. The procedure to assess it starts with screening of those endpoints that show a dose-dependent response to determine the lowest dose that significantly differs from the controls. This is the Lowest Observed Adverse Effect Level (LOAEL) for that endpoint, while the NOAEL is the dose below the LOAEL. This means that the NOAEL is smaller than the detectable effect size of the study, or in other words it could be anywhere between this size and zero. Nevertheless, in practice the NOAEL is simply considered as a dose where the effect is zero. Moreover, the NOAEL tends to be higher when fewer animals are used, while the opposite would be more appropriate as greater uncertainty should generate more conservative risk estimates [306]. Based on these considerations we can conclude that the unknown uncertainty in the NOAEL value is probably large.

Other key sources of uncertainty are the inter- and intraspecies EF. These default values were defined for regular chemical substances based on historical precedence and could be inappropriate for nanomaterials. In order to reduce this type of uncertainty it may be necessary to establish nano-specific EF based on extensive analysis of the already available large body of nano-specific physicochemical and toxicity data by means of *in silico* tools. Such tools can be for instance pharmacokinetic models that are useful to derive the ADME dynamics of the nanomaterials in experimental animals and to compare them to humans, including the sensitive sub-populations (children, older or diseased people).

There might also be unknown uncertainties arising from inappropriately using mass as the dose metric for dose-response assessment. Indeed, other metrics such as particle number or surface area might be more adequate if we assume nanoparticle-induced effects. The extrapolation of one dose metric to another can be done (for instance when estimating surface area from particle size distribution of the number concentration for spherical nanoparticles) and should be considered as often as possible in dose-response assessments.

Other sources of uncertainty in this study may result from the fact that only external doses were considered, while the uptake and the translocation of the nanoparticles in the organism were not taken into account. In fact, the size distribution of nanoparticles can strongly influence their deposition in the lungs. However, the number of ultrafine particles can quickly decline due to aggregation, agglomeration or surface deposition [307]. This means that nanoparticles measured close to the emission source can easily be eliminated by these processes and may never deposit in the lungs. Although the assessed uncertainty is quite large, the identification of the sources of uncertainty can help stakeholder to have a clear picture on which parameter/information caused this uncertainty and should be further assessed to decrease the

total uncertainty on the provided results. This is a different approach compered to control banding or risk screening approaches which apply the Precautionary Principle to facilitate risk management decisions in the context of large (often unknown) uncertainty (by basically hiding the uncertainty in their results). Indeed, while control bunding and risk screening approaches are useful to make pragmatic decisions, they do no clearly communicate the actual range of uncertainty which makes them unacceptable for regulatory risks assessment.

The use of a probabilistic risk assessment procedure raised the fundamental question of what levels of risk are acceptable. We tried to answer this question by a comprehensive analysis of the literature and by organising a workshop with relevant experts to identify adequate risk acceptance classes. We decided to be on the safe side by defining these classes as precautionary as possible in accordance with the conservative perspective of regulators. Nevertheless, the understanding of which risks are acceptable varies across sectors, communities and countries. To be able to develop a system that safely gives the opportunity to different stakeholders to set their own risk acceptability levels we need to perform more research on this subject. This has the benefit of extending the application domain of the SUNDS module beyond high-tier regulatory HHRA to allow its use by industries and SMEs also for other purposes such as prioritisation of safety by design or other measures in order to better decide on investments into their risk management portfolios.

In general, nanomaterials are offered in many different grades optimized for specific applications. This heterogeneity of sizes at nanoscale introduces a huge variability of properties that may exhibit different exposure potentials or biological effects. In the presented study, this issue was avoided as the organic pigment Red 256 nanomaterials used in the exposure studies are the same or similar to the ones used in the hazard studies. Therefore, we performed a case-specific HHRA, but considering the large variety of nanoforms, doing this for each of them individually would require excessive case-by-case testing. To avoid this, it is essential to develop approaches to group them based on physico-chemical, release, exposure, bio-kinetic and/or toxicological information. Grouping can facilitate also read-across between nanoforms and/or analogous (bulk) materials, which could optimise testing, thus reducing both costs and use of experimental animals.

6.5 Conclusions

This work introduced the SUNDS probabilistic HHRA methodology and presented one of its first applications to a real case study: Red254 organic nanopigment for coloration of plastic automotive parts. The proposed modelling approach successfully assessed the risks along the lifecycle of this product and characterised the associated sources of uncertainty. Our analysis demonstrated that the main source of uncertainty is the extrapolation from subacute to long-term exposure, which was necessary due to the lack of (sub)chronic in vivo studies with the investigated substance. Considerable uncertainties also stemmed from the use of default inter- and intra-species EF for conventional chemicals since such EF for NMs are presently unavailable. The proposed approach is currently unable to assess the uncertainties stemming from the use of NOAEL as a PoD, the selection of appropriate dose metrics, the behaviour of NMs in the air and in humans, and the use of data from studies involving different nanoforms of the same material. Therefore, although the proposed model is very suitable to apply for case-by-case risk analyses as currently required by regulations, its application to each nanoform separately would require excessive data. Therefore, in order to increase the efficiency of the

risk assessments it would be necessary to equip the proposed tool with grouping and read-across algorithms as it is planned in the recently funded EU Horizon 2020 Gracious project.

The results of our study showed that although the uncertainty in the risk estimates is high, which made them more conservative, the risks are acceptable for all exposure scenarios. Therefore, we can confidently conclude that the particular nanoscale organic pigment Red 254 application is safe in each stage of its lifecycle.

7 A quantitative Human Health Risk Assessment along the lifecycle of nano-scale copper-based wood preservatives using SUNDS

The work presented in this chapter is based on the following journal article:
D.Hristozov, L.Pizzol, **G.Basei**, A.Zabeo, J.Habicht, N.Neubauer, W.Wohlleben, A.Sanchez Jimenez, E.Semenzin, V.Subramanian, I.Gosens, F.R.Cassee, W.De Jong, S.F.Hansen, A.Mackevica, A.J.Koivisto, K.A.Jensen, V.Stone, and A.Marcomini, *Probabilistic Human Health Risk Assessment along the Lifecycle of Copper-Based Wood Preservatives*, Nanotoxicology, Volume 12, Issue 7, Pages 747-765, 2018 (DOI: 10.1080/17435390.2018.1472314).

7.1 Introduction

Preservation treatment is essential for increasing the service life of timber by imparting it with fungicidal and insecticidal properties. Copper-based preservatives have been widely used to treat softwood intended for commercial use due to their high performance and relatively low mammalian toxicity [308,309].

In response to the identified health risks from the chromated copper arsenate (CCA), chemical formulations without arsenic and chromium using ionic copper as the primary insecticide and fungicide were developed in the late 80s. Some key examples include the alkaline copper quaternary (ACQ), copper azole, and copper xyligen. Since then ionic copper formulations have become the dominant treatment for outdoor residential applications such as decking, gardening, fencing, and playground equipment in Europe. However, while they were effective in timber preservation, increased leaching of copper ions into the surrounding environment resulted in the degradation of metal fasteners and subsequent structural failure.

Micronized copper has been promoted as an alternative to ionic copper that can address these corrosion and treatment life issues [308]. It has limited market penetration in the EU due to a lack of regulatory approval, but over 75% of the residential lumber produced in the USA is nowadays treated with micronized copper [310] produced by mechanical grinding of compounds such as basic copper carbonate ($Cu_2(OH)_2CO_3$) or copper oxide (CuO) with dispersing agents in a carrier solution [308]. The size of the resulting particles ranges from 1 to 25000 nm, with typically 90% of the particles below the size of 1000 nm [308]. Leaching is significantly controlled in micronized wood treatments as compared to ionic wood treatments, and less than 5% of it was in particulate form [311]. While a proportion of micronized copper formulations are nano-sized [308], the potential additional advantage offered by copper formulations within the nano-size range are even more substantially being considered [312–314]. Clausen (2007) argues that dispersion stability coupled with controlled particle size in nano-sized wood preservative formulations may greatly improve preservative penetration, treatability of refractory wood species and stability of finishes and coatings for above ground applications. Accordingly, nanoparticles of CuO and $Cu_2(OH)_2CO_3$have been increasingly considered for micronized wood treatment formulations [313–315].

The increased use of nano-scale CuO and $Cu_2(OH)_2CO_3$ as timber preservatives has raised concerns about the potential of these substances to cause undesirable human health effects. In spite of the fact

that ionic copper formulations are currently thoroughly reviewed in Europe for their human and environmental risks under the Biocidal Products regulation (Regulation (EU) No 528/2012), there are only few studies that attempted to assess their risks [316,317]. Therefore, we performed a quantitative human health risk assessment (HHRA) of nano-scale CuO and $Cu_2(OH)_2CO_3$ along the lifecycles of antimicrobial/antifungal coatings and impregnations. This is the first quantitative estimation of the risks from these products from lifecycle perspective.

In the work described in this chapter, we applied the HHRA framework for regular chemicals as it has been considered by the European Scientific Committee on Emerging and Newly Identified Health Risks (SCENIHR) applicable to nanomaterials [318]. This approach consists of hazard identification, dose-response assessment, exposure assessment and risk characterization steps [306]. We applied it as a probabilistic methodology designed to quantitatively estimate and communicate the uncertainties in each of these steps in order to demonstrate how they influence the final results [319,320]. Then we implemented this methodology as a software module in the web-based EU FP7 SUN project's Decision Support System (SUNDS), which enabled it to estimate occupational, consumer and public health risks from manufactured nanomaterials along the lifecycles of nano-enabled products.

This chapter demonstrates the SUNDS HHRA module with dose-response data from in vivo experiments specifically designed to measure the subacute effects following inhalation and oral uptake of nanoscale CuO and $Cu_2(OH)_2CO_3$. The dose-response relationships were compared to external human exposure concentrations estimated for 13 relevant exposure scenarios (ES), which were formulated based on release data and contextual information on a CuO-based acrylic coating and a $Cu_2(OH)_2CO_3$-containing impregnation.

7.2 Methods

7.2.1 Case study products

7.2.1.1 CuO used in an antimicrobial/antifungal wood protective coating

CuO pristine nanoparticles were obtained as a black powder from the company PlasmaChem GmbH, Berlin, Germany. They were synthesized by thermal decomposition of an inorganic precursor in solid phase. The synthesized and dry-milled $Cu_2(OH)_2CO_3$ precursor was decomposed at approximately 350°C for several hours. The derived crystalline powder had a TEM particle size of 15–20 nm, a Brunauer–Emmett–Teller (BET) specific surface area of 47 g/m^2 and a bulk material density of 6.3 g/cm^3 according to the supplier. To check consistency with these data and complement them, we performed detailed physicochemical characterisation of size (distribution), shape, crystallite phases, dispersibility, agglomeration/aggregation, stability, surface area and chemistry, chemical composition and impurities. The adopted methods and the obtained results are described in detail in Table 36.

The CuO nanopowder was dispersed in a solution by mixing according to an established BASF protocol [321]. Specifically, we added it to a high-gloss acrylic wood coating, where the anticipated antimicrobial activity of the CuO would provide the additional functionalities of sealing the wood and serving decorative purposes. The wood coating liquid was then applied either by spraying or brushing onto the surface of blocks of pine wood with dimensions of 2.5 x 2.5 x 1 cm (n=70). Some of the blocks were coated entirely with a CuO-free (TiO2) coating to serve as a negative control. The rest of them were coated on one side with the TiO2/CuO coating on a chemically inert substrate (Teflon or Poly Ethylene)

and dried for a week in preparation for release experiments intended to generate data for formulating ES (cf. 7.2.2). The coatings were thoroughly characterised, and the results are reported in Pantano et al. (2018) [322] and in Table 37 and Table 38.

Table 36: Physicochemical characteristics of pristine CuO (SYNTHESIS).

Parameter	**Technique**	**Results**
Primary size distribution Min- Max (average) Mode (1st quartile … 3rd quartile) [nm]	TEM	3-35 (12) 10 (9.2.14)
Shape	TEM	Semi-spherical particles
Average crystallite size [nm]	XRD	9.3
Crystallite phases (%)	XRD	Tenorite 100%
Dispersibility in water: D_{50} [nm]; average agglomeration number (AAN)	DLS	139.5 ± 4.6; 346
Dispersibility in modified MEM provided by the Heriot -Watt University: D_{50} [nm]; average agglomeration number (AAN)	DLS	85.2±2.7; 77
Z potential in UP water [mV]	ELS	+28.1 ± 0.6
Isoelectric point [pH]	ELS	10.3
Photocatalysis: photon efficiency [unitless]	Methylene blue	$1.5x10^4$
Specific Surface Area [$m^2\ g^{-1}$]	degradation BET	47.0 ± 1.7
Pore sizes [nm]	BET	13.5 ± 1.6 (BJH) 23.0 ± 0.9 (AVG)
Surface chemistry [atomic fraction]	XPS	Cu = 0.46±0.05 O = 0.47±0.05 C= 0.07±0.01
Structure	FT-IR and/or RAMAN	Match with CuO database
Chemical impurities [mg kg^{-1}]	ICP-MS	Na: 505±30 Pb: 36±2 Ag: 13±4

Table 37: Physicochemical characteristics of CuO acrylate coating and micronized $Cu_2(OH)_2CO_3$ suspension (FORMULATION).

	CuO acrylate coating	**Micronized $Cu_2(OH)_2CO_3$ suspension**
Nanomaterials content (w/w)	1.5%	54%
Cu content (w/w)	1.2%	30%
Cu ion content (w/w)	N/A	0.5%
Other particulate content (w/w)	52% acrylic binder 43% non-nano TiO2	-
Nanomaterials agglomerate size	range 30 to 100 nm in volume metrics	Median 124 nm in volume metrics, median 34 nm in number metrics.

Table 38: Physicochemical characteristics of CuO coated and micronized $Cu_2(OH)_2CO_3$ impregnated woods (USE).

	CuO acrylate coating on wood	**Micronized $Cu_2(OH)_2CO_3$ impregnated wood**
Cu content related to specimen surface	1.7 g/m²	N/A
Cu content related to specimen mass	0.16 g/m³	1 kg/m³ 2 kg/m³
Application	Wet brushing	Pressure treatment

7.2.1.2 $Cu_2(OH)_2CO_3$ used in an antimicrobial/antifungal wood protective impregnation

Dispersed $Cu_2(OH)_2CO_3$ nanoparticles were obtained from PlasmaChem GmbH, Berlin, Germany. In the process of formulating an impregnation solution, the basic copper carbonate was wet milled until it reached nano-sized particles. The $Cu_2(OH)_2CO_3$ was then combined with water, stabilisers and co-biocides to make the stock solution. Small wood blocks were then immersed/soaked in this impregnation dispersion. This was adequate for research purposes, but on industrial scale pressure impregnation is typically carried out in steel cylinders or retorts. The wood is loaded on special tram cars and moved into the retort, which is then closed, evacuated and subsequently filled with preservative solution. Then pressure forces the preservative into the wood until the desired amount is absorbed.
The results of the performed detailed physicochemical characterisation of the micronized $Cu_2(OH)_2CO_3$ suspension and the impregnated wood are reported in Pantano et al. (2018) [323] and in Table 37 and Table 38.

7.2.2 Risk assessment by means of SUNDS

The SUNDS framework was previously described [268], where the computational risk assessment approach illustrated in this chapter is part of the SUNDS Tier 2 and is described in more detail in Chapter 5. This probabilistic HHRA module is designed to quantitatively estimate and communicate the uncertainties in each step of the risk analysis. The system can simultaneously assess risks in different lifecycle stages, targets, activities and routes of exposure based on in vivo toxicity data and ES. It is schematically depicted in Figure 36.
For each ES, based on a combination of the exposure assessment (estimation of external concentration) and hazard assessment (estimation of human effect threshold dose) the system produces a discrete value or a probability distribution of risk and the associated uncertainty. To do this, SUNDS uses exposure measurements, or if such are not available exposure can be estimated by means of models (e.g. NanoSafer, Ingestion Exposure Tool) that are either integrated in the system or interact with it externally. To assess a human effect threshold SUNDS can use in vivo raw data to perform dose-response analysis by means of a dedicated model and then to correct the obtained Point of Departure (PoD) (i.e. Benchmark Dose (BMD)) and extrapolate it to a human dose (HD) by means of the APROBA tool, which is integrated in the system. In some cases, the PoD (e.g. BMD or No-observed

Adverse Effect Level (NOAEL)) is available from the published literature and therefore can be directly imported in the system instead of analysing raw data. This is the case of this risk assessment, where the dose-response analysis involved PoD estimated in other studies, which were only corrected and extrapolated to HD by means of SUNDS/APROBA as it is described in 5.2.2.2.

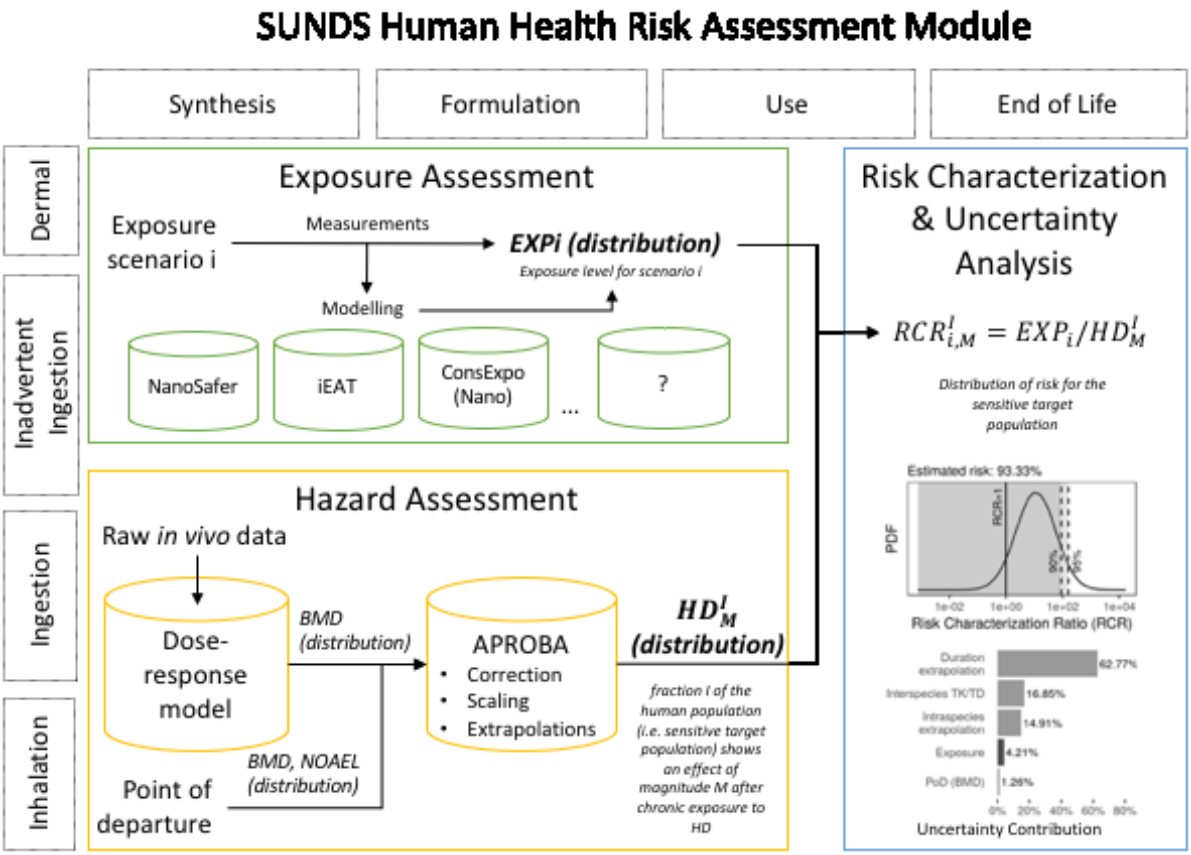

Figure 36: Structure, models, inputs and outputs of the human health risk assessment module of the SUN Decision Support System (SUNDS).

The following sections 5.2.2.1-5.2.2.3 describe how the SUNDS HHRA module was applied for exposure and hazard assessment of the case-studies presented in 5.2.1 to assess occupational and consumer risks along their lifecycles and to communicate the associated uncertainties.

7.2.2.1 Exposure assessment

7.2.2.1.1 Formulation of exposure scenarios

To gather the knowledge and expertise needed to formulate realistic workplace and consumer ES we performed a literature review, organised a dedicated workshop and obtained additional contextual information from the industrial companies BASF and Koppers Inc.

Specifically, published literature from 2000 to 2016 was searched for relevant release and exposure assessment studies. To do this we queried the Web of Science database with combinations of the following keywords: nano, copper oxide, copper carbonate, micronized copper, CuO, $Cu_2(OH)_2CO_3$, impregnation, exposure assessment, release, emission, exposure, workplace, consumer, use. The literature search resulted in a small number of documents, which were carefully analysed. In addition,

mapping of release hot spots along the lifecycles of the investigated products was performed as part of the SUN project [324]. We used these results as a basis to design the exposure assessment expert workshop.

Table 39: Description of the exposure scenarios assessed for nanoscale CuO used in wood coating paints and nanoscale $Cu_2(OH)_2CO_3$ used in timber preserving impregnations.

Exposure scenario (ES)	LC stage	Target	Exposure route	Exposure level (EXP_i)	Additional information	Source
ES1: Laboratory scale CuO powder production, handling and packing	SYN	Worker	Inhalation	negligible	Breathing zone and far field respirable mass concentrations below the minimum detection limits of 161 and 26 µg m^{-3}, respectively, assuming background concentration level is 0 µg m^{-3}.	[325]
		Worker	Dermal	negligible	Surface contamination was not detected, and dermal and perioral exposure are negligible*	
ES2: Pouring CuO nanoscale powder in the wood coating matrix	FOR	Worker	Inhalation	NF 26 µg/m^3 and FF 10 µg/m^3	In case the fume cupboard was active the concentration was < 0.2 µg/m^3. If the fume cupboard would be switched off and pouring would be performed in a room the concentration would be in the NF 26 µg/m^3 and FF 10 µg/m^3 i.e. 130 times higher than with the fume cupboard.	SUN project deliverable 5.4
		Worker	Dermal	negligible	Surface contamination: dermal and perioral exposure are negligible*	
ES3: Applying CuO wood coating to the substrate	USE	Worker	Inhalation	negligible	Since CuO wood preservative is highly viscous (viscosity N/A) it is applied by brush to the substrate. Release of respirable ($PM_{4.5}$) CuO wood preservative droplets is assumed to be negligible during brush painting. Thus, the inhalation exposure is negligible.	[326]
		Worker	Dermal	negligible	Surface contamination: dermal and perioral exposure are negligible*	
ES4: Sanding, cutting, drilling and sawing wood treated with CuO preservative	USE	Worker, Consumer	Inhalation	93 µg/m^3	Modelled NF CuO_2 concentration during continuous outdoor sanding.	SUN project deliverable 5.4
		Worker, Consumer	Dermal, Perioral	Dermal: negligible Perioral: 6.11E-06 (SD 2.29E-06) mg/kg/day	Surface contamination: dermal exposure is negligible, while perioral exposure has been assessed for consumers based on the IEAT model and considering an average of 6.3 hand-to-mouth (oral or perioral) contacts per day.	SUN project deliverable 5.4, [327]
	EOL	Worker	Inhalation	negligible	The percentage of treated wood in the waste is very low, thus reducing the emission of CuO.	[328]
		Worker	Dermal	negligible		
ES5: Consumers transfer to skin from surfaces by rubbing	USE	Consumer	Dermal	negligible	The wiping test performed in the SUN project indicated insignificant transfer to the skin.	[329]

Exposure scenario (ES)	LC stage	Target	Exposure route	Exposure level (EXP_i)	Additional information	Source
ES6: $Cu_2(OH)_2CO_3$ powder production, handling and packing	SYN	Worker	Inhalation	negligible	In this study, we assume that the occupational exposure levels during $Cu_2(OH)_2CO_3$ production, handling and packaging are, like for CuO, below the detection limits, which were 161 µg m^{-3}, 70, and 200 µg m^{-3}, respectively, when assuming background concentration level is 0 µg m^{-3}.	[325]
		Worker	Dermal	negligible	Surface contamination: dermal and perioral exposure are negligible. According to the latest skin penetration tests performed in SUN, dermal exposure is not relevant since the penetration rate is negligible for nanomaterials	
ES7: Milling of $Cu_2(OH)_2CO_3$ slurry for the impregnation stock solution	FOR	Worker	Inhalation	negligible	We assume that for the formulation phase, no inhalation exposure will occur due to negligible emissions to the air	SUN project deliverable 2.3
		Worker	Dermal	negligible	Surface contamination: dermal exposure is negligible since emissions are negligible	
ES8: Workers impregnating wood in an industrial setting	USE	Worker	Inhalation	negligible	For the vacuum pressure treatment process in industrial scenario, the emissions to air are limited. So, no relevant exposure scenarios are assessed	[330]
		Worker	Dermal	negligible	Surface contamination: dermal and perioral exposure are negligible*	
ES9: Workers constructing garden fences, decking, cladding, playgrounds, vegetable gardens using the treated wood	USE	Worker	Inhalation	negligible	For waterborne preservatives, very low emissions to air	[330]
		Worker	Dermal	negligible	Surface contamination: dermal and perioral exposure are negligible. According to the latest skin penetration tests performed in SUN, dermal exposure is not relevant since the penetration rate is negligible for nanomaterials	
ES10: Consumer transfer to skin from surfaces by rubbing	USE	Consumer	Inhalation	negligible	Inhalation exposure is assumed negligible	[329]
		Consumer	Dermal	negligible	Surface contamination: dermal and perioral exposure are negligible. According to the latest skin penetration tests performed in SUN, dermal exposure is not relevant since the penetration rate is negligible for nanomaterials	
ES11: Children exposed directly to the treated wood by skin contact, transfer of copper to the month and related ingestion	USE	Consumer	Oral	0.07 (SD 0.03) mg/kg/d	Assuming an average weekly exposure of 1.11 mg/day, corresponding to three visits to the playground and dividing by the distribution of weights of children aged 8-36 months.	[311]

Exposure scenario (ES)	LC stage	Target	Exposure route	Exposure level (EXP_i)	Additional information	Source
ES12: Sanding, cutting, drilling and sawing wood treated with $Cu_2(OH)_2CO_3$ preservative	EOL	Worker	Inhalation	negligible	The percentage of treated wood in the waste is very low, thus reducing the emission of $Cu_2(OH)_2CO_3$.	328
		Worker	Dermal	negligible	Dermal deposition was considered negligible as the workers wear gloves.	
ES13: Leaching during contact with water and related potential human exposure (appl. to both CuO and $Cu_2(OH)_2CO_3$)	USE	Consumer	Oral	negligible	Leaching experiments performed in SUN showed that the released copper was solely in ionic form. Platten et al. (2014) [311] showed that mostly ionic copper (> ~95%) is released from the wood treated with $Cu_2(OH)_2CO_3$ and that the particulate copper that was released is attached to cellulose and is therefore not free in the solution.	311,323
	EOL	Public	Oral	negligible	The percentage of treated wood in the landfilled waste is very low. Release from landfills is negligible in general.	328

SYN = Synthesis; FOR = Formulation; EOL = End of life; * Workers are assumed to wear protective gloves (e.g. nitrile) which prevent direct skin exposure. Thus, the skin exposure is assumed to be insignificant. Perioral exposure is also assumed to be insignificant unless a worker puts dirty glove in her/his mouth.

The workshop took place on 22 January 2016 in Venice and was attended by 22 academic and industrial experts in human exposure assessment and copper-based timber preservatives from EU, US and Russia. The discussions resulted in generic ES, which were then further elaborated with information obtained from the literature and from the industrial companies BASF and Koppers Inc. The formulated ES covered the entire lifecycles (i.e. synthesis, formulation, use, end-of-life) of the investigated products and are listed in Table 39. In cases when estimations of exposure were not available in the literature, such were derived in the SUN project by means of the experimental and modelling methods described in 5.2.2.2.

7.2.2.1.2 Estimation of exposure

The following experimental and modelling activities were performed with our case study products (cf. 7.2.1) in order to derive exposure estimations for each of the formulated ES for performing risk assessment by means of SUNDS. The numbering of the different ES corresponds to Table 39.

ES 1 and 6 involving laboratory production, handling and packing of nanoscale CuO and $Cu_2(OH)_2CO_3$ powders

CuO and $Cu_2(OH)_2CO_3$ nanoscale powders are produced using sol gel synthesis. The sol gel synthesis and packing were performed in a fume hood where the bags were canned, and the cans were subsequently moved to a storage room. Occupational exposure measurements were performed, which resulted in breathing zone and far field respirable mass concentrations below the minimum detection limits of 161 and 26 µg m-3, respectively [325]. The surface wipe samples analysed with a Scanning Electron Microscope (SEM) did not reveal any CuO particles [325]. Therefore, based on these results we concluded that the exposure levels for ES 1 and 6 are negligible.

ES 2 and 7 involving pouring nanoscale CuO powders in the wood coating stock solutions

The nanoscale CuO pouring to the liquid matrix was not measured. The exposure levels were estimated by means of a one-box model [331]. Laboratory scale powder mixing was assumed to be performed without using any emission controls (i.e. worst-case scenario). The parameters used for modelling of manufacturing 100 L CuO preservative are the following: Dustiness index = 104 mg/kg (moderate); mass flow = 1 kg/min (careful pouring); handling energy = 1 (equivalent release as in dustiness test); local emission controls = 1 (no control); pouring amount = 2.5 kg (poured from 1 kg bags, 9 minutes between pouring); room volume = 20 m3 (small room); ventilation rate = 2 h-1. The results of the modelling are reported in Table 39.

ES 3 involving application of CuO wood coating to the substrate

Because the Cu-based acrylic formulation is highly viscous it is applied to the substrate by a brush. Release of respirable (PM4.5) droplets of this solution is assumed to be insignificant during brush painting [326], so the inhalation exposure is assumed negligible. Workers performing the brushing are supposed to wear protective gloves to prevent direct skin exposure. If the gloves are worn correctly at all times, the skin exposure is insignificant. Hand-to-mouth exposure is also assumed to be negligible unless the worker touches mouth with contaminated gloves.

ES 4 involving scraping, sanding and sawing wood treated with CuO preservative

The old CuO wood preservative coating is typically removed before surface treatment. Because the dry coating is viscoelastic (elasticity modulus of the matrix is 10-7 Pa) the coating is likely removed by scraping, which produces an insignificant amount of respirable particles: the smallest 10 % size fraction of particles were 20 μm in size [332].

Emission rates were estimated based on sanding and drilling release experiments, which were used to represent also sawing. The exposure levels were estimated based on these data by means of a single and two box models [331,333]. The parameters used for modelling of sanding are the following: Emission rate = 20 μg/sec where 2 % is CuO2 (sanding disc dimeter 150 mm, grit size 80, rotation speed 1550 rpm, and contact force 17 N); local emission controls = 1 (no control); room volume = 100 m3 (outdoor); FF ventilation rate = 10 h-1 (still air), near-field volume = 8 m^3 after [334]; near-field air flow = 10 m^3/min. This resulted to a near-field (NF) concentration of 93 μg/m3 during continuous process. The results of the modelling are reported in Table 39.

ES 5 involving transfer to consumers' skin from surfaces by rubbing

Consumers are assumed to be handling painted wood with their hands without wearing protective gloves, which can lead to direct skin exposure and subsequent inadvertent ingestion by touching the area around the mouth. Hand exposure was assessed by conducting dermal transfer tests in the SUN project by means of the surface wiping method based on the NIOSH guideline Elements on Wipes: Method 9102 [335]. The experimental set-up and the obtained results are described in detail in Mackevica et al. (submitted) [329].

Perioral exposure was estimated using a modified version of the Ingestion Exposure Tool (iEAT) [336], assuming that a person touches a wood surface painted with CuO that has released CuO particles as a consequence of wearing and touches inadvertently the area around the mouth with subsequent ingestion by licking. The transfer efficiency of nanomaterials from finger tips to the perioral area was estimated experimentally. A worst case was assessed, where all the copper released from the wood is transferred to the finger tips. Each surface to hand event was presented as a hypothetical scenario were someone (with low or high hand moisture) touches the wood and then touches the perioral area. We assumed the finger area of contact was 1 cm^2 and the perioral area of contact also 1 cm^2.

ES 11 involving children exposed directly to the $Cu_2(OH)_2CO_3$ impregnated wood by skin transfer of copper to the month and related ingestion

The most likely place for children to come into contact with copper-based impregnated wood is a playground, where its skin can be exposed to copper with subsequent transfer to the mouth and related ingestion. Estimations of children exposure have been provided by Platten et al. (2014) [311], where the wood surface area a child would come into contact with during a typical visit to a playground has been estimated along with potential transfer, ingested concentration per playground visit and number of visits per week.

ES 13 involving leaching during contact with water and related potential human exposure

General population can come in contact with nano-scale CuO or $Cu_2(OH)_2CO_3$ released by the wood during contact with water. To estimate the amount and form (particle or ion) of released copper, leaching experiments were performed in the SUN project according to the European standard EN 84 [337], which describes an accelerated aging test of pine specimens treated with wood preservative formulations for

simulating exposure to water [337]. The investigated material was the acrylic coating containing 1.5% CuO and 42.5% TiO2 (pigment grade, non-nano) which was applied on pine wood (dimension: 2.6 x 2.7 x 1.1 cm). The result from applying the test showed that the released copper was solely in ionic form [323].

In the case of nano $Cu_2(OH)_2CO_3$, Platten et al. (2014) [311] reported results from leaching tests indicating that mostly ionic copper (>~95%) was released from the treated wood and that the particulate copper that was released is attached to cellulose and is therefore not free in the leaching waters.

Based on these results, the human exposure to nanoparticles leaching during contact of CuO coatings and $Cu_2(OH)_2CO_3$ impregnations with water was considered negligible.

7.2.2.1.3 Derivation of exposure distributions

The above exposure levels were used to generate an exposure distribution (EXPi) for each scenario i by means of SUNDS. When only deterministic values were available, normal or lognormal distributions were used to describe the probabilistic distribution of exposure as recommended by the US Environmental Protection Agency [300]. Such distributions were created around the available deterministic values by fitting a one order of magnitude (+/-50%) wide confidence interval around the mean exposure estimate. The reason for this is that the exposure levels were estimated based on measurements or models, which introduce uncertainties in the EXPi. Indeed, measurements are obtained by instruments, which present known errors, but many other aspects (e.g. preparing the samples, positioning of the instrument) add more uncertainties (often larger than the instrument errors). Moreover, the application of the one box and two box exposure models [331,338] also introduced uncertainties associated with certain assumptions.

7.2.2.2 Hazard assessment

7.2.2.2.1 Hazard identification

To identify the hazards of CuO and $Cu_2(OH)_2CO_3$ nanoparticles, a literature review was performed, which showed that dedicated in vivo inhalation or oral studies that considered multiple exposure doses (and were therefore suitable for dose-response assessment) did not exist [287]. Therefore, we designed and performed short-term inhalation and short-term oral studies in order to derive subacute data that according to the REACH Guidance on Chemical Safety Assessment [288] and the Guidance on Biocides Legislation [339] can be extrapolated for use in long-term HHRA. The used pristine nanomaterials and dispersions were the same described in section 5.2.1. The study designs are only shortly outlined in this section as they are described in detailed in Gosens et al (2016) [287] and de Jong et al (submitted) [340].

Short-term inhalation exposure

After an acclimatization period, rats (8 weeks old, HsdCpb: WU) were exposed nose-only to a single generated exposure concentration of CuO nanoparticles or to clean air as a control for 5 consecutive days. By exposing the animals for various durations (18 min, 36 min, 90 min, 3 h, and 6 h), different dose levels were obtained. A 6 h concentration equivalent was derived by multiplying the duration of exposure by the exposure concentration (designated as dose C x T) and scaling it to the highest exposure duration of 6 h to 13.2 mg/m^3 (for animals dedicated for toxicological examination) or 11.6 mg/m^3 (for animals dedicated for organ burden analysis). Repeated exposures to CuO nanoparticles via inhalation resulted in a linear increase in the determined lung burden, justifying the applied C x T concept.

Short -term oral exposure

Male rats (RjHan: WI, bred Specific Pathogen Free, barrier maintained during experiment) of 8-9 weeks old were obtained from Janvier Labs (Le Genest-Saint-Isle, Saint Berthevin, France). The CuO nanoparticle dispersions were orally administered by gavage using the following exposure doses: vehicle control, 1, 2, 4, 8, 16, 32, mg/kg body weight (b.w.) and a pilot study with 64 mg/kg b.w. The doses were chosen based on information in the literature of soluble non-nano CuSO4, which indicated a No-observed Adverse Effect Level (NOAEL) of 16.3 mg/kg [341]. The dose was administered as 0.1 ml per 20 g (1 ml per 200 g). In an additional study one group of animals (n=4) was exposed to a high dose of 512 mg/kg b.w. For the $Cu_2(OH)_2CO_3$ nanoparticles the administered doses were, vehicle control, 4, 8, 16, 32, 64, and 128 mg/kg b.w. The animals were treated on five consecutive days (days 1-5) and autopsy was performed 24 hours after the last oral administration (day 6). In addition, a recovery period of 3 weeks was included in the experiments to evaluate recuperation and possible persistence of the nanomaterials in the body. Autopsy of the recovery groups was performed on day 26, after three weeks of recovery.

7.2.2.2.2 Dose-response assessment

The dose-response assessment of the raw inhalation data was not performed by means of SUNDS because it was done by Gosens et al. (2016) [287] using the PROAST model. PROAST estimates a benchmark dose (BMD), which corresponds to a pre-defined benchmark response (BMR). The uncertainty of the BMD is reflected by providing a 90% confidence interval with an upper (BMDU) and lower (BMDL) limit.

The dose-response assessment of the ingestion data was also not performed by means of SUNDS, but by de Jong et al (submitted) [340], who derived a Lowest Observed Adverse Effect Level (LOAEL) for decrease of total body weight, which was then divided by an uncertainty factor (UF) of 3 to calculate a NOAEL.

The BMD and NOAEL values derived from the two studies were imported in SUNDS, and used by the system as PoD, which were "corrected" to account for exposure duration differences between the animal experiments and the ES. In addition, allometric scaling was performed in case of oral studies to consider physiological differences between the experimental animals and humans. These "corrected" probability distributions were then extrapolated to human effect threshold distributions by applying appropriate inter- and intra-species extrapolation factors (EF) [288].

The correction, allometric scaling and extrapolations were performed by means of APROBA, which is a Microsoft Excel tool developed by the World Health Organisation's International Programme on Chemical Safety (IPCS-WHO) [266] and is programmed in SUNDS. It is able to perform approximate probabilistic (as well as deterministic) analysis of human dose extrapolation starting from animal dose-response results. The result of the probabilistic hazard assessment is a human effect threshold, called human dose HD_M^I at which a fraction I of the human population shows an effect of magnitude M after chronic exposure, with a specific confidence interval (e.g. 90%). This fraction I represents the sensitive target population, which is the portion of population that is more vulnerable to effects of exposure to the substance due to e.g. age or poor health status. APROBA contains default algorithms and values for performing correction and allometric scaling based on input information (cf. 7.3.2.2 and Table 42) [266]. It also uses default extrapolation factors, which were proposed by the IPCS-WHO and are reported in Table 40.

Table 40: Generic Uncertainty (Extrapolation) Factors (UF) for different aspects of the dose-response assessment assuming lognormal uncertainty distributions. Source: IPCS-WHO guidance document on evaluation and communication of uncertainty in hazard characterisation [266].

Aspect of hazard characterization	**Lognormal P50**	**Lognormal P95/P50**	**Lognormal (P05, P95)**	**Comments**
PoD uncertainty for NOAEL*: $AF_{PoD\text{-}NOAEL}$				
Continuous endpoint, chronic/subchronic study	1/3	4.7	(0.07, 1.6)	Ratio of NOAEL to BMD_{05} (5% relative change)
Continuous endpoint, developmental study	1/3	7.0	(0.05, 2.3)	Ratio of NOAEL to BMD_{05} (5% relative change)
Deterministic quantal endpoint	2/9	5	(0.04, 1.1)	Ratio of NOAEL to ED_{50} (50% response)
Stochastic quantal endpoint	2/3	4.7	(0.14, 3.2)	Ratio of NOAEL to BMD_{10} (10% extra risk)
Exposure duration: AF_{Dur}				
Subchronic → Chronic	2	4	(1/2, 8)	--
Subacute → Chronic	5	8	(5/8, 40)	--
Interspecies body size adjustment: $AF_{Inter\text{-}BS}$				
Oral	$\left(\frac{bw_{human}}{bw_{test\ species}}\right)^{0.3}$	$\left(\frac{bw_{human}}{bw_{test\ species}}\right)^{0.04}$	$\left(\frac{bw_{human}}{bw_{test\ species}}\right)^{(0.26,0.34)}$	Use case-specific body weights
Inhalation	1/RDDR or 1/RGDR	2	(0.5, 2)/RDDR or (0.5, 2)/RGDR	Use case-specific RDDR (particle) or RGDR** (gas)
Interspecies TK/TD differences: $AF_{Inter\text{-}TK/TD}$				
Oral	1	3	(1/3, 3)	Given lack of alternative, can also be used for inhalation
Intraspecies differences for incidence *I*: $AF_{Intra\text{-}I}$				
I = 5%	5.0	2.8	(1.8, 14)	Log(GSD_H) P50 = 0.32 and P95/P50 = 2.2
I = 1%	9.7	4.3	(2.2, 42)	
I = 0.1%	20.4	7.0	(2.9, 143)	

BMD_x: benchmark dose for x% benchmark response; bw: body weight; ED_{50}: median effective dose; GSD_H: geometric standard deviation for interindividual variability in the human equipotent dose distribution; NOAEL: no-observed-adverse-effect level; P05: 5th percentile; P50: 50th percentile; P95: 95th percentile; PoD: point of departure; RDDR: regional deposited dose ratio; RGDR: regional gas dose ratio; TK/TD: toxicokinetic/toxicodynamic. *When using a NOAEL as the PoD, the uncertainty includes both the fact that the NOAEL is an approximation for the BMDL as well as the uncertainty in the underlying BMD (a ratio of 3 is assumed between the median estimate of the BMD and the BMDL). ** For gases, the RGDR is often assumed to be 1.

7.2.2.3 Risk characterization & Uncertainty analysis

Risk was calculated by means of SUNDS based on the Risk Characterization Ratio ($RCR^{I}_{i,M}$) approach, which takes into account uncertainty and variability related to the incidence goal sensitive population. $RCR^{I}_{i,M} = EXP_i/HD^{I}_{M}$, where EXPi represents an exposure level for scenario i. The $RCR^{I}_{i,M}$ distribution is classified as "non-acceptable" when it is above 1 for more than 10% of the sensitive population. The variability related to the rest of population is not taken into account in HD^{I}_{M} because when the sensitive population is at risk we assume that also the general population is at risk. The exposure situation "needs further consideration" when the $RCR^{I}_{i,M}$ is above 1 in 5% to 10%, and the risk is "acceptable" when it is above 1 for less than 5% of the sensitive population. These risk acceptability classes were defined based on the literature, which suggests that (in the case of probabilistic risk assessment) the risk can be acceptable if the 90th percentile of the population is safe, but more conservative values (i.e. the 95th percentile or the 99th percentile) can also be selected [298–300].

RCR distributions were generated for each of the ES by sampling the HD^{I}_{M} and EXP_i distributions in over 10 000 Monte Carlo simulations. The probablity distribution of the RCR is affected by 1) the assumptions/considerations applied in the probabilistic hazard assessment and 2) the uncertainties associated with the exposure estimations. In the first case, selecting a specific population incidence goal (e.g. 5%) in the dose-response assessment implies that the resulting probabilistic distribution of the RCR protects 95% of the population, thus the RCR probability distribution represents the variability and uncertainty around the 95% of the assessed population.

The contribution of different sources to the overall uncertainty in the RCR was estimated for each ES by means of Monte Carlo. In each of the 10 000 simulations RCR was numerically estimated by randomly sampling 10 000 elements from the distributions of the PoD, exposure and UF. The contribution of each of these factors to the uncertainty in the risk estimate was quantified by assessing the level of correlation between the factor and the resulting RCR by means of the squared Spearman's rank correlation coefficient.

7.3 Results

7.3.1 Exposure assessment

13 ES were formulated that covered the entire lifecycles (i.e. synthesis, formulation, use, end-of-life) of our case-study products: CuO-based coating paint and $Cu_2(OH)_2CO_3$-containing impregnation (Table 39).

The exposure assessment of the CuO-based coating demonstrated that release of nanoparticles is possible at each lifecycle stage and can lead to both worker and consumer exposure in different formulations: as nanopowder, as liquid paint, or as a cured surface coating on wood. The handling of dry powders led to some significant exposure potential in the formulation lifecycle stage. If paint spraying is avoided, inhalation exposure to paint is assumed negligible during its application, but dermal and oral exposure could be relevant for both workers and consumers either via accidental dermal deposition when treating (painting) the wood or via hand-to-mouth (i.e. inadvertent oral) exposure. However, according to the latest studies dermal exposure is insignificant [342]. Moreover, the dermal transfer testing of the painted wooden blocks (cf. 7.2.2.2) showed that there was nearly no release of nanoscale CuO from the paint matrix during surface wiping tests [329]. However, after sanding of the paint

surface, the observed CuO release was magnitudes higher. Accordingly, inhalation and inadvertent oral exposures were assessed in the case of occupational and consumer use during sanding activities and the results were used to represent also sawing operations.

The analysis of the literature on $Cu_2(OH)_2CO_3$-impregnated wood showed that the release of copper nanoparticles is typically negligible. The US EPA report provided an estimate of exposure for the concerning ES11 that involves children exposed directly to the treated wood by skin contact, transfer of copper to the month and subsequent ingestion [311]. Moreover, two other common exposure pathways were identified and assessed: leaching during contact with water and transfer during physical contact (Table 39).

We used SUNDS to generate EXP_i probability distributions for each ES based on the estimated exposure levels, which demonstrated significant exposure potential for scenarios 2, 4 and 11 (Table 41). To account for unknown uncertainties due to measurement and modelling errors we established a one order of magnitude wide confidence interval around the deterministic inhalation exposure estimates for ES2 and ES4 (0.026 mg/m^3 and 0.36 mg/m^3, respectively) and fitted the corresponding normal distributions. In ES11, starting from an exposure of 1.11 mg/day derived by averaging three visits to the playground over a week [311], we built a normal distribution representing uncertainty in the number of weekly visits characterized by the 5th percentile at 1.11/3 mg/day and the 95th percentile at 1.11 mg/day. This bell-shaped curve was then divided by a uniform mixture of normal distributions representing the variability of weights of children (girls) aged from 8 to 36 months (mean: 10.95 kg, SD: 2.18, $CI_{5\%}$: 7.6 kg, $CI_{95\%}$: 14.68 kg).

Table 41: Summary of exposure distributions (EXP_i) for each scenario i.

	ES1	**ES2 Inhalation**	**ES2 Dermal**	**ES3**	**ES4 Inhalation (Consumer and Worker)**	**ES4 Perioral (Consumer and Worker)**	**ES4 End of Life**	**ES5**
5%	Negligible	1.30E-02	Negligible	Negligible	1.60E-01	2.35E-06	Negligible	Negligible
95%		3.90E-02			4.80E-01	9.87E-06		
50% (Median)		2.60E-02			3.20E-01	6.11E-06		
Mean		2.60E-02			3.20E-01	6.11E-06		
Mode		2.60E-02			3.20E-01	6.11E-06		
SD		7.90E-03			9.73E-02	2.29E-06		
	ES6	**ES7**	**ES8**	**ES9**	**ES10**	**ES11**	**ES12**	**ES13**
5%	Negligible	Negligible	Negligible	Negligible	Negligible	3.23E-02	Negligible	Negligible
95%						1.18E-01		
50% (Median)						6.80E-02		
Mean						7.06E-02		
Mode						6.30E-02		
SD						2.63E-02		

7.3.2 Hazard Assessment

7.3.2.1 Hazard identification

The detailed results from the short-term inhalation exposure are available in Gosens et al. (2016) [287], while the results from the short-term oral exposure are reported in De Jong et al (submitted) [340]. Therefore, only the main findings of relevance for the dose-response analysis (cf. 7.3.2.2) are outlined below.

Short-term inhalation exposure

Twenty-four hours after a 5-day exposure to CuO pristine nanoparticles, dose-dependent lung inflammation and cytotoxicity were observed as well as histological alterations of the nose epithelium. Lung histopathological examinations indicated alveolitis, bronchiolitis, vacuolation of the respiratory epithelium and emphysema in the lung starting at a 6 h-concentration equivalent of 2.4 mg/m^3.

After a recovery period of 22 days, limited lung inflammation was still observed leaving a small but significant elevation of macrophages in the airspace (at the highest dose of 13.2 mg/m^3. This inflammation was not accompanied by pathological changes or elevated biochemical markers of fibrosis. The histological alterations of the olfactory epithelium in the nose restored completely after 22 days. No histopathological changes were detected in the brain, olfactory bulb, spleen, kidney and liver. In conclusion, a 5-day, 6-hour/day exposure equivalent to an aerosol of agglomerated CuO nanoparticles resulted in a dose-dependent toxicity in rats, which almost completely resolved during a 3-week post-exposure period. The data for all endpoints measured were compared via the BMD calculated by PROAST. This allowed a ranking of the relative sensitivity of each endpoint to the inhaled CuO nanoparticles with biochemical markers and inflammatory cell number in the bronchoalveolar lavage fluid providing to be the most sensitive indicators for lung toxicity [287].

Short-term oral exposure

Copper oxide: In the dose response study with a maximum dose of 64 mg/kg, no signs of toxicity were noted. After treatment of 5 consecutive days there was no difference in body weight between day 1 (start of treatment) and day 6 (24 hours after end of treatment). In the additional group of animals treated with 512 mg/kg some indications for toxicity were observed based on changes in the body weight. Moreover, the results of the clinical chemistry showed that at day 6 alterations in the level of alkaline phosphatase and aspartate aminotransferase enzymes indicated the presence of liver toxicity. At the dose of 64 mg/kg lactate dehydrogenase levels were also increased indicating cell and organ damage. Animals treated with 512 mg/kg showed similar alterations in clinical chemistry (low level of alkaline phosphatase, high level of aspartate aminotransferase, and high level of lactate dehydrogenase), and histopathological alterations in the liver (e.g. inflammation, hepatocellular hypertrophy, hepatocellular necrosis) thus supporting the data of the dose response study. Therefore, the dose 512 mg/kg was taken as the LOAEL.

Copper carbonate: For $Cu_2(OH)_2CO_3$ nanoparticles a dose response study was performed with the highest dose being 128 mg/kg b.w. Repeated (5 times) oral administration of the highest dose induced severe toxic responses in the treated animals as indicated by the behaviour of the animals, frequent washing and piloerection. Based on these observations the animals scheduled for prolonged observation (autopsy after a recovery period at day 26 after treatment) were autopsied prematurely at days 6 and 7, respectively 24 and 48 hours after the last (day 5) treatment.

For animals treated with a dose up to 64 mg/kg b.w. both at day 6 and day 26 after treatment both body and organ weights did not show a difference with the vehicle treated control animals. These results were consistent with the results from the haematological and clinical chemistry analyses. However, for the animals treated with 128 mg/kg b.w. at day 6 a decrease in body weight and weight of heart, liver, spleen, thymus was observed whereas adrenal weights were increased, the latter probably indicating a stress response due to the toxicity of the $Cu_2(OH)_2CO_3$ nanoparticles. In addition, several clinical chemistry parameters in the blood were affected (e.g. white blood cell increase, red blood cell decrease, and increases in ALT, AST, and LDH) Histopathological lesions were observed in various organs, notably the liver (hepatocellular vacuolation, hypertrophy, and necrosis, and single cell necrosis) [340].

7.3.2.2 Dose-response Analysis

Deriving the PoD

The inhalation study argued that changes in the total number of inflammatory cells in the BAL can be considered a critical endpoint for inhalation risk assessment and proposed a BMR of 100% based on previous studies (Gosens et al. 2016). This BMR was used to calculate a BMDL of 0.16 mg/m^3 and a BMDU of 0.29 mg/m^3 by means of PROAST [287]. This BMD lognormal distribution was used as the PoD for risk assessment.

As far as CuO ingestion toxicity is concerned, based on the short-term oral exposure de Jong et al (submitted) [340] a LOAEL for decrease of total body weight corresponding to 512 mg/kg was estimated. We divided this value by an UF of 3 to calculate a NOAEL of 170.67 mg/kg. The short term oral study of the $Cu_2(OH)_2CO_3$ derived a LOAEL of 128 mg/kg, which we similarly divided by an UF of 3 to estimate a NOAEL of 42,67 mg/kg b.w. These NOAEL values were corrected by means of APROBA (when needed) for differences in human and experimental exposure conditions and in respiratory volumes between experimental animals (at rest) and humans (light activity) and then used as PoD for risk assessment.

Selecting the Uncertainty Factors

The selected UF for CuO are for interspecies scaling, interspecies toxicokinetic and toxicodynamic, intraspecies differences and differences in duration of exposure for both ingestion and inhalation. The selected UF for $Cu_2(OH)_2CO_3$ are interspecies scaling, interspecies toxicokinetic and toxicodynamic, intraspecies differences and differences in duration of exposure for the ingestion pathway. The probabilistic distributions of these factors are the default values suggested by APROBA and reported in Table 40.

Deriving the distributions of HD

The PoD were used as inputs to APROBA, which was applied with the above inter- and intra-species scaling and uncertainty factors as shown in Table 42 to derive lognormal distributions of long-term HDs for local and systemic effects due to both inhalation and ingestion of CuO and only ingestion of $Cu_2(OH)_2CO_3$. The results are reported in Table 43.

Table 42: APROBA input data and output results

	Notes	CuO Inhalation	CuO Ingestion	$Cu_2(OH)_2CO_3$ Ingestion
Inputs to APROBA				
Data type		Continuous	Continuous	Continuous
Target BMR		100%	5%	5%
PoD type		BMDL	NOAEL	NOAEL
PoD unit of measure		mg/m^3	mg/kg bw/day	mg/kg bw/day
PoD value		0.16	170.67	42.67
BMDU (in case of using the BMD approach)		0.29	---	---
Reference to support the PoD selection		287	340	340
Factor used to correct PoD to consider differences in human and experimental exposure conditions	Workers are assumed to be exposed 8 hours per day. This correction factor applies in case of inhalation studies.	0.375	n.a.	n.a.
Exposure conditions		3 h/day	n.a.	n.a.
Factor used to correct PoD for differences in respiratory volumes between experimental animals (at rest) and humans (light activity).	This correction factor applies in case of inhalation studies.	0.67	n.a.	n.a.
Corrected PoD value (BMDL)	PoD (BMDL) and BMDU values corrected multiplying original values by the correction factors, in case of inhalation studies.	0.040	---	---
Corrected BMDU (in case of using the BMD approach)		0.073	---	---
Data route		Inhalation	Oral	Oral
Study type		Subacute	Subacute	Subacute
Test species		Rat	Rat	Rat
Species weight (average)		0.332 kg	0.228 kg	0.366 kg
Human weight		70 kg	70 kg	10 kg
Population Incidence Goal (I)		5%	5%	1%

	Notes	CuO Inhalation	CuO Ingestion	$Cu_2(OH)_2CO_3$ Ingestion
Probabilistic Coverage Goal		95%	95%	95%
Overall deterministic UF		100	100	100
Outputs from APROBA				
NOAEL to BMD (LCL)	Uncertainty in transforming a NOAEL to BMD	1	0.07	0.07
NOAEL to BMD (UCL)		1	1.57	1.57
Interspecies scaling (LCL)	This aspect addresses the interspecies adjustment to take into account differences in body size (e.g. allometric scaling).	1	4.43	2.36
Interspecies scaling (UCL)		1	7.01	3.08
Interspecies TK/TD (LCL)	This aspect addresses remaining interspecies TK and TD (toxicokinetic and toxicodynamic differences) differences after accounting for body size differences.	0.333	0.333	0.333
Interspecies TK/TD (LCL)		3	3	3
Duration Extrapolation (LCL)	This aspect addresses uncertainty in using a less-than-chronic study (as specified in "Study type" previously) to estimate a chronic PoD.	0.625	0.625	0.625
Duration Extrapolation (UCL)		40	40	40
Intraspecies (LCL)	This aspect addresses the uncertainty in the amount of human variability in sensitivity. It depends directly on the "population incidence goal" entered previously	1.77	1.77	2.24
Intraspecies (UCL)		14.02	14.02	41.88
RESULTS				
	HD distribution (lognormally distributed)	long term HD local effects	long term HD systemic effects	long term HD systemic effects
	Unit of measure	mg/m3	mg/kg body weight per day	mg/kg body weight per day
	LCL (P05)	1.63-04	7.85E-02	0.041
	UCL (P95)	2.88E-02	4.55E+01	23.5

Table 43: Long-term HD log-normal probability distributions statistics for CuO (ingestion and inhalation routes) and for $Cu_2(OH)_2CO_3$ (ingestion route).

	CuO Inhalation	CuO Ingestion	$Cu_2(OH)_2CO_3$ Ingestion
5%	1.63E-04	1.81E-01	4.09E-02
95%	2.88E-02	7.44E+01	2.35E+01
50% (median)	2.17E-03	3.67E+00	9.80E-01
Mean	7.48E-03	1.96E+01	6.33E+00
GM	2.17E-03	3.67E+00	9.80E-01
SD factor	4.82E+00	6.23E+00	6.90E+00

7.3.3 Risk characterization

Figure 37 and Table 44 display the risks along the lifecycles of the investigated products and the associated sources of uncertainty estimated by means of SUNDS. 3 out of the 13 occupational and consumer ES resulted in RCR distributions ≥ 1 (i.e. risk present). The formulation stage ES2 had a high probability of risk compared to the other scenarios in the formulation lifecycle stage, with nearly 93.33% of the Monte-Carlo simulation results being ≥ 1 (i.e. 6.67% of the RCR resulted in no risk to the exposed sensitive population). Nearly 95.79% of the variation in this result were caused by uncertainty in the UFs, mainly the factor used for extrapolation from subacute to chronic effects (62.77%). In the use-stage ES4, a worst-case exposure estimation of 0.32 mg/m^3 determined a non-acceptable inhalation risk for 99.87% of the sensitive population of both workers and consumers. 95.8% of the uncertainty in this result was again due to the UFs as the main underlying source was the extrapolation from subacute data to chronic effects. The perioral intake in ES4, instead, resulted in a safe scenario even for the most sensitive population. In contrast, the ES11 involving children exposed to the $Cu_2(OH)_2CO_3$ through inadvertent ingestion is non-acceptable for 8.48% of the population. Similarly, to the other concerning scenarios, 94.08% of the uncertainty in this result was caused by the UFs, but this time the contribution of the underlying sources was different: extrapolation from subacute to chronic effects = 41.62%; extrapolation from NOAEL to BMD = 22.69%; intraspecies extrapolation = 20.26%; interspecies toxicokinetic/dynamics = 11.34%; allometric scaling = 0.17%. The remaining 3.92% were from variation in exposure factors (i.e. exposure of the substance to sensitive children accounted for 2.86% of the uncertainty, while children weights contributed for 1.06%).

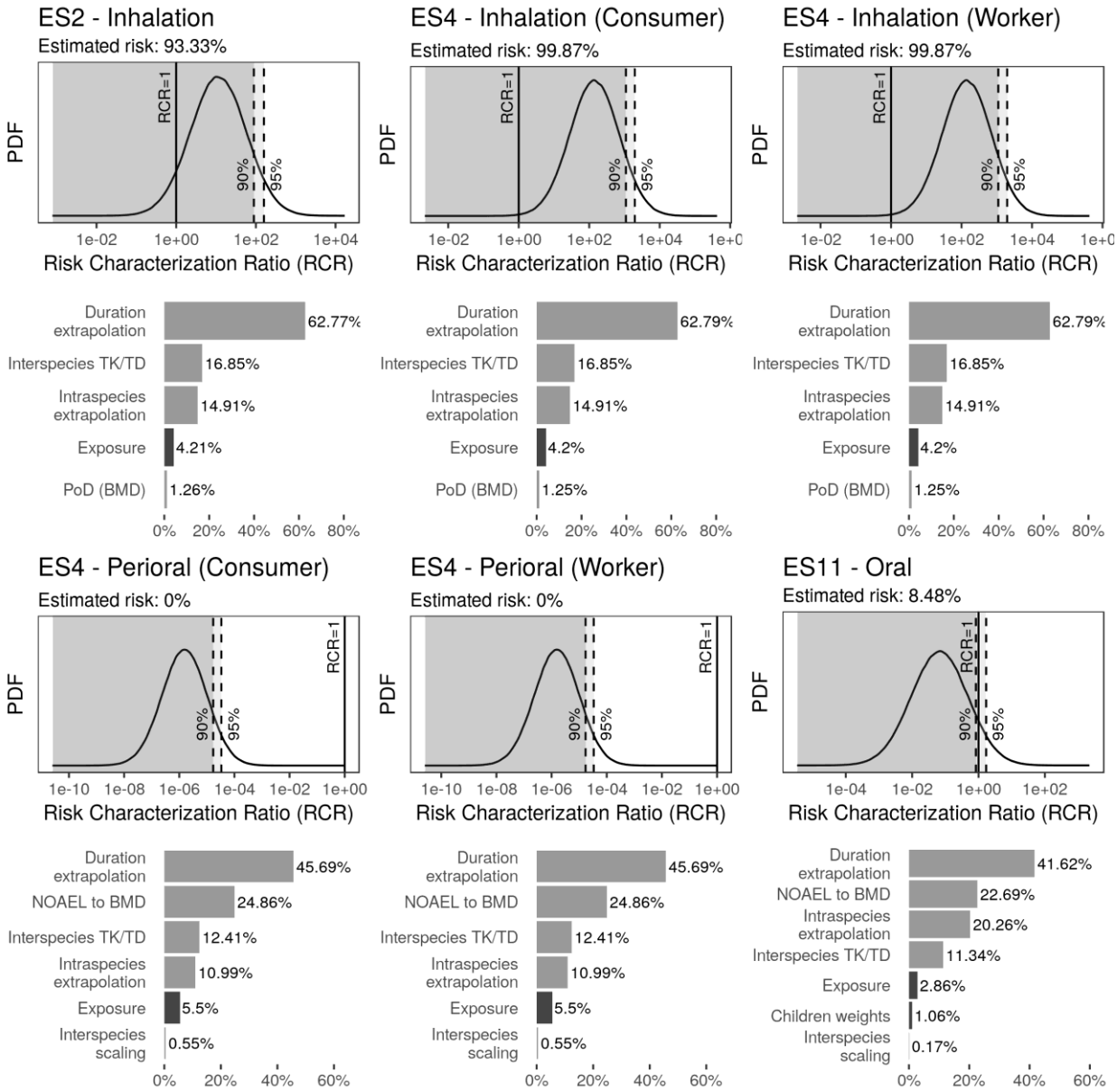

Figure 37: Risks along the lifecycles of the CuO and $Cu_2(OH)_2CO_3$ based products for all concerning exposure scenarios (ES). Contributions of the different sources of uncertainty to the total uncertainty, derived from over 10 000 Monte Carlo simulations, are highlighted.

Table 44: Risk Characterisation Ratio (RCR) distributions of risk for all assessed exposure scenarios (ES). These statistics are the result from over 10 000 Monte Carlo simulations.

	ES1	**ES2 Inhalation**	**ES2 Dermal**	**ES3**	**ES4 Inhalation (Consumer and Worker)**	**ES4 Perioral (Consumer and Worker)**	**ES4 End of Life**	**ES5**
5%	No Risk (Negligible exposure)	7.90E-01	No Risk (Negligible exposure)	No Risk (Negligible exposure)	9.74E+00	6.79E-08	No Risk (Negligible exposure)	No Risk (Negligible exposure)
95%		1.60E+02			1.97E+03	3.37E-05		
50%		1.12E+01			1.38E+02	1.51E-06		
Mean		4.13E+01			5.09E+02	8.96E-06		
GM		1.12E+01			1.38E+02	1.51E-06		
SD factor		5.02E+00			5.02E+00	6.60E+00		

Risk (Prob. RCR > 1)		93.33%			99.87%	0.00%		
	ES6	**ES7**	**ES8**	**ES9**	**ES10**	**ES11**	**ES12**	**ES13**
5%	No Risk (Negligible exposure)	No Risk (Negligible exposure)	No Risk (Negligible exposure)	No Risk (Negligible exposure)	No Risk (Negligible exposure)	2.59E-03	No Risk (Negligible exposure)	No Risk (Negligible exposure)
95%						1.70E+00		
50%						6.63E-02		
Mean						4.63E-01		
GM						6.63E-02		
SD factor						7.18E+00		
Risk (Prob. RCR > 1)						8.48%		

7.3.4 Uncertainty assessment

Uncertainty contribution to RCR by each involved factor was estimated through a Monte Carlo approach with 10.000 trials. At each trial, the RCR was numerically estimated by randomly sampling 10.000 elements from the PoD distribution, exposure distribution(s), and from each EF's distribution, and then computing the resulting RCR. The contribution to uncertainty of each factor was quantified by assessing the (normalized to 100) level of correlation between the factor and the resulting RCR by means of squared Spearman's rank correlation coefficient. Curve statistics of Exposure(s), PoD and EFs's distributions are summarized in Table 45 (Inhalation route of exposure of ES2), Table 46 (Inhalation route of exposure, for both Consumers and Workers of ES4), Table 47 (Perioral route of exposure, for both Consumers and Workers of ES4), and Table 48 (Oral route of exposure, children aged 8 to 36 months). Resulting distributions for each source of uncertainty are presented in Figure 38 (Inhalation route of exposure of ES2), Figure 39 (Inhalation route of exposure, for both Consumers and Workers of ES4), Figure 40 (Peri-oral route of exposure, for both Consumers and Workers of ES4), and Figure 41 (Oral route of exposure, children aged 8 to 36 months), together with the corresponding curve statistics. The contribution of each EF was selected as the arithmetic mean of each resulting curve. All the computations were performed using an internally developed script in R language, with resulting pictures generated thanks to the *ggplot2* package. SUNDS, on the other hand, integrates an approximation of this analysis, where only the uncertainties of HD_M^I and EXP_i with respect to the resulting RCR are performed as described above. An approximation of the Uncertainty analysis of PoD and UFs with respect to HD_M^I distribution is indeed provided by the APROBA tool included in our DSS, thus in SUNDS such contributions are normalized to the uncertainty of HD_M^I with respect to the RCR.

Table 45: Curve statistics for Exposure, PoD and EFs for Inhalation route of exposure of ES2. Mean and SD was computed for Normally distributed factors, while mean, GeoMean and GeoSD factor was computed for Lognormally distributed factors.

	Exposure	**PoD**	**Interspecies TKTD**	**Intraspecies extrap.**	**Duration extrap.**
Distribution	Normal	Lognormal	Lognormal	Lognormal	Lognormal
5%	1.30E-02	4.00E-02	3.33E-01	1.77E+00	6.25E-01
95%	3.90E-02	7.30E-02	3.00E+00	1.40E+01	4.00E+01

	Exposure	PoD	Interspecies TKTD	Intraspecies extrap.	Duration extrap.
50% (Median)	2.60E-02	5.40E-02	9.99E-01	4.98E+00	5.00E+00
Mean	2.60E-02	5.49E-02	1.25E+00	6.07E+00	1.11E+01
SD	7.90E-03	---	---	---	---
GM	---	5.40E-02	9.99E-01	4.98E+00	5.00E+00
GSD	---	1.20E+00	1.95E+00	1.88E+00	3.54E+00

Table 46: Curve statistics for Exposure, PoD and EFs for Inhalation route of exposure of ES4, for both consumers and workers. Mean and SD was computed for Normally distributed factors, while mean, GeoMean and GeoSD factor was computed for Lognormally distributed factors.

	Exposure	PoD	Interspecies TKTD	Intraspecies extrap.	Duration extrap.
Distribution	Normal	Lognormal	Lognormal	Lognormal	Lognormal
5%	1.60E-02	4.00E-02	3.33E-01	1.77E+00	6.25E-01
95%	4.80E-02	7.30E-02	3.00E+00	1.40E+01	4.00E+01
50% (Median)	3.20E-02	5.40E-02	9.99E-01	4.98E+00	5.00E+00
Mean	3.20E-02	5.49E-02	1.25E+00	6.07E+00	1.11E+01
SD	9.73E-03	---	---	---	---
GM	---	5.40E-02	9.99E-01	4.98E+00	5.00E+00
GSD	---	1.20E+00	1.95E+00	1.88E+00	3.54E+00

Table 47: Curve statistics for Exposure, PoD and EFs for Perioral route of exposure of ES4, for both consumers and workers. Mean and SD was computed for Normally distributed factors, while mean, GeoMean and GeoSD factor was computed for Lognormally distributed factors.

	Exposure	NOAEL to BMD	Interspecies TK/TD	Interspecies scaling	Intraspecies extrap.	Duration extrap.
Distribution	Normal	Lognormal	Lognormal	Lognormal	Lognormal	Lognormal
5%	2.35E-06	7.09E-02	3.33E-01	4.43E+00	1.77E+00	6.25E-01
95%	9.87E-06	1.57E+00	3.00E+00	7.01E+00	1.40E+01	4.00E+01
50% (Median)	6.11E-06	3.33E-01	9.99E-01	5.57E+00	4.98E+00	5.00E+00
Mean	6.11E-06	5.19E-01	1.25E+00	5.63E+00	6.07E+00	1.11E+01
SD	2.29E-06	---	---	---	---	---
GM	---	3.33E-01	9.99E-01	5.57E+00	4.98E+00	5.00E+00
GSD	---	2.56E+00	1.95E+00	1.15E+00	1.88E+00	3.54E+00

Table 48: Curve statistics for Exposure, PoD and EFs for Oral route of exposure of ES11, involving children aged 8 to 36 months. Mean and SD was computed for Normally distributed factors, while mean, GeoMean and GeoSD factor was computed for Lognormally distributed factors.

	Exposure	Children weights	NOAEL to BMD	Interspecies TK/TD	Interspecies scaling	Intraspecies extrap.	Duration extrap.
Distrib.	Normal	Mixture of Gaussians	Lognormal	Lognormal	Lognormal	Lognormal	Lognormal
5%	3.70E-01	7.60E+00	7.09E-02	3.33E-01	2.36E+00	2.24E+00	6.25E-01

	Exposure	Children weights	NOAEL to BMD	Interspecies TK/TD	Interspecies scaling	Intraspecies extrap.	Duration extrap.
95%	1.11E+00	1.47E+01	1.57E+00	3.00E+00	3.08E+00	4.19E+01	4.00E+01
50% (Median)	7.40E-01	1.08E+01	3.33E-01	9.99E-01	2.70E+00	9.69E+00	5.00E+00
Mean	7.40E-01	1.09E+01	5.19E-01	1.25E+00	2.70E+00	1.44E+01	1.11E+01
SD	2.25E-01	2.18E+00	---	---	---	---	---
GM	---	---	3.33E-01	9.99E-01	2.70E+00	9.69E+00	5.00E+00
GSD	---	---	2.56E+00	1.95E+00	1.08E+00	2.44E+00	3.54E+00

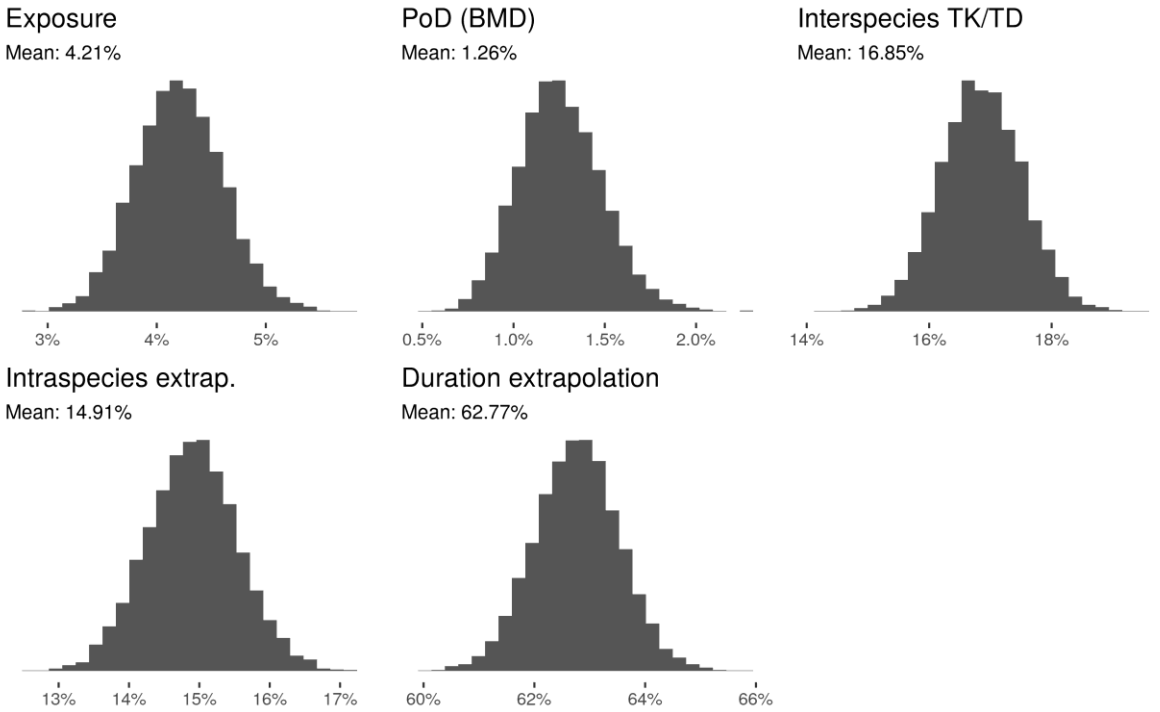

Figure 38: Distributions of uncertainties in ES2 Inhalation scenario, numerically derived after 10 000 Monte Carlo simulations. The corresponding curve statistics are summarized in Table 49.

Table 49: Curve statistics of distribution of uncertainty of each factor in ES2 Inhalation scenario, quantified by the (normalized to 1) level of correlation between the factor and the resulting RCR by means of squared Spearman's rank correlation coefficient.

	Exposure	PoD	Interspecies TK/TD	Intraspecies extrapolation	Duration extrapolation
5%	3.55E-02	8.97E-03	1.58E-01	1.39E-01	6.15E-01
95%	4.88E-02	1.64E-02	1.79E-01	1.59E-01	6.40E-01
50% (Median)	4.20E-02	1.24E-02	1.69E-01	1.49E-01	6.28E-01
Mean	4.20E-02	1.25E-02	1.69E-01	1.49E-01	6.28E-01
SD	4.01E-03	2.27E-03	6.59E-03	6.38E-03	7.63E-03

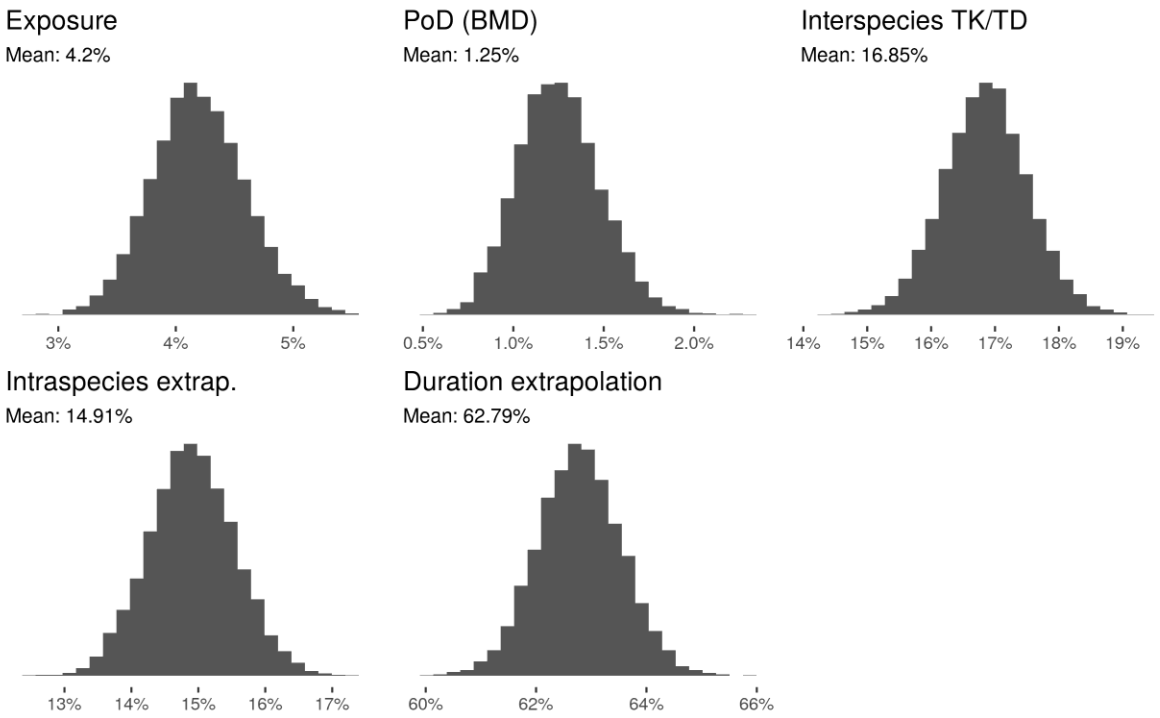

Figure 39: distributions of uncertainties in ES4 Inhalation scenario, numerically derived after 10 000 Monte Carlo simulations. The corresponding curve statistics are summarized in Table 50.

Table 50: Curve statistics of distribution of uncertainty of each factor in ES4 Inhalation scenario, quantified by the (normalized to 1) level of correlation between the factor and the resulting RCR by means of squared Spearman's rank correlation coefficient.

	Exposure	**PoD**	**Interspecies TK/TD**	**Intraspecies extrapolation**	**Duration extrapolation**
5%	3.57E-02	9.04E-03	1.58E-01	1.38E-01	6.16E-01
95%	4.88E-02	1.63E-02	1.79E-01	1.60E-01	6.40E-01
50% (Median)	4.19E-02	1.25E-02	1.68E-01	1.49E-01	6.28E-01
Mean	4.20E-02	1.25E-02	1.69E-01	1.49E-01	6.28E-01
SD	4.00E-03	2.24E-03	6.64E-03	6.40E-03	7.60E-03

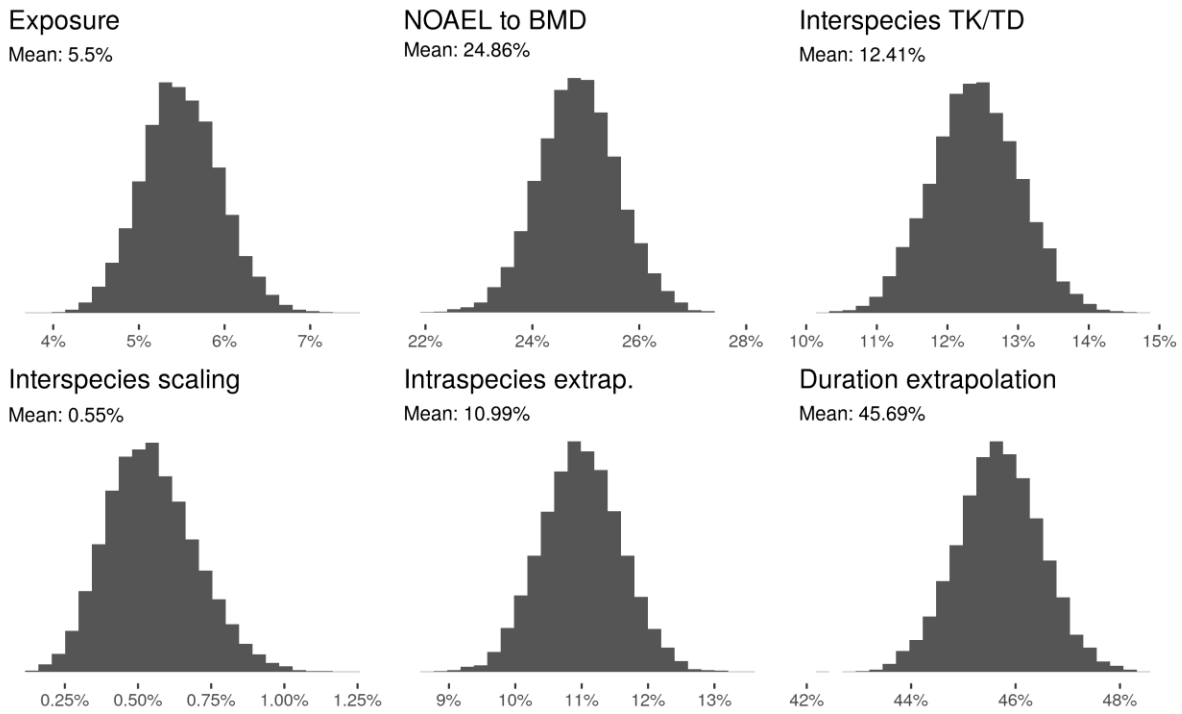

Figure 40: distributions of uncertainties in ES4 Peri-oral scenario, for both consumers and workers, numerically derived after 10 000 Monte Carlo simulations. The corresponding curve statistics are summarized in Table 51.

Table 51: Curve statistics of distribution of uncertainty of each factor in ES4 Perioral scenario, quantified by the (normalized to 1) level of correlation between the factor and the resulting RCR by means of squared Spearman's rank correlation coefficient.

	Exposure	**NOAEL to BMD**	**Interspecies TK/TD**	**Interspecies scaling**	**Intraspecies extrapolation**	**Duration extrapolation**
5%	4.76E-02	2.36E-01	1.14E-01	3.13E-03	1.00E-01	4.43E-01
95%	6.28E-02	2.61E-01	1.34E-01	8.16E-03	1.20E-01	4.70E-01
50% (Median)	5.48E-02	2.49E-01	1.24E-01	5.37E-03	1.10E-01	4.57E-01
Mean	5.50E-02	2.49E-01	1.24E-01	5.46E-03	1.10E-01	4.57E-01
SD	4.62E-03	7.53E-03	6.21E-03	1.53E-03	6.00E-03	8.08E-03

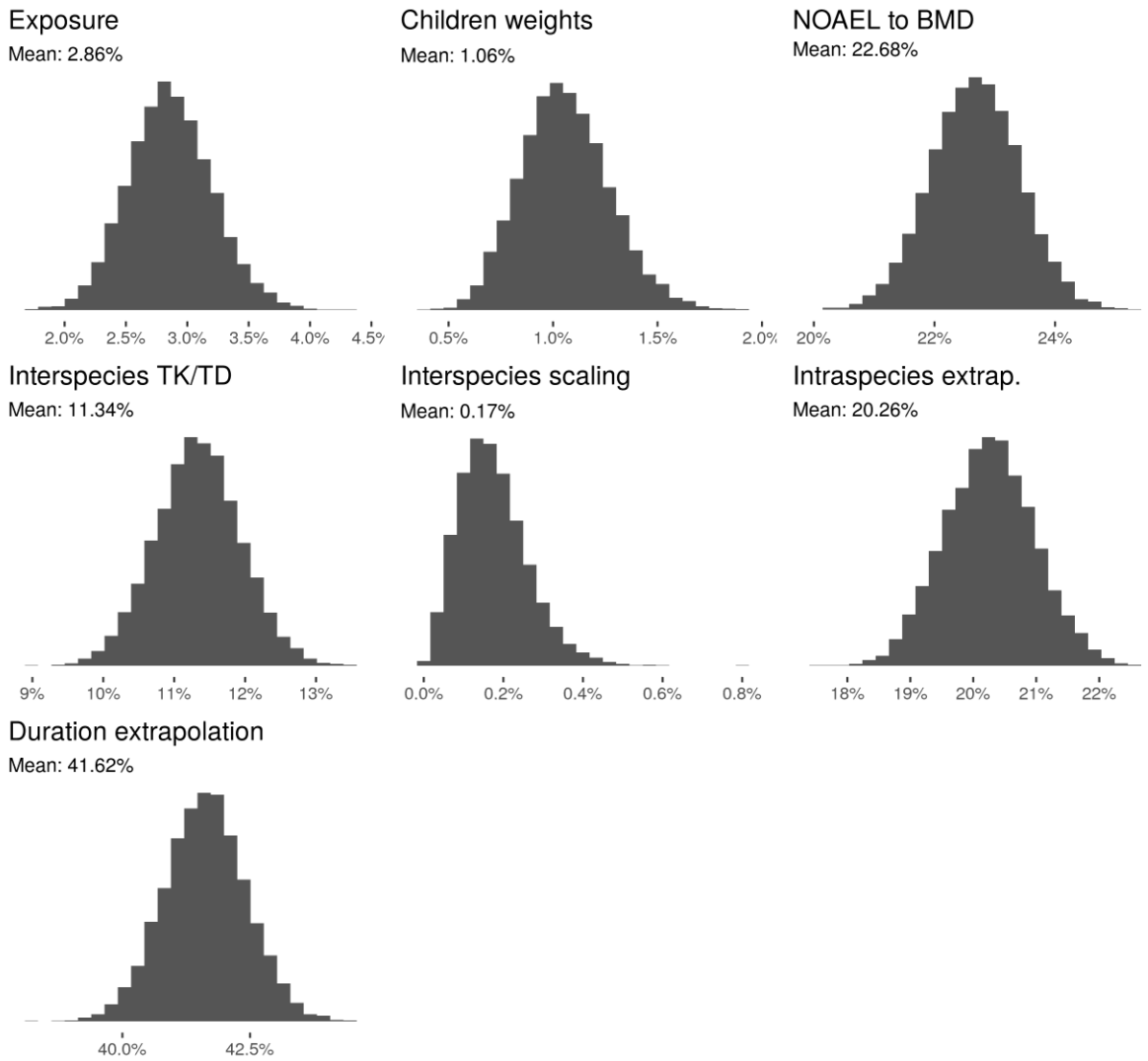

Figure 41: distributions of uncertainties in ES11 Oral scenario, for children (girls) aged 8 to 36 months, numerically derived after 10 000 Monte Carlo simulations. The corresponding curve statistics are summarized in Table 52.

Table 52: Curve statistics of distribution of uncertainty of each factor in ES11 Oral scenario, quantified by the (normalized to 1) level of correlation between the factor and the resulting RCR by means of squared Spearman's rank correlation coefficient.

	Exposure	Children weights	NOAEL to BMD	Interspecies TK/TD	Interspecies scaling	Intraspecies extrapolation	Duration extrapolation
5%	2.32E-02	7.36E-03	2.15E-01	1.03E-01	5.59E-04	1.91E-01	4.03E-01
95%	3.44E-02	1.42E-02	2.39E-01	1.23E-01	3.33E-03	2.15E-01	4.29E-01
50% (Median)	2.85E-02	1.05E-02	2.27E-01	1.13E-01	1.65E-03	2.03E-01	4.16E-01
Mean	2.86E-02	1.06E-02	2.27E-01	1.13E-01	1.75E-03	2.03E-01	4.16E-01
SD	3.41E-03	2.10E-03	7.33E-03	6.00E-03	8.63E-04	7.23E-03	7.90E-03

7.4 Discussion

This is the first quantitative HHRA of nanoscale CuO and $Cu_2(OH)_2CO_3$ used for antimicrobial and antifungal treatment of wood. In contrast to the more classical deterministic approach our probabilistic methodology was able to discriminate and communicate the different sources of uncertainty in the risk

analysis to better inform the generation of additional data and/or the adoption of adequate risk management measures.

Specifically, it was possible to assess the uncertainty in the dose-response data by means of parametric bootstrapping. This enabled us to discover the largest source of uncertainty in the assessment, which was due to the extrapolation of the BMD derived from subacute animal experiments to long-term human HD. Therefore, in order to increase the confidence in our results it is important to repeat the analysis once (sub)chronic in vivo inhalation and ingestion data become available.

Other considerable sources of uncertainty were the inter- and intraspecies EF. These default values were defined for regular chemicals based on historical precedence and if we assume that the CuO and $Cu_2(OH)_2CO_3$ nanoforms act according to different mechanisms of toxicity, then these factors may turn out to be inaccurate. In order to reduce this type of uncertainty it may be necessary to establish nano-specific EF based on extensive analysis of the available physicochemical and toxicity data for nanomaterials. This requires the development of data management and curation capabilities to check the quality of data prior to their analysis.

The results from the dose-response analysis largely depend on the BMR. There is a lack of consensus among toxicologists regarding what effect size may demarcate adverse from non-adverse and there is an agreement that the BMR may differ significantly among endpoints. Therefore, some authors suggested the evaluation of an uncertainty distribution for the BMR [343], but we did not do this in our study. Instead, we used predefined values, which helped to communicate which BMR corresponds to which BMD distribution, but prevented us from considering this important parameter in the uncertainty analysis.

Other uncertainty arises from the fact that from the short-term exposure studies it is difficult to predict that no (sub)chronic endpoints like sustained inflammation or fibrosis will be affected at longer exposures. In the short-term inhalation study, we found that lung inflammation was not completely resolved after 22 days but did not lead to fibrosis, while copper levels in the lung returned to baseline levels [287].

The exposure assessment of the dry nanoscale powders in this study was determined for worst-case scenarios, as risk management measures (e.g. emission controls, efficiency of local exhaust ventilation) that may reduce their airborne concentrations were not considered. Therefore, the impact of possible overestimations of exposures from powder handling in the workplace may have been significant in determining the high estimated risks associated with these scenarios. Therefore, these risks could be easily managed by applying appropriate risk management measures (e.g. engineering controls, personal protective equipment).

The potential risks of ES11 that involves children ingesting CuO or $Cu_2(OH)_2CO_3$ nanoparticles by skin contact, transfer of copper to the month and related ingestion would be more difficult to control. In this case, the potentially most effective measures to be considered involve safety by design measures to reduce the release potential and/or the hazard of the material as well as consumer labelling and safety instructions.

Other sources of uncertainty in the exposure assessment may result from the fact that only external doses were considered in this study, while due to insufficient data the uptake and the translocation of the substances in the organism were not considered. Particle size distributions strongly influence the

deposition pattern of nanoparticles in the lungs and their dissolution kinetics in cases of soluble particles such as CuO or $Cu_2(OH)_2CO_3$ [287].

There are also considerable uncertainties in the measured external exposure concentrations in the air as they may quickly decline due to aggregation, agglomeration or surface deposition [307]. This means that nanoscale fractions measured close to the emission source may be eliminated by the time the particles are deposited in the lungs. Some specific sources of uncertainty that were not explicitly defined in this study include for example the time length of each work activity, the time-length of pauses between work activities. Exact values of these parameters will not always be known but can have a significant influence on nano-specific transformation processes such as aggregation and thus the inhalation exposure to nanoparticles.

In the lungs or the intestine, the particles might completely dissolve, which would mean that only ions are uptaken in the systemic circulation and are translocated to the secondary organs. These phenomena could differ between species and the effects observed in animals could follow different mechanisms of toxicity as compared to the actual effects in humans. In order to reduce these uncertainties, it is essential to perform kinetic studies and to appropriately measure or model the dissolution as well as the absorption, distribution, metabolization and excretion (ADME) kinetics of the investigated substances. The results from the kinetic studies that we performed in the SUN project showed that after short-term inhalation of CuO pristine nanoparticles, no other organs besides the nose and lung were affected based on histological analysis and organ weights. This could be explained by the lack of any increase in Cu levels compared to background levels in the liver, blood, brain, bone marrow, heart, kidney, and spleen at the applied exposure levels. After oral administration of CuO nanoparticles at day 6 increased levels of Cu was noted mainly in liver and lung starting at a dose of 32 mg/kg b.w. After oral administration of $Cu_2(OH)_2CO_3$nanoparticles increased Cu levels were observed in liver, lung, kidney, spleen, thymus, mesenteric lymp nodes, and to a lesser extent in testes and brain. This clearly shows that the two investigated materials have very different ADME profiles, but as long as we do not understand their dissolution kinetics we can only guess what the underlying reasons for this are.

In general nanomaterials (incl. CuO and $Cu_2(OH)_2CO_3$) are offered in many different grades that are optimized in terms of physicochemical properties for integration into specific applications. This study is a case-specific risk assessment where the nanomaterials used in the exposure and the hazard studies are similar. This is however often not the case in order to avoid excessive case-by-case testing we should search for possibilities to group them based on physico-chemical, release, exposure, bio-kinetic or toxicological information in order to facilitate read-across, which could reduce testing costs and the use of experimental animals.

7.5 Conclusions

Our assessment demonstrated unacceptable inhalation risks of CuO for worst-case ES involving handling of dry powders and sanding operations. In addition, we identified potentially unacceptable ingestion risks for the sensitive population of children exposed to $Cu_2(OH)_2CO_3$nanoparticles by hand to mouth contact with impregnated wood. It should be noted, however, that there are significant uncertainties in these results, which should be resolved by additional testing. Therefore, the conclusion “unacceptable risk” may stem from the safety margin of extrapolations to fill data gaps and is therefore not a proof of actual risks.

Our analysis demonstrated that the main source of uncertainty is the extrapolation from subacute to long-term exposure, which was necessary due to the lack of (sub)chronic in vivo studies with CuO and $Cu_2(OH)_2CO_3$. Considerable uncertainties also stemmed from the use of default inter- and intra-species UF for chemicals. The proposed approach is currently suited only for case-by-case risk assessments but will be extended to enable also grouping and read-across for more efficient analysis.

8 Ecological risk along the lifecycle of nano-enabled products by means of SUNDS Environmental Risk Assessment module

The work presented in this chapter will be submitted as a journal article, currently in preparation:
E.Semenzin, **G.Basei**, A.Caballero-Guzman, J.J.Scott-Fordsmand, F.Gottschalk, V.Ricottone, V.Subramanian, A.Zabeo, E.Giubilato, B.Nowack, D.Hristozov, and A.Marcomini, *Ecological risk along the lifecycle of nano-enabled products*, to be submitted to Environmental Pollution (in prep.).

8.1 Introduction

Within SUNDS, the Ecological Risk Assessment (ERA) sub-module implements a quantitative methodology for the estimation of risks along the lifecycle of specific nanoapplications to key environmental compartments e.g. surface water, soil (natural and urban or sludge), air, and sediments.
As described in Chapter 7, copper-based preservatives have been widely used to treat softwood intended for commercial use due to their high performance [308,309], and chemical formulations without arsenic and chromium including ACQ were adopted in place of the more toxic chromated copper arsenate (CCA). Micronized copper has been promoted as a better alternative to ionic copper [308]. It has still limited market penetration in the EU due to a lack of regulatory approval, but over 75% of the residential lumber produced in the USA is nowadays treated with micronized copper [310] produced by mechanical grinding of compounds such as basic copper carbonate ($Cu_2(OH)_2CO_3$) or copper oxide (CuO) with dispersing agents in a carrier solution [308]. The increased use of nano-scale CuO and $Cu_2(OH)_2CO_3$ as timber preservatives has raised concerns not only for Human Health, but also for the environment. Therefore, we performed a quantitative Environmental Risk Assessment (ERA) of nano-scale CuO and $Cu_2(OH)_2CO_3$, and for comparison purposes also of ACQ, along the lifecycles of antimicrobial/antifungal coatings and impregnations.
On the other hand, as already mentioned in chapter 6, nanoscale organic pigment used in the automotive industry are highly relevant as the market of high-performance pigments is in expansion [277]. These pigments can have several advantages as colorants in coatings and polymers [279]. Our case study specifically targets pigment-coloured automotive plastics. Nano-pigments can be defined as organic or inorganic substances, insoluble, chemically and physically inert into the substrate or binders, with a particle size less than 100 nm [280,281]. Such plastics are widely used in interior, exterior, and under bonnet components to reduce automobile weight, improve aesthetics, vibration and noise control, and cabin insulation [282]. Specifically, the “Ferrari Red” Organic Pigment (Hydrogen-bonded diketopyrrolopyrrole Red 254 (DPP)) was selected in the SUN project as case study for Risk Assessment.
The ERA methodology has indeed been applied to the nano-copper oxide-based biocidal paint and plastic automotive part (bumper) coloured with nano-sized organic pigment case studies, according to the exposure and effect data generated in the frame of the SUN project. In this chapter the first quantitative estimation of the risks for the environment of these products from lifecycle perspective is presented.

8.2 Materials and methods

8.2.1 Case study products

Two case studies were selected, namely biocidal paint for wood preservation and paint for plastic bumper of cars. For the first case study, two nanomaterials were tested (CuO and $Cu_2(OH)_2CO_3$) plus a conventional chemical for reference (ACQ), while in the second case study, only DPP was tested in SUN project. Physicochemical characterizations were performed in SUN project for pristine DPP and CuO and were presented in Chapters 6 and 7 (cf. 6.2.1 and 7.2.1).
Similarly, total amounts of case studies NMs used in the reference system (EU27) was estimated during the SUN project and are summarized in Table 53.

Table 53: Total amount of case studies NMs used in EU 27, as estimated during SUN project.

Application	NM	NM related enhancement	Year of the study	Total quantity sold	NM content (%)	NM mass (tons)
Car bumper	DPP	Colour tone not reached by traditional pigments.	2014	226800 cars (1.54 kg of product each)	1	3.3
Wood preservation	CuO	Protection against weathering and organisms (e.g. fungi).	2011	3850 tons	1.5	58
Wood preservation	CuCO3	Protection against weathering and organisms (e.g. fungi).	2011	3850 tons	18	693
Wood preservation	ACQ*	Conventional chemical, one of the main types of wood coating sold.	2011	269500 tons	9.6*	25872

* ACQ is not a NM, but we included it as reference product for the Wood coating case study.

8.2.2 Exposure assessment

8.2.2.1 PMFA model

As mentioned in Chapter 5, the Probabilistic Material Flow Analysis (PMFA) package is included in SUNDS to derive PECs for all lifecycle stages. PMFA aims at tracking the release of potential contaminants into natural and technical compartments as well as to quantify their quantities in those environments. The application of such model is not new, and its methodological and study based overview was already provided in the literature [344–350]. However, so far this approach was applied in a comprehensive way, while in this study we derived PEC values for all lifecycle stages.
The model follows the "box-flow" framework: each compartment is placed in a box, as well as fluxes between compartments, and statistical functions are used to simulate the transfer between such compartments. Usually, a time frame equal to one epoch is selected, but in principle it is possible to simulate the behaviour in the system in a continuous time frame, by increasing the *time* parameter provided to the model. In addition to *time*, there are three other types of inputs required by the model:

- material input in the box: the periodical material input in the system in form of a mass per period must be known, for example tons per year. This material input usually takes place in one single box, i.e. the initial main box. The indexing of all boxes is explained below. Material

input comprises material synthesizing as well as material import from outside of the system. Such import may also occur as material ingredient of imported use products/articles.

- material fate inside the box: this, in SUNDS, comprises two possible situations, namely material elimination inside the compartment (for instance, material burnt by the Waste Incineration Plant), and material deposition insider the compartment; the original model allows two additional type of fates, namely transport delay (material not transported further in the target time period, which is useful in cases of simulating a continuous time frame) and unknown material fate inside the compartment.
- material transfers from the box: all the material which was eliminated or deposited into the compartment is assumed to be transferred to other compartments; the model does not pose any restrictions on such transfers, while in SUNDS we decided to allow only the most common transfers among compartments. Such transfers are highlighted in Figure 29 (cf. Chapter 5).

All the transfers parameters, except to time, are quantified as a fraction that lies between 0 and 1 including the borders, and as already mentioned in Chapter 5 (cf. Section 5.2.3.1.1), user can choose between four different types of distributions for the inputs (material input, material fate, and material transfer), specifically, he can choose between uniform distribution, triangular distribution, normal distribution (which is fixed for material input in the initial compartment), and bootstrapping.

8.2.2.2 Material transfer and fate coefficients among compartments

The system parameters refer to the transfer coefficients that determine the flow among technical compartments and between these and the natural compartments. The data was taken from Sun et al. (2014) [349], except where indicated. These coefficients, reported below, are fixed for all case studies.

From Wastewater to:

- To Waste Water Treatment Plant (connection rate) (WWTP): 70-90%
- To Surface Water (WW not connected to the sewage): 10-30%

From Waste Water Treatment Plant (WWTP) to:

- WWTP to Surface Water (overflow, i.e., not filtered due to overcapacity): 3.2% (SD: 0.4%)
- WWTP to Sludge (removal efficiency): see Table 54
    - Sludge to Incineration (WIP): 25%
    - Sludge to Landfill (LF): 20%
    - Sludge to Soil ("Sludge Treated Soil"): 55%

From Waste incineration Plant (WIP) to:

- Destroyed during incineration: see Table 54
- Incineration to Bottom Ash: 81%
    - From Bottom Ash to Landfill: 58%
    - From Bottom Ash to Recycling: 42%
- Incineration to Filter: 19%
    - From Filter to Landfill (filter removal efficiency): 99.5-99.9%
    - From Filter to Air: 0.05-0.25%
    - From Filter to Wet Scrubber: 0.05-0.25%
        - From Wet Scrubber to Landfill: 99.9%
        - From Wet Scrubber to Air: 0.1%

From Air to:

- Natural and Urban Soil: 97%

- Surface Water: 3%

Surface Water

- From Surface Water to Sediments: 97%
- Remains in Surface Water: 3%

Soil

- From Soil to Surface Water: 0.5%
- Remains in Soil: 99.5%

Case specific coefficient are instead reported in Table 54, together with the corresponding references. In the table, DoB stands for "Degree of Belief", which is a measure of confidence on the source that we set upon expert judgement. In the model, DoB was assessed by using bootstrapping: for instance, in the case of CuO there are 4 sources that account for a 20% of DoB, and a single source that accounts for 80% of DoB; we selected the most conservative value provided by the first set of sources (i.e.: 80%) and we selected four times each value between 95% and 99%. The 90% value in the set of references with 20% DoB was neglected, having no influence because exactly between the extremes, while the other are comprised in the 80% DoB values. Similar judgments were done in the other case studies.

Table 54: Case specific Fate coefficient for all the case studies, together with the references and, when applicable, a Degree of Belief (DoB).

	DPP	**CuO**	**$Cu_2(OH)_2CO_3$**	**ACQ****
WWTP Removal Efficiency	95-98% [351], 80-98% [352], 96-98% [353], 96-97% [354], 90% [355]	**DoB 20%** 95-98% [351], 80-98% [352], 96-98% [353], 96-97% [354], 90% [355]	**DoB 20%** 95-98% [351], 80-98% [352], 96-98% [353], 96-97% [354], 90% [355]	**DoB 20%** 95-98% [351], 80-98% [352], 96-98% [353], 96-97% [354], 90% [355]
		DoB 80% 95-99%*	**DoB 80%** 95-99%*	**DoB 80%** 95-99%*
Elimination during Incineration	98% [349]	0%	0%	0%

* Personal communication on April 2016 with dr. R.Kaegi (EAWAG, https://www.eawag.ch/). ** Original studies were related to nanoscale materials only. ACQ is not a nanomaterial, but we decided to assume the same coefficients for comparison. Note that this is a conservative assumption.

8.2.2.2 Environmental Compartments volumes

Once the PECs are evaluated for each lifecycle stage, before computing risks, it is necessary to divide it by the volume of the compartment in the system of reference. By default, SUNDS uses the EU 27 data, for which residence times in the system were included (residence time of 10 days in the system EU was assumed for Air, while a residence time of 40 days in the system EU was assumed for Surface Water). Such volumes are reported in Table 55.

Table 55: Default volumes of Environmental compartments. These volumes refer to EU 27 data, for which resident times in the system have already been included. Data was originally reported in Sun et al. (2014) [349].

Environmental compartment	Volume	Unite of measure
Atmosphere	1.629E+17	m^3
Soil (Natural and Urban)	7.435E+14	kg
Soil (Sludge treated)	5.757E+12	kg
Surface water	3.665E+15	L
Sediments	1.044E+12	kg

8.2.3 Hazard assessment

As described in Chapter 5 (cf. 5.2.3.1.1), to derive a PNEC in SUNDS, user is asked to insert information on available (eco)toxicological data. If at least 10 long-term NOECs are available from different species (covering at least 8 taxonomic groups), it is possible to derive a probabilistic PNEC starting from Probability Species Sensitivity Distribution (pSSD) model, by taking the 5th percentile from each SSD, which corresponds to the hazardous concentration for the five percent of the species (HC5), otherwise a deterministic PNEC is derived according to REACH.

It is worth noting that applications of such model have already been provided in the literature [356,357] as well as alternative approaches that will be included in SUNDS in the forthcoming months [358]. The main difference is that in SUNDS the resulting PNEC is approximated by a Lognormal distribution generated starting from the confidence intervals of the derived PNEC. SUNDS displays to the user the original curve and the approximated one. As will be discussed in the following sections, this approximation is reasonable for PNECs.

An indication that this approximation is reasonable is feasible even when performing a low (i.e. <1000) number of simulations is displayed in Figure 42, where we plotted the calculated vs approximated PNEC on a synthetic dataset, by increasing the number of simulations performed by pSSD model.

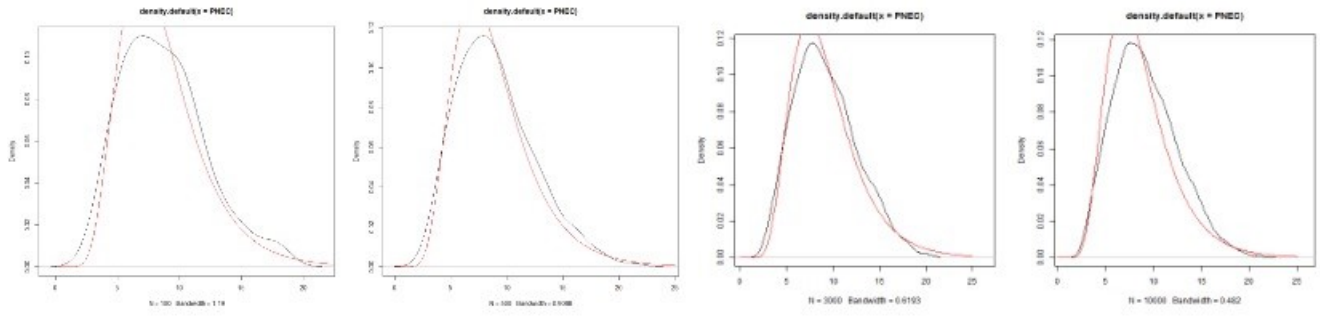

Figure 42: Computed PNECs (in black) vs PNECs approximated by a lognormal, on synthetic data. From left to right: 100 simulations, 500 simulations, 3000 simulations and 10000 simulations.

8.2.4 Risk characterization

3.2.4.1 Risk characterisation ratio (RCR)

Ecological risk is calculated by integrating outputs from: i) environmental exposure models deriving Predicted Environmental Concentrations (PECs) in different environmental compartments, and ii)

deterministic procedures or Species Sensitivity Distributions (SSDs)-based probabilistic procedures [267] that estimate Predicted No Effect Concentrations (PNECs) for various species in the specific environmental compartment. An ecological risk portfolio along the lifecycle is calculated by choosing the maximum risk for each lifecycle stage to characterize it. The resulting ecological risk is either deterministic (i.e. PEC/PNEC) or probabilistic (i.e. percentage of Risk Characterization Ratio (RCR) distribution greater or equal than 1) depending on the nature of exposure and effect input data. In case both PEC and PNEC being probabilistic, a Monte Carlo simulation is performed by sampling with replacement from the two distributions an equal number of elements and dividing the two resulting vectors. In this case, thus, the risk is computed as the percentage of samples with value greater or equal than 1 in the resulting vector.

3.2.4.2 Risk acceptability classification

Once the risk is estimated, it is classified in terms of acceptability according to an approach based on confidence intervals. Specifically, in case the risk is presented deterministically, two classes are identified: acceptable (ratio below one) and non-acceptable (ratio above one). As probabilistic risk distributions typically follow a right-skewed log-normal distribution, it is too rare to have a completely acceptable risk. To select the most suitable risk acceptability classes we studied the literature and in addition asked relevant experts by means of a questionnaire specifically designed for this purpose. Ten experts were chosen from our personal networks. SurveyMonkey platform was used to implement the online questionnaire. Their responses pointed us to the following three classes: 1) acceptable (when the threshold of one is higher than the 99th percentile of the risk characterization ratio distribution), 2) needs further consideration (threshold of one between the 95th and 99th percentile) and 3) non-acceptable (threshold of one below the 95th percentile). The selection of the percentiles for this pre-defined risk acceptability classification profile can be changed depending on specific assessment needs.

8.3 Results

8.3.1 Exposure assessment results

Data based on the scenarios created to assess the potential consumption of the application and the NM mass consumed is summarized in Table 53 . Values in the last column (NM mass) were fed to PMFA package as input, after splitting those value in different lifecycle stages as described in the following subsections.

8.3.1.1 “Ferrari Red” organic pigment (DPP)

In addition to transfer coefficients described in Section 8.2.2.2, specific coefficients for the DPP case study, as assessed in SUN project, are reported in Table 56.

Table 56: Transfer coefficients for Car Bumper with DPP by life cycle stages. Mass released column indicates how the total material input in the system is split among all the lifecycles, while each row indicates the proportion of the material directly being transfer into natural and technical compartments. Source: SUN project.

		Natural compartments			Technical compartments				
	Mass released	Air	Soil	SW	WW	EXP	LF	REC	WIP
Production	0.0003	0.013	-	-	0.013	-	-	-	0.974
Manufacture	0.017	-	-	-	0.37	-	-	-	0.63
Use	0.0002	-	-	-	0.5	-	-	-	0.5
End-of-Life	0.9825	0.01	-	-	0.01	-	0.26	0.46	0.26

SW: Surface Water; WW: Waste Water; EXP: Exportation; REC: Recycling; WIP: Waste Incineration Plant.

A schematic picture of the material transfers among all the system compartments is provided in Figure 43, the number on the arrows corresponds to the mean value of the material transferred from a compartment to another. Values are expressed in tons. The mean values of the quantities deposited into the natural compartments (divided by the compartments volumes reported in Table 55) and used for Risk Assessment, instead, are reported in Table 57.

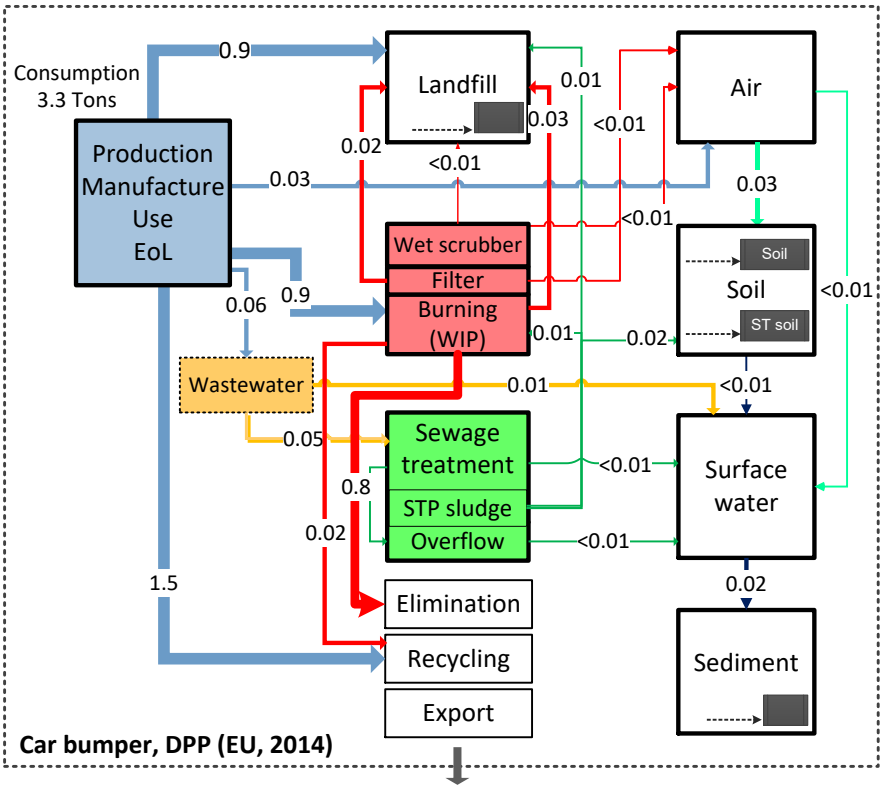

Figure 43: Mass flows in tons of Ferrari Red Organic Pigment for the case study assessments in all lifecycle stages. Units are expressed in tons. The numbers correspond to the mean values of the probability distributions generated.

Table 57: Mean value of material concentration in Environmental compartments computed by the PMFA model (divided by the compartment's volumes reported in Table 55) for the CuO case study, together with their relative weights with respect to the total material concentration in all lifecycle stages.

	Concentrations, absolute values (mean)						Relative weights (%)			
Environmental Compartment	**Syn**	**For**	**Use**	**EoL**	**All LCS**	**Units**	**Syn**	**For**	**Use**	**EoL**
Atmosphere	8.627E-11	8.73E-12	8.76E-14	2.02E-07	2.02E-07	µg/m^3	0.04%	0.00%	0.00%	99.95%
Sediments	3.759E-06	5.13E-03	8.12E-05	8.83E-03	1.41E-02	µg/kg·y	0.03%	36.54%	0.58%	62.86%
Soil (Natural and Urban)	1.833E-08	1.86E-09	1.86E-11	4.30E-05	4.30E-05	µg/kg·y	0.04%	0.00%	0.00%	99.95%
Soil (Sludge treated)	1.653E-06	2.57E-03	4.07E-05	3.89E-03	6.50E-03	µg/kg·y	0.03%	39.59%	0.63%	59.76%
Surface water	1.104E-09	1.51E-06	2.38E-08	2.59E-06	4.13E-06	µg/L	0.03%	36.54%	0.58%	62.86%

Syn: Synthesis; For: Formulation; EoL: End of Life; LCS: Lifecycle stage.

8.3.1.2 Copper Oxide (CuO)

In addition to transfer coefficients described in Section 8.2.2.2, specific coefficients for the CuO case study, as assessed in SUN project, are reported in Table 58.

Table 58: Transfer coefficients for Wood Preservation with CuO by life cycle stages. Mass released column indicates how the total material input in the system is split among all the lifecycles, while each row indicates the proportion of the material directly being transfer into natural and technical compartments. Source: SUN project.

		Natural compartments			Technical compartments				
	Mass released	**Air**	**Soil**	**SW**	**WW**	**EXP**	**LF**	**REC**	**WIP**
Production	0	-	-	-	-	-	-	-	-
Manufacture	0.02	-	0.001	-	0.999	-	-	-	-
Use	0.065	-	0.57	-	0.2	-	-	-	0.23
End-of-Life	0.915	-	0.1	-	-	-	-	-	0.9

SW: Surface Water; WW: Waste Water; EXP: Exportation; REC: Recycling; WIP: Waste Incineration Plant.

A schematic picture of the material transfers among all the system compartments is provided in Figure 44, the number on the arrows corresponds to the mean value of the material transferred from a compartment to another. Values are expressed in tons. The mean values of the quantities deposited into the natural compartments (divided by the compartments volumes reported in Table 55) and used for Risk Assessment, instead, are reported in Table 59.

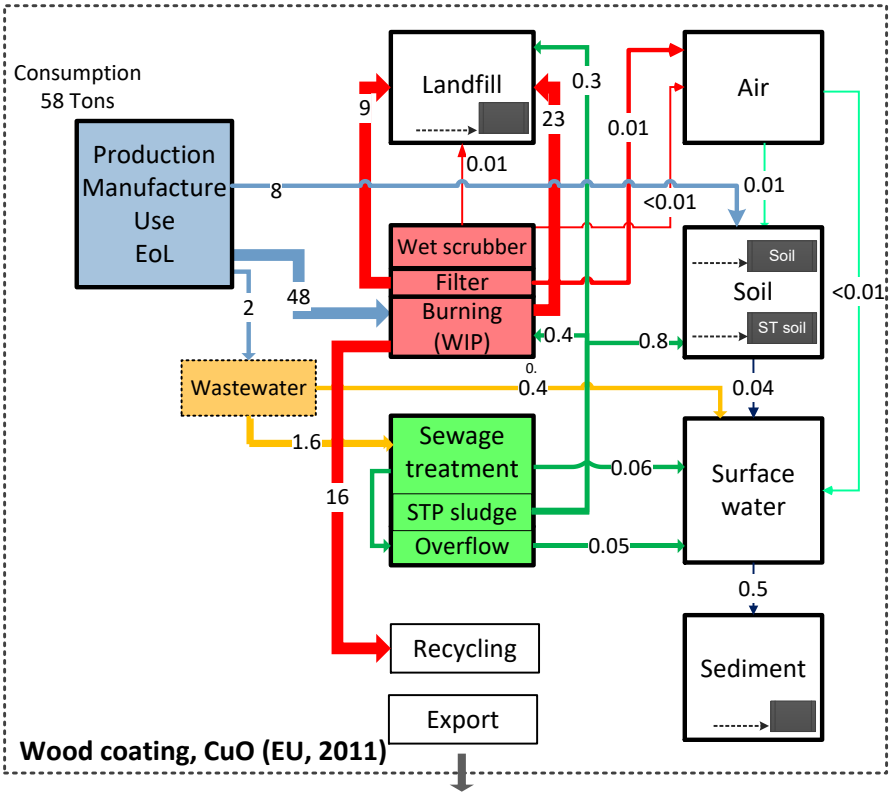

Figure 44: Mass flows in tons of Copper Oxide for the case study assessments in all lifecycle stages. Units are expressed in tonnes. The numbers correspond to the mean values of the probability distributions generated.

Table 59: Mean value of material concentration in Environmental compartments computed by the PMFA model (divided by the compartment's volumes reported in Table 55) for the CuO case study, together with their relative weights with respect to the total material concentration in all lifecycle stages.

	Concentrations, absolute values (mean)						Relative weights (%)			
Environmental Compartment	**Syn**	**For**	**Use**	**EoL**	**All LCS**	**Units**	**Syn**	**For**	**Use**	**EoL**
Atmosphere	0	4.03E-10	1.87E-09	8.43E-08	8.66E-08	µg/m^3	0%	0.46%	2.16%	97.38%
Sediments	0	2.84E-01	1.97E-01	2.75E-02	5.08E-01	µg/kg·y	0%	55.86%	38.73%	5.41%
Soil (Natural and Urban)	0	1.78E-06	2.98E-03	7.36E-03	1.03E-02	µg/kg·y	0%	0.02%	28.78%	71.21%
Soil (Sludge treated)	0	1.42E-01	9.30E-02	0.00	2.35E-01	µg/kg·y	0%	60.43%	39.57%	0%
Surface water	0	8.33E-05	5.78E-05	8.08E-06	1.49E-04	µg/L	0%	55.85%	38.73%	5.41%

Syn: Synthesis; For: Formulation; EoL: End of Life; LCS: Lifecycle stage.

8.3.1.3 Copper Carbonate ($Cu_2(OH)_2CO_3$)

In addition to transfer coefficients described in Section 8.2.2.2, specific coefficients for the $Cu_2(OH)_2CO_3$) case study, as assessed in SUN project, are reported in Table 60.

Table 60: Transfer coefficients for Wood Preservation with $Cu_2(OH)_2CO_3$ by life cycle stages. Mass released column indicates how the total material input in the system is split among all the lifecycles, while each row indicates the proportion of the material directly being transfer into natural and technical compartments. Source: SUN project.

		Natural compartments			Technical compartments				
	Mass released	**Air**	**Soil**	**SW**	**WW**	**EXP**	**LF**	**REC**	**WIP**
Production	0	-	-	-	-	-	-	-	-
Manufacture	0.05	-	0.001	-	0.999	-	-	-	-
Use	0.065	-	0.57	-	0.2	-	-	-	0.23
End-of-Life	0.885	-	0.1	-	-	-	-	-	0.9

SW: Surface Water; WW: Waste Water; EXP: Exportation; REC: Recycling; WIP: Waste Incineration Plant.

A schematic picture of the principal material transfers among all the system compartments is provided in Figure 45, the number on the arrows corresponds to the mean value of the material transferred from a compartment to another. Values are expressed in tons. The mean values of the quantities deposited into the natural compartments (divided by the compartments volumes reported in Table 55) and used for Risk Assessment, instead, are reported in Table 61.

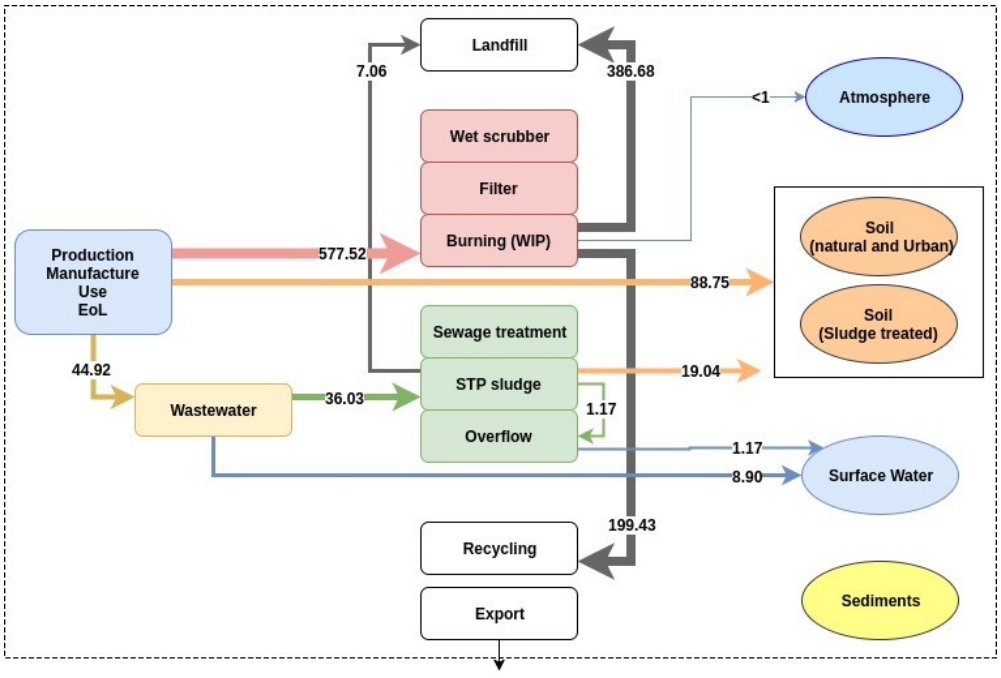

Figure 45: Principal mass flows in tons of Copper Carbonate for the case study assessments in all lifecycle stages. Units are expressed in tonnes. The numbers correspond to the mean values of the probability distributions generated.

Table 61: Mean value of material concentration in Environmental compartments computed by the PMFA model (divided by the compartment's volumes reported in Table 55) for the CuO case study, together with their relative weights with respect to the total material concentration in all lifecycle stages.

	Concentrations, absolute values (mean)						Relative weights (%)			
Environmental Compartment	**Syn**	**For**	**Use**	**EoL**	**All LCS**	**Units**	**Syn**	**For**	**Use**	**EoL**
Atmosphere	0	1.22E-08	2.19E-08	9.88E-07	1.02E-06	µg/m^3	0.00%	1.19%	2.15%	96.66%
Sediments	0	7.50E+00	2.08E+00	2.98E-01	9.88E+00	µg/kg·y	0.00%	75.91%	21.07%	3.02%
Soil (Natural and Urban)	0	5.04E-05	3.54E-02	8.48E-02	1.20E-01	µg/kg·y	0.00%	0.04%	29.45%	70.51%
Soil (Sludge treated)	0	4.36E+00	1.15E+00	0	5.51E+00	µg/kg·y	0.00%	79.15%	20.85%	0.00%
Surface water	0	2.20E-03	6.11E-04	8.75E-05	2.90E-03	µg/L	0.00%	75.90%	21.08%	3.02%

Syn: Synthesis; For: Formulation; EoL: End of Life; LCS: Lifecycle stage.

8.3.1.4 Alkaline copper quaternary (ACQ)

In addition to transfer coefficients described in Section 3.2.2.2, specific coefficients for ACQ case study, as assessed in SUN project, are reported in Table 62.

Table 62: Transfer coefficients for Wood Preservation with ACQ by life cycle stages. Mass released column indicates how the total material input in the system is split among all the lifecycles, while each row indicates the proportion of the material directly being transfer into natural and technical compartments. Source: SUN project.

		Natural compartments			Technical compartments				
	Mass released	**Air**	**Soil**	**SW**	**WW**	**EXP**	**LF**	**REC**	**WIP**
Production	0	-	-	-	-	-	-	-	-
Manufacture	0.05	-	0.001	-	0.999	-	-	-	-
Use	0.16	-	0.57	-	0.2	-	-	-	0.23
End-of-Life	0.79	-	0.1	-	-	-	-	-	0.9

SW: Surface Water; WW: Waste Water; EXP: Exportation; REC: Recycling; WIP: Waste Incineration Plant.

A schematic picture of the principal material transfers among all the system compartments is provided in Figure 46, the number on the arrows corresponds to the mean value of the material transferred from a compartment to another. Values are expressed in tons. The mean values of the quantities deposited into the natural compartments (divided by the compartments volumes reported in Table 55) and used for Risk Assessment, instead, are reported in Table 63.

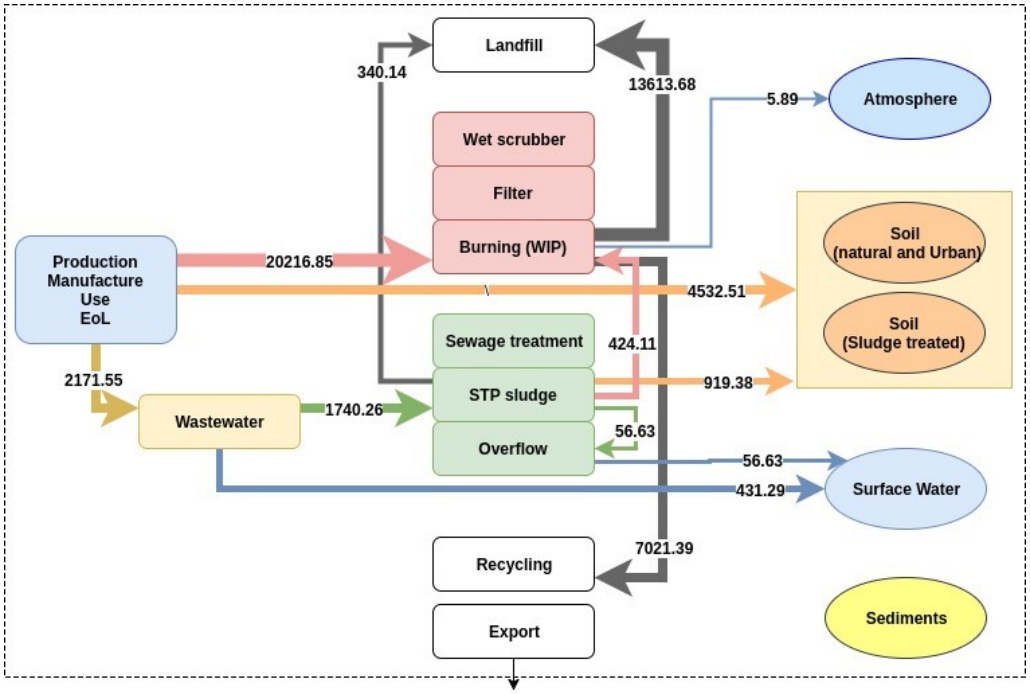

Figure 46: Principal mass flows in tons of Alkaline Copper Quaternary for the case study assessments in all lifecycle stages. Units are expressed in tonnes. The numbers correspond to the mean values of the probability distributions generated.

Table 63: Mean value of material concentration in Environmental compartments computed by the PMFA model (divided by the compartment's volumes reported in Table 55) for the CuO case study, together with their relative weights with respect to the total material concentration in all lifecycle stages.

	Concentrations, absolute values (mean)						Relative weights (%)			
Environmental Compartment	**Syn**	**For**	**Use**	**EoL**	**All LCS**	**Units**	**Syn**	**For**	**Use**	**EoL**
Atmosphere	0	4.51E-07	2.02E-06	3.35E-05	3.60E-05	µg/m3	0.00%	1.25%	5.62%	93.13%
Sediments	0	2.76E+02	1.92E+02	1.01E+01	4.78E+02	µg/kg·y	0.00%	57.67%	40.23%	2.10%
Soil (Natural and Urban)	0	1.86E-03	3.24E+00	2.87E+00	6.11E+00	µg/kg·y	0.00%	0.03%	52.99%	46.98%
Soil (Sludge treated)	0	1.62E+02	1.05E+02	0	2.67E+02	µg/kg·y	0.00%	60.60%	39.40%	0.00%
Surface water	0	8.10E-02	5.65E-02	2.95E-03	1.41E-01	µg/L	0.00%	57.67%	40.22%	2.10%

Syn: Synthesis; For: Formulation; EoL: End of Life; LCS: Lifecycle stage.

8.3.2 Hazard assessment results

8.3.2.1 "Ferrari Red" organic pigment (DPP)

For DPP, ecotoxicological data for Soils and for Surface Water were available. Such results are presented in Table 64, together with the rationale for applying assessment factors. Depending on the incorporation of the NM into the final chemical matrix and the properties of such matrix, different methods are necessary to produce fragmented products (FP). The obtained FP represent a form of the matrix with a greatly increased surface area, but constitute otherwise the identical material to the one

in the real products [332]. For DPP it was possible to estimate PNEC also for FPs. Thus, we used the data derived on pristine NM in the Synthesis and Formulation lifecycle stages, while we used the data on fragmented NM for the Use and End of Life lifecycle stages.

Table 64: Available ecotoxicological data and computed PNEC for DPP. Source: SUN project.

Dpp type	Pristine*	Fragmented**	Pristine
Type of species	Terrestrial	Terrestrial	Aquatic
Toxicological endpoint	EC10	HONEC	EC50; EC50
Taxonomic group	Invertebrate	Invertebrate	Invertebrate
Test organism	Enchytraeus crypticus	Enchytraeus crypticus	Daphnia magna
Concentration	1600	>3200	1644
Exposure time	28 days (chronic)	28 days (chronic)	48 h (acute)
AF no effect (where applicable)	-	10	-
Calculated NOEC	-	320	-
Rationale for PNEC derivation (based on REACH [262])	EC10 data for a long term available	NOEC for one long-term toxicity test available	Short term EC50 on invertebrates (not covering three trophic levels).
AF	100	100	1000
PNEC	16*	3.2**	1.644
Unite of measure	mg/kg	mg/kg	µg/l

* Data used in Synthesis and Formulation lifecycle stages; ** Data used in Use and End of Life lifecycle stages; AF: Assessment Factor; EC10: Effective Concentration at 10% inhibition; EC50: Effective Concentration at 50% inhibition; HONEC: Highest Observed No-Effect Level; NOEC: No Observed Effect Concentration.

8.3.2.2 Copper Oxide (CuO)

For CuO, ecotoxicological data for Soils and for Surface Water were available. Such results are presented in Table 65, together with the rationale for applying assessment factors.

Table 65: Available ecotoxicological data and computed PNEC for CuO. Source: SUN project.

Dpp type	Pristine	Pristine
Type of species	Terrestrial	Aquatic
Toxicological endpoint	EC10	EC10 (mortality endpoint); NOAEC (from EC20 weight endpoint)
Taxonomic group	Invertebrate	Invertebrate; Invertebrate
Test organism	Enchytraeus crypticus	Lymnaea stagnalis; Lymnaea stagnalis
Concentration	19	314; 29.5
Exposure time	28 days (chronic)	30 days (chronic); 30 days (chronic);

Dpp type	Pristine	Pristine
Type of species	Terrestrial	Aquatic
Rationale for PNEC derivation (based on REACH [262])	EC10 data for a long term available	NOEC/EC10 for long-term toxicity test, but not covering more than one trophic level. The lowest is selected.
AF	100	100
PNEC	0.19	0.295
Unite of measure	mg/kg	µg/l

AF: Assessment Factor; EC10: Effective Concentration at 10% inhibition; EC20: Effective Concentration at 20% inhibition; NOEC: No Observed Effect Concentration.

In addition, during the SUN project tests were performed on five additional Terrestrial species. Such results are reported in Table 66. REACH requires that at least ten NOECs (No Observed Effect Concentrations), and preferably more than 15, for different species covering at least eight taxonomic groups are available for deriving an HC5 from a SSD (Sensitivity Species Distribution) and use it as a PNEC [262]. However, for comparison purposes and to demonstrate the ability of SUNDS of dealing with a probabilistic PNEC (derived from HC5), we derived it from the available data.
Note that in Table 66 there is not the value of 19 mg/kg reported in Table 65 for *Enchytraeus crypticus*, this is because the value is based on cocoon production endpoint from a full life cycle test. This endpoint is thus not directly comparable to the endpoints in Table 66 which are based on the population number endpoint.

Table 66: Ecotoxicological results for Terrestrial species, used for SSD derivation. Source: SUN project.

Toxicological endpoint	Taxonomic group	Test organism	Concentration (mg/Kg)	Details on concentration	Exposure time (d)	AF no-effect	Calculated NOEC (mg/Kg)
EC10	Invertebrate	Enchytraeus crypticus	160	<160 mg Cu/kg, dry soil*	28	10	16
EC10	Invertebrate	Folsomia candida	227	227 (159-395) mg Cu/kg dry soil	28	1	227
EC10	Invertebrate	Protaphorura minuta	294	294 (168-420) mg Cu/kg dry soil	28	1	294
EC10	Invertebrate	Hyposatrura assimilis	300	300 (77-523) mg Cu/kg dry soil	28	1	300
EC10	Invertebrate	Mesaphorura macrochaeta	160	<160 mg Cu/kg dry soil*	28	10	16
EC10	Invertebrate	Hypoaspis aculeifer	329	329 (17-640) mg Cu/kg dry soil	28	1	329

* No negative effects were observed at the highest dose tested; EC10: Effective Concentration at 10% inhibition; NOEC: No Observed Effect Concentration.

The cumulative distribution function (CDF) computed by SUNDS after 10000 simulations, with the corresponding confidence intervals, of the resulting SSD curves computed is presented in Figure 47.

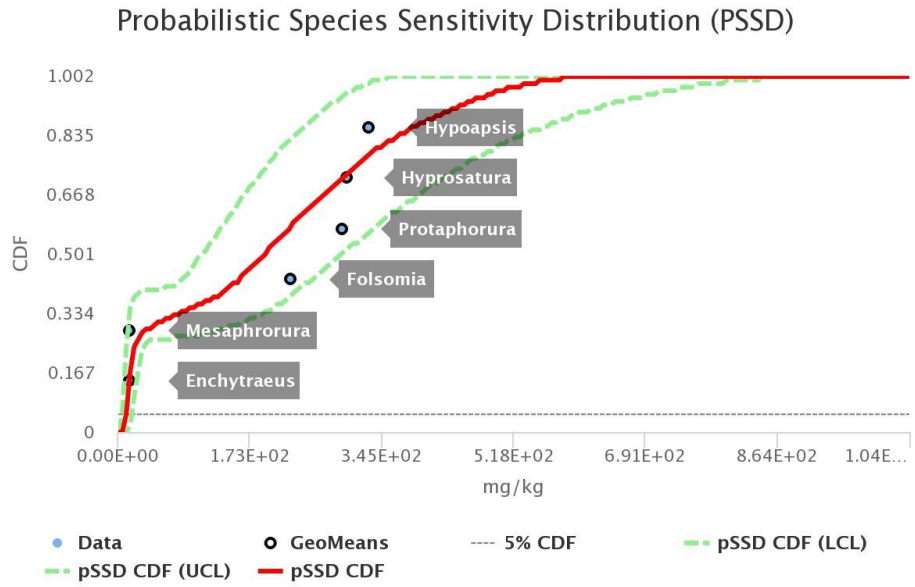

Figure 47: CDF of the SSD curves with confidence intervals, computed by SUNDS after 10000 simulations.

From the 5% of each SSD curve (HC5), SUNDS derived a probabilistic PNEC, which was approximated to a lognormal, as displayed in Figure 48 together with the original one.

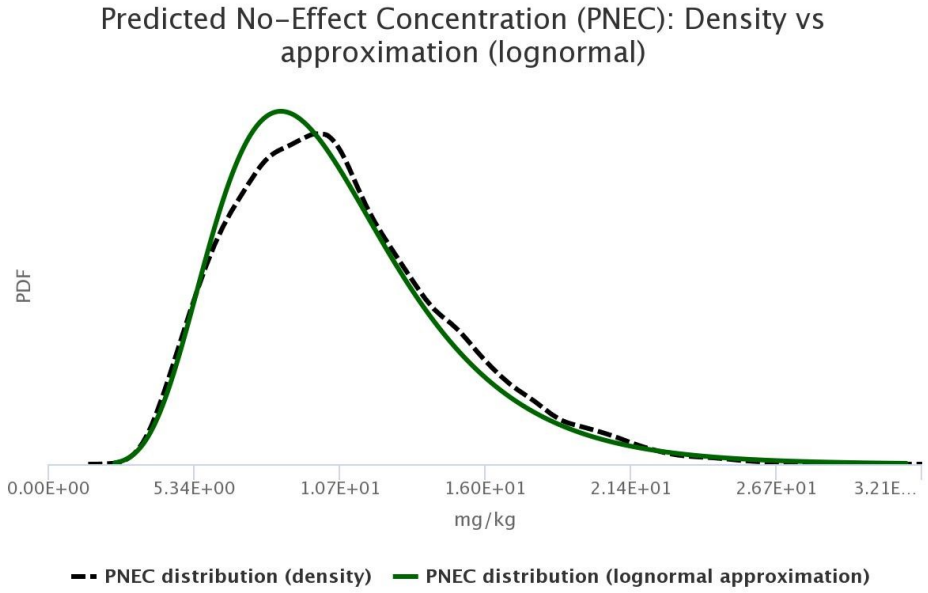

Figure 48: Computed PNEC and lognormal that approximate it and is used for Risk assessment.

From the figure, it is evident that it is reasonable to approximate probabilistic PNEC derived from HC5 of SSDs by using a lognormal distribution. The statistics of both curves are presented in Table 67.

Table 67: Curve characterization of the original PNEC and the approximated one. In case of lognormal distributions, in place of Mean and SD GeoMean and GeoSD (SD factor) are used.

Curve	Distribution	5%	25%	50%	75%	95%	(Geo)Mean	(Geo)SD
Original	Empirical	5.4e+00	7.81e+00	1.01e+01	1.31e+01	1.79e+01	1.08e+01	4.01e+00
Approximated	Lognormal	5.4e+00	7.69e+00	9.84e+00	1.26e+01	1.79e+01	(9.84e+00)	(1.44e+00)

8.3.2.3 Copper Carbonate ($Cu_2(OH)_2CO_3$) and Alkaline copper quaternary (ACQ)

For $Cu_2(OH)_2CO_3$ and ACQ, PNEC data was retrieved from a Danish report of 2015 (Environmental project No. 1788) [359], and are is summarized in Table 68.

Table 68: PNEC values for Cu2(OH)2CO3 and ACQ, retrieved from a Danish report of 2015 [359].

NM	Terrestrial	Aquatic
$Cu_2(OH)_2CO_3$	-	0.34 µg/l
ACQ	65 mg/kg	7.8 µg/l

8.3.3 Risk characterization results

If both PEC and PNEC values/distribution were available for an environmental compartment at a specific lifecycle stage, the corresponding risk were computed. Results are presented in the following sections.

8.3.3.1 "Ferrari Red" organic pigment (DPP)

Probabilistic Risk Characterization Ratios (RCRs) for the available Environmental compartments in all life cycle stages are reported in Figure 49 (Terrestrial compartments) and in Figure 50 (Aquatic compartments).

These results highlight that no risk is present in any of the Terrestrial and Aquatic compartments for DPP, in all the lifecycle stages. Due to the lack of ecotoxicological data for Air and Sediments, no conclusion can be drawn on these two Environmental compartments.

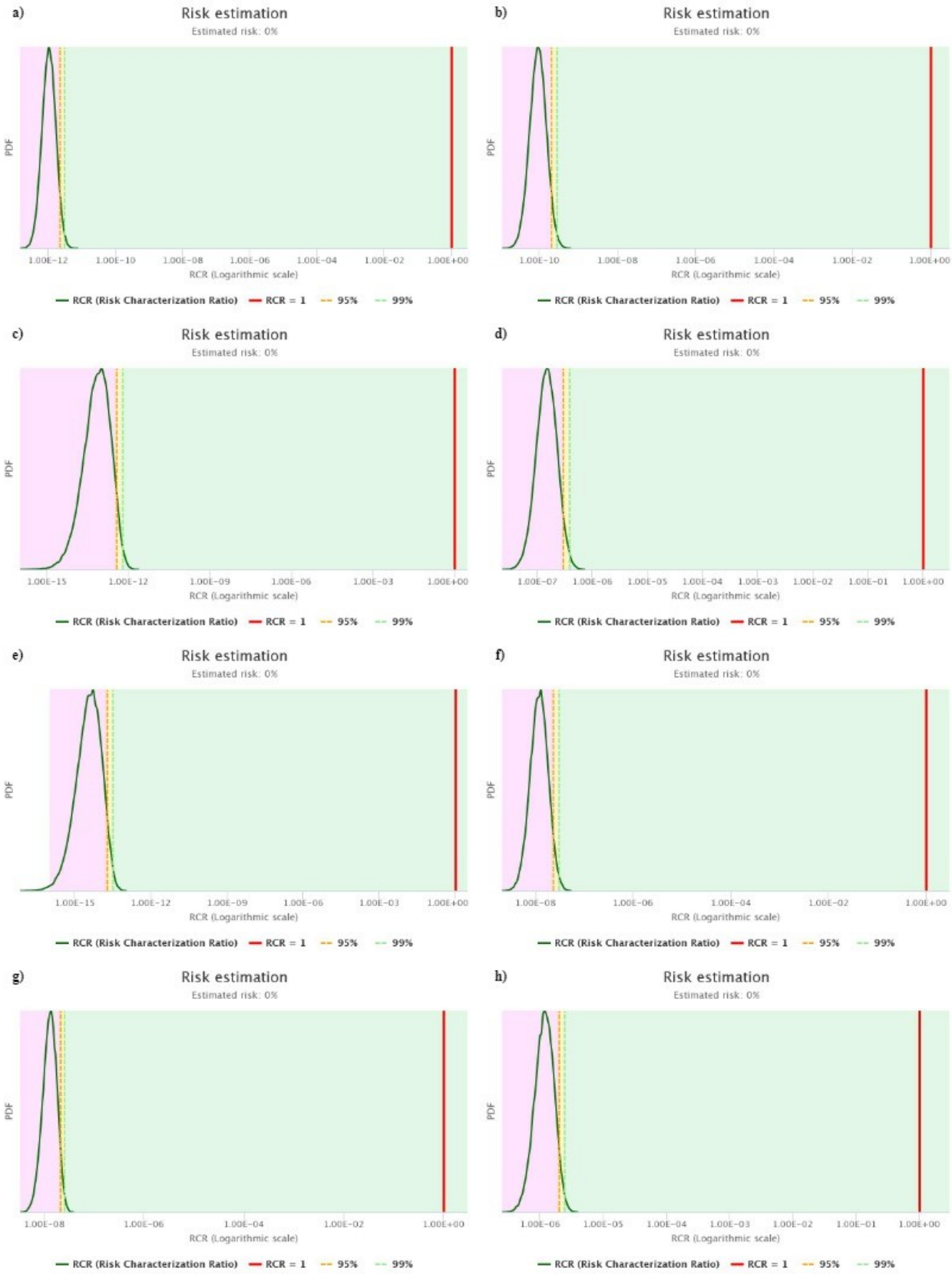

Figure 49: RCRs for terrestrial compartments in all lifecycle stages for DPP.
FORMULATION: a) Natural and Urban soils, b) Sludge Treated soil; SYNTHESIS: c) Natural and Urban soils, d) Sludge Treated soil; USE: e) Natural and Urban soils, f) Sludge Treated soil; END OF LIFE: g) Natural and Urban soils, h) Sludge Treated soil.

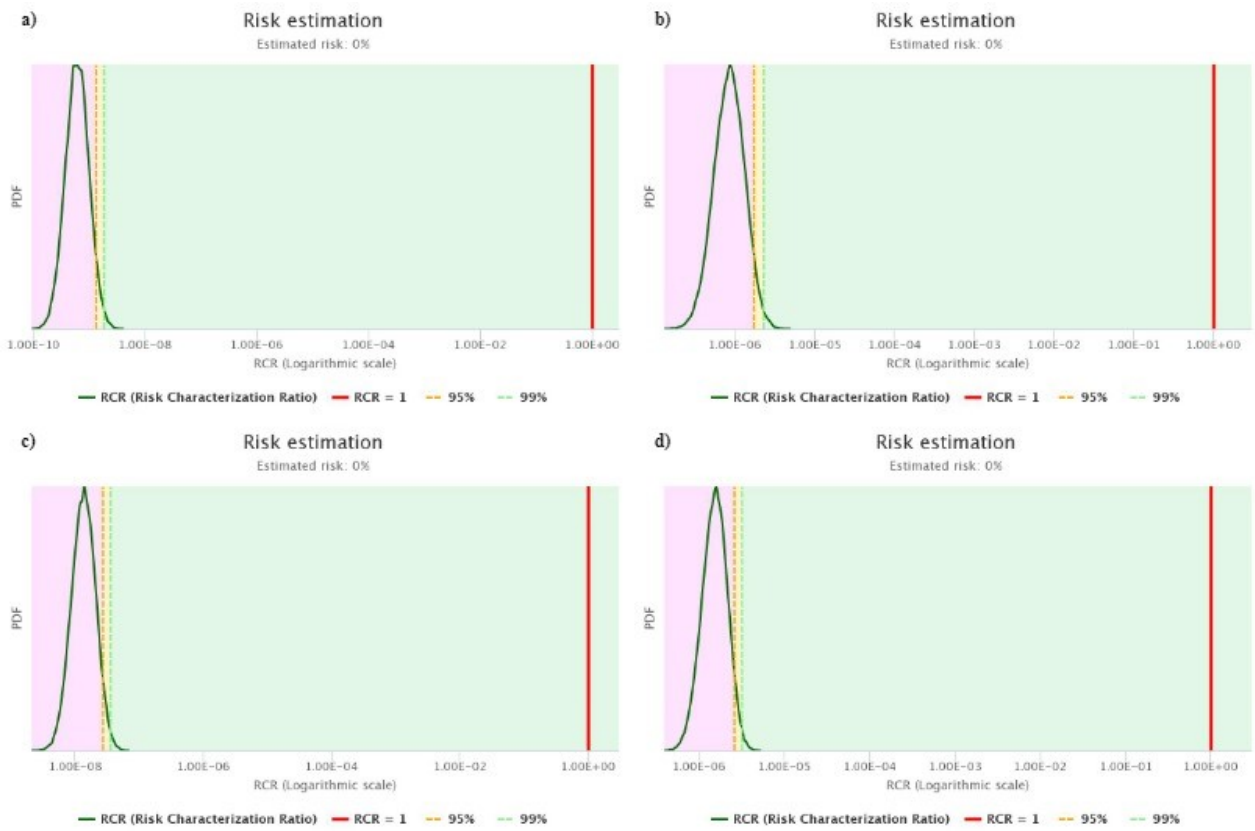

Figure 50: RCRs for the Surface Water Environmental compartment in all lifecycle stages for DPP.
a) FORMULATION; b) SYNTHESIS; c) USE; d) END OF LIFE.

8.3.3.2 Copper Oxide (CuO)

Probabilistic and Deterministic Risk Characterization Ratios (RCRs) for the available Environmental compartments in all life cycle stages are reported in Figure 51 (Terrestrial compartments) and in Figure 52 (Aquatic compartments).

These results highlight that no risk is present in any of the Terrestrial and Aquatic compartments for CuO, in all the lifecycle stages. Due to the lack of ecotoxicological data for Air and Sediments, no conclusion can be drawn on these two Environmental compartments.

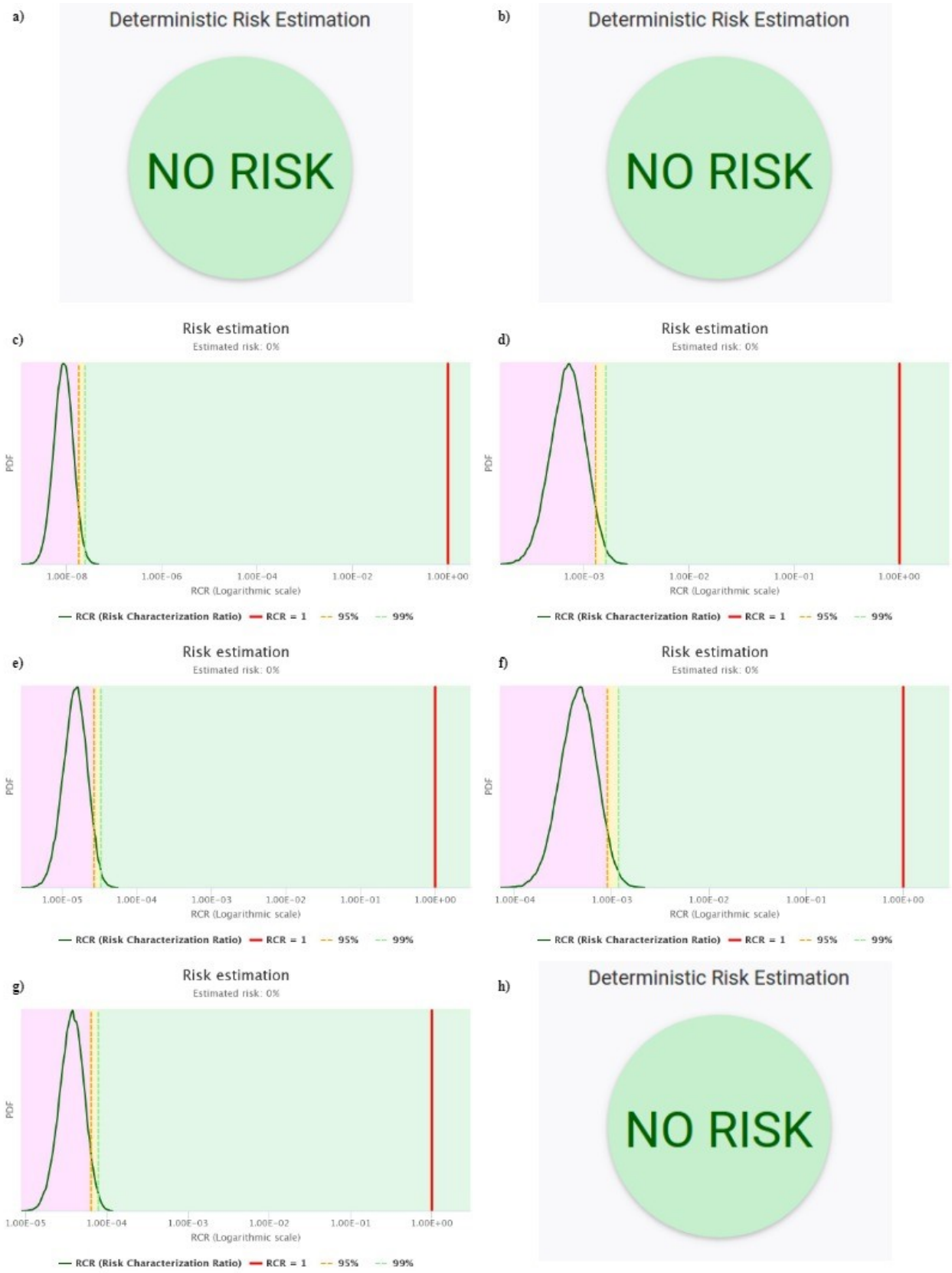

Figure 51: RCRs for terrestrial compartments in all lifecycle stages for CuO.
FORMULATION: a) Natural and Urban soils, b) Sludge Treated soil; SYNTHESIS: c) Natural and Urban soils, d) Sludge

Treated soil; USE: e) Natural and Urban soils, f) Sludge Treated soil; END OF LIFE: g) Natural and Urban soils, h) Sludge Treated soil.

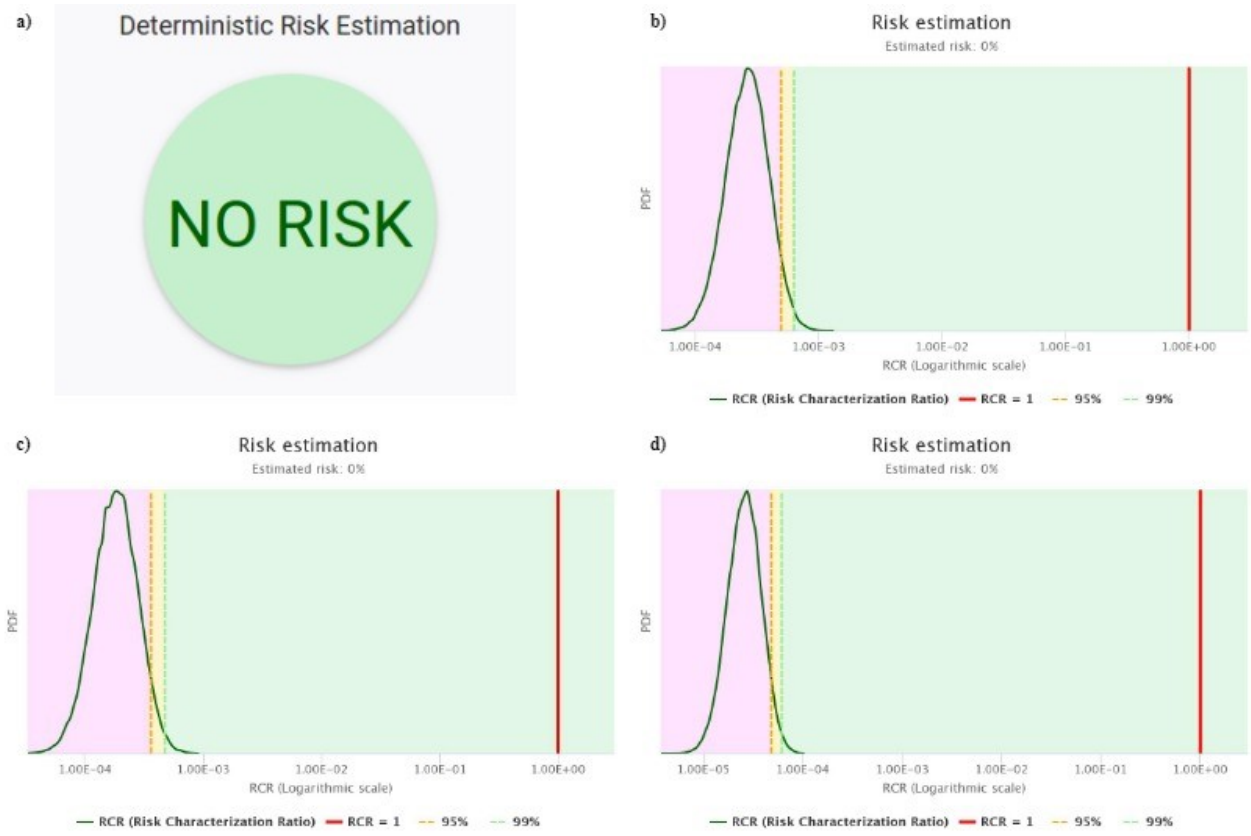

Figure 52: RCRs for the Surface Water Environmental compartment in all lifecycle stages for CuO.
a) FORMULATION; b) SYNTHESIS; c) USE; d) END OF LIFE.

In the case of CuO, since we derived also probabilistic PNECs for terrestrial compartments, it is possible to generate a probabilistic RCR by sampling with replacement from both PEC and PNEC distributions. The results of such analysis are displayed in Figure 53. It is worth nothing that the RCRs are more far than the red line with respect to the corresponding ones in Figure 51. This is expected, since the PNEC derived from as SSD is generally bigger than one derived deterministically. Specifically, in this case we used only 6 species from the same taxonomic group (invertebrates): it is important to stress out again that this analysis is provided just for comparison purposes and to demonstrate the functionalities of SUNDS. For Risk Assessment one has to use the more conservative deterministic PNECs.

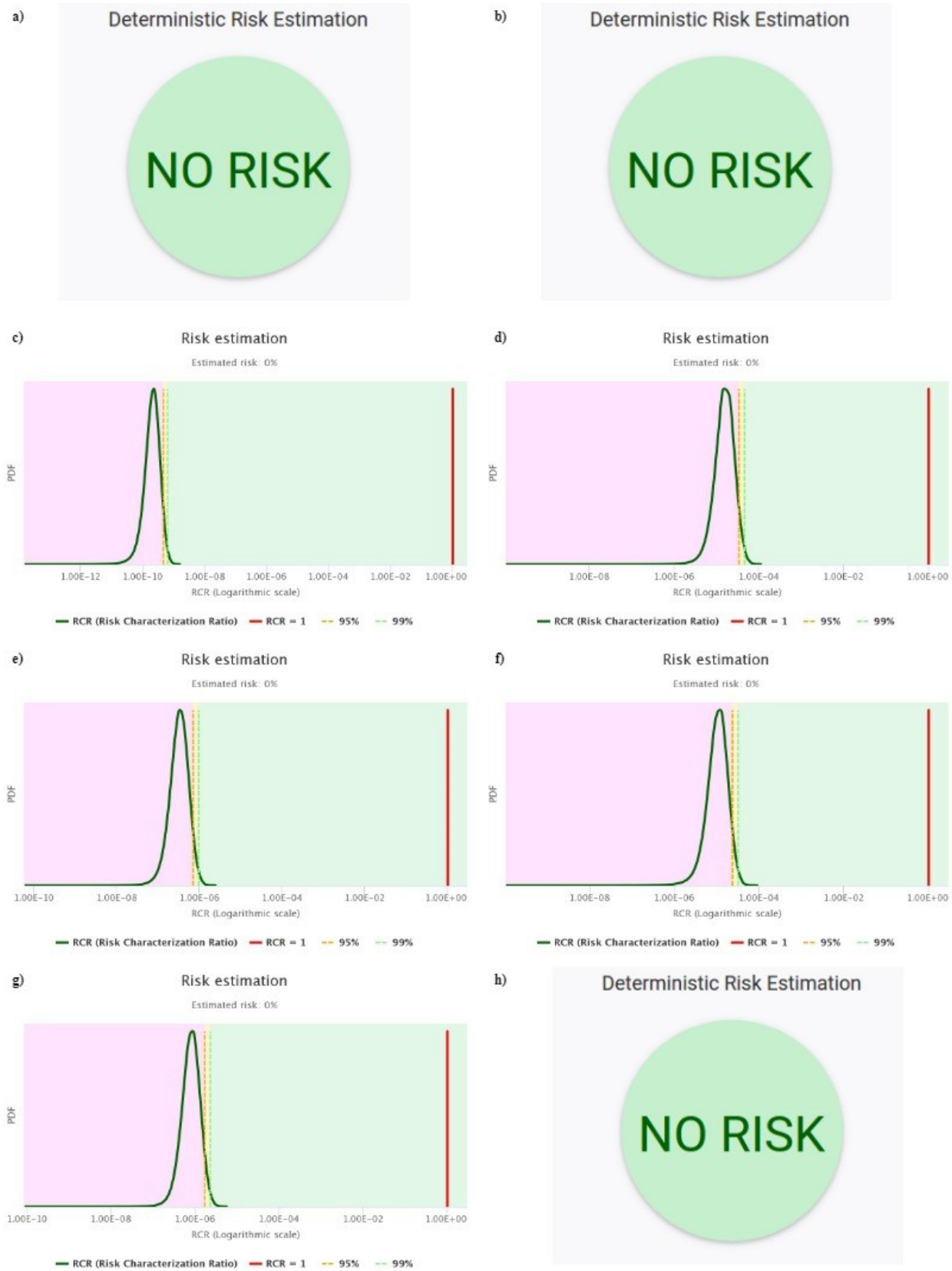

Figure 53: RCRs for terrestrial compartments in all lifecycle stages for CuO, derived from probabilistic PNECs. FORMULATION: a) Natural and Urban soils, b) Sludge Treated soil; SYNTHESIS: c) Natural and Urban soils, d) Sludge Treated soil; USE: e) Natural and Urban soils, f) Sludge Treated soil; END OF LIFE: g) Natural and Urban soils, h) Sludge Treated soil.

8.3.3.3 Copper Carbonate ($Cu_2(OH)_2CO_3$)

Probabilistic and Deterministic Risk Characterization Ratios (RCRs) for the available Environmental compartments in all life cycle stages are reported in Figure 54 (Aquatic compartments).

These results highlight that no risk is present in any of the Aquatic compartments for CuO, in all the lifecycle stages. Due to the lack of ecotoxicological data for Soils, Air and Sediments, no conclusion can be drawn on these three Environmental compartments.

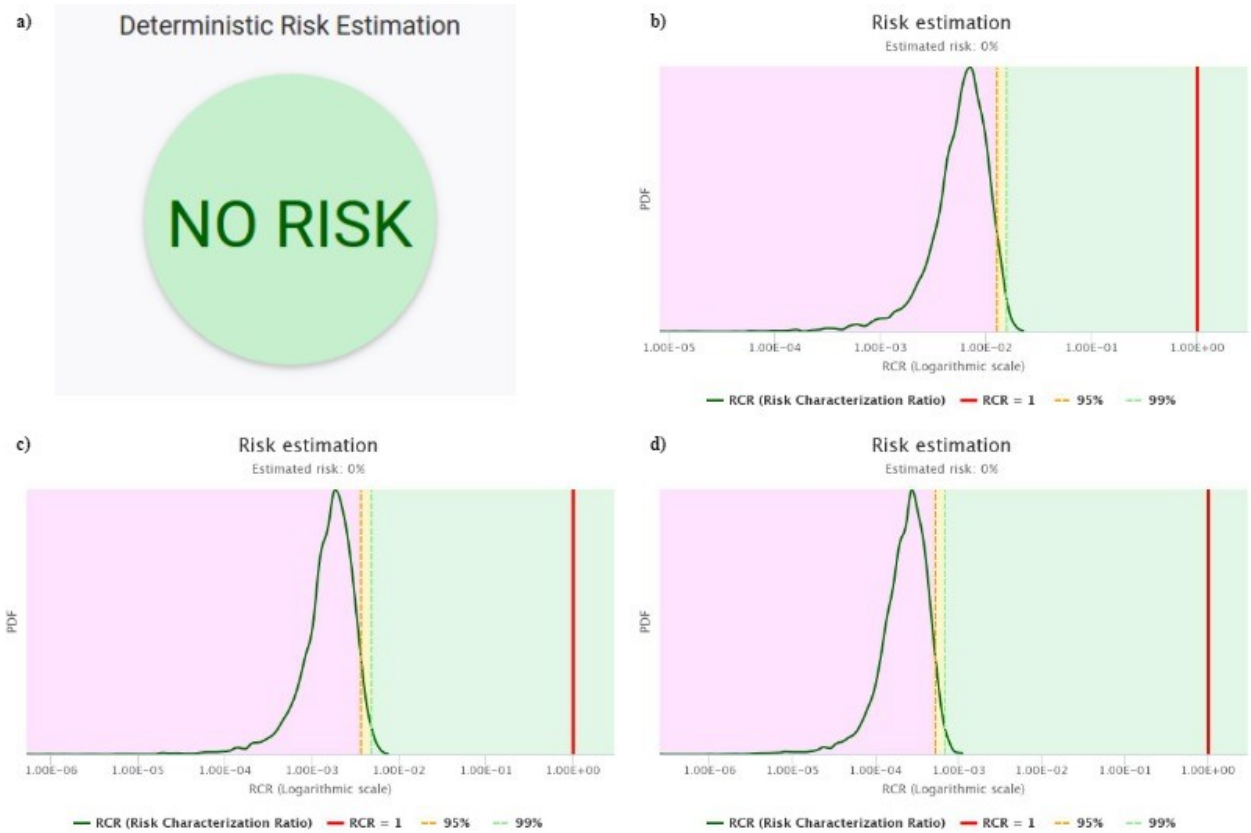

Figure 54: RCRs for the Surface Water Environmental compartment in all lifecycle stages for $Cu_2(OH)_2CO_3$.
a) FORMULATION; b) SYNTHESIS; c) USE; d) END OF LIFE.

8.3.3.4 Alkaline copper quaternary (ACQ)

Probabilistic and Deterministic Risk Characterization Ratios (RCRs) for the available Environmental compartments in all life cycle stages are reported in Figure 55 (Terrestrial compartments) and in Figure 56 (Aquatic compartments). These results highlight that no risk is present in any of the Terrestrial and Aquatic compartments for ACQ, in all the lifecycle stages. Due to the lack of ecotoxicological data for Air and Sediments, no conclusion can be drawn on these two Environmental compartments.

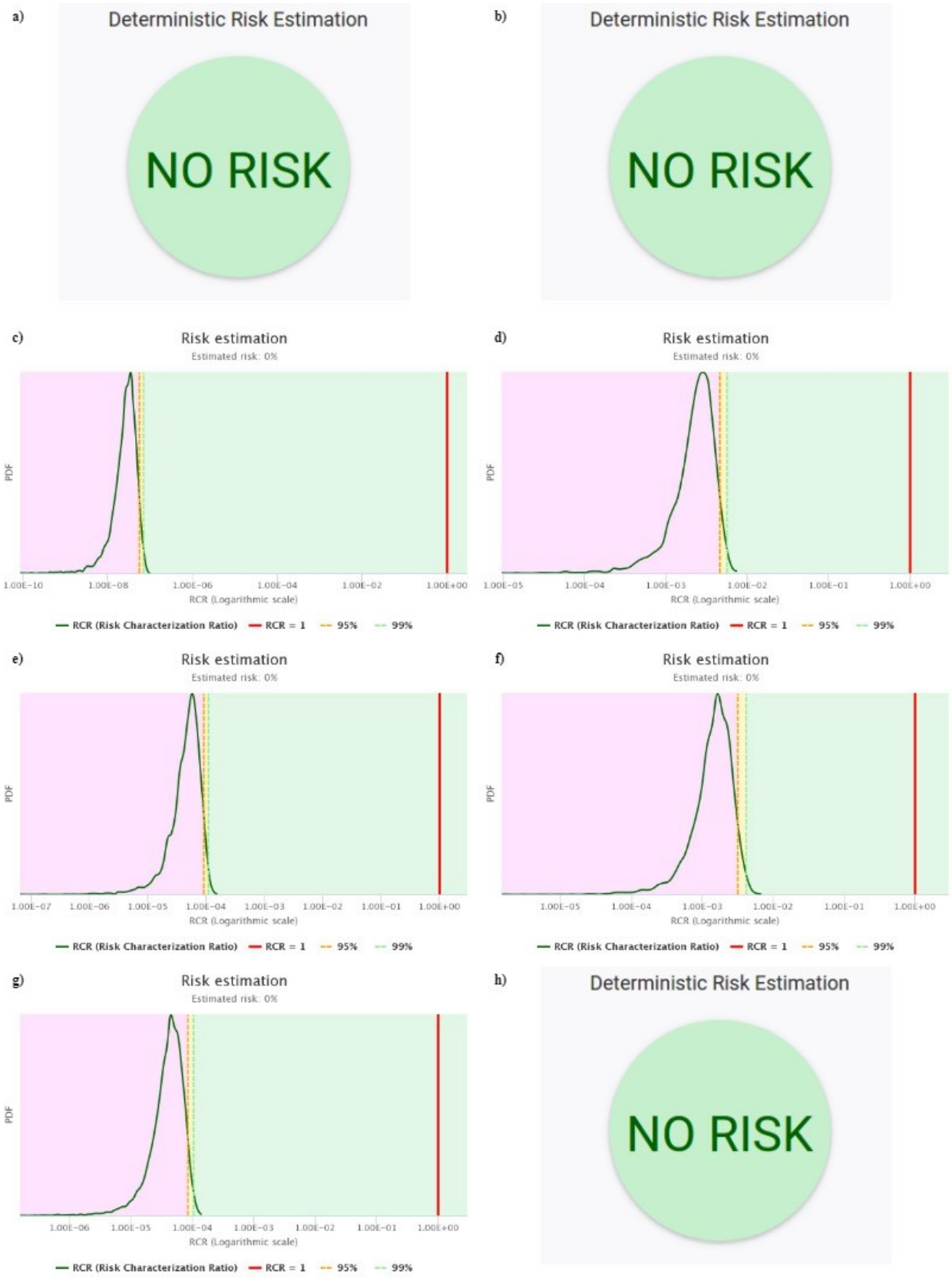

Figure 55: RCRs for terrestrial compartments in all lifecycle stages for ACQ.
FORMULATION: a) Natural and Urban soils, b) Sludge Treated soil; SYNTHESIS: c) Natural and Urban soils, d) Sludge

Treated soil; USE: e) Natural and Urban soils, f) Sludge Treated soil; END OF LIFE: g) Natural and Urban soils, h) Sludge Treated soil.

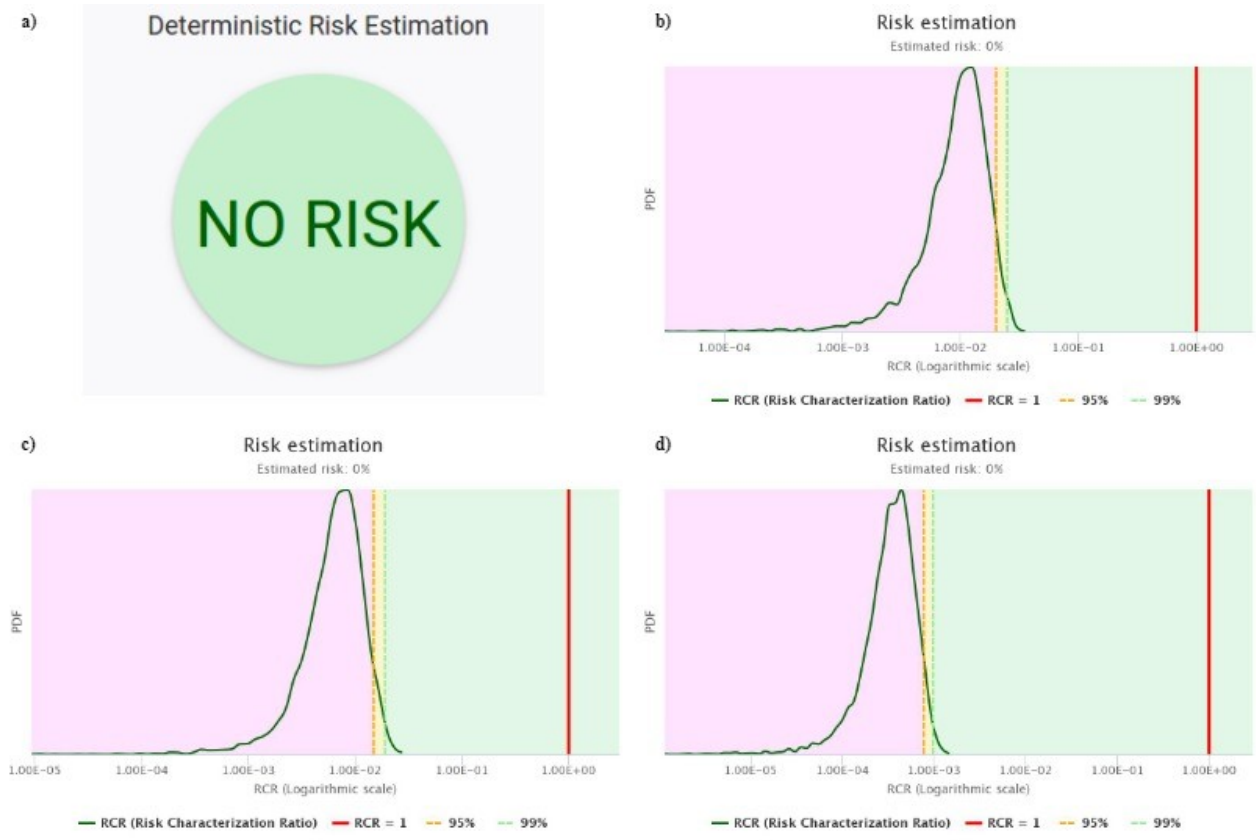

Figure 56: RCRs for the Surface Water Environmental compartment in all lifecycle stages for ACQ.
a) FORMULATION; b) SYNTHESIS; c) USE; d) END OF LIFE.

8.4 Conclusions

In this chapter the SUNDS ERA methodology was applied for two different case studies, namely nano-copper oxide-based biocidal paint and plastic automotive part (bumper) coloured with nano-sized organic pigment, according to the exposure and effect data generated in the frame of the SUN project.
The risk assessment highlighted no risk for Aquatic Environmental compartments in all the case studies (DPP, CuO, $Cu_2(OH)_2CO_3$, and ACQ), and for CuO, DPP and ACQ our analysis show that no risk is present for Natural and Urban soils and for Sludge treated soils used for agriculture. It was not possible to assess the risk for the Air and Sediments Environmental compartments (and for Soils compartments in the case of $Cu_2(OH)_2CO_3$) due to the lack of ecotoxicological data.
Furthermore, we demonstrated the ability of SUNDS to deal with both probabilistic and deterministic PECs and PNECs.

9 Conclusions and future work

This thesis was built upon the Cooper Stage-Gate innovation model [11] for the development of a SbD concept for NMs which could be implemented by industry and accounted as a reference tool by regulators. Specifically, the application of computational models for the safety assessment of NM was discussed through the thesis, and novel approaches aimed at informing SbD practices were provided.

The first part of this thesis, indeed, discussed predictive *in silico* models, which can be contextualized in screening level modelling in the early stages of NEP development (up to stage 3 of the Cooper Stage Gate innovation model). Current *in silico* tools that make use of ML techniques to predict hazard endpoints were reviewed, and two novel models were proposed: one was aimed at categorizing NFs of the same NM into stability classes with respect to their colloidal stability in different environmental media, while the other proposed a novel ML approach based on subspace clustering for the Read-Across and Classification of NMs. My plan for the forthcoming months is to further follow the path addressed by the first 4 chapters of this thesis: our approach that make use of subspace clustering will be indeed further investigated, trying to apply it to predict quantitatively (and not only qualitatively) endpoint values. If the good results achieved in the preliminary tests provided in chapter 4 will be achieved also with this new setting, this will surely be a big step forward the development of predictive *in silico* tools for the safety assessment of NMs. In addition, a sensitivity and uncertainty analysis of this tool will be provided also for the case studies described in the chapter. In the forthcoming months I will also work further in studying how surface functionalization affect the colloidal stability and the risks of NMs: we are indeed performing tests on different NMs and on different test conditions.

On the other hand, the second part of the thesis dealt with regulatory risk assessment and management to allow the NEPs to go the market (stage 5 of the Copper Stage Gate innovation model), describing SUNDS, the DSS developed in the SUN project, and its application in different case studies for the evaluation of risks for the Human Health and the Environment. In the forthcoming month, chapter 8 (the one that dealt Environmental Risk Assessment in SUNDS) will be further elaborated: a discussion from a risk assessment perspective will be provided, and an article will be submitted to a peer-reviewed journal. Moreover, SUNDS will be further developed, to enable also grouping and read-across for more efficient analysis.

Thus, what presented in this thesis and its future development will contribute to go a step further in the implementation of NMs with desired properties and controlled risks for Human Health and the Environment.

References

1. Potočnik, J. Commission recommendation of 18 October 2011 on the definition of nanomaterial (2011/696/EU). *Off. J. Eur. Union* (2011). doi:10.2777/13162
2. Piccinno, F., Gottschalk, F., Seeger, S. & Nowack, B. Industrial production quantities and uses of ten engineered nanomaterials in Europe and the world. *J. Nanoparticle Res.* **14,** 1109 (2012).
3. European Comission. Regulation (EC) 1907/2006 of the European Parliament and of teh Council of 18 December 2006 - REACH. *Off. J. Eur. Union* (2006). doi:http://eur-lex.europa.eu/LexUriServ/LexUriServ.do?uri=OJ:L:2006:396:0001:0849:EN:PDF
4. OECD. Important Issues on Risk Assessment of Manufactured Nanomaterials. *OECD Environ. Heal. Saf. Publ. Ser. Saf. Manuf. Nanomater. ENV/JM/MONO(2012)/8* (2012).
5. ECHA. Appendix R . 6-1 : Recommendations for nanomaterials applicable to the Guidance on QSARs and Grouping. 29 (2017). doi:10.2823/884050
6. Hutchison, J. E. The Road to Sustainable Nanotechnology: Challenges, Progress and Opportunities. *ACS Sustain. Chem. Eng.* **4,** 5907–5914 (2016).
7. Kraegeloh, A., Suarez-Merino, B., Sluijters, T. & Micheletti, C. Implementation of Safe-by-Design for Nanomaterial Development and Safe Innovation: Why We Need a Comprehensive Approach. *Nanomaterials* (2018). doi:10.3390/nano8040239
8. Rivera-Gil, P. *et al.* The challenge to relate the physicochemical properties of colloidal nanoparticles to their cytotoxicity. *Acc. Chem. Res.* (2013). doi:10.1021/ar300039j
9. Goesmann, H. & Feldmann, C. Nanoparticulate functional materials. *Angewandte Chemie - International Edition* (2010). doi:10.1002/anie.200903053
10. Reinosa, J. J., Docio, C. M. Á., Ramírez, V. Z. & Lozano, J. F. F. Hierarchical nano ZnO-micro TiO2composites: High UV protection yield lowering photodegradation in sunscreens. *Ceram. Int.* (2018). doi:10.1016/j.ceramint.2017.11.028
11. Cooper, R. G. Idea-to-Launch Gating Systems: Better, Faster, and More Agile. *Res. Manag.* (2017). doi:10.1080/08956308.2017.1255057
12. EC. Amendments of the Annexes to REACH for registration of nanomaterials | European Commission. (2017).
13. Burden, N. *et al.* The 3Rs as a framework to support a 21st century approach for nanosafety assessment. *Nano Today* **12,** 10–13 (2017).
14. Hristozov, D. *et al.* Frameworks and tools for risk assessment of manufactured nanomaterials. *Environment International* **95,** 36–53 (2016).
15. ECHA. *Appendix R . 6-1 : Recommendations for nanomaterials applicable to the Guidance on QSARs and Grouping*. (2017). doi:10.2823/884050
16. OECD. *Guidance Document on the Validation of (Quantitative) Structure-Activity Relationship [(Q)SAR] Models*. *ENV/JM/MONO(2007)2* **2,** (OECD Publishing, 2007).
17. RCC. Nanotechnology Initiative Work Element 2 , Priority Setting : Development of a Joint Nanomaterials Classification Scheme. 18 (2013).
18. RCC. Nanotechnology Initiative Work Element 3 : Risk Assessment / Risk Management. 42 (2013).
19. Lynch, I., Weiss, C. & Valsami-Jones, E. A strategy for grouping of nanomaterials based on key physico-chemical descriptors as a basis for safer-by-design NMs. *Nano Today* **9,** 266–270 (2014).
20. ECHA. Read-Across Assessment Framework (RAAF). (2017). doi:10.2823/619212
21. Mech, A. *et al.* Insights into possibilities for grouping and read-across for nanomaterials in EU chemicals legislation. *Nanotoxicology* 1–23 (2018). doi:10.1080/17435390.2018.1513092
22. Hardy, A. *et al. Guidance on risk assessment of the application of nanoscience and nanotechnologies in the food and feed chain: Part 1, human and animal health*. *EFSA Journal* **16,** (2018).
23. Oomen, A. G. *et al.* Risk assessment frameworks for nanomaterials: Scope, link to regulations, applicability, and outline for future directions in view of needed increase in efficiency.

NanoImpact **9,** 1–13 (2018).
24. Lamon, L., Aschberger, K., Asturiol, D., Richarz, A.-N. & Worth, A. Grouping of nanomaterials to read-across hazard endpoints: a review. *Nanotoxicology* doi:10.1080/17435390.2018.1506060
25. Arts, J. H. E. *et al.* A critical appraisal of existing concepts for the grouping of nanomaterials. *Regul. Toxicol. Pharmacol.* **70,** 492–506 (2015).
26. Arts, J. H. E. *et al.* A decision-making framework for the grouping and testing of nanomaterials (DF4nanoGrouping). *Regul. Toxicol. Pharmacol.* **71,** S1–S27 (2015).
27. Lamon, L., Aschberger, K., Asturiol, D., Richarz, A.-N. & Worth, A. Grouping of nanomaterials to read-across hazard endpoints: a review. *Accept. by Nanotoxicology*
28. Oberdörster, G. & Kuhlbusch, T. A. J. In vivo effects: Methodologies and biokinetics of inhaled nanomaterials. *NanoImpact* **10,** 38–60 (2018).
29. Rasmussen, K. *et al.* Physico-chemical properties of manufactured nanomaterials - Characterisation and relevant methods. An outlook based on the OECD Testing Programme. *Regul. Toxicol. Pharmacol.* **92,** 8–28 (2018).
30. Stone, V. *et al.* ITS-NANO - Prioritising nanosafety research to develop a stakeholder driven intelligent testing strategy. *Part. Fibre Toxicol.* **11,** 9 (2014).
31. Fourches, D. *et al.* Computer-aided design of carbon nanotubes with the desired bioactivity and safety profiles. *Nanotoxicology* **10,** 374–383 (2016).
32. Puzyn, T. *et al.* Using nano-QSAR to predict the cytotoxicity of metal oxide nanoparticles. *Nat. Nanotechnol.* **6,** 175–178 (2011).
33. Winkler, D. A. *et al.* Applying quantitative structure-activity relationship approaches to nanotoxicology: Current status and future potential. *Toxicology* **313,** 15–23 (2013).
34. Oksel, C., Ma, C. Y., Liu, J. J., Wilkins, T. & Wang, X. Z. (Q)SAR modelling of nanomaterial toxicity: A critical review. *Particuology* **21,** 1–19 (2015).
35. Cedervall, T. *et al.* Understanding the nanoparticle-protein corona using methods to quantify exchange rates and affinities of proteins for nanoparticles. *Proc. Natl. Acad. Sci.* **104,** 2050–2055 (2007).
36. Lynch, I. & Dawson, K. A. Protein-nanoparticle interactions. *Nano Today* **3,** 40–47 (2008).
37. Monopoli, M. P., Åberg, C., Salvati, A. & Dawson, K. A. Biomolecular coronas provide the biological identity of nanosized materials. *Nat. Nanotechnol.* **7,** 779–786 (2012).
38. Tsiliki, G., Nymark, P., Kohonen, P., Grafström, R. & Sarimveis, H. Enriching Nanomaterials Omics Data: An Integration Technique to Generate Biological Descriptors. *Small Methods* **1,** 1700139 (2017).
39. Lubinski, L. *et al.* Evaluation criteria for the quality of published experimental data on nanomaterials and their usefulness for QSAR modelling. *SAR QSAR Environ. Res.* (2013). doi:10.1080/1062936X.2013.840679
40. Gajewicz, A., Jagiello, K., Cronin, M. T. D., Leszczynski, J. & Puzyn, T. Addressing a bottle neck for regulation of nanomaterials: quantitative read-across (Nano-QRA) algorithm for cases when only limited data is available. *Environ. Sci. Nano* (2017). doi:10.1039/c6en00399k
41. Gajewicz, A., Cronin, M. T. D., Rasulev, B., Leszczynski, J. & Puzyn, T. Novel approach for efficient predictions properties of large pool of nanomaterials based on limited set of species: Nano-read-across. *Nanotechnology* **26,** (2015).
42. Puzyn, T., Leszczynska, D. & Leszczynski, J. Toward the development of 'Nano-QSARs': Advances and challenges. *Small* **5,** 2494–2509 (2009).
43. Tantra, R. *et al.* Nano(Q)SAR: Challenges, pitfalls and perspectives. *Nanotoxicology* **9,** 636–642 (2015).
44. Oksel, C., Ma, C. Y., Liu, J. J., Wilkins, T. & Wang, X. Z. in *Advances in Experimental Medicine and Biology* **947,** 103–142 (2017).
45. Jones, D. E., Ghandehari, H. & Facelli, J. C. A review of the applications of data mining and machine learning for the prediction of biomedical properties of nanoparticles. *Computer Methods and Programs in Biomedicine* **132,** 93–103 (2016).
46. Sizochenko, N. & Leszczynski, J. Review of Current and Emerging Approaches for Quantitative Nanostructure-Activity Relationship Modeling. *J. Nanotoxicology Nanomedicine* **1,** 1–16 (2016).

47. Chen, G., Vijver, M. G., Xiao, Y. & Peijnenburg, W. J. G. M. A review of recent advances towards the development of (quantitative) structure-activity relationships for metallic nanomaterials. *Materials* (2017). doi:10.3390/ma10091013
48. Chen, G., Peijnenburg, W., Xiao, Y. & Vijver, M. Current Knowledge on the Use of Computational Toxicology in Hazard Assessment of Metallic Engineered Nanomaterials. *Int. J. Mol. Sci.* **18,** 1504 (2017).
49. Quik, J. T. K. *et al.* Directions in QPPR development to complement the predictive models used in risk assessment of nanomaterials. *NanoImpact* (2018). doi:10.1016/j.impact.2018.02.003
50. Lamon, L. *et al.* Physiologically based mathematical models of nanomaterials for regulatory toxicology: a review. *Comput. Toxicol. (In Press.*
51. Steinhäuser, K. G. & Sayre, P. G. Reliability of methods and data for regulatory assessment of nanomaterial risks. *NanoImpact* **7,** 66–74 (2017).
52. Jones, D. E., Igo, S., Hurdle, J. & Facelli, J. C. Automatic Extraction of NanoParticle properties using natural language processing: NanoSifter an application to acquire pamam dendrimer properties. *PLoS One* **9,** (2014).
53. Lewinski, N. A. & McInnes, B. T. Using natural language processing techniques to inform research on nanotechnology. *Beilstein J. Nanotechnol.* (2015). doi:10.3762/bjnano.6.149
54. Maojo, V. *et al.* Nanoinformatics: A new area of research in nanomedicine. *International Journal of Nanomedicine* (2012). doi:10.2147/IJN.S24582
55. Smith-Unna, R. & Murray-Rust, P. The ContentMine scraping stack: Literature-scale content mining with community-maintained collections of declarative scrapers. *D-Lib Mag.* (2014). doi:10.1045/november14-smith-unna
56. Jeliazkova, N. *et al.* The eNanoMapper database for nanomaterial safety information. *Beilstein J. Nanotechnol.* **6,** 1609–1634 (2015).
57. Chomenidis, C. *et al.* Jaqpot Quattro: A Novel Computational Web Platform for Modeling and Analysis in Nanoinformatics. *J. Chem. Inf. Model.* (2017). doi:10.1021/acs.jcim.7b00223
58. Oecd. OECD principles for the validation, for regulatory purposes, of (quantitative) structure-activity relationships models. *Biotechnology* 1–2 (2004).
59. Dearden, J. C., Cronin, M. T. D. & Kaiser, K. L. E. How not to develop a quantitative structure-activity or structure-property relationship (QSAR/QSPR). *SAR QSAR Environ. Res.* **20,** 241–266 (2009).
60. Beleites, C., Neugebauer, U., Bocklitz, T., Krafft, C. & Popp, J. Sample size planning for classification models. *Anal. Chim. Acta* **760,** 25–33 (2013).
61. Eriksson, L. *et al.* Methods for reliability and uncertainty assessment and for applicability evaluations of classification- and regression-based QSARs. *Environmental Health Perspectives* **111,** 1361–1375 (2003).
62. Dudek, A. Z., Arodz, T. & Gálvez, J. Computational methods in developing quantitative structure-activity relationships (QSAR): a review. *Comb. Chem. High Throughput Screen.* **9,** 213–28 (2006).
63. Golbraikh, A. & Tropsha, A. Beware of q2! in *Journal of Molecular Graphics and Modelling* **20,** 269–276 (2002).
64. Gramatica, P. & Sangion, A. A Historical Excursus on the Statistical Validation Parameters for QSAR Models: A Clarification Concerning Metrics and Terminology. *Journal of Chemical Information and Modeling* **56,** 1127–1131 (2016).
65. Gramatica, P. Principles of QSAR models validation: Internal and external. *QSAR and Combinatorial Science* **26,** 694–701 (2007).
66. Tropsha, A., Gramatica, P. & Gombar, V. The Importance of Being Earnest: Validation is the Absolute Essential for Successful Application and Interpretation of QSPR Models. *QSAR Comb. Sci.* **22,** 69–77 (2003).
67. Alexander, D. L. J., Tropsha, A. & Winkler, D. A. Beware of R^2: Simple, Unambiguous Assessment of the Prediction Accuracy of QSAR and QSPR Models. *J. Chem. Inf. Model.* **55,** 1316–1322 (2015).
68. Roy, P. P. & Roy, K. On Some Aspects of Variable Selection for Partial Least Squares Regression Models. *QSAR Comb. Sci.* **27,** 302–313 (2008).
69. Chirico, N. & Gramatica, P. Real external predictivity of QSAR models: How to evaluate It?

Comparison of different validation criteria and proposal of using the concordance correlation coefficient. *J. Chem. Inf. Model.* **51,** 2320–2335 (2011).
70. Chirico, N. & Gramatica, P. Real external predictivity of QSAR models. Part 2. New intercomparable thresholds for different validation criteria and the need for scatter plot inspection. *J. Chem. Inf. Model.* **52,** 2044–2058 (2012).
71. Jaworska, J., Nikolova-Jeliazkova, N. & Aldenberg, T. QSAR applicability domain estimation by projection of the training set in descriptor space: A review. *ATLA Alternatives to Laboratory Animals* **33,** 445–459 (2005).
72. Hristozov, D. *et al.* Demonstration of a modelling-based multi-criteria decision analysis procedure for prioritisation of occupational risks from manufactured nanomaterials. *Nanotoxicology* **10,** 1215–1228 (2016).
73. Sizochenko, N., Gajewicz, A., Leszczynski, J. & Puzyn, T. Causation or only correlation? Application of causal inference graphs for evaluating causality in nano-QSAR models. *Nanoscale* **8,** 7203–7208 (2016).
74. Sizochenko, N. *et al.* Causal inference methods to assist in mechanistic interpretation of classification nano-SAR models. *RSC Adv.* **5,** 77739–77745 (2015).
75. Panneerselvam, S. & Choi, S. Nanoinformatics: Emerging databases and available tools. *Int. J. Mol. Sci.* **15,** 7158–7182 (2014).
76. Kohonen, P. *et al.* Cancer biology, toxicology and alternative methods development go hand-in-hand. *Basic Clin. Pharmacol. Toxicol.* **115,** 50–58 (2014).
77. Jeliazkova, N. *et al.* The first eNanoMapper prototype: A substance database to support safe-by-design. in *Proceedings - 2014 IEEE International Conference on Bioinformatics and Biomedicine, IEEE BIBM 2014* 1–9 (2014). doi:10.1109/BIBM.2014.6999367
78. Oksel, C., Ma, C. Y. & Wang, X. Z. Current situation on the availability of nanostructure–biological activity data. *SAR QSAR Environ. Res.* **26,** 79–94 (2015).
79. Hendren, C. O., Powers, C. M., Hoover, M. D. & Harper, S. L. The Nanomaterial Data Curation Initiative: A collaborative approach to assessing, evaluating, and advancing the state of the field. *Beilstein J. Nanotechnol.* **6,** 1752–1762 (2015).
80. Powers, C. M. *et al.* Nanocuration workflows: Establishing best practices for identifying, inputting, and sharing data to inform decisions on nanomaterials. *Beilstein J. Nanotechnol.* **6,** 1860–1871 (2015).
81. Marchese Robinson, R. L. *et al.* How should the completeness and quality of curated nanomaterial data be evaluated? *Nanoscale* **8,** 9919–9943 (2016).
82. Thomas, D. G. *et al.* ISA-TAB-Nano: A Specification for Sharing Nanomaterial Research Data in Spreadsheet-based Format. *BMC Biotechnol.* **13,** 2 (2013).
83. Thomas, D. G., Pappu, R. V. & Baker, N. A. NanoParticle Ontology for cancer nanotechnology research. *J. Biomed. Inform.* (2011). doi:10.1016/j.jbi.2010.03.001
84. Karcher, S. *et al.* Integration among databases and data sets to support productive nanotechnology: Challenges and recommendations. *NanoImpact* (2018). doi:10.1016/j.impact.2017.11.002
85. Mills, K. C., Murry, D., Guzan, K. A. & Ostraat, M. L. Nanomaterial registry: Database that captures the minimal information about nanomaterial physico-chemical characteristics. *J. Nanoparticle Res.* (2014). doi:10.1007/s11051-013-2219-8
86. George, S. *et al.* Use of a high-throughput screening approach coupled with in vivo zebrafish embryo screening to develop hazard ranking for engineered nanomaterials. *ACS Nano* **5,** 1805–1817 (2011).
87. George, S. *et al.* Use of a rapid cytotoxicity screening approach to engineer a safer zinc oxide nanoparticle through iron doping. *ACS Nano* (2010). doi:10.1021/nn901503q
88. Zhang, H. *et al.* Use of metal oxide nanoparticle band gap to develop a predictive paradigm for oxidative stress and acute pulmonary inflammation. *ACS Nano* **6,** 4349–4368 (2012).
89. Chen, R. *et al.* Nanoparticle surface characterization and clustering through concentration-dependent surface adsorption modeling. *ACS Nano* **8,** 9446–56 (2014).
90. Xia, X. R., Monteiro-Riviere, N. A. & Riviere, J. E. An index for characterization of nanomaterials in biological systems. *Nat. Nanotechnol.* (2010). doi:10.1038/nnano.2010.164
91. Liu, R. *et al.* Evaluation of Toxicity Ranking for Metal Oxide Nanoparticles via an in Vitro

Dosimetry Model. *ACS Nano* **9,** 9303–13 (2015).
92. Gajewicz, A. *et al.* Towards understanding mechanisms governing cytotoxicity of metal oxides nanoparticles: Hints from nano-QSAR studies. *Nanotoxicology* **9,** 313–325 (2015).
93. Helma, C., Rautenberg, M. & Gebele, D. Nano-Lazar: Read across predictions for nanoparticle toxicities with calculated and measured properties. *Front. Pharmacol.* (2017). doi:10.3389/fphar.2017.00377
94. Walkey, C. D. *et al.* Protein corona fingerprinting predicts the cellular interaction of gold and silver nanoparticles. *ACS Nano* **8,** 2439–2455 (2014).
95. Varsou, D. D. *et al.* ToxFlow: A Web-Based Application for Read-Across Toxicity Prediction Using Omics and Physicochemical Data. *J. Chem. Inf. Model.* (2018). doi:10.1021/acs.jcim.7b00160
96. Sizochenko, N. *et al.* How the toxicity of nanomaterials towards different species could be simultaneously evaluated: A novel multi-nano-read-across approach. *Nanoscale* **10,** 582–591 (2018).
97. Pathakoti, K., Huang, M. J., Watts, J. D., He, X. & Hwang, H. M. Using experimental data of Escherichia coli to develop a QSAR model for predicting the photo-induced cytotoxicity of metal oxide nanoparticles. *J. Photochem. Photobiol. B Biol.* **130,** 234–240 (2014).
98. Wang, D., Gao, Y., Lin, Z., Yao, Z. & Zhang, W. The joint effects on Photobacterium phosphoreum of metal oxide nanoparticles and their most likely coexisting chemicals in the environment. *Aquat. Toxicol.* (2014). doi:10.1016/j.aquatox.2014.05.023
99. Kaweeteerawat, C. *et al.* Toxicity of metal oxide nanoparticles in Escherichia coli correlates with conduction band and hydration energies. *Environ. Sci. Technol.* (2015). doi:10.1021/es504259s
100. Aruoja, V. *et al.* Toxicity of 12 metal-based nanoparticles to algae, bacteria and protozoa. *Environ. Sci. Nano* (2015). doi:10.1039/c5en00057b
101. Titma, T., Shimmo, R., Siigur, J. & Kahru, A. Toxicity of antimony, copper, cobalt, manganese, titanium and zinc oxide nanoparticles for the alveolar and intestinal epithelial barrier cells in vitro. *Cytotechnology* (2016). doi:10.1007/s10616-016-0032-9
102. Lamon, L. *et al.* Grouping of nanomaterials to read-across hazard endpoints: From data collection to assessment of the grouping hypothesis by application of chemoinformatic techniques. *Part. Fibre Toxicol.* **15,** (2018).
103. OECD. *Titanium dioxide dossier (NM100-NM105)*. (2015).
104. Guichard, Y. *et al.* Cytotoxicity and Genotoxicity of Nanosized and Microsized Titanium Dioxide and Iron Oxide Particles in Syrian Hamster Embryo Cells. *Ann. Occup. Hyg.* **56,** 631–644 (2012).
105. NanoGenoTox Joint Action. *NANOGENOTOX Final report. Facilitating the safety evaluation of manufactured nanomaterials by characterising their potential genotoxic hazard*. (2013).
106. Aschberger, K. *et al.* Grouping of multi-walled carbon nanotubes to read-across genotoxicity: A case study to evaluate the applicability of regulatory guidance. *Comput. Toxicol.* **9,** 22–35 (2019).
107. Lamon, L. *et al.* Grouping of nanomaterials to read-across hazard endpoints: from data collection to assessment of the grouping hypothesis by application of chemoinformatic techniques. *Part. Fibre Toxicol.* **15,** 37 (2018).
108. Nantasenamat, C., Isarankura-Na-Ayudhya, C., Naenna, T. & Prachayasittikul, V. A practical overview of quantitative structure-activity relationship. *EXCLI Journal* **8,** 74–88 (2009).
109. Verma, J., Khedkar, V. M. & Coutinho, E. C. 3D-QSAR in drug design--a review. *Curr. Top. Med. Chem.* **10,** 95–115 (2010).
110. Fourches, D. *et al.* Quantitative Nanostructure−Activity Relationship Modeling. *ACS Nano* **4,** 5703–5712 (2010).
111. Shaw, S. Y. *et al.* Perturbational profiling of nanomaterial biologic activity. *Proc. Natl. Acad. Sci.* **105,** 7387–7392 (2008).
112. Weissleder, R., Kelly, K., Sun, E. Y., Shtatland, T. & Josephson, L. Cell-specific targeting of nanoparticles by multivalent attachment of small molecules. *Nat. Biotechnol.* **23,** 1418–1423 (2005).
113. Burello, E. & Worth, A. P. A theoretical framework for predicting the oxidative stress potential

of oxide nanoparticles. *Nanotoxicology* (2011). doi:10.3109/17435390.2010.502980
114. Sayes, C. & Ivanov, I. Comparative Study of Predictive Computational Models for Nanoparticle-Induced Cytotoxicity. *Risk Anal.* **30,** 1723–1734 (2010).
115. Liu, R. *et al.* Classification NanoSAR development for cytotoxicity of metal oxide nanoparticles. *Small* **7,** 1118–1126 (2011).
116. Epa, V. C. *et al.* Modeling biological activities of nanoparticles. *Nano Lett.* **12,** 5808–5812 (2012).
117. Toropov, A. A. *et al.* Novel application of the CORAL software to model cytotoxicity of metal oxide nanoparticles to bacteria Escherichia coli. *Chemosphere* **89,** 1098–1102 (2012).
118. Toropov, A. A., Toropova, A. P., Benfenati, E., Leszczynska, D. & Leszczynski, J. SMILES-based optimal descriptors: QSAR analysis of fullerene-based HIV-1 PR inhibitors by means of balance of correlations. *J. Comput. Chem.* **31,** 381–392 (2010).
119. Chau, Y. T. & Yap, C. W. Quantitative Nanostructure-Activity Relationship modelling of nanoparticles. *RSC Adv.* (2012). doi:10.1039/c2ra21489j
120. Ghorbanzadeh, M., Fatemi, M. H. & Karimpour, M. Modeling the Cellular Uptake of Magnetofluorescent Nanoparticles in Pancreatic Cancer Cells: A Quantitative Structure Activity Relationship Study. *Ind. Eng. Chem. Res.* (2012). doi:10.1021/ie3006947
121. Shao, C. Y. *et al.* Dependence of QSAR models on the selection of trial descriptor sets: A demonstration using nanotoxicity endpoints of decorated nanotubes. *J. Chem. Inf. Model.* (2013). doi:10.1021/ci3005308
122. Zhou, H. *et al.* A nano-combinatorial library strategy for the discovery of nanotubes with reduced protein-binding, cytotoxicity, and immune response. *Nano Lett.* **8,** 859–865 (2008).
123. Liu, R. *et al.* Development of structure-activity relationship for metal oxide nanoparticles. *Nanoscale* (2013). doi:10.1039/c3nr01533e
124. Zhang, H. *et al.* Use of metal oxide nanoparticle band gap to develop a predictive paradigm for oxidative stress and acute pulmonary inflammation. *ACS Nano* **6,** 4349–4368 (2012).
125. Liu, R. *et al.* Nano-SAR development for bioactivity of nanoparticles with considerations of decision boundaries. *Small* **9,** 1842–1852 (2013).
126. Horev-Azaria, L. *et al.* Predictive Toxicology of cobalt ferrite nanoparticles: comparative in-vitro study of different cellular models using methods of knowledge discovery from data. *Part. Fibre Toxicol.* **10,** 32 (2013).
127. Toropov, A. A. *et al.* QSAR as a random event: Modeling of nanoparticles uptake in PaCa2 cancer cells. *Chemosphere* (2013). doi:10.1016/j.chemosphere.2013.03.012
128. Kar, S., Gajewicz, A., Puzyn, T. & Roy, K. Nano-quantitative structure-activity relationship modeling using easily computable and interpretable descriptors for uptake of magnetofluorescent engineered nanoparticles in pancreatic cancer cells. *Toxicol. Vitr.* **28,** 600–606 (2014).
129. Rogers, D. & Hopfinger, A. J. Application of Genetic Function Approximation to Quantitative Structure-Activity Relationships and Quantitative Structure-Property Relationships. *J. Chem. Inf. Comput. Sci.* **34,** 854–866 (1994).
130. Singh, K. P. & Gupta, S. Nano-QSAR modeling for predicting biological activity of diverse nanomaterials. *RSC Adv.* **4,** 13215–13230 (2014).
131. Durdagi, S., Mavromoustakos, T., Chronakis, N. & Papadopoulos, M. G. Computational design of novel fullerene analogues as potential HIV-1 PR inhibitors: Analysis of the binding interactions between fullerene inhibitors and HIV-1 PR residues using 3D QSAR, molecular docking and molecular dynamics simulations. *Bioorganic Med. Chem.* **16,** 9957–9974 (2008).
132. Kleandrova, V. V. *et al.* Computational tool for risk assessment of nanomaterials: Novel QSTR-perturbation model for simultaneous prediction of ecotoxicity and cytotoxicity of uncoated and coated nanoparticles under multiple experimental conditions. *Environ. Sci. Technol.* (2014). doi:10.1021/es503861x
133. Luan, F. *et al.* Computer-aided nanotoxicology: Assessing cytotoxicity of nanoparticles under diverse experimental conditions by using a novel QSTR-perturbation approach. *Nanoscale* (2014). doi:10.1039/c4nr01285b
134. Kar, S., Gajewicz, A., Puzyn, T., Roy, K. & Leszczynski, J. Periodic table-based descriptors to encode cytotoxicity profile of metal oxide nanoparticles: A mechanistic QSTR approach.

Ecotoxicol. Environ. Saf. **107,** 162–169 (2014).
135. Toropova, A. P. *et al.* Optimal descriptor as a translator of eclectic information into the prediction of membrane damage: The case of a group of ZnO and TiO2nanoparticles. *Ecotoxicol. Environ. Saf.* **108,** 203–209 (2014).
136. Winkler, D. A. *et al.* Modelling and predicting the biological effects of nanomaterials. *SAR QSAR Environ. Res.* (2014). doi:10.1080/1062936X.2013.874367
137. Toropova, A. P., Toropov, A. A., Benfenati, E. & Korenstein, R. QSAR model for cytotoxicity of SiO2 nanoparticles on human lung fibroblasts. *J. Nanoparticle Res.* (2014). doi:10.1007/s11051-014-2282-9
138. Xu, Z., Chou, L. & Sun, J. Effects of SiO2nanoparticles on HFL-I activating ROS-mediated apoptosis via p53 pathway. *J. Appl. Toxicol.* (2012). doi:10.1002/jat.1710
139. Sizochenko, N. *et al.* From basic physics to mechanisms of toxicity: the "liquid drop" approach applied to develop predictive classification models for toxicity of metal oxide nanoparticles. *Nanoscale* **6,** 13986–13993 (2014).
140. Melagraki, G. & Afantitis, A. Enalos InSilicoNano platform: An online decision support tool for the design and virtual screening of nanoparticles. *RSC Adv.* (2014). doi:10.1039/c4ra07756c
141. Bigdeli, A., Hormozi-Nezhad, M. R. & Parastar, H. Using nano-QSAR to determine the most responsible factor(s) in gold nanoparticle exocytosis. *RSC Adv.* **5,** 57030–57037 (2015).
142. Oh, N. & Park, J. H. Surface chemistry of gold nanoparticles mediates their exocytosis in macrophages. *ACS Nano* **8,** 6232–6241 (2014).
143. Jones, D. E., Ghandehari, H. & Facelli, J. C. Predicting cytotoxicity of PAMAM dendrimers using molecular descriptors. *Beilstein J. Nanotechnol.* **6,** 1886–1896 (2015).
144. Papa, E., Doucet, J. P. & Doucet-Panaye, A. Linear and non-linear modelling of the cytotoxicity of TiO2 and ZnO nanoparticles by empirical descriptors. *SAR QSAR Environ. Res.* (2015). doi:10.1080/1062936X.2015.1080186
145. Oksel, C., Ma, C. Y. & Wang, X. Z. Structure-activity relationship models for hazard assessment and risk management of engineered nanomaterials. in *Procedia Engineering* **102,** 1500–1510 (2015).
146. Wang, X. Z. *et al.* Principal component and causal analysis of structural and acute in vitro toxicity data for nanoparticles. *Nanotoxicology* **8,** 465–476 (2014).
147. Liu, R., Jiang, W., Walkey, C. D., Chan, W. C. W. & Cohen, Y. Prediction of nanoparticles-cell association based on corona proteins and physicochemical properties. *Nanoscale* (2015). doi:10.1039/c5nr01537e
148. Tsiliki, G. *et al.* RRegrs: An R package for computer-aided model selection with multiple regression models. *J. Cheminform.* (2015). doi:10.1186/s13321-015-0094-2
149. Oksel, C., Winkler, D. A., Ma, C. Y., Wilkins, T. & Wang, X. Z. Accurate and interpretable nanoSAR models from genetic programming-based decision tree construction approaches. *Nanotoxicology* **10,** 1001–1012 (2016).
150. Mu, Y. *et al.* Predicting toxic potencies of metal oxide nanoparticles by means of nano-QSARs. *Nanotoxicology* **10,** 1207–1214 (2016).
151. Kar, S., Gajewicz, A., Roy, K., Leszczynski, J. & Puzyn, T. Extrapolating between toxicity endpoints of metal oxide nanoparticles: Predicting toxicity to Escherichia coli and human keratinocyte cell line (HaCaT) with Nano-QTTR. *Ecotoxicol. Environ. Saf.* (2016). doi:10.1016/j.ecoenv.2015.12.033
152. Papa, E., Doucet, J. P., Sangion, A. & Doucet-Panaye, A. Investigation of the influence of protein corona composition on gold nanoparticle bioactivity using machine learning approaches. *SAR QSAR Environ. Res.* (2016). doi:10.1080/1062936X.2016.1197310
153. Pan, Y. *et al.* Nano-QSAR modeling for predicting the cytotoxicity of metal oxide nanoparticles using novel descriptors. *RSC Adv.* (2016). doi:10.1039/C6RA01298A
154. Basant, N. & Gupta, S. Multi-target QSTR modeling for simultaneous prediction of multiple toxicity endpoints of nano-metal oxides. *Nanotoxicology* (2017). doi:10.1080/17435390.2017.1302612
155. Gajewicz, A. *et al.* Decision tree models to classify nanomaterials according to the DF4nanoGrouping scheme. *Nanotoxicology* (2018). doi:10.1080/17435390.2017.1415388
156. Driessen, M. D. *et al.* Proteomic analysis of protein carbonylation: A useful tool to unravel

nanoparticle toxicity mechanisms. *Part. Fibre Toxicol.* (2015). doi:10.1186/s12989-015-0108-2
157. Roy, K., Kar, S. & Ambure, P. On a simple approach for determining applicability domain of QSAR models. *Chemom. Intell. Lab. Syst.* (2015). doi:10.1016/j.chemolab.2015.04.013
158. Cherkasov, A. *et al.* QSAR modeling: Where have you been? Where are you going to? *Journal of Medicinal Chemistry* (2014). doi:10.1021/jm4004285
159. Lamon, L. *et al.* Computational models in manufactured nanomaterials risk assessment: development of model reporting standards and mapping of the model landscape. *Submitt. to Comput. Toxicol.*
160. Rücker, C., Rücker, G. & Meringer, M. Y-randomization and its variants in QSPR/QSAR. *J. Chem. Inf. Model.* (2007). doi:10.1021/ci700157b
161. De Jong, M. *et al.* A Statistical Learning Framework for Materials Science: Application to Elastic Moduli of k-nary Inorganic Polycrystalline Compounds. *Sci. Rep.* (2016). doi:10.1038/srep34256
162. Zhang, Y. & Ling, C. A strategy to apply machine learning to small datasets in materials science. *npj Comput. Mater.* (2018). doi:10.1038/s41524-018-0081-z
163. Gajewicz, A. *et al.* Decision tree models to classify nanomaterials according to the *DF4nanoGrouping* scheme. *Nanotoxicology* **12,** 1–17 (2018).
164. Mooney, R. J. & Bunescu, R. Mining knowledge from text using information extraction. *ACM SIGKDD Explor. Newsl.* (2005). doi:10.1145/1089815.1089817
165. Liu, X. *et al.* Predictive modeling of nanomaterial exposure effects in biological systems. *Int. J. Nanomedicine* (2013). doi:10.2147/IJN.S40742
166. Kovalishyn, V. *et al.* Modelling the toxicity of a large set of metal and metal oxide nanoparticles using the OCHEM platform. *Food Chem. Toxicol.* (2018). doi:10.1016/j.fct.2017.08.008
167. Chen, G., Peijnenburg, W. J. G. M., Kovalishyn, V. & Vijver, M. G. Development of nanostructure-activity relationships assisting the nanomaterial hazard categorization for risk assessment and regulatory decision-making. *RSC Adv.* (2016). doi:10.1039/c6ra06159a
168. Aggarwal, C. C., Hinneburg, A. & Keim, D. A. in *Database theory* (2001).
169. Verleysen, M. & François, D. The Curse of Dimensionality in Data Mining. *Analysis* (2005). doi:10.1007/11494669_93
170. Donoho, D. L. Aide-Memoire. High-Dimensional Data Analysis: The Curses and Blessings of Dimensionality. *Am. Math. Soc. Lect. Challenges 21st Century* (2000). doi:10.1.1.329.3392
171. Peduzzi, P., Concato, J., Kemper, E., Holford, T. R. & Feinstem, A. R. A simulation study of the number of events per variable in logistic regression analysis. *J. Clin. Epidemiol.* (1996). doi:10.1016/S0895-4356(96)00236-3
172. Dolnicar, S. *A review of unquestioned standards in using cluster analysis for data-driven market segmentation*. *Faculty of Commerce-Papers* (2002).
173. Kaplan, R. M., Chambers, D. A. & Glasgow, R. E. Big data and large sample size: A cautionary note on the potential for bias. *Clinical and Translational Science* **7,** 342–346 (2014).
174. Heckman, J. J. Sample Selection Bias as a Specification Error. *Econometrica* **47,** 153 (1979).
175. Toomet, O. & Henningsen, A. Sample Selection Models in R: Package sampleSelection. *J. Stat. Softw.* **27,** 1–23 (2008).
176. Zadrozny, B. Learning and evaluating classifiers under sample selection bias. in *Twenty-first international conference on Machine learning - ICML '04* 114 (2004). doi:10.1145/1015330.1015425
177. Pan, S. J. & Yang, Q. A survey on transfer learning. *IEEE Transactions on Knowledge and Data Engineering* **22,** 1345–1359 (2010).
178. Weiss, K., Khoshgoftaar, T. M. & Wang, D. D. A survey of transfer learning. *J. Big Data* **3,** (2016).
179. Lecun, Y., Bengio, Y. & Hinton, G. Deep learning. *Nature* (2015). doi:10.1038/nature14539
180. Liu, B., Wei, Y., Zhang, Y. & Yang, Q. Deep neural networks for high dimension, low sample size data. in *IJCAI International Joint Conference on Artificial Intelligence* (2017). doi:10.24963/ijcai.2017/318
181. Razavian, A. S., Azizpour, H., Sullivan, J. & Carlsson, S. CNN features off-the-shelf: An astounding baseline for recognition. in *IEEE Computer Society Conference on Computer Vision*

and Pattern Recognition Workshops (2014). doi:10.1109/CVPRW.2014.131
182. Oquab, M., Bottou, L., Laptev, I. & Sivic, J. Learning and transferring mid-level image representations using convolutional neural networks. in *Proceedings of the IEEE Computer Society Conference on Computer Vision and Pattern Recognition* (2014). doi:10.1109/CVPR.2014.222
183. Shin, H. C. *et al.* Deep Convolutional Neural Networks for Computer-Aided Detection: CNN Architectures, Dataset Characteristics and Transfer Learning. *IEEE Trans. Med. Imaging* (2016). doi:10.1109/TMI.2016.2528162
184. Japkowicz, N. & Stephen, S. The class imbalance problem: A systematic study. *Intell. Data Anal.* (2002). doi:10.1.1.711.8214
185. Longadge, R., Dongre, S. S. & Malik, L. Class imbalance problem in data mining: review. *Int. J. Comput. Sci. Netw.* (2013). doi:10.1109/SIU.2013.6531574
186. Sayes, C. M., Alex Smith, P. & Ivanov, I. V. A framework for grouping nanoparticles based on their measurable characteristics. *Int. J. Nanomedicine* **8,** 45–56 (2013).
187. Wang, X. Z. *et al.* Principal component and causal analysis of structural and acute in vitro toxicity data for nanoparticles. *Nanotoxicology* **8,** 465–476 (2014).
188. Tantra, R. *et al.* A method for assessing nanomaterial dispersion quality based on principal component analysis of particle size distribution data. *Particuology* (2015). doi:10.1016/j.partic.2014.10.004
189. Brunelli, A. *et al.* Effects of organic modifiers on the colloidal stability of TiO2nanoparticles. A methodological approach for NPs categorization by multivariate statistical analysis. *NanoImpact* (2018). doi:10.1016/j.impact.2018.03.001
190. Patlewicz, G. *et al.* Read-across approaches - Misconceptions, promises and challenges ahead. *Arch. Med. Vet.* **46,** 387–396 (2014).
191. Sharma, V. K., Siskova, K. M., Zboril, R. & Gardea-Torresdey, J. L. Organic-coated silver nanoparticles in biological and environmental conditions: Fate, stability and toxicity. *Adv. Colloid Interface Sci.* **204,** 15–34 (2014).
192. Ortelli, S. *et al.* Colloidal characterization of CuO nanoparticles in biological and environmental media. *Environ. Sci. Nano* **4,** 1264–1272 (2017).
193. Canesi, L. & Corsi, I. Effects of nanomaterials on marine invertebrates. *Sci. Total Environ.* **565,** 933–940 (2016).
194. Arts, J. H. E. *et al.* Case studies putting the decision-making framework for the grouping and testing of nanomaterials (DF4nanoGrouping) into practice. *Regul. Toxicol. Pharmacol.* **76,** 234–261 (2016).
195. Hühn, J. *et al.* Selected Standard Protocols for the Synthesis, Phase Transfer, and Characterization of Inorganic Colloidal Nanoparticles. *Chem. Mater.* **29,** 399–461 (2017).
196. Mitrano, D. M., Motellier, S., Clavaguera, S. & Nowack, B. Review of nanomaterial aging and transformations through the life cycle of nano-enhanced products. *Environ. Int.* **77,** 132–147 (2015).
197. Gonçalves, R. H., Schreiner, W. H. & Leite, E. R. Synthesis of TiO2 Nanocrystals with a High Affinity for Amine Organic Compounds. *Langmuir* **26,** 11657–11662 (2010).
198. Savić, T. D. *et al.* The effect of substituents on the surface modification of anatase nanoparticles with catecholate-type ligands: A combined DFT and experimental study. *Phys. Chem. Chem. Phys.* **16,** 20796–20805 (2014).
199. Kobayashi, N. & Arai, R. Design and construction of self-assembling supramolecular protein complexes using artificial and fusion proteins as nanoscale building blocks. *Curr. Opin. Biotechnol.* **46,** 57–65 (2017).
200. Burger, A. *et al.* Layer-by-Layer Assemblies of Catechol-Functionalized TiO<inf>2</inf> Nanoparticles and Porphyrins through Electrostatic Interactions. *Chem. - A Eur. J.* **21,** 5041–5054 (2015).
201. Wei, Q., Becherer, T., Noeske, P.-L. M., Grunwald, I. & Haag, R. A universal approach to crosslinked hierarchical polymer multilayers as stable and highly effective antifouling coatings. *Adv. Mater.* **26,** 2688–2693 (2014).
202. Selli, D. & Di Valentin, C. Ab initio investigation of polyethylene glycol coating of TiO<inf>2</inf> surfaces. *J. Phys. Chem. C* **120,** 29190–29201 (2016).

203. ISO. ISO/TR 13097:2013. Guidelines for the Characterization of Dispersion Stability. (2013).
204. Bishop, C. M. *Pattern Recognition and Machine Learning (Information Science and Statistics)*. (Springer-Verlag New York, Inc. Secaucus, NJ, USA, 2006).
205. Tantra, R. *et al.* Dispersion stability of nanoparticles in ecotoxicological investigations: The need for adequate measurement tools. *J. Nanoparticle Res.* **13,** 3765–3780 (2011).
206. Brunelli, A., Pojana, G., Callegaro, S. & Marcomini, A. Agglomeration and sedimentation of titanium dioxide nanoparticles (n-TiO2) in synthetic and real waters. *J. Nanoparticle Res.* **15,** (2013).
207. OECD Guidelines for Testing of Chemicals N° 203 - Fish Acute Toxicity Test (Annex 2 Composition of the recommended reconstituted water). OECD Guidelines for Testing of Chemicals No. 203. Fish, Acute Toxicity Test (Annex 2 Composition of the recommended reconstituted water). 1–9 (1992).
208. ASTM D1141-98 (Reapproved 2003). Standard Practice for the Preparation of Substitute Ocean Water. ASTM D1141-98, Standard Practice for the Preparation of Substitute Ocean Water, Re-approved. (2003).
209. Taurozzi, J. S., Hackley, V. A. & Wiesner, M. R. *Preparation of Nanoparticle Dispersions from Powdered Material Using Ultrasonic Disruption*. (2012). doi:http://dx.doi.org/10.6028/NIST.SP.1200-2
210. Burger, A. *et al.* Layer-by-Layer Assemblies of Catechol-Functionalized TiO2 Nanoparticles and Porphyrins through Electrostatic Interactions. *Chem. - A Eur. J.* **21,** 5041–5054 (2015).
211. Suttiponparnit, K. *et al.* Role of Surface Area, Primary Particle Size, and Crystal Phase on Titanium Dioxide Nanoparticle Dispersion Properties. *Nanoscale Res. Lett.* **6,** 27 (2011).
212. Zhang, Y., Chen, Y., Westerhoff, P., Hristovski, K. & Crittenden, J. C. Stability of commercial metal oxide nanoparticles in water. *Water Res.* **42,** 2204–2212 (2008).
213. Bhattacharjee, S. DLS and zeta potential - What they are and what they are not? *J. Control. Release* **235,** 337–351 (2016).
214. Kim, K.-M. *et al.* Surface treatment of silica nanoparticles for stable and charge-controlled colloidal silica. *Int. J. Nanomedicine* **9,** 29–40 (2014).
215. Almeida, T. C. A., Larentis, A. L. & Ferraz, H. C. Ã. Evaluation of the stability of concentrated emulsions for lemon beverages using sequential experimental designs. *PLoS One* **10,** 1–18 (2015).
216. Brunelli, A., Zabeo, A., Semenzin, E., Hristozov, D. & Marcomini, A. Extrapolated long-term stability of titanium dioxide nanoparticles and multi-walled carbon nanotubes in artificial freshwater. *J. Nanoparticle Res.* **18,** 113 (2016).
217. Lerche, D. Dispersion Stability and Particle Characterization by Sedimentation Kinetics in a Centrifugal Field. *J. Dispers. Sci. Technol.* **23,** 699–709 (2002).
218. Saeed, F., Salim, N. & Abdo, A. Voting-based consensus clustering for combining multiple clusterings of chemical structures. *J. Cheminform.* **4,** 37 (2012).
219. Hubert, L. & Arabie, P. Comparing partitions. *J. Classif.* **2,** 193–218 (1985).
220. Milligan, G. W. & Cooper, M. C. A Study of the Comparability of External Criteria for Hierarchical Cluster Analysis. *Multivariate Behav. Res.* **21,** 441–458 (1986).
221. Santos, J. M. & Embrechts, M. in (eds. Alippi, C., Polycarpou, M., Panayiotou, C. & Ellinas, G.) 175–184 (Springer Berlin Heidelberg, 2009). doi:10.1007/978-3-642-04277-5_18
222. R Core Team. R: A language and environment for statistical computing. (2016).
223. Meyer, D., Dimitriadou, E., Hornik, K., Weingessel, A. & Leisch, F. e1071: Misc Functions of the Department of Statistics, Probability Theory Group (Formerly: E1071). (2015).
224. Venables, W. N. & Ripley, B. D. *Modern Applied Statistics with S*. (Springer Publishing Company, 2010).
225. Kakuma, Y., Nosaka, A. Y. & Nosaka, Y. Difference in TiO2 photocatalytic mechanism between rutile and anatase studied by the detection of active oxygen and surface species in water. *Phys. Chem. Chem. Phys.* **17,** 18691–18698 (2015).
226. Janković, I. A., Šaponjić, Z. V., Čomor, M. I. & Nedeljkovic, J. M. Surface modification of colloidal tiO2 nanoparticles with bidentate benzene derivatives. *J. Phys. Chem. C* **113,** 12645–12652 (2009).
227. León, A. *et al.* FTIR and raman characterization of TiO<inf>2</inf> nanoparticles coated with

polyethylene glycol as carrier for 2-methoxyestradiol. *Appl. Sci.* **7,** 49 (2017).
228. Manorama, S. V. *et al.* Photostabilization of dye on anatase titania nanoparticles by polymer capping. *J. Phys. Chem. Solids* **63,** 135–143 (2001).
229. Kosmulski, M. pH-dependent surface charging and points of zero charge. IV. Update and new approach. *J. Colloid Interface Sci.* **337,** 439–448 (2009).
230. Praetorius, A. *et al.* Heteroaggregation of titanium dioxide nanoparticles with model natural colloids under environmentally relevant conditions. *Environ. Sci. Technol.* **48,** 10690–10698 (2014).
231. Rodríguez, R., Blesa, M. A. & Regazzoni, A. E. Surface Complexation at the TiO2(anatase)/Aqueous Solution Interface: Chemisorption of Catechol. *J. Colloid Interface Sci.* **177,** 122–131 (1996).
232. Mandzy, N., Grulke, E. & Druffel, T. Breakage of TiO2 agglomerates in electrostatically stabilized aqueous dispersions. *Powder Technol.* **160,** 121–126 (2005).
233. Selli, D. & Di Valentin, C. Ab initio investigation of polyethylene glycol coating of TiO2 surfaces. *J. Phys. Chem. C* **120,** 29190–29201 (2016).
234. Gabriel, K. R. The biplot graphic display of matrices with application to principal component analysis. *Biometrika* (1971). doi:10.1093/biomet/58.3.453
235. Loosli, F., Le Coustumer, P. & Stoll, S. TiO2 nanoparticles aggregation and disaggregation in presence of alginate and Suwannee River humic acids. pH and concentration effects on nanoparticle stability. *Water Res.* **47,** 6052–6063 (2013).
236. Beyer, K., Goldstein, J., Ramakrishnan, R. & Shaft, U. in *Database Theory — ICDT'99* (1999). doi:10.1007/3-540-49257-7_15
237. Lamon, L. *et al.* Grouping of nanomaterials to read-across hazard endpoints: from data collection to assessment of the grouping hypothesis by application of chemoinformatic techniques. *Submitt. to Part. Fibre Toxicol.*
238. Saeys, Y., Inza, I. & Larrañaga, P. A review of feature selection techniques in bioinformatics. *Bioinformatics* (2007). doi:10.1093/bioinformatics/btm344
239. Parsons, L., Haque, E. & Liu, H. Subspace clustering for high dimensional data: a review. *ACM SIGKDD Explor. Newsl.* (2004). doi:10.1145/1007730.1007731
240. Kolhe, P., Misra, E., Kannan, R. M., Kannan, S. & Lieh-Lai, M. Drug complexation, in vitro release and cellular entry of dendrimers and hyperbranched polymers. *Int. J. Pharm.* (2003). doi:10.1016/S0378-5173(03)00225-4
241. Wood, K. C., Little, S. R., Langer, R. & Hammond, P. T. A family of hierarchically self-assembling linear-dendritic hybrid polymers for highly efficient targeted gene delivery. *Angew. Chemie - Int. Ed.* (2005). doi:10.1002/anie.200502152
242. Gillies, E. R. & Fréchet, J. M. J. Dendrimers and dendritic polymers in drug delivery. *Drug Discovery Today* (2005). doi:10.1016/S1359-6446(04)03276-3
243. Palmerston Mendes, L., Pan, J. & Torchilin, V. Dendrimers as Nanocarriers for Nucleic Acid and Drug Delivery in Cancer Therapy. *Molecules* (2017). doi:10.3390/molecules22091401
244. Greish, K. *et al.* Size and surface charge significantly influence the toxicity of silica and dendritic nanoparticles. *Nanotoxicology* (2012). doi:10.3109/17435390.2011.604442
245. Xu, Q., Wang, C.-H. & Wayne Pack, D. Polymeric Carriers for Gene Delivery: Chitosan and Poly(amidoamine) Dendrimers. *Curr. Pharm. Des.* (2010). doi:10.2174/138161210791920469
246. Yellepeddi, V. K., Kumar, A. & Palakurthi, S. Surface modified poly(amido)amine dendrimers as diverse nanomolecules for biomedical applications. *Expert Opin. Drug Deliv.* (2009). doi:10.1517/17425240903061251
247. Zhang, H. *et al.* Use of metal oxide nanoparticle band gap to develop a predictive paradigm for oxidative stress and acute pulmonary inflammation. *ACS Nano* (2012). doi:10.1021/nn3010087
248. Artemenkoa, A. G. *et al.* Qsar analysis of the toxicity of nitroaromatics in tetrahymena pyriformis: Structural factors and possible modes of action. *SAR QSAR Environ. Res.* (2011). doi:10.1080/1062936X.2011.569950
249. Newman, M. C., McCloskey, J. T. & Tatara, C. P. Using metal-lingand binding characteristics to predict metal toxicity: Quantitative ion charater-activity relationships (QICARs). *Environ. Health Perspect.* **106,** 1419–1425. (1998).
250. Pearl, J. *Causality: Models, reasoning, and inference, second edition*. *Causality: Models,*

Reasoning, and Inference, Second Edition (2011). doi:10.1017/CBO9780511803161
251. Peng, C. H. *et al.* Causal inference of gene regulation with subnetwork assembly from genetical genomics data. *Nucleic Acids Res.* (2014). doi:10.1093/nar/gkt1277
252. Sizochenko, N. *et al.* Causal inference methods to assist in mechanistic interpretation of classification nano-SAR models. *RSC Adv.* (2015). doi:10.1039/c5ra11399g
253. Landsiedel, R. *et al.* Application of short-term inhalation studies to assess the inhalation toxicity of nanomaterials. *Part. Fibre Toxicol.* (2014). doi:10.1186/1743-8977-11-16
254. Wiemann, M. *et al.* An in vitro alveolar macrophage assay for predicting the short-term inhalation toxicity of nanomaterials. *J. Nanobiotechnology* (2016). doi:10.1186/s12951-016-0164-2
255. Agrawal, R., Gehrke, J., Gunopulos, D. & Raghavan, P. Automatic subspace clustering of high dimensional data. *Data Min. Knowl. Discov.* (2005). doi:10.1007/s10618-005-1396-1
256. Auria, L. & Moro, R. A. *Support Vector Machines (SVM) as a Technique for Solvency Analysis*. *SSRN* (2009). doi:10.2139/ssrn.1424949
257. Interface, T. *et al.* Package 'subspace': Interface to OpenSubspace. (2015).
258. van Harmelen, T. *et al.* LICARA nanoSCAN - A tool for the self-assessment of benefits and risks of nanoproducts. *Environ. Int.* (2016). doi:10.1016/j.envint.2016.02.021
259. TUV SUD Industrie Service. *Certification Standard CENARIOS ®*. (2013).
260. Widler, T. *et al.* in 219–235 (Springer, Cham, 2016). doi:10.1007/978-3-319-32392-3_12
261. Tno. *LICARA Guidelines for the sustainable competitiveness of nanoproducts*.
262. Echa. Guidance on information requirements and chmical safety assessment. Chapter R.10: Characterisation of dose [concentration]-response for environment. *Eur. Chem. Agency* 1–65 (2008). doi:10.2823/128621
263. Gottschalk, F. & Nowack, B. A probabilistic method for species sensitivity distributions taking into account the inherent uncertainty and variability of effects to estimate environmental risk. *Integr. Environ. Assess. Manag.* **9,** 79–86 (2013).
264. Echa. *Guidance on information requirements and chemical safety assessment Chapter R . 7b : Endpoint specific guidance*. *Echa* (2017). doi:10.2823/84188
265. ECHA. Proposal for Harmonised Classification and Labelling Based on Regulation (EC) No 1272/2008 (CLP Regulation), Annex VI, Part 2; Substance Name: Lead metal. *CLH Rep.* (2017).
266. IPCS-WHO. *Guidance document on evaluating and expressing uncertainty in hazard characterization*. (World Health Organisation, 2014).
267. ECHA. *Guidance on information requirements and chemical safety assessment Chapter R.8: Characterisation of dose [concentration]-response for human health*. (2012).
268. Subramanian, V. *et al.* Sustainable nanotechnology decision support system: bridging risk management, sustainable innovation and risk governance. *J. Nanoparticle Res.* **18,** 1–13 (2016).
269. Goedkoop, M. *et al. ReCiPe 2008*. *Potentials* (2009). doi:10.029/2003JD004283
270. Guinee, J. *et al.* Handbook on Life Cycle Assessment: Operational Guide to the ISO Standards. *Kluwer Acad. Publ.* (2002). doi:10.1007/0-306-48055-7
271. Schmidt, I. *et al.* SEEbalance. *Greener Manag. Int.* (2004). doi:10.9774/GLEAF.3062.2004.sp.00007
272. Fransman, W. *et al.* Development and evaluation of an Exposure Control Efficacy Library (ECEL). *Ann. Occup. Hyg.* (2008). doi:10.1093/annhyg/men054
273. Leeuwen, C. & Vermeire, T. *Risk Assessment of Chemicals*. *Springer* (2007). doi:10.1007/978-1-4020-6102-8
274. Subramanian, V. *et al.* Sustainable nanotechnology decision support system: bridging risk management, sustainable innovation and risk governance. *J. Nanoparticle Res.* **18,** 1–13 (2016).
275. Pang, C. *et al.* Probabilistic approach for assessing infants' health risks due to ingestion of nanoscale silver released from consumer products. *Environ. Int.* **99,** 199–207 (2017).
276. Tsang, M. P. *et al.* Probabilistic risk assessment of emerging materials: case study of titanium dioxide nanoparticles. *Nanotoxicology* **11,** 558–568 (2017).
277. GrandViewResearch. High Performance Pigments Market availalbe at https://www.grandviewresearch.com/press-release/global-high-performance-pigments-market. (2016).
278. CPMA. Color Pigment Manufacturers Association, Inc. accessed at https://colour-

index.com/definitions-of-a-dye-and-a-pigment in September 2018. (2018).
279. Christie, R. M. in 485–498 (Springer, Dordrecht, 1998). doi:10.1007/978-94-011-5862-6_53
280. Cain, M. & Morrell, R. Nanostructured ceramics: a review of their potential. *Appl. Organomet. Chem.* **15,** 321–330 (2001).
281. Cavalcante, P. M. T., Dondi, M., Guarini, G., Raimondo, M. & Baldi, G. Colour performance of ceramic nano-pigments. *Dye. Pigment.* **80,** 226–232 (2009).
282. Research and Markets Report. Automotive Plastics Market for Passenger Cars. Summary available via http://www.researchandmarkets.com/reports/3339984/automotive-plastics-market-for-passenger-cars-by. (2015).
283. Norman, M. The story behind Pigment Red 254, nicknamed 'Ferrari Red'. Available via http://blog.cleveland.com/pdextra/2007/10/pollock_cuts.html. (2007).
284. Farnum, D. G., Mehta, G., Moore, G. G. I. & Siegal, F. P. Attempted reformatskii reaction of benzonitrile, 1,4-diketo-3,6-diphenylpyrrolo[3,4-C]pyrrole. A lactam analogue of pentalene. *Tetrahedron Lett.* **15,** 2549–2552 (1974).
285. Iqbal, A. and C. L. Process for colouring highly molecular organic material and polycyclic pigments. Eur. Pat. Appl. 61426. (1982).
286. Davis, J. A., Gift, J. S. & Zhao, Q. J. Introduction to benchmark dose methods and U.S. EPA's benchmark dose software (BMDS) version 2.1.1. *Toxicol. Appl. Pharmacol.* **254,** 181–191 (2011).
287. Gosens, I. *et al.* Organ burden and pulmonary toxicity of nano-sized copper (II) oxide particles after short-term inhalation exposure. *Nanotoxicology* (2016). doi:10.3109/17435390.2016.1172678
288. ECHA. Guidance on information requirements and chemical safety assessment. Chapter R.8: Characterisation of dose concentration -response for human health. *Eur. Chem. Agency* (2008).
289. Slob, W., Bakker, M. I., Biesebeek, J. D. te & Bokkers, B. G. H. Exploring the Uncertainties in Cancer Risk Assessment Using the Integrated Probabilistic Risk Assessment (IPRA) Approach. *Risk Anal.* **34,** 1401–1422 (2014).
290. IPCS. GUIDANCE DOCUMENT ON EVALUATING AND EXPRESSING UNCERTAINTY IN HAZARD CHARACTERIZATION. http://www.who.int/ipcs/methods/harmonization/uncertainty_in_hazard_characterization.pdf?ua=1. (2017).
291. Chiu, W. A. & Slob, W. A unified probabilistic framework for dose–response assessment of human health effects. *Environmental Health Perspectives* (2015). doi:10.1289/ehp.1409385
292. Barlow, S. *et al.* Guidance of the scientific committee on a request from EFSA on the use of the benchmark dose approach in risk assessment. *EFSA J.* **1150,** 1–72 (2009).
293. Boonruksa, P. *et al.* Exposures to nanoparticles and fibers during injection molding and recycling of carbon nanotube reinforced polycarbonate composites. *J. Expo. Sci. Environ. Epidemiol.* **27,** 379–390 (2017).
294. Koivisto, A. J. *et al.* First order risk assessment for nanoparticle inhalation exposure during injection molding of polypropylene composites and production of tungsten-carbide-cobalt fine powder based upon pulmonary inflammation and surface area dose. *NanoImpact* **6,** 30–38 (2017).
295. Amorim, M. J. B. *et al.* Environmental Impacts by Fragments Released from Nanoenabled Products: A Multiassay, Multimaterial Exploration by the SUN Approach. *Environ. Sci. Technol.* (2018). doi:10.1021/acs.est.7b04122
296. Wohlleben, W. & Neubauer, N. Quantitative rates of release from weathered nanocomposites are determined across 5 orders of magnitude by the matrix, modulated by the embedded nanomaterial. *NanoImpact* **1,** 39–45 (2016).
297. Sotiriou, G. A. *et al.* Thermal decomposition of nano-enabled thermoplastics: Possible environmental health and safety implications. *J. Hazard. Mater.* **305,** 87–95 (2016).
298. USEPA. Risk Assessment Forum White Paper: Probabilistic Risk Assessment Methods and Case Studies. EPA/100/R-09/001A. Washington, D.C.: Risk Assessment Forum, Office of the Science Advisor,. (2014).
299. USEPA. Probabilistic Risk Assessment to Inform Decision M; D.C.: Risk Assessment Forum; Office of th e Science Advisor; USEPA. http://epa.gov/raf/prawhitepaper/index.htm. (2014).

300. USEPA. Risk Assessment Guidance for Superfund (RAGS) Volume III - Part A: Process for Conducting Probabilistic Risk Assessment, Appendix B. *Off. Emerg. Remedial Response U.S. Environ. Prot. Agency* **III,** 1–385 (2001).
301. Helton, J. C. & Davis, F. J. Latin hypercube sampling and the propagation of uncertainty in analyses of complex systems. *Reliability Engineering and System Safety* **81,** 23–69 (2003).
302. Ma-Hock, L. *et al.* Development of a Short-Term Inhalation Test in the Rat Using Nano-Titanium Dioxide as a Model Substance. *Inhal. Toxicol.* **21,** 102–118 (2009).
303. Hofmann, T. *et al.* Comparative short-term inhalation toxicity of five organic diketopyrrolopyrrole pigments and two inorganic iron-oxide-based pigments. *Inhal. Toxicol.* **28,** 463–479 (2016).
304. Bundesanstalt für Arbeitsschutz und Arbeitsmedizin. *BekGS 527 Hergestellte Nanomaterialien. Bekanntmachung zu Gefahrstoffen*. (2013).
305. Störmer, A., Bott, J., Kemmer, D. & Franz, R. Critical review of the migration potential of nanoparticles in food contact plastics. *Trends in Food Science and Technology* **63,** 39–50 (2017).
306. Van Leeuwen, C. & Vermeire, T. *Risk assessment of chemicals: An introduction*. **2,** (Springer, 2007).
307. Schneider, T. & Jensen, K. Relevance of aerosol dynamics and dustiness for personal exposure to manufactured nanoparticles. *J Nanopart Res* **11,** 1637–1650 (2009).
308. Freeman, B. M. H. & McIntyre, C. R. A Comprehensive Review of Copper-Based Wood Preservatives with a focus on new micronized or dispersed copper systems. *For. Prod. J.* (2008).
309. Lebow, S. T. & Foster, D. Environmental concentrations of copper, chromium, and arsenic released from a chromated-copper-arsenate-(CCA-C-) treated wetland boardwalk. *For. Prod. journal. Vol. 55, no. 2 (Feb. 2005) p. 62-70.* (2005).
310. Freeman, M. H. & McIntyre, C. Micronized Copper Wood Preservatives: Strong Indications of the Reservoir Effect. International Research Group on Wood Protection, 1 (2013).
311. Platten, W. *et al.* Release of Micronized Copper Particles from Pressure Treated Wood Products. U.S. Environmental Protection Agency, Washington, (2014).
312. Clausen, C. A. Nanotechnology: Implications for the Wood Preservation Industry. *38th annual meeting of The International Research Group for Wood Preservation* (2007).
313. Evans, P., Matsunaga, H. & Kiguchi, M. Large-scale application of nanotechnology for wood protection. *Nature Nanotechnology* (2008). doi:10.1038/nnano.2008.286
314. Kartal, S. N., Green, F. & Clausen, C. A. Do the unique properties of nanometals affect leachability or efficacy against fungi and termites? *Int. Biodeterior. Biodegrad.* (2009). doi:10.1016/j.ibiod.2009.01.007
315. Clausen, C. A. Nanotechnology: Implications for the Wood Preservation Industry. *38th annual meeting of The International Research Group for Wood Preservation* (2007).
316. Chen, J., Mottl, N., Lindheimer, T. & Cook, N. *A Probabilistic Risk Assessment for Children Who Contact CCA-Treated Playsets and Decks Final Report*. (2008).
317. Civardi, C., Schwarze, F. W. M. R. & Wick, P. Micronized copper wood preservatives: An efficiency and potential health risk assessment for copper-based nanoparticles. *Environmental Pollution* (2015). doi:10.1016/j.envpol.2015.02.018
318. SCENIHR. *Risk assessment of products of nanotechnologies*. (Scientific Committee on Emerging and Newly Identified Health Risks, 2009).
319. Tsang, M. P. *et al.* Probabilistic risk assessment of emerging materials: case study of titanium dioxide nanoparticles. *Nanotoxicology* **11,** 558–568 (2017).
320. Pang, C. *et al.* Probabilistic approach for assessing infants' health risks due to ingestion of nanoscale silver released from consumer products. *Environ. Int.* **99,** 199–207 (2017).
321. Tiarks, F. *et al.* Formulation effects on the distribution of pigment particles in paints. *Prog. Org. Coatings* **48,** 140–152 (2003).
322. Pantano, D. *et al.* Transformations of Nanoenabled Copper Formulations Govern Release, Antifungal Effectiveness, and Sustainability throughout the Wood Protection Lifecycle. *Environ. Sci. Technol.* **52,** 1128–1138 (2018).
323. Pantano, D. *et al.* Transformations of Nanoenabled Copper Formulations Govern Release, Antifungal Effectiveness, and Sustainability throughout the Wood Protection Lifecycle. *Environ. Sci. Technol.* **52,** 1128–1138 (2018).

324. Steinfeldt, M. Hot Spot Release Mapping of Nanomaterials – A Visual Exposure Assessment Method for Preliminary Assessment. *New Tools and Approaches for Nanomaterials Safety Assessment* (2017).
325. Fonseca, A. S. *et al.* Particle release and control of worker exposure during laboratory-scale synthesis, handling and simulated spills of manufactured nanomaterials in fume hoods. *J. Nanoparticle Res.* (2018). doi:10.1007/s11051-018-4136-3
326. ECHA. Recommendation no. 10 of the BPC Ad hoc Working Group on Human Exposure: The most appropriate model to be used for the scenario of non-professional application of paints by brushing and rolling. (2016).
327. Gorman, M. *et al.* The Relationship Between Inadvertent Ingestion and Dermal Exposure Pathways: A New Integrated Conceptual Model and a Database of Dermal and Oral Transfer Efficiencies. *Ann. Occup. Hyg.* **56,** 1000–1012 (2012).
328. Heggelund, L., Hansen, S. F., Astrup, T. F. & Boldrin, A. Semi-quantitative analysis of solid waste flows from nano-enabled consumer products in Europe, Denmark and the United Kingdom – Abundance, distribution and management. *Waste Manag.* (2016). doi:10.1016/j.wasman.2016.05.030
329. Mackevica, A., Olsson, M., Mines, P., Heggelund, L. & Hansen, S. Estimation of dermal transfer of nanoparticles from consumer articles by wipe sampling. *submitted*
330. EPA, U. in *Emissions Factors and AP 42. 5th ed. US74* (1995).
331. Hewett, P. & Ganser, G. H. Models for nearly every occasion: Part I - One box models. *J. Occup. Environ. Hyg.* (2017). doi:10.1080/15459624.2016.1213392
332. Nowack, B. *et al.* Meeting the Needs for Released Nanomaterials Required for Further Testing—The SUN Approach. *Environ. Sci. Technol.* **50,** 2747–2753 (2016).
333. Ganser, G. H. & Hewett, P. Models for nearly every occasion: Part II - Two box models. *J. Occup. Environ. Hyg.* **14,** 58–71 (2017).
334. Cherrie, J. W. The effect of room size and general ventilation on the relationship between near and far-field concentrations. *Appl. Occup. Environ. Hyg.* **14,** 539–46 (1999).
335. NIOSH. in *NIOSH Manual of Analytical Methods* (National Institute for Occupational Safety and Health, 2003).
336. Gorman, M. *et al.* The Relationship Between Inadvertent Ingestion and Dermal Exposure Pathways: A New Integrated Conceptual Model and a Database of Dermal and Oral Transfer Efficiencies. *Ann. Occup. Hyg.* **56,** 1000–1012 (2012).
337. ISO. DS/EN 84: Wood preservatives. Accelerated ageing of treated wood prior to biological testing. Leaching procedure. (1997).
338. Ganser, G. H. & Hewett, P. Models for nearly every occasion: Part II - Two box models. *J. Occup. Environ. Hyg.* **14,** 58–71 (2017).
339. ECHA. Guidance on the Biocidal Products Regulation - Volume III Human Health - Assessment & Evaluation (Parts B+C). (2017).
340. de Jong, W., Stone, V., Cassee, F. & Gosens, I. A 28-day oral toxicity study in rats with copper oxide and copper carbonate nanoparticles. *submitted*
341. Hébert, C. *NTP Technical Report on toxicity studies of cupric sulphate (CAS N°7758-99-8) administered in drinking water and feed to F344/N rats and B6C3F1 mice*. (National Toxicology Program, U.S. Department of Health and Human Services, 1993).
342. Platten, W. E. *et al.* Estimating dermal transfer of copper particles from the surfaces of pressure-treated lumber and implications for exposure. *Sci. Total Environ.* **548–549,** 441–449 (2016).
343. Van Der Voet, H. & Slob, W. Integration of probabilistic exposure assessment and probabilistic hazard characterization. *Risk Anal.* **27,** 351–371 (2007).
344. Gottschalk, F., Sonderer, T., Scholz, R. W. & Nowack, B. Possibilities and limitations of modeling environmental exposure to engineered nanomaterials by probabilistic material flow analysis. *Environ. Toxicol. Chem.* **29,** n/a-n/a (2010).
345. Gottschalk, F., Scholz, R. W. & Nowack, B. Probabilistic material flow modeling for assessing the environmental exposure to compounds: Methodology and an application to engineered nano-TiO2 particles. *Environ. Model. Softw.* **25,** 320–332 (2010).
346. Gottschalk, F., Scholz, R. W. & Nowack, B. Probabilistic material flow modeling for assessing the environmental exposure to compounds: Methodology and an application to engineered nano-

TiO2 particles. *Environ. Model. Softw.* (2010). doi:10.1016/j.envsoft.2009.08.011
347. Gottschalk, F., Sonderer, T., Scholz, R. W. & Nowack, B. Modeled environmental concentrations of engineered nanomaterials (TiO2, ZnO, Ag, CNT, fullerenes) for different regions. *Environ. Sci. Technol.* (2009). doi:10.1021/es9015553
348. Walser, T. & Gottschalk, F. Stochastic fate analysis of engineered nanoparticles in incineration plants. *J. Clean. Prod.* (2014). doi:10.1016/j.jclepro.2014.05.085
349. Sun, T. Y., Gottschalk, F., Hungerbühler, K. & Nowack, B. Comprehensive probabilistic modelling of environmental emissions of engineered nanomaterials. *Environ. Pollut.* **185,** 69–76 (2014).
350. Gottschalk, F., Lassen, C., Kjoelholt, J., Christensen, F. & Nowack, B. Modeling flows and concentrations of nine engineered nanomaterials in the Danish environment. *International Journal of Environmental Research and Public Health* (2015). doi:10.3390/ijerph120505581
351. Limbach, L. K. *et al.* Removal of oxide nanoparticles in a model wastewater treatment plant: Influence of agglomeration and surfactants on clearing efficiency. *Environ. Sci. Technol.* (2008). doi:10.1021/es800091f
352. Westerhoff, P., Song, G., Hristovski, K. & Kiser, M. A. Occurrence and removal of titanium at full scale wastewater treatment plants: Implications for TiO2 nanomaterials. *J. Environ. Monit.* (2011). doi:10.1039/c1em10017c
353. Wang, Y., Deng, L., Caballero-Guzman, A. & Nowack, B. Are engineered nano iron oxide particles safe? an environmental risk assessment by probabilistic exposure, effects and risk modeling. *Nanotoxicology* (2016). doi:10.1080/17435390.2016.1242798
354. Gartiser, S. *et al.* Behavior of nanoscale titanium dioxide in laboratory wastewater treatment plants according to OECD 303 A. *Chemosphere* (2014). doi:10.1016/j.chemosphere.2013.11.015
355. Johnson, A. C. *et al.* An assessment of the fate, behaviour and environmental risk associated with sunscreen TiO2nanoparticles in UK field scenarios. *Sci. Total Environ.* (2011). doi:10.1016/j.scitotenv.2011.03.040
356. Coll, C. *et al.* Probabilistic environmental risk assessment of five nanomaterials (nano-TiO2, nano-Ag, nano-ZnO, CNT, and fullerenes). *Nanotoxicology* (2016). doi:10.3109/17435390.2015.1073812
357. Gottschalk, F., Kost, E. & Nowack, B. Engineered nanomaterials in water and soils: A risk quantification based on probabilistic exposure and effect modeling. *Environ. Toxicol. Chem.* **32,** 1278–1287 (2013).
358. Semenzin, E. *et al.* Species sensitivity weighted distribution for ecological risk assessment of engineered nanomaterials: The n-TiO2 case study. *Environ. Toxicol. Chem.* (2015). doi:10.1002/etc.3103
359. Kjølholt, J. *et al. Environmental assessment of nanomaterial use in Denmark*. (2015).